Centre for Hydrogeology
and Geothermics (CHYN)
University of Neuchâtel
www.unine.ch/chyn

Isotope fractionation due to diffusion and sorption of chlorinated hydrocarbons and its implications for identifying reactive processes in aquifer - aquitard systems

PhD thesis presented to the Faculty of Sciences of the University of Neuchâtel to satisfy the requirements for the degree of Doctor of Philosophy in Science

by

Philipp Wanner

Private defense date: September 22, 2016
Public defense date: November, 25, 2016

Jury members:
Prof. Dr. Daniel Hunkeler, University of Neuchâtel, Switzerland (thesis director)
Prof. Dr. Beth Parker, University of Guelph, Canada
Prof. Dr. Philip Brunner, University of Neuchâtel, Switzerland
PD. Dr. Martin Elsner, Helmholtz Zentrum München, Germany

UNIVERSITÉ DE NEUCHÂTEL

Faculté des sciences
Secrétariat-décanat de Faculté
Rue Emile-Argand 11
2000 Neuchâtel - Suisse
Tél: + 41 (0)32 718 2100
E-mail: secretariat.sciences@unine.ch

IMPRIMATUR POUR THESE DE DOCTORAT

La Faculté des sciences de l'Université de Neuchâtel autorise l'impression de la présente thèse soutenue par

Monsieur Philipp Wanner

Titre:

"Isotope fractionation due to diffusion and sorption of chlorinated hydrocarbons and its implications for identifying reactive processes in aquifer-aquitard systems"

sur le rapport des membres du jury composé comme suit:

- Prof. Daniel Hunkeler, directeur de thèse, Université de Neuchâtel, Suisse
- Prof. Philip Brunner, Université de Neuchâtel, Suisse
- Prof. Beth L. Parker, University of Guelph, Canada
- Dr Martin Elsner, Helmholtz Zentrum München, Allemagne

Neuchâtel, le 14 novembre 2016 Le Doyen, Prof. R. Bshary

Acknowledgment

The present PhD thesis would not have been possible without the help of numerous people. First of all I would like to thank my PhD thesis director Prof. Daniel Hunkeler. I was always impressed how fast he comprehended complicated contexts and could give helpful inputs, which greatly improved the quality of this PhD thesis. Beside Prof. Daniel Hunkeler's outstanding research qualities, I also appreciated the always very positive atmosphere during our discussions. Furthermore, I would like to thank all the people from the Centre for Hydrogeology and Geothermics (CHYN) at the University of Neuchâtel for feeling very comfortable during the four years of my PhD, as everybody was very friendly and helpful. A special thank goes to the people from the Hydrochemistry and Contaminants group: Simon Jeannottat, Daniel Bouchard, Jordi Palau, Bibiane Schlunegger, Christian Moeck, Yuexia Wu, Alice Badin, Clara Torrento, Violaine Ponsin, Vincent Gruber and Simone Hintze. Moreover, I would also like to thank Prof. Beth Parker and her research group G360 at the University of Guelph in Canada for letting me participate in the unique controlled release field experiments in Borden and Sarnia in Canada. In this context I would also like to thank Steven Chapman for organizing the fieldwork in Sarnia and Borden and Bob Ingleton and Paul Johnson for operating the Geoprobe rig to retrieve the clay cores. Furthermore, I would like to thank Ryan Kroeker, Dan Elliot and Kellin Scully for their valuable contributions to the fieldwork and Maria Gorecka and Rashmi Jadeja for their analytical support in the laboratory. It was pleasure to work with so many skilled people in Canada. Furthermore, I also would like to express my gratitude to Prof. Ian Bourg from the University of Princeton in the USA. He helped me to perform the molecular dynamic simulations by giving me access to the Supercomputer at the University of Berkeley. I appreciated the constructive discussion with him and was very thankful that he took a lot of time for me even though I was not a student of him. Moreover, I am thankful for the financial support by the Swiss National Science Foundation (SNSF).

The greatest support during my PhD I experienced at home from my wife Sophie and my son Elia. I cannot express in words how thankful I am that Sophie kept my back free during my PhD and how she supported me mentally during every stage of the PhD thesis. Furthermore it was priceless how Elia made me smile after every working day. Moreover I would like to thank my parents who also supported my throughout my PhD.

Summary

Chlorinated hydrocarbons are anthropogenic contaminants, which are known to be possibly carcinogenic to humans. Although the peak production of chlorinated hydrocarbons in the 1970ties was followed by a dramatic decrease in the subsequent decades, chlorinated hydrocarbons are still frequently detected in aquifer systems demonstrating their long-term persistence. When chlorinated hydrocarbons are released at the surface as dense non-aqueous phase liquid (DNAPL), they rapidly migrate in to the subsurface and penetrate aquifer systems due to their highly mobile behavior (high density, low viscosity). During the transportation in the saturated zone, DNAPLs accumulate on top of low permeability sediments such as aquitards and are slowly dissolved. The dissolved DNAPL compounds are transported by advection in the aquifer creating a contaminant plume downstream of the source zone and diffuse into the low permeable units. During the migration in aquifer and aquitards, chlorinated hydrocarbons are retarded due to sorption, which occurs predominately on organic matter. After cessation of the DNAPL release at surface, chlorinated hydrocarbons back-diffuse from the low permeable layers towards the aquifer expanding the longevity of the contamination source. Chlorinated hydrocarbons are degradable under reducing conditions as they can act as electron acceptors under oxygen free conditions. Such reducing conditions are often encounterd in low permeable units such as aquitards.

Stable isotope methods have been increasingly used for identifying and quantifying reactive transformation in the subsurface of organic compounds such as chlorinated hydrocarbons. The method general relies on the assumption that only reactive processes are associated with an isotope effect. However, recent studies revealed that physical processes in the vadose zone (volatilization, gas phase diffusion and air-water partitioning) also fractionate isotopes, which might impair the identification of reactive processes by using stable isotope methods. In contrast to the vadose zone, the effect of physical processes in aquifer – aquitard systems on isotope ratios has received little attention so far. It remains especially uncertain as to what extent aqueous phase diffusion and sorption have a significant influence on isotope ratios of organic compounds. Thus, it remains unclear if stable isotope methods can be used to track reactive processes in systems such as aquitards, where transport is controlled by diffusion and significant sorption occurs. Furthermore, it in this context it has not yet been investigated,

whether stable isotope methods can be used to gain insight into the relation between reactive processes in aquitards and plume persistence in aquifers due to back-diffusion.

To address these gaps in knowledge, the present PhD thesis addressed the four following research questions: A) Does aqueous phase diffusion and sorption lead to measurable shifts of isotope ratios? B) Are isotope effects due to diffusion and sorption detectable under field conditions? C) Do isotope effects associated with sorption and diffusion impair the identification of reactive processes in aquifer - aquitard systems? and D) Can stable isotope methods provide insight into the impact of reactive processes in aquitards on plume persistence in aquifers? In the following, the key findings regarding the four main research questions are summarized.

A) Does aqueous phase diffusion and sorption lead to measurable shifts of isotope ratios?

Isotope fractionation associated with aqueous phase diffusion and sorption was investigated by laboratory experiments. The magnitude of isotope fractionation due to aqueous phase diffusion was quantified for two chlorinated hydrocarbons (TCE and 1,2-DCA) by conducting a modified Stokes' diffusion cell experiment. A measurable shift of isotope ratios due to aqueous phase diffusion was detected, whereby TCE and 1,2-DCA isotopocules (molecules differing in isotopic composition) containing light isotopes were transported faster by diffusion compared to those with heavy isotopes. The isotope enrichment factors were larger for chlorine ($\varepsilon_{Cl,TCE}$ = -0.37‰, $\varepsilon_{Cl,1,2\text{-}DCA}$ = -0.61‰) compared to carbon isotopes ($\varepsilon_{C,TCE}$ = -0.22‰, $\varepsilon_{C,1,2\text{-}DCA}$ = -0.23‰), which was in agreement with the larger absolute mass difference between stable chlorine (two mass units) compared to carbon isotopes (one mass unit). The diffusion coefficient (D) showed a weaker power law mass dependency ($D \propto m^{-\beta}$) with β values in the range between 0.023 and 0.031 than observed in the gas phase, where $D \propto m^{-0.5}$. The determined beta values were inconsistent with standard diffusion models (Fick's, Einstein's, Maxwell-Stefan's and Langevin's diffusion theory), which predicted either a kinetic mass dependency of D ($D \propto m^{-0.5}$) as observed in the gas phase, no mass dependency of D or a mass dependency of D in the opposite direction (i.e. faster for heavy compared to light isotopes) than the kinetic theory. To provide a theoretical basis to our laboratory observations, molecular dynamic (MD) simulations of TCE and 1,2-DCA carbon and chlorine isotopocules were for the first time performed. During MD simulations the individual motion of isotopocules are simulated, whereby all interactions with water molecules were taken into account using high performance computing. The MD

simulation results were consistent with the experimental data showing also lower beta values than predicted by the kinetic theory. The MD simulations revealed that the weak power law mass dependency of the diffusive transport rate can be explained by the mode-coupling theory showing that the overall isotope effect is the result of a competition between mass independent long-term hydrodynamic and strongly mass dependent short-term kinetic modes of motion.

Sorption induced isotope fractionation was quantified by repeated exposure of a water sample to a mass of uncontaminated natural aquitard material, which generated a higher shift of isotope ratios and thus, led to a higher precision of the determined isotope fractionation factor compared to a single step batch experiment. The multistep sorption experiment, which was conducted for two chlorinated hydrocarbons (1,2-DCA and DCM), revealed an unusual inverse isotope trend showing that carbon and chlorine isotopocules containing light isotopes were preferentially sorbed. This enhances the mobility of isotopically heavy species, which is opposite to what was observed for the diffusive transport processes during which isotopically light species are transported faster compared to heavy. The detected preferential sorption of isotopocules with light compared to isotopocules with heavy isotopes can be likely explained by changes of vibrational frequencies due to changing nonbonding interactions during the transition between the aqueous solution and the sorbent material. In the sorbent material the vibrational frequencies slow down compared to the aqueous solution caused by the stronger nonbonding interactions of the molecules with the sorbent material. Therefore, the zero point energy levels for the light and heavy isotopocules are lower and closer together in the sorbent material compared to the aqueous solution. This results in a smaller difference of the zero point energy level between sorbed and dissolved compounds in the aqueous solution for heavy than for light isotopocules. Consequently, slightly less energy is required for the heavy isotopocule to go into the aqueous phase than for the light isotopocules leading to a depletion of heavy isotopocules in the sorbent material. The determined sorption induced isotope enrichment factors were in same range for 1,2-DCA carbon and chlorine isotopes ($\varepsilon_{C,1,2\text{-}DCA}$ = -0.40‰, $\varepsilon_{Cl,1,2\text{-}DCA}$ = -0.55‰) as for the DCM carbon isotopes ($\varepsilon_{C,DCM}$ = -0.54‰).

B) Are isotope effects due to diffusion and sorption detectable under field conditions?

To investigate if diffusion and sorption leads to significant shifts of isotope ratios under field conditions and to examine how isotope fractionation due diffusion and sorption interact, two

field studies were conducted in saturated low permeability sediment, where transport is dominated by diffusion. Saturated low permeability sediments provide the advantage that the advancing concentration front can be located very precisely and sampled at a high spatial resolution. The two sites differed by the amount of organic carbon in the sediments and thus, by the extent of sorption. For both sites the contamination source was well characterized (volume, composition, spill time). At the first site (Sarnia site) a controlled release field experiment had been carried out, while at the second site the contamination was caused by a chemical waste landfill with a well-known history. At the Sarnia site, a DNAPL source had been created by emplacing 2L of 1,2-DCA and DCM. In this study, clay cores were retrieved below the DNAPL sources about 15.5 years (5672 days) after source emplacement. Carbon and chlorine isotope ratio profiles in the retrieved cores showed trends in opposite directions in the low-permeable unit. 1,2-DCA and DCM became enriched in ^{13}C with depth ($\Delta\delta^{13}C$ = 2.0‰ – 2.4‰) as sorption induced isotope fractionation dominated for carbon. In contrast for chlorine the diffusive isotope effect was larger as the absolute mass difference is two for stable chlorine compared to one for carbon isotopes overruling the sorption effect and leading to a depletion of ^{37}Cl in 1,2-DCA with depth ($\Delta\delta^{37}Cl$ =1.3‰). At the chemical waste landfill site, cores were retrieved 45 years after the waste was deposited and analyzed for TCE, the predominant organic contaminant. In contrast to the Sarnia site both elements (C and Cl) in the TCE molecule became depleted in the heavy isotope with depth, i.e. sorption no longer overruled the diffusion effect for carbon. This consistent with the five times lower organic matter content, which reduces the extent of sorption. Hence, isotope fractionation due to diffusion dominated for both TCE carbon and chlorine isotopes leading to the observed depletion in ^{13}C and ^{37}Cl with depth. The simulation of isotope fractionation for different diffusion periods in low permeability sediments at the contaminated site revealed that the diffusion time scales have an impact on the magnitude of isotope fractionation. During short diffusion periods the shift of isotope ratios is largest, while for longer diffusion period the heavy isotopes catch up and the magnitude of isotope fractionation becomes smaller. Generally, the results of the two field studies demonstrated for the first time that sorption and diffusion induced isotope fractionation for both C and Cl is detectable under field conditions.

C) Do isotope effects associated with sorption and diffusion impair the identification of reactive processes in aquifer - aquitard systems?

To evaluate if reactive processes can be tracked by stable isotope analysis despite of the isotope effect associated with diffusion and sorption, an additional field study was carried out at the Borden site. At this site, 50L of a three components DNAPL mixture (45 vol% PCE, 45 vol% TCE, 10 vol% TCM) was released in a sandy aquifer with an underlying clayey-silty aquitard on April 8, 1999. Cores were retrieved from the aquitard nearly 15 years (5281 days) after the DNAPL release and subsampled with depth to examine whether depth-discrete isotope ratio profiles can be attributed to degradation processes. Carbon isotope ratios became depleted in ^{13}C with depth as expected for a diffusion isotope effect but opposite to what is expected for reactive processes. However, the isotopic shift was much larger (up to 24‰) than observed at the chemical landfill site without degradation. The unusual large inverse isotope trend could be explained by a delay of the start of the degradation activities in the aquitard followed by non-uniformly distributed degradation activities in the aquitard, which were strongest close to the aquifer – aquitard interface and decreased exponentially with increasing depth within the upper 10 cm of the aquitard. Such a profile of degradation activities could be caused by nutrients that had diffused from the aquifer into the aquitard. Numerical modelling suggests that reactive processes started around 2500 days after DNAPL release in the aquifer indicating that isotope ratio profiles in aquitards not only provide information about the spatial distribution of degradation activities but also about their temporal evolution when intitial conditions are reasonably constrained. Furthermore, based on the numerical model degradation rates affecting chlorinated hydrocarbon in the aquitard could be estimated. The field investigations at the Borden site demonstrated for the first time that stable isotope methods can be used to identify and quantify reactive processes including spatial and temporal variability in saturated low permeability sediments

D) Can stable isotope methods provide insight into the impact of reactive processes in aquitards on plume persistence in aquifers?

To examine whether stable isotope methods provide insight into the relation between reactive processes in aquitards and plume persistence due to back-diffusion a previously developed numerical model of a dissolved TCE plume emanating from a TCE DNAPL source in

an aquifer – aquitard system was adopted by adding a single step degradation of TCE to cDCE. Three different aquitard degradation scenarios were simulated: A no-degradation scenario, a uniform and a non-uniform degradation scenario. In the latter, the same degradation rates were used as in the Borden site study (i.e. the rates decreased exponentially in the upper 10 cm of the aquitard). The degradation scenarios showed that plume persistence due to back-diffusion depends on degradation activities in the aquitard and on their vertical distribution. In the no-degradation scenario a long-term TCE tailing persists in the aquifer after source removal due to back-diffusion with concentrations above the Maximum Contamination Level (MCL) for more than 100 years. In contrast in the uniform degradation scenario, TCE disappeared completely five years after source removal but the produced cDCE was transported by diffusion from the aquitard towards the aquifer generating concentrations above the MCL for more than 100 years after source removal. Hence, as cDCE was not further degraded uniform degradation activities in the aquitard were not preventing the formation of a long-term tailing due to back-diffusion. In the non-uniform degradation scenario the parent (TCE) as well as the daughter compound (cDCE) persisted in the aquifer due to back-diffusion from the aquitard at concentrations above the MCL for more than a century. This showed that the partial degradation of TCE in the non-uniform aquitard degradation scenario led to a dual contamination and aggravated plume persistence due to back-diffusion compared to the simulated no-degradation and the uniform degradation scenario.

In the aquitard degradation scenarios, isotope enrichment was not only detectable in the aquitard but also in the aquifer during the presence as well as absence of an upgradient DNAPL source. The isotope enrichment was however, stronger once the DNAPL was removed due to the back-diffusion of heavy TCE and cDCE from the aquitard. Hence, reactive processes in the aquitard have an impact on carbon isotope ratios in the aquifer and thus, they can be tracked by measuring the temporal isotope ratio evolution before and after source removal in the aquifer. This facilitates the tracking of reactive processes in aquitards as aquifers are usually easier to access than aquitards. To investigate if the obtained carbon isotope ratio pattern for reactive processes in the aquitard are different from those for reactive processes occurring in the aquifer, an aquifer degradation scenario was simulated as well for comparison. For the aquifer degradation scenario a continuous enrichment of heavy carbon isotopes along the plume axis was observed, which was equal before and after source removal. In contrast for the aquitard

degradation scenarios (uniform/non-uniform), a sudden enrichment of heavy carbon isotopes was observed along the plume axis after source removal due to back-diffusion of heavy TCE and cDCE from the aquitard. This shows that degradation in the aquitard can also be distinguished from reactive processes occurring in the aquifer by using stable isotope methods. When reactive processes occur in the aquitard, carbon isotope ratio measurements along the plume axis are also beneficial to assess the success of the remediation of DNAPL sources located in the aquifer as the contaminants become enriched in ^{13}C when the DNAPL is completely removed.

This final paragraph provides some concluding remarks on a key question of the thesis i.e. whether isotope fractionation due to diffusion and/or sorption can impair the identification of reactive processes. For field studies, it is generally accepted that the shift of carbon or chlorine isotope ratios should be at least 2‰ to provide solid evidence for a reactive process (e.g. US EPA ;Hunkeler et al., 2008). In this research, shifts above this threshold were sometimes measured despite the absence of degradation, but the threshold was only slightly exceeded. The numerical simulation showed that in exceptional situations (strong sorption behavior, early transient diffusion), higher shifts of isotope ratios can occur. But fortunately, the field experiments and simulations also showed that the diffusion and sorption induced isotope effects are opposite and in many cases nearly cancel each other. Nevertheless, when only relatively small shifts of isotope ratios in the range of the threshold mentioned above are observed, their attribution to reactive processes should be made with caution. Such a situation is mainly expected if degradation is very slow or associated with a small isotope enrichment factor as for example for degradation of BTEX. However, for reductive dechlorination of chlorinated hydrocarbons, which is of key interest for aquitards in which generally reducing conditions prevail, isotope enrichment factors tend to be large, and thus, shifts in isotope ratios that greatly exceed the threshold are expected. This can be nicely illustrated with the Borden case study. Although the shift was in the same direction as for isotope fractionation by diffusion, it could unequivocally be attributed to reactive processes due to its large magnitude. Thus overall, this PhD thesis provides a solid basis to apply isotope methods in low permeable systems such as aquitards, where transport is governed by aqueous diffusion and attenuated by sorption. This PhD thesis also demonstrates the high potential of the CSIA method to gain insight into the effect of degradation activities in low permeability sediments on plume persistence in adjacent aquifers systems and provides guidance on suitable CSIA monitoring strategies.

Keywords:

Chlorinated hydrocarbons, aquifer – aquitard systems, stable isotope methods, carbon and chlorine isotope fractionation, diffusion, sorption, degradation

Table of contents

Chapter 1: Introduction

1.1. Context and aim of the thesis

1.1.1. History of subsurface contamination by chlorinated solvents

The production of synthetic chlorinated organic liquids such as Trichloroethene (TCE), Tetrachloroethene (PCE), cis-dichloroethene (cDCE), 1,2-Dichloroethane (1,2-DCA) or Dichloromethane (DCM) commenced at the beginning of the 20th century (Pankow and Cherry, 1996). Due to the frequent usage as solvents for dry-cleaning and degreasing applications, the synthetically produced chlorinated organic liquids were denoted as chlorinated solvents. Because of their inflammability, low reactivity, rapid evaporation and their ability to efficiently dissolve organic substances, chlorinated solvents were superior to the previously used petroleum solvents (Doherty, 2000). During the post-World War II economic expansion from the 1950ties until 1970ties, the production and use of chlorinated solvents increased dramatically, as also the food and the pharmaceutical industry started to use chlorinated solvents for extracting and synthetizing other substances (Stroo and Ward, 2010). The largest quantities of chlorinated solvents were produced in the 1970ties. For instance 200'000 tons of TCE and 350'000 tons of PCE per year were manufactured in the United States (Doherty, 2000). Due to the widespread use and the lack of understanding about potential subsurface contamination and the carcinogenic effect to humans, chlorinated solvents were used carelessly and often improperly disposed. Consequently, chlorinated solvents were often released near the surface due accidental spills or leaking storage tanks and migrated into the subsurface (Pankow and Cherry, 1996). Groundwater contamination by chlorinated solvents was discovered for the first time in the mid 1970ties (Brass et al., 1977; Symons et al., 1975). Following-up investigations revealed that groundwater contamination by chlorinated solvents is widespread and affects also many aquifers used for drinking water supply (Dowty et al., 1975; Giger and Schaffner, 1981; Page, 1981; Petura, 1981; Pojasek, 1977; Speth et al., 1981; Zoeteman et al., 1981). However, the far-reaching problems of subsurface contamination by chlorinated solvents were not yet fully understood, until a decade later the first comprehensive conceptual models describing the subsurface behavior of chlorinated solvents were developed (Pankow and Cherry, 1996). It became clearer that large quantities of chlorinated solvents have migrated into the subsurface persisting and contaminating large water bodies for decades or even centuries. Due to the increasing awareness of the severity of groundwater contamination by chlorinated solvents, the usage of chlorinated solvents became regulated and

the annual production decreased. Furthermore, considerable efforts have been made to remediate sites contaminated by chlorinated solvents. However, extensive survey studies, conducted before and after the turn of the century, (Moran et al., 2007; Rivett et al., 2005; Rivett et al., 2012; Squillace et al., 1999) demonstrated that chlorinated solvents persist in the groundwater despite the remediation of many contamination sites. For instance Squillace et al. (1999) revealed that around 7% of the ambient groundwater resources of the United States, which is used by 30 – 50 million people, contain at least one of the 60 most frequent chlorinated solvents. This is especially disquieting considering the carcinogenic effect of chlorinated hydrocarbons to humans. Hence, the legacy of subsurface contamination by chlorinated solvents of previous generations is not yet eliminated and poses further challenges for the present and future generations to ensure a contaminant free drinking water supply.

1.1.2. Behavior of chlorinated solvents in the subsurface

After releasing chlorinated solvents near the surface as dense non-aqueous phase liquid (DNAPL), rapid vertical migration into the subsurface occurs due to their high density, low viscosity and low interfacial tension (Pankow and Cherry, 1996; Schwille, 1988). In the vadose zone chlorinated solvents are partly volatilized due to their high vapor pressure forming a vapor phase contaminant plume (Christophersen et al., 2005; Conant et al., 1996; Silka, 1988) (Fig. 1A). When large quantities are released, DNAPLs migrate to greater depth reaching the water table and penetrating aquifer systems due to their higher density compared to water (Pankow and Cherry, 1996; Schwille, 1988). During the transportation in the saturated zone, DNAPLs form pools on top of low permeability layers, which are slowly dissolved (McKay et al., 1993; Pankow and Cherry, 1996; Parker et al., 1994) (Fig. 1-1A). The dissolved DNAPL compounds are transported by advection in the aquifer creating a contaminant plume downstream of the source zone and diffuse into low permeable units (Fig. 1-1A). The rate of the diffusive mass loading into the low permeability layers depends on retardation due to sorption, which occurs predominantly on organic matter (Allen-King et al., 2002; Allen-King et al., 1996). Initially, it has been assumed that only the slow dissolution process of accumulated DNAPL pools on top of low permeability sediments contributes to the longevity of DNAPL contamination sources (Anderson et al., 1992; Berglund, 1997; Hunt et al., 1988; Johnson and Pankow, 1992; Pankow and Cherry, 1996). However, in the early to mid-2000s it has been discovered that the contamination persist after the

complete dissolution of accumulated DNAPL pools. It turned out that after disappearance of DNAPL pools, the contaminant mass in the low permeability unit is transported by back-diffusion towards the aquifer due to the reversal of the concentration gradient (lower concentration in aquifer than in low permeable unit). Several field and modelling studies revealed that back-diffusion can expand the longevity of the contamination source to decades or even centuries (Chapman and Parker, 2005; Liu and Ball, 2002; Parker et al., 2008; West and Kueper, 2010) (Fig. 1-1B). The relative contribution of DNAPL dissolution versus back-diffusion to the longevity of contamination sources depends strongly on the dissolution rate of the contaminant (Seyedabbasi et al., 2012). For a compound with a high solubility a major portion of the source longevity can be attributed to back-diffusion (e.g. 97% for DCM), while for a compound with a low solubility the contribution of back-diffusion is of minor importance (e.g. 17% for PCE) (Seyedabbasi et al., 2012). Furthermore, more recent studies showed that due to the more reducing conditions, (bio)degradation of chlorinated hydrocarbons possibly occurs in saturated low permeability sediments despite the small pore sizes (Damgaard et al., 2013; Takeuchi et al., 2011). When chlorinated hydrocarbons are completely (bio)degraded in saturated low permeability sediments, the back-diffusive transport period might be shortened, which reduces the longevity of contamination sources in low permeability sediments. This is especially important for contaminants with high solubilities, as for these contaminants back-diffusion is the predominant contribution to the longevity of the contamination sources (Seyedabbasi et al., 2012). In contrast, when only partial (bio)degradation of chlorinated hydrocarbons occurs in saturated low permeability sediments, more toxic intermediate compounds might be produced and released to the aquifer by back-diffusion, which aggravates the contamination of the adjacent aquifer. However, the relevance of (bio)degradation in saturated low permeability sediments and its effect on plume persistence due to back-diffusion has not yet been investigated in detail.

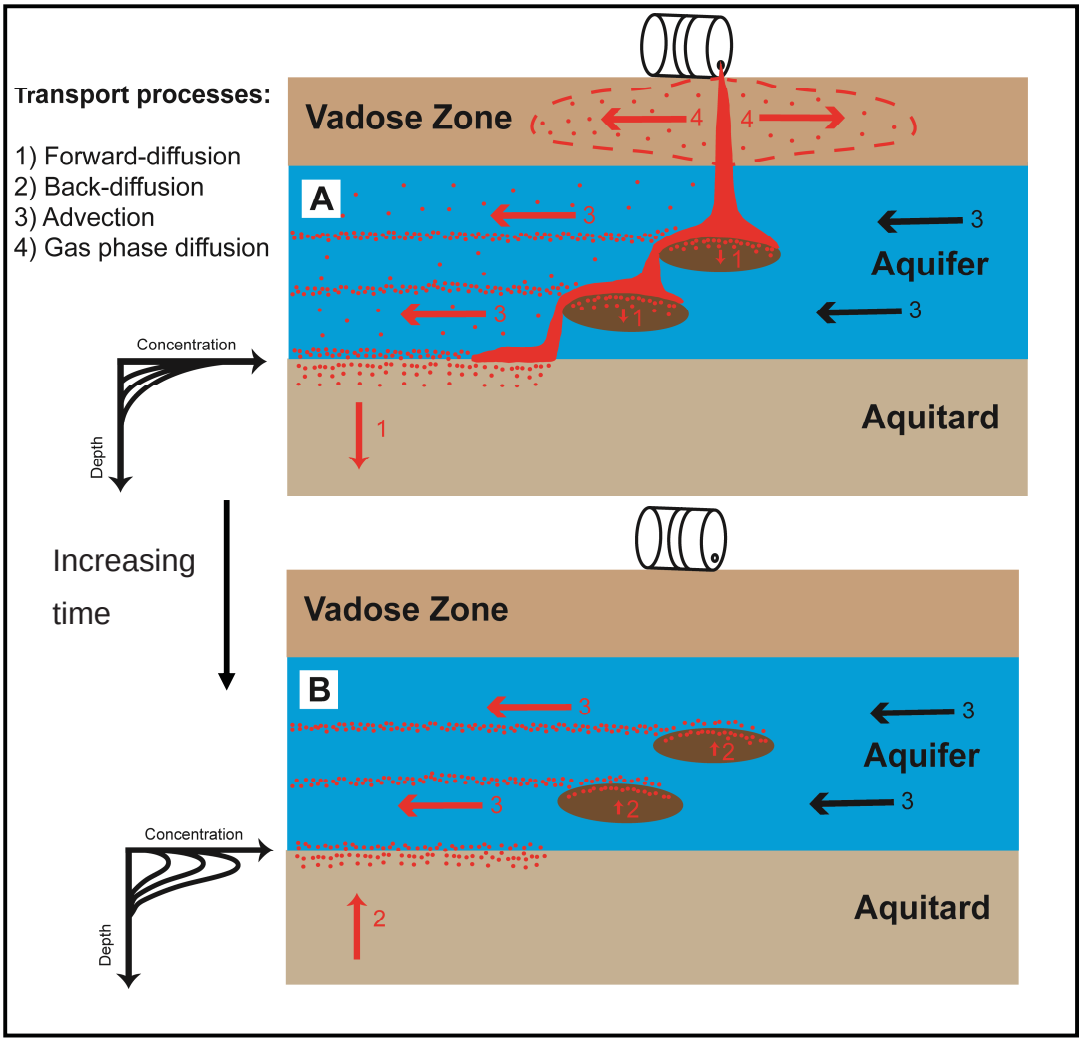

Figure 1-1. Conceptual scenario for the temporal evolution of DNAPL contamination in the subsurface. (Fig. 1-1A) Situation during DNAPLs release at the surface. Released DNAPLs form a vapor plume in the vadose zone and penetrate into the aquifer system, where they accumulate on top of low permeability zones within the aquifer and on top of the aquitard. With time, DNAPLs are dissolved and transported by advection in the aquifer and by diffusion into low permeable units. (Fig. 1-1B), Situation after cessation of DNAPL release at the surface. Back-diffusion of dissolved DNAPL mass occurs from the low permeable layers towards the aquifer contributing to the longevity of the contamination source affecting adjacent aquifers. Furthermore, possible complete or partial (bio)degradation of dissolved DNAPLs in saturated low permeable layers influence the longevity and the severity of the contamination source affecting adjacent aquifers due to back-diffusion.

1.1.3. The use of stable isotope methods in the environment

Stable isotope analysis has been increasingly used to investigate the behavior of chlorinated solvents in the subsurface. Compound-specific isotope analysis (CSIA) is an effective tool to identify and quantify in-situ (bio)degradation of organic compounds in the subsurface and to relate contaminant sources to downgradient contamination (Elsner et al., 2005; Hunkeler et al., 2011; Hunkeler et al., 2005; Hunkeler et al., 2008; Meckenstock et al., 2004). For tracking (bio)degradation, CSIA makes use of the preferential cleavage of bonds between light compared to heavy isotopes, which leads to a progressive enrichment of heavy isotopes in the educt compared to the product compound. Initially, CSIA was mainly applied for carbon isotope measurements to quantify (bio)degradation rates and for contaminant source allocation. However, recently developed new analytical techniques for compound-specific chlorine and hydrogen isotope analysis opened the possibility to apply a dual or a multi-element isotope approach i.e. to measure carbon, chlorine and hydrogen isotope signatures for the same compound. It has been demonstrated that dual and multi-element isotope approaches improve the identification of NAPL contamination sources (Shouakar-Stash et al., 2003; Wang et al., 2013; Wang and Smith, 2010) and enhances the unraveling of different degradation pathways of organic compounds (Badin et al., 2014; Kuder et al., 2013; Palau et al., 2014; Vogt et al., 2014). The CSIA method is generally based on the assumption that only reactive processes are associated with an isotope effect. However, recent studies have shown that, especially in the unsaturated zone, physical processes also fractionate isotopes potentially impairing the CSIA applications for tracking reactive processes and for allocating contaminant sources to down gradient contamination (Bouchard et al., 2008a; Bouchard et al., 2008b; Harrington et al., 1999; Huang et al., 1999; Jeannottat and Hunkeler, 2012; Jeannottat and Hunkeler, 2013; Kuder et al., 2013; Poulson and Drever, 1999). In contrast to the vadose zone, the effect of physical processes in the saturated zone on isotope ratios has received little attention in research so far. It remains especially uncertain as to what extent aqueous phase diffusion and sorption have a significant influence on isotope ratios of organic compounds, which might influence the identification and quantification of degradation activities in aquifer – aquitard systems. Furthermore, not much is known about how isotope ratios evolve during interaction of these processes.

1.1.4. General aims of the thesis

The main goals of this PhD thesis are to investigate isotope effects associated with aqueous phase diffusion and sorption of chlorinated hydrocarbons and to evaluate their effect on stable isotope methods for the identification of reactive processes in aquifer-aquitard systems. Based on these investigations it is also explored whether stable isotope methods can provide insight into the relation between reactive processes in aquitards and plume persistence in aquifers.

1.2. Fundamentals of stable isotope methods

Before outlining the research approach and content of the thesis, fundamental aspects of stable isotope methods are briefly covered. Stable isotopes are defined as chemically identical atoms having different masses due to the different number of neutrons, which do not decay. For all elements constituting chlorinated solvents (carbon, chlorine, hydrogen) two stable isotopes exist, whereby the light isotope always shows the higher natural abundance (Tab. 1-1). The abundance of stable isotopes is commonly quantified as the ratio between the most abundant heavy and the dominant light isotope (Tab. 1-1).

Table 1-1. Natural abundance of the stable isotopes of C, Cl, and H after De Laeter et al. (2003)

Element	**Stable Isotopes and Natural Abundance (%)**	
Carbon	^{12}C (98.93)	^{13}C (0.0115)
Chlorine	^{35}Cl (75.76)	^{37}Cl (24.24)
Hydrogen	^{1}H (99.9885)	^{2}H (0.0115)

As the variations of stable isotope ratios are usually small, isotope measurements are reported as deviation from internationally referenced standards (Tab. 1-2) using the delta notation (Coplen, 2011):

$$\delta_X = \left(\frac{R_{Sample} - R_{S\,tan\,dard}}{R_{S\,tan\,dard}} \right) \quad (1\text{-}1)$$

where δ_X is the delta value of the isotope ratio of element X, R_{Sample} is ratio between the heavy and the light isotope of element X and $R_{Standard}$ corresponds to the ratio of the international standard between the heavy and light isotope of element X.

Table 1-2. International references of isotope ratios for major elements constituting organic compounds.

Element	**Ratio of Isotopes**	**Standard**	**Abbrevation**	**Ratio of isotope standard[a]**
Carbon	$^{13}C/^{12}C$	Carbonate from Vienna Pee Dee	VPDB	0.011237
Chlorine	$^{37}Cl/^{35}Cl$	Chlorine ion in ocean water	SMOC	0.324
Hydrogen	$^{2}H/^{1}H$	Vienna Standard Mean Ocean Water	VSMOW	$1.5575 \cdot 10^{-4}$

[a]From Clark and Fritz (1997)

To quantify (bio)degradation of organic compounds by stable isotope methods, the Rayleigh equation is commonly used as (bio)degradation corresponds to a kinetic process:

$$ln(R_t/R_0) = (\alpha - 1) \cdot ln\ f \qquad \text{with} \quad \alpha = \frac{R_{Pr\,oduct}}{R_{Re\,ac\,tan\,t}} \quad (1\text{-}2)$$

where R_t is the isotope ratio at time t, R_0 corresponds to the initial isotope ratio at time zero and α is the fractionation factor, where $R_{Product}$ and $R_{Reactant}$ refer to the isotope ratios of the instantaneously produced product and remaining educt, respectively.

As the difference in the isotope ratios of the product and the reactant are normally small, fractionation factors (α) are frequently indicated as enrichment factors (ε):

$$\varepsilon = (\alpha - 1) \quad (1\text{-}3)$$

1.3. Isotope fractionation during physical processes

In the following two sections the current knowledge about isotope fractionation due to aqueous phase diffusion and sorption is summarized pinpointing to the need of further research for investigating the effect of these processes on isotope ratios, especially for chlorinated hydrocarbons.

1.3.1. Isotope fractionation due to aqueous phase diffusion

The fractionation factor (α) due to aqueous phase diffusion can be expressed as the ratio between the diffusion coefficients of the isotopically heavy (D_H) and the isotopically light species (D_L), respectively (Bourg et al., 2010; Richter et al., 2006):

$$\alpha = \frac{D_H}{D_L} \tag{1-4}$$

Some studies assumed that the diffusive transport rate in the aqueous phase is independent of the mass of the diffusing species (α = 1) (Berkowitz and Wan, 1987; Biswas and Bagchi, 1997; Chernyavsky and Wortmann, 2007; Chong and Hirata, 1998; McManus et al., 2002; Wolynes, 1978), while others hypothesized that the magnitude of isotope fractionation due to aqueous phase diffusion is similar as for the gas phase following the kinetic theory (Appelo and Postma, 2005; Clark and Fritz, 1997; Desaulniers et al., 1985; Donahue et al., 2008; LaBolle et al., 2008; Peeters et al., 2003; Senftle and Bracken, 1954):

$$\alpha = \frac{D_H}{D_L} = \left(\frac{\mu_L}{\mu_H} \right)^{0.5} \tag{1-5}$$

where, μ_L and μ_H refer to the reduced masses ($\mu_i = m_i M_i / m_i + M_i$) of the light and heavy species respectively, while m_i and M_i are the solute and solvent molecular masses.

For the case when the mass of the solvent molecules is infinitely large compared to the diffusing species ($M_i >> m_i$) the reduced mass can be replaced by the molecular mass of the diffusing species as $u_i \rightarrow m_i$, since $m_i + M_i \rightarrow M_i$:

$$\alpha = \frac{D_H}{D_L} = \left(\frac{m_L}{m_H} \right)^{0.5} \quad (1\text{-}6)$$

where, m_L and m_H refer to molecular mass of the light and heavy species, respectively.

Early diffusion experiments (Kunze and Fuoss, 1962; Pikal, 1972) provided evidence that the kinetic theory (eq. 1-6) overestimates the magnitude of isotope fractionation due to aqueous phase diffusion. Pikal (1972) and Kunze and Fuoss (1962) obtained a value 0.023 for the exponent in equation 1-6 for Na and Li isotopes (Tab. 1-3), which is clearly lower than 0.5 postulated by the kinetic theory. More recent experimental investigations (Bourg et al., 2010; Eggenkamp and Coleman, 2009; Richter et al., 2006; Rodushkin et al., 2004), which addressed isotope fractionation during aqueous phase diffusion for a wide spectra of dissolved ions (Mg^{2+}, Ca^{2+}, Fe^{2+}, Zn^{2+}, K^{+}, Li^{+} Cl^{-}, Br^{-}), resulted in values ranging between 0.000 and 0.025 for the exponent in equation 1-6 (Tab. 1-3). These studies confirmed that the kinetic theory overestimates the magnitude of isotope fractionation and proposed the introduction of a more general inverse power law model with an exponent $\beta < 0.5$ (Tab. 1-3):

$$\alpha = \frac{D_H}{D_L} = \left(\frac{m_L}{m_H} \right)^{\beta} \quad (1\text{-}7)$$

Tyroller et al. (2014) and Tempest and Emerson (2013) showed that also for neutral species such as noble gases (Ar, Ne), the kinetic theory overestimates the magnitude of isotope fractionation due to aqueous phase diffusion as indicated by beta values (eq. 1-7) of 0.0371 for Ar and of 0.104 and 0.0727 for Ne isotopes. Thus, these studies reinforced the validity of more general power law (eq. 1-7) for describing the magnitude of diffusion induced isotope fractionation in the aqueous phase.

In contrast to dissolved ions, organic compounds are dissolved in water as neutral molecules similar to noble gases. Isotopically distinct organic molecules are constituted by several stable isotopes (C, Cl, H, O, N, S) and denoted as isotopocules. The term isotopocules encompasses isotopologues (molecules differing in isotopic composition) as well as isotopomers (molecules having the same number of isotopes but at different positions).

Table 1-3. Experimental results for isotope fractionation due to aqueous phase diffusion

Species	**$\alpha=D_H/D_L$ (eq. 1-4)**	**β (eq. 1-7)**	**Reference**
Na Isotopes	$D_{24Na}/D_{22Na} = 0.998$	0.023	(Pikal, 1972)
Li Isotopes	$D_{7Li}/D_{6Li} = 0.9965$	0.023	(Kunze and Fuoss, 1962)
	$D_{7Li}/D_{6Li} = 0.99772$	0.015	(Richter et al., 2006)
Fe Isotopes	$D_{56Fe}/D_{54Fe} = 0.99991$	0.0024	(Rodushkin et al., 2004)
Zn Isotopes	$D_{66Zn}/D_{64Zn} = 0.99994$	0.0019	(Rodushkin et al., 2004)
Mg Isotopes	$D_{25Mg}/D_{24Mg} = 1.00003$	~ 0.000	(Richter et al., 2006)
Cl Isotopes	$D_{37Cl}/D_{35Cl} = 0.99857$	0.025	(Richter et al., 2006)
	$D_{37Cl}/D_{35Cl} = 0.99841$[a]	0.029	(Eggenkamp and Coleman, 2009)
Br Isotopes	$D_{81Br}/D_{79Br} = 0.99920$[a]	0.032	(Eggenkamp and Coleman, 2009)
Ca Isotopes	$D_{44Ca}/D_{40Ca} = 0.99957$	0.0045	(Bourg et al., 2010)
K Isotopes	$D_{41K}/D_{39K} = 0.99790$	0.042	(Bourg et al., 2010)
Ne Isotopes	$D_{22Ne}/D_{20Ne} = 0.99001$	0.104	(Tyroller et al., 2014)
	$D_{22Ne}/D_{20Ne} = 0.9931$	0.0727	(Tempest and Emerson, 2013)
Ar Isotopes	$D_{36Ar}/D_{40Ar} = 0.9961$	0.0371	(Tempest and Emerson, 2013)
C Isotopocules CH_4	$D_{13CH_4}/D_{12CH_4} = 0.99776$[b]	0.037	(Zhang and Krooss, 2001)
	$D_{13CH_4}/D_{12CH_4} = 0.99783$[c]	0.036	(Schloemer and Krooss, 2004)
C Isotopocules C_2H_6	$D_{13C_2H_6}/D_{12C_2H_6} = 0.99877$[c]	0.038	(Schloemer and Krooss, 2004)
Deuterated and non-deuterated isopropanol (IPA)	$D_{IPA}/D_{DeutIPA} = 0.99305$	0.063	(LaBolle et al., 2008)
Deuterated and non-deuterated tertiary butyl alcohol (TBA)	$D_{TBA}/D_{DeutTBA} = 0.99741$	0.023	(LaBolle et al., 2008)
Deuterated and non-deuterated toluene	$D_{Tol}/D_{DeutTol} = 0.96246$	0.455	(Jin et al., 2014)
Deuterated and non-deuterated ethylbenzene	$D_{ethb}/D_{Deutethb} = 0.96061$	0.455	(Jin et al., 2014)
Cl Isotopocules cDCE	Not indicated	0.088	(Jin et al., 2014)
Cl Isotopocules TCE	Not indicated	0.043	(Jin et al., 2014)

[a]Average of sevenfold and threefold D_H/D_L measurement for Cl and Br isotopes, respectively reported by Eggenkamp and Coleman (2009)
[b]Average of fivefold D_H/D_L measurements reported by Zhang and Krooss (2001)
[c]Average of twofold D_H/D_L measurement reported by Schloemer and Krooss (2004)

Hence, fractionation between distinct isotopically species of organic compounds occurs between isotopocules instead of isotopes. In contrast to inorganic species only little is known about isotopocule fractionation of organic compounds during diffusion in the aqueous phase. Some of the few experimental studies used deuterated versus non-deuterated compounds, to facilitate the determination of beta values. However, the obtained results are contradictory as some studies received beta values being consistent with the kinetic theory (eq. 1-6) (e.g. 0.455 for tuolene and ethylbenzene) (Jin et al., 2014), whereas others determined beta values, which are consistent with the more general inverse power law model (eq. 1-7) (e.g. 0.063 for isopropanol and 0.023 for tertiary butyl alcohol) (LaBolle et al., 2008). This spells some doubt whether deuterated versus non-deuterated compounds are representative for isotopocule fractionation during aqueous phase

diffusion at natural abundance. Only a few studies were carried out at natural abundance: Zhang and Krooss (2001) and Schloemer and Krooss (2004) determined the magnitude of carbon isotopocule fractionation of methane and ethane, whereas Jin et al. (2014) examined the magnitude of chlorine isotopocule fractionation of chlorinated hydrocarbons (cDCE and TCE). The obtained beta values (methane and ethane: 0.036 – 0.037, cDCE: 0.088, TCE: 0.043) were lower than 0.5 postulated by the kinetic theory (eq. 1-6), consistent with the observations for diffusing ions (Tab. 1-3).

1.3.2. Isotope fractionation due to sorption

The partitioning of organic compounds between groundwater or pore water and sorbent materials can be quantified by the soil-water distribution coefficient K_d. As organic compounds sorb predominantly on organic matter, K_d is commonly expressed as the product between the fraction of organic matter (f_{OC}) and the constant organic carbon-pore water partitioning coefficient (K_{OC}): (Pankow and Cherry, 1996; Wiedemeier, 1999):

$$q_e = K_d \cdot C_e \quad \text{with} \quad K_d = K_{OC} \cdot f_{OC} \tag{1-8}$$

where q_e (mg/kg) and C_e (mg/L) are the equilibrium sorbed and solution concentrations, respectively. K_{OC} values can be estimated based on the octanol-water partition coefficient (K_{OW}) (Schwarzenbach et al., 2003).

The fractionation factor due to sorption for isotopically distinct organic compounds is expressed as the ratio of the partitioning sorption constants of the heavy and light isotope, respectively (Imfeld et al., 2014; Kopinke et al., 2005):

$$\alpha = \frac{{}^{H}K_{OC}}{{}^{L}K_{OC}} \tag{1-9}$$

In analytical chemistry it has been recognized that sorption has a significant influence on isotope ratios during liquid chromatographic separation (Caimi and Brenna, 1993; Caimi and Brenna, 1997; Filer, 1999; Klein et al., 1964; Poulson et al., 1997) and in ion exchange columns (Spedding et al., 1955). It has been observed that light isotopes are preferentially sorbed on the

stationary phase leading to an enrichment of heavy isotopes in the mobile phase. Despite this evidence that sorption for sorption-induced isotope fractionation, it is currently under controversial debate if sorption fractionates isotopically distinct organic compounds in natural systems to a detectable level. Some laboratory studies suggested that sorption induced isotope fractionation can be neglected (Schüth et al., 2003; Slater et al., 2000), while others revealed a significant effect (Höhener and Yu, 2012; Imfeld et al., 2014; Kopinke et al., 2005) (Tab. 1-4). Modelling studies, which were performed based on laboratory determined enrichment factors suggest a significant sorption-induced isotope effect at the fringe of contamination plumes in aquifers (Höhener and Atteia, 2010; Van Breukelen and Prommer, 2008). However, verification of these modelling results is challenging as it can be difficult to locate and to sample the expanding plume front, where isotope fractionation might occur, at a high spatial resolution. Furthermore, other isotope fractionation processes occur at the edge of contaminant plumes such as mixing enhanced degradation or dispersion impairing the identification of isotope fractionation by sorption. Moreover, as the laboratory experiments use distinct sorbent material compared to the field, there is some doubt if the extrapolation between laboratory and the field scale is valid. Hence, up to present it remains unclear as to what extent sorption fractionates isotopically distinct species of organic compounds, especially under field conditions.

Table 1-4. Experimental results for sorption induced isotope fractionation

Species	$\varepsilon_{Sorption}$ **(‰)**	**Reference**
C Isotopocules MTBE	0.00	(Kopinke et al., 2005)
C Isotopocules Benzene	-0.44	(Kopinke et al., 2005)
C Isotopocules Toluene	-0.60	(Kopinke et al., 2005)
C Isotopocules Benzene	-0.13[a]	(Höhener and Yu, 2012)
C Isotopocules TCE	-0.52[a]	(Höhener and Yu, 2012)
Deuterated and non-deuterated Benzene	-19.0[a]	(Höhener and Yu, 2012)
Deuterated and non-deuterated cyclohexane	-64.0[a]	(Höhener and Yu, 2012)
C Isotopocules Benzene	-1.04[b]	(Imfeld et al., 2014)
C Isotopocules Toluene	-0.58[b]	(Imfeld et al., 2014)
H Isotopocules Benzene	-44.89[b]	(Imfeld et al., 2014)
H Isotopocules Toluene	-9.12[b]	(Imfeld et al., 2014)

[a]Determined based on vapor-liquid isotope effects using linear free energy relationships (LFERs)
[b]Determined by measuring sorption induced isotope fractionation due to partitioning between aqueous phase and different solvents. Indicated values correspond to the average of the reported values by Imfeld et al. (2014)

1.4. Research approach and overview of the thesis

The specific aim of the present PhD thesis was to address the following four research questions: A) Does aqueous phase diffusion and sorption lead to measurable shifts of isotope ratios? B) Are isotope effects due to diffusion and sorption detectable under field conditions? C) Do isotope effects associated with sorption and diffusion impair the identification of reactive processes in aquifer - aquitard systems? and D) Can stable isotope methods provide insight into the impact of reactive processes in aquitards on plume persistence in aquifers? To answer these four research question a research approach consisting of a combination between laboratory, field and modeling methods was applied as outlined in the following paragraph.

Isotope fractionation associated with diffusion and sorption was constrained with laboratory experiment. The mechanism of isotope fractionation during aqueous phase diffusion was investigated in more detail by using molecular dynamic simulation. To evaluate if diffusion- and sorption-induced fractionation also occurs at the field scale, controlled-release experiments were used thanks to the collaboration with the University of Guelph in Canada. Such experiments open the possibility to attribute shifts of isotope ratios to individual or combined processes with a high certainty in contrast to accidental spill sites, where the initial conditions of the contamination source (composition, spill time, volume) are often unknown. Two such controlled release experiments were performed at sites with and without occurrence of (bio)degradation. By investigating these contrasting sites, insight can also be gained as to what extend isotope fractionation associated with sorption and diffusion affects the identification of reactive processes and whether isotope data can be used to demonstrated (bio)degradation in low permeability sediments. Furthermore, it was investigated how (bio)degradation in low permeability sediments affects groundwater quality by using numerical modelling. The described studies are presented in this PhD thesis in the different chapters as follows:

In chapter 2, existing standard diffusion models were reviewed under the aspect if and how a mass dependency of the diffusive transport rate is conceptualized to provide a theoretical background for assessing the magnitude of isotope fractionation due to aqueous phase diffusion.

In chapter 3, the magnitude of diffusion-induced isotope fractionation was quantified on the laboratory scale for two chlorinated hydrocarbons by performing a Rayleigh type diffusion cell experiment. At the field scale, a water-saturated clay core was retrieved from the bottom of a

contaminated site and subsampled as a function of depth to investigate shifts of isotope ratios during downward diffusion into the clay. To compare field and laboratory data, field isotope ratio profiles were simulated using a 1D-diffusion model based on the experimentally determined magnitude of isotope fractionation due to diffusion.

In chapter 4, molecular dynamic (MD) simulations were performed to gain molecular scale insights into the mass dependency of the diffusive transport rate for isotopically distinct chlorinated hydrocarbons. Furthermore, the determined diffusion coefficients from MD simulations were compared with the laboratory determined magnitude of isotope fractionation due to aqueous phase diffusion in chapter 3.

In chapter 5, the goal was to quantify the magnitude of sorption induced isotope fractionation at the laboratory scale and to assess whether sorption induced isotope fractionation is also detectable at the field scale. Moreover, it was assessed how isotope ratios evolve when sorption and diffusion interact. At the laboratory scale a multistep sorption experiment was conducted to quantify sorption induced isotope enrichment factors. At the field scale a long-term field experiment was performed by emplacing two different DNAPL phases into a non-reactive clay unit, where diffusion and sorption occur together. About 15.5 years after emplacement isotope ratio profiles were determined in clay unit to investigate whether isotope shifts with depth can be assigned to diffusion and/or sorption processes. Moreover, to relate laboratory with field observation, determined isotope ratio profiles were compared with a 2D axisymmetrical numerical model, which included laboratory determined enrichment factors for sorption and diffusion.

In chapter 6, the aim was to evaluate whether stable isotope methods can be used to quantify degradation processes in saturated low permeability sediments. For that purpose a second long-term field experiment was conducted by infiltrating 50 liters of a three-component DNAPL mixture into an aquifer overlying an aquitard, in which degradation was expected. Nearly 14.5 years after DNAPL infiltration (5281 days), it was assess whether depth discrete isotope ratio profiles of chlorinated hydrocarbons, which had diffused into the aquitard, can be attributed to reactive processes in the aquitard.

In chapter 7, the effect of chlorinated hydrocarbon degradation in aquitards on plume persistence due to back-diffusion was investigated. Furthermore it was evaluated whether stable isotope methods can be used to track vertically varying aquitard degradation conditions. For that

purpose three different aquitard degradation scenarios were simulated: No-degradation, uniform degradation and non-uniform degradation by adopting a previously described numerical model of an aquifer – aquitard system. In addition an aquifer degradation scenario was simulated and compared with the different aquitard degradation scenarios to assess whether stable isotope methods can also be used to distinguish between degradation activities in the aquifer and the aquitard.

In chapter 8, the general conclusions of this PhD thesis are provided and new research questions are listed, which have been risen during this PhD.

1.5. References

Allen-King, R.M., Grathwohl, P., Ball, W.P., 2002. New modeling paradigms for the sorption of hydrophobic organic chemicals to heterogeneous carbonaceous matter in soils, sediments, and rocks. Advances in Water resources, 25(8): 985-1016.

Allen-King, R.M., Groenevelt, H., Warren, C.J., Mackay, D.M., 1996. Non-linear chlorinated-solvent sorption in four aquitards. Journal of contaminant hydrology, 22(3): 203-221.

Anderson, M.R., Johnson, R.L., Pankow, J.F., 1992. Dissolution of dense chlorinated solvents into ground water: 1. Dissolution from a well-defined residual source. Ground Water, 30(2): 250-256.

Appelo, C.A.J., Postma, D., 2005. Geochemistry, groundwater and pollution. CRC Press Amsterdam, Netherlands.

Badin, A., Buttet, G., Maillard, J., Holliger, C., Hunkeler, D., 2014. Multiple dual C–Cl isotope patterns associated with reductive dechlorination of tetrachloroethene. Environmental science & technology, 48(16): 9179-9186.

Berglund, S., 1997. Aquifer remediation by pumping: A model for stochastic-advective transport with nonaqueous phase liquid dissolution. Water resources research, 33(4): 649-661.

Berkowitz, M., Wan, W., 1987. The Limiting Ionic Conductivity of Na+ and CL- Ions in Aqueous Soluttions - Molecular Dynamics Simulation. Journal of Chemical Physics, 86(1): 376-382.

Biswas, R., Bagchi, B., 1997. Limiting ionic conductance of symmetrical, rigid ions in aqueous solutions: Temperature dependence and solvent isotope effects. Journal of the American Chemical Society, 119(25): 5946-5953.

Bouchard, D., Hohener, P., Hunkeler, D., 2008a. Carbon Isotope Fractionation During Volatilization of Petroleum Hydrocarbons and Diffusion Across a Porous Medium: A Column Experiment. Environmental Science & Technology, 42(21): 7801-7806.

Bouchard, D. et al., 2008b. Carbon isotope fractionation during diffusion and biodegradation of petroleum hydrocarbons in the unsaturated zone: Field experiment at Vaerlose airbase, Denmark, and modeling. Environmental Science & Technology, 42(2): 596-601.

Bourg, I.C., Richter, F.M., Christensen, J.N., Sposito, G., 2010. Isotopic mass dependence of metal cation diffusion coefficient in liquid water. Geochimica et Cosmochimica, 74: 2249 - 2256.

Brass, H. et al., 1977. The national organic monitoring survey: samplings and analyses for purgeable organic compounds. Drinking water quality enhancement through source protection: 393-416.

Caimi, R.J., Brenna, J.T., 1993. High-precision liquid chromatography-combustion isotope ratio mass spectrometry. Analytical chemistry, 65(23): 3497-3500.

Caimi, R.J., Brenna, J.T., 1997. Quantitative evaluation of carbon isotopic fractionation during reversed-phase high-performance liquid chromatography. Journal of Chromatography A, 757(1): 307-310.

Chapman, S.W., Parker, B.L., 2005. Plume persistence due to aquitard back diffusion following dense nonaqueous phase liquid source removal or isolation. Water Resources Research, 41(12).

Chernyavsky, B.M., Wortmann, U.G., 2007. REMAP: A reaction transport model for isotope ratio calculations in porous media. Geochemistry Geophysics Geosystems, 8.

Chong, S.H., Hirata, F., 1998. Dynamics of solvated ion in polar liquids: An interaction-site-model description. Journal of Chemical Physics, 108(17): 7339-7349.

Christophersen, M. et al., 2005. Transport of hydrocarbons from an emplaced fuel source experiment in the vadose zone at Airbase Værløse, Denmark. Journal of contaminant hydrology, 81(1): 1-33.

Clark, I.D., Fritz, P., 1997. Environmental Isotopes in Hydrogeology. CRC Press, United States of Americ, 328 pp.

Conant, B.H., Gillham, R.W., Mendoza, C.A., 1996. Vapor transport of trichloroethylene in the unsaturated zone: Field and numerical modeling investigations. Water Resources Research, 32(1): 9-22.

Coplen, T.B., 2011. Guidelines and recommended terms for expression of stable-isotope-ratio and gas-ratio measurement results. Rapid Communications in Mass Spectrometry, 25(17): 2538-2560.

Damgaard, I. et al., 2013. Identification of chlorinated solvents degradation zones in clay till by high resolution chemical, microbial and compound specific isotope analysis. Journal of Contaminant Hydrology, 146: 37-50.

De Laeter, J.R. et al., 2003. Atomic weights of the elements. Review 2000 (IUPAC Technical Report). Pure and Applied Chemistry, 75(6): 683-800.

Desaulniers, D.E., Kaufmann, R.S., Cherry, J.A., Bentley, H.W., 1985. ^{37}Cl - ^{35}Cl variations in a diffusion-controlled groundwater system. Geochimica et Cosmochimica, 50: 1757 - 1764.

Doherty, R.E., 2000. A History of the Production and Use of Carbon Tetrachloride, Tetrachloroethylene, Trichloroethylene and 1, 1, 1-Trichloroethane in the United States: Part 1--Historical Background; Carbon Tetrachloride and Tetrachloroethylene. Environmental forensics, 1(2): 69-81.

Donahue, M.A., Werne, J.P., Meile, C., Lyons, T.W., 2008. Modeling sulfur isotope fractionation and differential diffusion during sulfate reduction in sediments of the Cariaco Basin. Geochimica Et Cosmochimica Acta, 72(9): 2287-2297.

Dowty, B.J., Carlisle, D.R., Laseter, J.L., 1975. New Orleans drinking water sources tested by gas chromatography-mass spectrometry. Occurrence and origin of aromatics and halogenated aliphatic hydrocarbons. Environmental Science & Technology, 9(8): 762-765.

Eggenkamp, H.G.M., Coleman, M.L., 2009. The effect of aqueous diffusion on the fractionation of chlorine and bromine stable isotopes. Geochimica et Cosmochimica Acta, 73(12): 3539-3548.

Elsner, M., Zwank, L., Hunkeler, D., Schwarzenbach, R.P., 2005. A new concept linking observable stable isotope fractionation to transformation pathways of organic pollutants. Environmental Science & Technology, 39(18): 6896-6916.

Filer, C.N., 1999. Isotopic fractionation of organic compounds in chromatography. Journal of Labelled Compounds and Radiopharmaceuticals, 42(2): 169-197.

Giger, W., Schaffner, C., 1981. Groundwater pollution by volatile organic chemicals. Studies in Environmental Science, 17: 517-522.

Harrington, R.R., Poulson, S.R., Drever, J.I., Colberg, P.J.S., Kelly, E.F., 1999. Carbon isotope systematics of monoaromatic hydrocarbons: vaporization and adsorption experiments. Organic Geochemistry, 30(8A): 765-775.

Höhener, P., Atteia, O., 2010. Multidimensional analytical models for isotope ratios in groundwater pollutant plumes of organic contaminants undergoing different biodegradation kinetics. Advances in Water Resources, 33(7): 740-751.

Höhener, P., Yu, X., 2012. Stable carbon and hydrogen isotope fractionation of dissolved organic groundwater pollutants by equilibrium sorption. Journal of contaminant hydrology, 129: 54-61.

Huang, L., Sturchio, N.C., Abrajano, T., Heraty, L.J., Holt, B.D., 1999. Carbon and chlorine isotope fractionation of chlorinated aliphatic hydrocarbons by evaporation. Organic Geochemistry, 30(8A): 777-785.

Hunkeler, D. et al., 2011. Assessing chlorinated ethene degradation in a large scale contaminant plume by dual carbon-chlorine isotope analysis and quantitative PCR. Journal of Contaminant Hydrology, 119(1-4): 69-79.

Hunkeler, D., Aravena, R., Berry-Spark, K., Cox, E., 2005. Assessment of degradation pathways in an aquifer with mixed chlorinated hydrocarbon contamination using stable isotope analysis. Environmental Science & Technology, 39(16): 5975-5981.

Hunkeler, D., Meckenstock, R.U., Sheerwood Lollar, B., Schmidt, T.C., Wilson, J.T., 2008. A Guide for Assessing Biodegradation and Source Identification of Organic Ground Water Contaminants using Compound Specific Isotope Analysis. Environental Protection Agency (EPA), 600(R-08): 68.

Hunt, J.R., Sitar, N., Udell, K.S., 1988. Nonaqueous phase liquid transport and cleanup: 1. Analysis of mechanisms. Water Resources Research, 24(8): 1247-1258.

Imfeld, G., Kopinke, F.D., Fischer, A., Richnow, H.H., 2014. Carbon and hydrogen isotope fractionation of benzene and toluene during hydrophobic sorption in multistep batch experiments. Chemosphere, 107: 454-461.

Jeannottat, S., Hunkeler, D., 2012. Chlorine and Carbon Isotopes Fractionation during Volatilization and Diffusive Transport of Trichloroethene in the Unsaturated Zone. Environmental Science & Technology, 46(6): 3169-3176.

Jeannottat, S., Hunkeler, D., 2013. Can Soil Gas VOCs be Related to Groundwater Plumes Based on Their Isotope Signature? Environmental Science & Technology, 47(21): 12115-12122.

Jin, B., Rolle, M., Li, T., Haderlein, S.B., 2014. Diffusive Fractionation of BTEX and Chlorinated Ethenes in Aqueous Solution: Quantification of Spatial Isotope Gradients. Environmental Science & Technology, 48(11): 6141-6150.

Johnson, R.L., Pankow, J.F., 1992. Dissolution of Dense Chlorinated Solvents Into Groundwater. 2. Source Functions for Pools of Solvent. Environmental Science & Technology, 26(5): 896-901.

Klein, P., Simborg, D., Szczepanik, P.A., 1964. Detection and computation of isotope fractionation in the adsorption chromatography of dual-labelled compounds. Pure and Applied Chemistry, 8(3-4): 357-370.

Kopinke, F.D., Georgi, A., Voskamp, M., Richnow, H.H., 2005. Carbon isotope fractionation of organic contaminants due to retardation on humic substances: Implications for natural attenuation studies in aquifers. Environmental Science & Technology, 39(16): 6052-6062.

Kuder, T., van Breukelen, B.M., Vanderford, M., Philp, P., 2013. 3D-CSIA: Carbon, chlorine, and hydrogen isotope fractionation in transformation of TCE to ethene by a Dehalococcoides culture. Environmental science & technology, 47(17): 9668-9677.

Kunze, R.W., Fuoss, R.M., 1962. Conductance of the Alkali Halides. III. The Isotopic Lithium Chlorides. The Journal of Physical Chemistry, 66(5): 930-931.

LaBolle, E.M., Fogg, G.E., Eweis, J.B., Gravner, J., Leaist, D.G., 2008. Isotopic fractionation by diffusion in groundwater. Water Resources Research, 44(7).

Liu, C.X., Ball, W.P., 2002. Back diffusion of chlorinated solvent contaminants from a natural aquitard to a remediated aquifer under well-controlled field conditions: Predictions and measurements. Ground Water, 40(2): 175-184.

McKay, L.D., Gillham, R.W., Cherry, J.A., 1993. Field experiments in a fractured clay till: 2. Solute and colloid transport. Water Resources Research, 29(12): 3879-3890.

McManus, J., Nägler, T.F., Siebert, C., Wheat, C.G., Hammond, D.E., 2002. Oceanic molybdenum isotope fractionation: Diagenesis and hydrothermal ridge-flank alteration. Geochemistry, Geophysics, Geosystems, 3(12): 1-9.

Meckenstock, R.U., Morasch, B., Griebler, C., Richnow, H.H., 2004. Stable isotope fractionation analysis as a tool to monitor biodegradation in contaminated acquifers. Journal of Contaminant Hydrology, 75(3-4): 215-255.

Moran, M.J., Zogorski, J.S., Squillace, P.J., 2007. Chlorinated solvents in groundwater of the United States. Environmental Science & Technology, 41(1): 74-81.

Page, G.W., 1981. Comparison of groundwater and surface water for patterns and levels of contamination by toxic substances. Environmental Science & Technology, 15(12): 1475-1481.

Palau, J. et al., 2014. C and Cl isotope fractionation of 1,2-dichloroethane displays unique δ13C/δ37Cl patterns for pathway identification and reveals surprising C-Cl bond involvement during microbial oxidation. Environmental Science & Technology.

Pankow, J.F., Cherry, J.A., 1996. Dense Chlorinated Solvents and Other DNAPLs in Groundwater Waterloo. Press. Portland, OR., 522 pp.

Parker, B.L., Chapman, S.W., Guilbeault, M.A., 2008. Plume persistence caused by back diffusion from thin clay layers in a sand aquifer following TCE source-zone hydraulic isolation. Journal of Contaminant Hydrology, 102(1-2): 86-104.

Parker, B.L., Gillham, R.W., Cherry, J.A., 1994. Diffusive Disappearance of Immiscible-Phase Organic Liquids in Fractured Geologic Media. Groundwater, 32(5): 805-820.

Peeters, F. et al., 2003. Improving noble gas based paleoclimate reconstruction and groundwater dating using Ne-20/Ne-22 ratios. Geochimica Et Cosmochimica Acta, 67(4): 587-600.

Petura, J.C., 1981. Trichloroethylene and methyl chloroform in groundwater: A problem assessment. Journal (American Water Works Association): 200-205.

Pikal, M.J., 1972. Isotope effects in tracer diffusion. Comparison of the diffusion coefficients of $^{24}Na^{+}$ and $^{22}Na^{+}$ in aqueous electrolytes. J. Phys. Chem., 76: 3038 - 3040.

Pojasek, R., 1977. How to protect drinking water sources. Environmental Science & Technology, 11(4): 342-347.

Poulson, S.R., Drever, J.I., 1999. Stable isotope (C, Cl, and H) fractionation during vaporization of trichloroethylene. Environmental Science & Technology, 33(20): 3689-3694.

Poulson, S.R., Drever, J.I., Colberg, P.J., 1997. Estimation of K oc values for deuterated benzene, toluene, and ethylbenzene, and application to ground water contamination studies. Chemosphere, 35(10): 2215-2224.

Richter, F.M. et al., 2006. Kinetic isotopic fractionation during diffusion of ionic species in water. Geochimica et Cosmochimica, 70: 277 - 289.

Rivett, M., Shepherd, K., Keeys, L., Brennan, A., 2005. Chlorinated solvents in the Birmingham aquifer, UK: 1986–2001. Quarterly journal of engineering geology and hydrogeology, 38(4): 337-350.

Rivett, M.O., Turner, R.J., Glibbery, P., Cuthbert, M.O., 2012. The legacy of chlorinated solvents in the Birmingham aquifer, UK: Observations spanning three decades and the challenge of future urban groundwater development. Journal of contaminant hydrology, 140: 107-123.

Rodushkin, I., Stenberg, A., Andrén, H., Malinovsky, D., Baxter, D.C., 2004. Isotopic fractionation during diffusion of transition metal ions in solution. Analytical Chemistry, 76: 2148 - 2151.

Schloemer, S., Krooss, B.M., 2004. Molecular transport of methane, ethane and nitrogen and the influence of diffusion on the chemical and isotopic composition of natural gas accumulations. Geofluids, 4(1): 81-108.

Schüth, C., Bill, M., Barth, J.A., Slater, G.F., Kalin, R.M., 2003. Carbon isotope fractionation during reductive dechlorination of TCE in batch experiments with iron samples from reactive barriers. Journal of contaminant hydrology, 66(1): 25-37.

Schwille, F., 1988. Dense chlorinated solvents in porous and fractured media: model experiments. Boca Raton, FL, USA.

Senftle, F.E., Bracken, J.T., 1954. Theoretical effects of diffusion on isotopic abundance ratios in rocks and associated fluids. Geochimica et Cosmochimica, 7: 61 - 76.

Seyedabbasi, M.A., Newell, C.J., Adamson, D.T., Sale, T.C., 2012. Relative contribution of DNAPL dissolution and matrix diffusion to the long-term persistence of chlorinated solvent source zones. Journal of Contaminant Hydrology, 134: 69-81.

Shouakar-Stash, O., Frape, S.K., Drimmie, R.J., 2003. Stable hydrogen, carbon and chlorine isotope measurements of selected chlorinated organic solvents. Journal of Contaminant Hydrology, 60(3): 211-228.

Silka, L.R., 1988. Simulation of Vapor Transport Through the Unsaturated Zone—Interpretation of Soil-Gas Surveys. Groundwater Monitoring & Remediation, 8(2): 115-123.

Slater, G.F., Ahad, J.M.E., Lollar, B.S., Allen-King, R., Sleep, B., 2000. Carbon isotope effects resulting from equilibrium sorption of dissolved VOCs. Analytical Chemistry, 72(22): 5669-5672.

Spedding, F., Powell, J., Svec, H., 1955. A Laboratory Method for Separating Nitrogen Isotopes by Ion Exchange1. Journal of the American Chemical Society, 77(23): 6125-6132.

Speth, G., Harris, R., Yarn, J., 1981. Contamination of Ground Water by Toxic Organic Chemicals. Washington. DC: Council on Environmental Quality: 75-78.

Squillace, P.J. et al., 1999. Volatile organic compounds in untreated ambient groundwater of the United States, 1985-1995. Environmental Science & Technology, 33(23): 4176-4187.

Stroo, H.F., Ward, C.H., 2010. In situ remediation of chlorinated solvent plumes. Springer Science & Business Media.

Symons, J.M. et al., 1975. National organics reconnaissance survey for halogenated organics. Journal (American Water Works Association): 634-647.

Takeuchi, M. et al., 2011. Comparative study of microbial dechlorination of chlorinated ethenes in an aquifer and a clayey aquitard. Journal of Contaminant Hydrology, 124(1-4): 14-24.

Tempest, K.E., Emerson, S., 2013. Kinetic isotopic fractionation of argon and neon during air-water gas transfer. Marine Chemistry, 153: 39-47.

Tyroller, L., Brennwald, M.S., Mächler, L., Livingstone, D.M., Kipfer, R., 2014. Fractionation of Ne and Ar isotopes by molecular diffusion in water. Geochimica et Cosmochimica Acta, 136: 60-66.

Van Breukelen, B.M., Prommer, H., 2008. Beyond the Rayleigh equation: Reactive transport modeling of isotope fractionation effects to improve quantification of biodegradation. Environmental Science & Technology, 42(7): 2457-2463.

Vogt, C. et al., 2014. Monitoring BTEX degradation by CSIA-chances and challenges, EGU General Assembly Conference Abstracts, pp. 9875.

Wang, G. et al., 2013. A practical measurement strategy to estimate nonlinear chlorinated solvent sorption in low foc sediments. Groundwater Monitoring & Remediation, 33(1): 87-96.

Wang, Y., Smith, G.J., 2010. Advanced site diagnostic tool 3D-CSIA for in situ remediation. Remediation Journal, 21(1): 79-96.

West, M.R., Kueper, B.H., 2010. Plume detachment and recession times in fractured rock. Ground water, 48(3): 416-426.

Wiedemeier, T.H., 1999. Natural attenuation of fuels and chlorinated solvents in the subsurface. John Wiley & Sons.

Wolynes, P.G., 1978. Molecular theory of solvated ion dynamics. The Journal of Chemical Physics, 68(2): 473-483.

Zhang, T.W., Krooss, B.M., 2001. Experimental investigation on the carbon isotope fractionation of methane during gas migration by diffusion through sedimentary rocks at elevated temperature and pressure. Geochimica Et Cosmochimica Acta, 65(16): 2723-2742.

Zoeteman, B., De Greef, E., Brinkmann, F., 1981. Persistency of organic contaminants in groundwater, lessons from soil pollution incidents in the Netherlands. Science of the Total Environment, 21: 187-202.

Chapter 2: Mass dependency of diffusive transport rate – What do diffusion theories tell? – A review

2.1. Introduction

For simulating diffusive transport of solutes in the aqueous phase, several diffusion models have been developed. The models can be divided in two groups representing two different concepts: The first group of diffusion models assesses the average behavior of many solute molecules in a solution, while the second group investigates the random trajectory of one single solute molecule within the solvent. The former includes Fick's and Maxwell Stefan's diffusion theory, while the latter comprises Einstein's and Langevin's theory of diffusion.

As demonstrated in chapter 1, it is under controversial debate as to what extent isotope fractionation occurs due to aqueous phase diffusion. Three different assumptions can be found in the literature with respect the magnitude of diffusion-induced isotope fractionation: a) isotope fractionation due to aqueous phase diffusion is negligible (Berkowitz and Wan, 1987; Biswas and Bagchi, 1997; Chernyavsky and Wortmann, 2007; Chong and Hirata, 1998; McManus et al., 2002; Wolynes, 1978), b) isotope fractionation in the aqueous phase is similar to gas phase diffusion following the kinetic theory (eq. 1-5, chp. 1) (Appelo and Postma, 2005; Clark and Fritz, 1997; Desaulniers et al., 1985; Donahue et al., 2008; LaBolle et al., 2008; Peeters et al., 2003; Senftle and Bracken, 1954) and c) the magnitude of isotope fractionation caused by diffusion in the aqueous phase is significant but lower than in the kinetic theory (eq. 1-5, chp. 1) following a more general power law model with the exponent $\beta < 0.5$ (eq. 1-6, chp. 1) (Eggenkamp and Coleman, 2009; Kunze and Fuoss, 1962; Pikal, 1972; Richter et al., 2006; Schloemer and Krooss, 2004; Tempest and Emerson, 2013; Wanner and Hunkeler, 2015; Zhang and Krooss, 2001).

Given these contradictory assumptions regarding isotope fractionation associated with diffusion in liquid water, this chapter reviews four different diffusion models (Fick, Maxwell-Stefan, Einstein, Langevin) to investigate if and how they conceptualize the mass dependency of the diffusive transport rate in the aqueous phase. Furthermore, it is examined whether the different diffusion models are consistent with one of the used assumptions in literature regarding the magnitude of isotope fractionation due to diffusion in liquid water.

2.2. Mass dependency of the diffusive transport rate in different diffusion theories

2.2.1. The Fickian theory of diffusion

Fick's theory of diffusion (Fick, 1855) is the most commonly applied model for describing the diffusive transport processes in the aqueous phase. The theory considers the average behavior of solute molecules and its interaction with a solvent and is based on two physical properties: The molecular density (concentration) and the solute molecular net flux. The molecular net flux is defined as the deviation of the concentration distribution in a given system (Fick's first law of diffusion):

$$F_{u,i} = -D_i \frac{\partial C_i}{\partial u} \qquad \text{(u=x,y,z)} \tag{2-1}$$

where $F_{u,i}$ (mol/s) is the flux in direction x,y and z of species i, D_i (m^2/s) is the diffusion coefficient of species i and $\partial C_i/\partial u$ (mol/m^3/m) is the spatial density (concentration) gradient along the axis x,y, and z of species i.

Furthermore, Fick (1855) related the molecular net flux (eq. 2-1) with the molecular density (concentration) by assuming that the change in molecular density inside an infinitesimal volume element dxdydz at position r must be equal to the average net molecular flux in all 3 dimensions during an infinitesimal time interval dt (Fig. 2-1):

$$\begin{aligned} &c(r,t+dt)\cdot dxdydz - c(r,t)\cdot dxdydz = \left(J_x(r,t)\cdot dydz\cdot dt - J_x(r+dx,t)\cdot dydz\cdot dt\right) \\ &+\left(J_y(r,t)\cdot dxdz\cdot dt - J_y(r+dy,t)\cdot dxdz\cdot dt\right) \\ &+\left(J_z(r,t)\cdot dxdy\cdot dt - J_z(r+dz,t)\cdot dxdy\cdot dt\right) \end{aligned} \tag{2-2}$$

Dividing equation 2-2 by dxdydzdt and letting all infinitesimals approaches zero, we obtain:

$$\frac{\partial C(r,t)}{\partial u} = -\frac{\partial J_x(r,t)}{\partial x} + \frac{\partial J_y(r,t)}{\partial y} + \frac{\partial J_z(r,t)}{\partial z} \tag{2-3}$$

Inserting equation 2-1 in equation 2-3 leads to Fick's second law of diffusion:

$$\frac{\partial C(r,t)}{\partial u} = D\left(\frac{\partial^2 C(r,t)}{\partial x^2} + \frac{\partial^2 C(r,t)}{\partial y^2} + \frac{\partial^2 C(r,t)}{\partial z^2}\right) \tag{2-4}$$

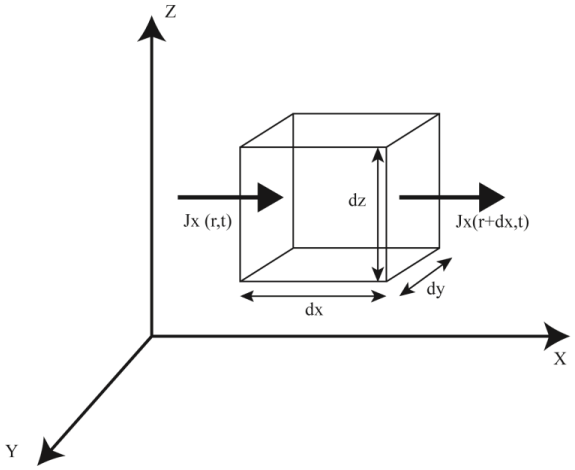

Figure 2-1. Schematic illustration of a representative infinitesimal volume element dxdydz for Fick's theory of diffusion. The net change of the molecular density (concentration) in the infinitesimal volume element during the infinitesimal time interval dt depends on the difference between the incoming flux from the left side Jx(r.t)· dydz · dt and the outgoing flux on the right side Jx(r+dx,t) dydz · dt.

A potential mass dependency of the diffusive transport rate in Fick's theory of diffusion can be investigated by assessing the different theoretical and empirical definitions of the Fickian diffusion coefficients (D; eq. 2-4). For the theoretical definitions two approaches are distinguished: the hydrodynamic and the kinetic theory. The hydrodynamic theory assumes that a solute molecule moves through a continuum solvent with a specific viscosity and the diffusion coefficient is commonly described by the Stokes-Einstein relation (Tyrrell and Harris, 1984):

$$D = \frac{k_B T}{6\pi\eta R_0} \tag{2-5}$$

where D (m^2/s) is the diffusion coefficient, k_B (J/K) is Boltzmann's constant, T (K) is the temperature, η (kg/ms) refers to the dynamic viscosity of the solvent and R_0 (m) is the solute radius.

The hydrodynamic definition of the Fickian diffusion coefficient includes no mass dependency, as the diffusion coefficient is radius but not mass dependent (eq. 2-5). Thus, the hydrodynamic theory predicts no fractionation between isotopically distinct species as an additional neutron increases the mass significantly but not necessarily the radius of a diffusing species. In contrary to the hydrodynamic theory, the kinetic theory assumes that the solute molecule diffuses in a dense hard-sphere fluid and the diffusion coefficient is commonly described by the Enskog relation (Alder et al., 1974; Tyrrell and Harris, 1984):

$$D = \frac{3}{8\rho R_{i0}^2} \frac{1}{g_{i0}\left(R_i + R_0\right)} \left(\frac{k_B T}{2\pi\mu_{i0}} \right)^{0.5} \tag{2-6}$$

where ρ is the density of the fluid, $g_{i0}(R_i+R_0)$ is the value of the solute radial distribution function at the point of contact of solute and solvent molecules, R_0 is the solvent molecule radius, $R_{i0} = (R_i + R_0)/2$, and μ_{i0} is the reduced mass of the solute solvent pair ($\mu_{i0}=m_i m_0/(m_i + m_0)$), where m_i and m_0 correspond to the molecular mass of the solute and solvent, respectively.

In contrast to the hydrodynamic theory, the kinetic theory (eq. 2-6) predicts a mass dependency of the diffusive transport rate showing an inverse proportionality of the diffusion coefficient to the square root of the reduced mass:

$$D \propto \mu^{-0.5} \tag{2-7}$$

where μ refers to the reduced mass (μ = mM/m+M), while m and M are the solute and solvent molecular masses, respectively.

For the case when the mass of the solvent molecules is infinitely large compared to the diffusing species, the reduced mass can be replaced by the molecular mass of the diffusing species as u → m, since m + M → M:

$$D \propto m^{-0.5} \tag{2-8}$$

where m is the molecular mass of the diffusion species

In addition to the theoretical definitions of the Fickian diffusion coefficient (hydrodynamic and kinetic), several empirical definitions can be found in literature. For instance Worch (1993) suggested the following empirical definition for the aqueous phase diffusion coefficient:

$$D = \frac{3.595 \cdot 10^{-11} T}{\eta m_s^{0.53}} \tag{2-9}$$

This definition of the diffusion coefficient by Worch (1993) is consistent with the kinetic theory showing a mass dependency of the diffusive transport rate, which is roughly inversely proportional to the square root of the molecular mass of the diffusing species:

$$D \propto m^{-0.53} \tag{2-10}$$

Furthermore, Wilke and Chang (1955) and Hayduk and Laudie (1974) correlated empirically diffusion coefficients for diffusing species in liquid water and in non-associated solvents exhibiting the following relationships:

$$D = \frac{7.4 \cdot 10^{-12} (xM)^{1/2} T}{\eta V^{0.6}} \quad \text{(Wilke and Chang, 1955)} \tag{2-11}$$

$$D = \frac{13.36 \cdot 10^{-9}}{\eta^{1.14} V^{0.589}} \quad \text{(Hayduk and Laudie, 1974)} \tag{2-12}$$

where x is the empirical association parameter of the solvent (2.6 for water and 1 for non-polar fluids), M is the molecular weight of the solvent and V corresponds to the molar volume of the diffusing substance.

In contrast to Worch (1993), the empirical diffusion coefficients defined by Wilke and Chang (1955) and Hayduk and Laudie (1974) are not directly dependent on the mass but on the volume of the diffusing species (eqs. 2-11 and 2-12). It has been demonstrated that isotopic substitution can have an influence on the molar volume of the diffusing species, especially when comparing deuterated vs. non-deuterated compounds (Bartell and Roskos, 1966; Lacks, 1995).

The effect originates from the longer C-H than the C-D bond length due to the greater zero point energy and the higher vibrational amplitude of the stretching vibrations for C-H compared to C-D bonds. Bartell and Roskos (1966) showed experimentally, that deuterated benzene, toluene, cyclohexane, and methyl cyclohexane have an about 0.3% smaller volume compared to their hydrogenated equivalents. Hence, the empirical diffusion coefficients defined by Wilke and Chang (1955) and Hayduk and Laudie (1974) include a mass dependency of the diffusing species via the molar volume as follows:

$D \propto V^{-0.6}$ (Wilke and Chang, 1955) (2-13)

$D \propto V^{-0.589}$ (Hayduk and Laudie, 1974) (2-14)

However, as the molar volume of the isotopically light compared to the isotopically heavy species is greater, the diffusive transport rate defined by Wilke and Chang (1955) and Hayduk and Laudie (1974) is expected to be faster for heavy compared to light isotopes. This is in fundamental contradiction with the kinetic theory (eq. 2-8) and the empirical definition of the diffusion coefficient defined by Worch (1993) (eq. 2-10), which show a mass dependency of the diffusive transport rate in the opposite way (faster for isotopically light compared to heavy species). Furthermore, the empirical diffusion coefficients defined by Wilke and Chang (1955) and Hayduk and Laudie (1974) are also not consistent with the hydrodynamic theory predicting no mass dependency of the diffusive transport rate.

2.2.2. Maxwell-Stefan's theory of diffusion

The Maxwell-Stefan theory of diffusion (Maxwell, 1866; Stefan, 1871) was developed based on the thermodynamic theory of ideal gases but it has been also widely applied for liquid solutions (Krishna and Wesselingh, 1997; Liu et al., 2013; Rehfeldt and Stichlmair, 2007; Rehfeldt and Stichlmair, 2010). The theory assumes that in a solution the chemical potential gradient of species i ($\nabla\mu_i$) is in equilibrium with the molecular friction between species i and j (Fig. 2-2).

$$\frac{x_i}{RT} \cdot \nabla \mu_i = -\sum_{j=1}^{n} \frac{x_i x_j}{\Im_{ij}} \left(v_i - v_j \right) \tag{2-15}$$

with

$$\mu_i = \mu_i^0 + RT \ln x_i \tag{2-16}$$

where $\nabla \mu_i$ is the chemical potential gradient of species i, R (8.3145 J/molK) is the gas constant, T (K) is the temperature, $\Im_{ij}$ (m^2/s) is the Maxwell-Stephan diffusion coefficient, x_i and x_j refer to the mole fractions of species i and j, respectively v_i - v_j (m/s) is the velocity difference between species i and j, μ_i^0 is the chemical potential of the pure species i and μ_i is the chemical potential for species i in a fluid mixture.

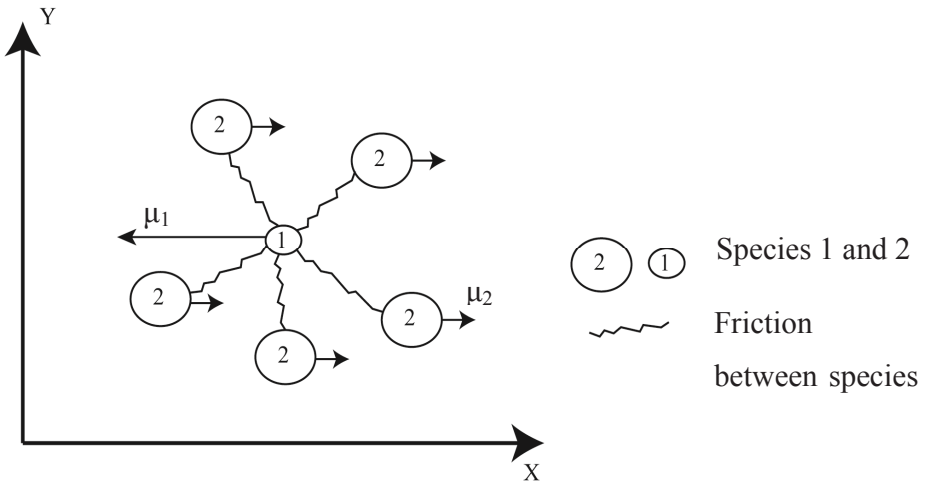

Figure 2-2. Schematic illustration of the force balance assumed by the Maxwell-Stefan theory of diffusion. The force acting per mole of species 1 in x-direction –dμ/dx is equal to the friction between species 1 and 2. Modified after Krishna and Wesselingh (1996).

Maxwell (1866) and Stefan (1871) assumed that every deviation from the equilibrium state between chemical potential gradient and molecular friction (eq. 2-15) leads to a diffusive movement of the dissolved species. In contrast to Fick's theory, the Maxwell-Stefan's theory of diffusion provides the advantage that it can be used for describing diffusive transport in multicomponent systems. On the contrary the theory has the disadvantage that the experimental

determination of the Maxwell-Stefan diffusion coefficient is only possible for binary systems and only via the Fickian diffusion coefficient and the thermodynamic correction factor (Γ_{ij}) as the chemical potential (eq. 2-16) is not directly measurable (Rehfeldt and Stichlmair, 2007; Rehfeldt and Stichlmair, 2010):

$$\Im_{ij} = \frac{D_i}{\Gamma_{ji}} \tag{2-17}$$

where $\Im_{ij}$ (m^2/s) is the Maxwell-Stefan diffusion coefficient of species i dissolved in species j, D_i (m^2/s) is the Fickian diffusion coefficient of dissolved species i and Γ_i is the thermodynamic correction factor.

It has been demonstrated by Rehfeldt and Stichelmair (2010) that experimentally determined Maxwell-Stefan diffusion coefficients, via the Fickian diffusion coefficient and the thermodynamic correction factor (eq. 2-17), are consistent with the predicted theoretical values (eq. 2-15) for thermodynamically ideal mixtures. In contrast for non-ideal systems predicted and measured Maxwell-Stefan diffusion coefficients were not consistent (Rehfeldt and Stichlmair, 2010). This indicates that the Maxwell-Stefan's diffusion theory is suitable for assessing diffusive transport in a solution with a thermodynamic ideal behavior, while for non-ideal mixtures the theory shows a high uncertainty.

Equation 2-15 suggests that the Maxwell-Stefan diffusion coefficient is not mass dependent. However, when the diffusive transport rate is determined via the Fickian diffusion coefficient (eq. 2-17), a mass dependency is observed similar to Fick's diffusion theory, depending on which definition of the Fickian diffusion coefficient is used for the transformation (eq. 2-17). When using the kinetic and the empirical definitions of the Fickian diffusion coefficient of Worch (1993) (eqs. 2-6 – 2-10), the diffusive transport rate is inversely dependent on the square root of the molecular mass of the diffusing species. In contrast when using the hydrodynamic thermodynamic definition of the Fickian diffusion coefficient (eq. 2-5), the Maxwell-Stefan diffusion coefficient shows no mass dependency, while when considering the empirical definition of Wilke and Chang (1955) and Hayduk and Laudie (1974) the diffusive transport is expected to be faster for heavy compared to light isotopes.

2.2.3. Einstein's theory of diffusion

In contrast to Fick's and Maxwell-Stefan's diffusion theory, which assesses the average behavior of solute molecules in a solution, Einstein's theory of diffusion (Einstein, 1906) is based on the probabilistic behavior of a single solute molecule within a solvent. In particular, Einstein (1906) assessed the probability that a single solute molecule changes its position due to its diffusive migration in the solvent. Einstein (1906) considered a time interval δt that is short enough for a solute molecule to collide several times with solvent molecules base on its random movement, but small enough that it can be considered infinitesimally small on the macroscopic scale. Afterwards a probability density function φ(Δ;δt) was defined, whereby φ(Δ;δt)dΔ gives the probability that a solute molecule changes its position along the x-axis of a system during δt by an amount between Δ and dΔ due to a collision with a solvent molecule. From the definition of φ(Δ;δt) Einstein calculated the average molecular density (concentration) between the spatial interval x and x + dx at time t+δt using the following equation:

$$\rho(x,t+\delta t)dx = \int_{\Delta=-\infty}^{\infty} \left[\rho(x+\Delta,t)dx\right]\cdot\left[\varphi(\Delta;\delta t)d\Delta\right] \tag{2-18}$$

The first factor in the brackets indicates the average number of solute molecules at the position x+Δ at time t, which is the average number of solute molecules prior collision with solvent molecules (Fig. 2-3). The second term is the probability that the solute molecules will be displaced along the x-axis during the time interval by an amount between Δ and dΔ and will therefore end up in the dx interval at time t+ δt. Einstein (1906) integrated equation 2-18 over all possible Δ values between +∞ and -∞ for obtaining the average number of solute molecules with the x coordinate between x+dx at time t+ δt. After integrating and rearranging equation 2-18, Einstein received the following equation for describing the diffusive transport process in three dimensions (for details, readers are referred to Einstein (1906)):

$$\frac{\partial C(r,t)}{\partial u} = D\left(\frac{\partial^2 C(r,t)}{\partial x^2} + \frac{\partial^2 C(r,t)}{\partial y^2} + \frac{\partial^2 C(r,t)}{\partial z^2}\right) \tag{2-19}$$

with:

$$D = \frac{1}{2\delta t}\int_{-\infty}^{\infty} \Delta^2 \varphi(\Delta;\delta t)\, d\Delta \qquad (2\text{-}20)$$

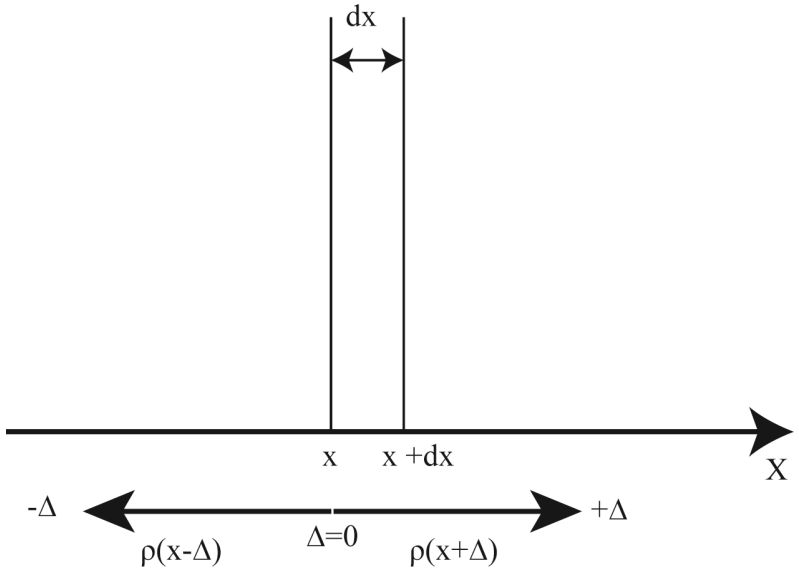

Figure 2-3. Schematic illustration of Einstein's perspective on the diffusion process. ρ(x+Δ) and ρ(x-Δ) are the molecular densities (concentrations) of solute molecules in positive and negative x direction from the considered dx interval at time t before the collision with the solvent molecules. These concentrations are multiplied with the PDF φ(Δ;δt) and then integrated over all Δ values in order to receive the solute molecular density in the dx interval after the collision of solute with solvent molecules at time t+δt.

Equations 2-19 and 2-20 show that Einstein (1906) obtained the same equation for describing the diffusive transport process as Fick (1855) (eq. 2-4) but with a different definition for the diffusion coefficient. Furthermore, Einstein (1906) revealed for the first time a relationship between the mean square displacement of a solute molecule and the diffusion coefficient D by showing that the mean square displacement increases with time at a rate 2dD, where d is the dimensionality of the system:

$$\left(r(t) - r(0)\right)^2 = 2dD\left(t - t_0\right) \qquad (2\text{-}21)$$

rearranging equation 2-21 gives:

$$D = \frac{\left(r(t) - r(0)\right)^2}{2d\left(t - t_0\right)} \tag{2-22}$$

where $(r(t)-r(0))^2$ (m^2) corresponds to the mean square displacement of a solute molecule during the time interval $t - t_0$ (s), D (m^2/s) refers to the diffusion coefficient and d indicates the dimensionality of the system.

Even tough Einstein's diffusion theory predicts not explicitly a mass dependency of the diffusive transport rate (eq. 2-20), the exhibition of a relationship between the mean square displacement and the diffusion coefficient (eq. 2-22) opened the possibility to asses a mass dependency of the diffusive transport rate by measuring the mean square displacement for isotopocially distinct species.

2.2.4. Langevin's theory of diffusion

Similar to Einstein's theory, Langevin's diffusion theory focuses on behavior of one solute molecule within a solvent. The diffusion theory was developed by examining a single solute molecule with mass m, which is exposed to forces coming from collisions with solvent molecules (Lemons and Gythiel, 1997). In contrast to Einstein's theory of diffusion, which is based on the probabilistic behavior of a solute molecule, Langevin used Newton's second law to explain the random motion of a solute molecule:

$$m\frac{dVx(t)}{dt} = -yVx(t) + X \tag{2-23}$$

Langevin assumed that the force F=ma (Newton's second law; left term eq. 2-23), which a solute molecule experiences during collision with solvent molecules equals the sum of two different forces. The first force (-yVx(t); first term right side of equation 2-23) is directly proportional to the velocity of the molecule but in negative direction, whereby the constant y represents the drag force ($y=6\pi\eta R$), which corresponds to the conventional drag force used in hydrodynamics. The second force (X; second term, right side of equation 2-23) equals to a random fluctuation forces,

which is independent of the velocity of the moving solute molecule. Langevin used this force cautiously and intuitively because their formal properties were not yet developed and not widely applied at this time, whereas today this force is defined and applied as the Gaussian white noise. For a detailed description of the Gaussian white noise readers are referred to Kuo (1996).

Similar to Einstein, Langevin's diffusion theory also yields an expression for the mean square displacement of solute molecule within a solvent. (For details of the deviation of the mean square displacement equations of Langevin's diffusion theory readers are referred to Gillespie and Seitaridou (2013)):

$$\left(r(t)-r(0)\right)^2 = 2d\,\frac{k_B T}{y}\left[(t-t_0)-\tau\left(1-e^{-(t-t_0)/\tau}\right)\right] \tag{2-24}$$

where k_B (J/K) is the Boltzmann constant, T (K) is the temperature, $y=6\pi\eta R$ (kg/ms) corresponds to the drag forces, where η is the viscosity of the solvent and R (m) is the solute radius, $t - t_0$ (s) is the time interval and τ (s) equals mD/k_BT, where m is the mass of the solute molecule.

For investigating the properties of Langevin's mean square displacement formula (eq. 2-24) with respect to a mass dependency the equation is considered for large and short time intervals. When taking a large time interval with respect to the constant τ ($t - t_0 >> \tau$), which has also units of time, the right most term $\tau\left(1-e^{-(t-t_0)/\tau}\right)$ in equation 2-24 becomes zero. Hence, the mean square displacement equation for long time intervals becomes:

$$\left(r(t)-r(0)\right)^2 = 2d\,\frac{k_B T}{6\pi\eta R}(t-t_0) = 2dD(t-t_0) \tag{2-25}$$

The expression in equation 2-25 corresponds to Einstein's means square displacement expression (eq. 2-23) showing that during large time intervals ($t - t_0 >> \tau$) Langevin's and Einstein's mean squared displacement formulas are identical. Hence, during large time intervals ($t - t_0 >> \tau$) the Langevin theory of diffusion is not predicting a mass dependency of the diffusive transport rate. In contrast when the time interval is taken small ($t - t_0 << \tau$) Langevin's mean square displacement equation expression becomes:

$$\left(r(t)-r(0)\right)^2 = 2d\,\frac{k_B T}{m}\left(t-t_0\right)^2 \qquad (2\text{-}26)$$

Equation 2-26 demonstrates that in contrast to large time intervals ($t - t_0 >> \tau$) (eq. 2-25), the mean square displacement is inversely proportional to the mass of the diffusion species during short time intervals ($t - t_0 << \tau$). Hence, in contrast to long time intervals, the mean square displacement equation for Langevin's theory of diffusion predicts a mass dependency for the movement of solute molecules during short time intervals.

2.3. Discussion

The different definitions of the Fickian diffusion coefficient (kinetic, hydrodynamic, empirical) are inconsistent with respect to their mass dependency. The mass dependency of the diffusive transport rate is either neglected shows an inverse proportionality to the square root of the molecular mass of the diffusing species or predicts a faster diffusive transport rate for heavy compared to light isotopes (eqs. 2-5 – 2-14). The same inconsistency regarding the mass dependency of the diffusive transport rate is also observed for the Maxwell-Stefan diffusion theory, as the Maxwell-Stefan diffusion coefficient is determined via the Fickian diffusion coefficient (eq. 2-17). Einstein's diffusion theory foresees not explicitly a mass dependence of the diffusive transport rate, being consistent with the hydrodynamic but in contradiction with the kinetic and the empirical definition of the Fickian diffusion coefficients. However, as mentioned in section 2.2.3. the relationship between the diffusion coefficient and the mean squared displacement by Einstein (1906) (eq. 2-24) enabled the possibility to investigate a potential mass dependency of the diffusive transport rate by measuring the mean square displacement for isotopically distinct species. However, Einstein's relationship between the diffusion coefficient and the mean square displacement contains also some limitations due to the inverse proportionality to the arbitrarily taken time interval δt (eq. 2-23). When the time interval δt is very small, the solute molecule might not experience enough collisions with the solvent molecules that its movement is randomly. Thus, during short time intervals, the solute molecule moves nearly straight (ballistic) at a nearly constant speed like in a diluted gas, which is not corresponding to a diffusive behavior. Therefore, at small time intervals it is not possible to

determine diffusion coefficient using Einstein's mean square displacement formula. In contrast to Einstein, Langevin's diffusion theory contributed to the solution that the mean square displacement can also be described during short time intervals. Langevin revealed an inverse proportionality between molecular movement of the solute and the mass of the diffusing species during short time intervals (eq. 2-26). However, the disadvantage of the expression in equation 2-26 is that although Langevin found a way to describe the mass dependent ballistic behavior during short time intervals, it cannot be related with a diffusive transport rate, as the term k_BT/m (eq. 2-26) is not corresponding to the diffusion coefficient. In contrast during long time intervals Langevin's diffusion theory proposed that the diffusive transport process is mass independent obtaining the same mean square displacement equation as Einstein (eq. 2-28). This is in agreement with the hydrodynamic definition of the diffusion coefficient but contradicts the kinetic and empirical definitions of the Fickian and the Maxwell-Stefan diffusion coefficients.

In addition to the contradictory results regarding the mass dependency of the diffusive transport rate non-of the described diffusion models was consistent with the recently proposed more general power law model by experimental studies (eq. 1-6, chp. 1). The different diffusion models either overestimated the magnitude of isotope fractionation (kinetic and Worch (1993) empirical definition of the Fickian diffusion), predicted an isotope fractionation in the opposite way (empirical definition of Fickian diffusion coefficient by Hayduk and Laudie (1974) and Wilke and Chang (1955)) or underestimated the mass dependency of the diffusive transport rate compared to the power law model (Einstein's, Maxwell-Stefan's and Langevin's diffusion models). Therefore, non-of the standard diffusion models provide a theoretical rationale for the general power law model proposed by recent experimental studies (eq. 1-6, chp. 1). Alternatively, to the standard diffusion models, molecular dynamic simulations have been increasingly used to investigate the mass dependency of the diffusive transport rate in aqueous solutions. The basic concept relies on the quantification of the diffusive transport rate for isotopically distinct species by determining the solute's mean square displacement using Einstein's equation (eq. 2-22) for a time interval being large enough to ensure a random movement of the solute in the solvent. In contrast to the standard diffusion models, molecular dynamic simulations (Bourg et al., 2010; Bourg and Sposito, 2007; Bourg and Sposito, 2008) for isotopically distinct ions and noble gases, revealed a consistency between the mass dependency of the diffusive transport and the power law model (eq. 2-2). Hence, Bourg and Sposito (2007), Bourg and Sposito (2008) and Bourg et al.

(2010) provided for the first time a theoretical rationale for the more general power law model (eq. 1-6, chp. 1) supporting its validity for estimating the magnitude of isotope fractionation due to aqueous phase diffusion. Furthermore, the performance of molecular dynamic simulations opened the possibility to gain more insight into the mechanism of the mass dependency of the diffusive transport rate. Bourg et al. (2010) and Bhattacharyya and Bagchi (2000) revealed that two competing effects determine the mass dependency of the diffusive transport rate in the aqueous phase: The strongly mass dependent short time kinetic-like friction and the mass independent long time hydrodynamic friction, which will be discussed in more detail in chapter 4. This outcome is to some extent consistent with the Langevin's theory of diffusion proposing a mass dependency during short but not during long time intervals (eqs. 2-24 – 2-26). However, Langevin's diffusion theory is not providing an equation, which includes both time interval considerations to predict correctly the mass dependency of the diffusive transport rate in the aqueous phase.

2.4. Conclusions

The review of four standard diffusion theories (Fick, Maxwell-Stefan, Einstein, Langevin) revealed equivocal results regarding the mass dependency of the diffusive transport rate in the aqueous phase. In addition to the provision of ambiguous results, non-of the four diffusion theories is coherent with the general power law model (eq. 1-6, chp. 1), exhibited by recent experiment studies. In contrast to the standard diffusion models, molecular dynamic simulations were able to reproduce the weaker power law mass dependency of the diffusive transport rate than postulated by the kinetic theory being consistent with recent experimental studies. Thus, the molecular dynamic simulation results reinforce the validity of the more general power law model (eq. 1-6, chp. 1). However, so far molecular dynamic simulations were only performed for isotopically distinct inorganic species. Thus, the confirmation of the validity of the more general power law model for isotopically distinct organic species has not yet been provided by molecular dynamic simulations.

2.5. References

Alder, B.J., Alley, W.E., Dymond, J.H., 1974. Studies In Molecular-Dynamics .14. Mass and Size Dependence of Binary Diffusion Coefficients. Journal of Chemical Physics, 61(4): 1415-1420.

Appelo, C.A.J., Postma, D., 2005. Geochemistry, groundwater and pollution. CRC Press Amsterdam, Netherlands.

Bartell, L., Roskos, R., 1966. Isotope effects on molar volume and surface tension: simple theoretical model and experimental data for hydrocarbons. The Journal of Chemical Physics, 44(2): 457-463.

Berkowitz, M., Wan, W., 1987. The Limiting Ionic Conductivity of Na+ and Cl- Ions in Aqueous Soluttions - Molecular Dynamics Simulation. Journal of Chemical Physics, 86(1): 376-382.

Bhattacharyya, S., Bagchi, B., 2000. Power law mass dependence of diffusion: A mode coupling theory analysis. Physical Review E, 61(4): 3850-3856.

Biswas, R., Bagchi, B., 1997. Limiting ionic conductance of symmetrical, rigid ions in aqueous solutions: Temperature dependence and solvent isotope effects. Journal of the American Chemical Society, 119(25): 5946-5953.

Bourg, I.C., Richter, F.M., Christensen, J.N., Sposito, G., 2010. Isotopic mass dependence of metal cation diffusion coefficient in liquid water. Geochimica et Cosmochimica, 74: 2249 - 2256.

Bourg, I.C., Sposito, G., 2007. Molecular dynamics simulations of kinetic isotope fractionation during the diffusion of ionic species in liquid water. Geochimica et Cosmochimica Acta, 71(23): 5583-5589.

Bourg, I.C., Sposito, G., 2008. Isotopic fractionation of noble gases by diffusion in liquid water: Molecular dynamics simulations and hydrologic applications. Geochimica Et Cosmochimica Acta, 72(9): 2237-2247.

Chernyavsky, B.M., Wortmann, U.G., 2007. REMAP: A reaction transport model for isotope ratio calculations in porous media. Geochemistry Geophysics Geosystems, 8.

Chong, S.H., Hirata, F., 1998. Dynamics of solvated ion in polar liquids: An interaction-site-model description. Journal of Chemical Physics, 108(17): 7339-7349.

Clark, I.D., Fritz, P., 1997. Environmental Isotopes in Hydrogeology. CRC Press, United States of Americ, 328 pp.

Desaulniers, D.E., Kaufmann, R.S., Cherry, J.A., Bentley, H.W., 1985. ^{37}Cl - ^{35}Cl variations in a diffusion-controlled groundwater system. Geochimica et Cosmochimica, 50: 1757 - 1764.

Donahue, M.A., Werne, J.P., Meile, C., Lyons, T.W., 2008. Modeling sulfur isotope fractionation and differential diffusion during sulfate reduction in sediments of the Cariaco Basin. Geochimica Et Cosmochimica Acta, 72(9): 2287-2297.

Eggenkamp, H.G.M., Coleman, M.L., 2009. The effect of aqueous diffusion on the fractionation of chlorine and bromine stable isotopes. Geochimica et Cosmochimica Acta, 73(12): 3539-3548.

Einstein, A., 1906. Über die von der molekularkinetischen Theorie der Wärme geforderte Bewegung von in ruhenden Flüssigkeiten suspendierten Teilchen Einstein. Annalen der Physik, 17: 549 - 560.

Fick, A., 1855. Über Diffusion. Annalen der Physik, 170: 59 - 86.

Gillespie, D.T., Seitaridou, E., 2013. Simple brownian diffuison. Oxford University Press, Oxford, 273 pp.

Hayduk, W., Laudie, H., 1974. Prediction of Diffusion-Coefficients for Non-Electrolytes in Dilute Aqueous-Solutions. Aiche Journal, 20(3): 611-615.

Krishna, R., Wesselingh, J.A., 1997. The Maxwell-Stefan approach to mass transfer. Chemical Engineering Science, 52(6): 861 - 911.

Kunze, R.W., Fuoss, R.M., 1962. Conductance of the Alkali Halides. III. The Isotopic Lithium Chlorides. The Journal of Physical Chemistry, 66(5): 930-931.

Kuo, H.K., 1996. White Noise Distribution Theory. CRC Press Inc., United States of America, Florida, 378 pp.

LaBolle, E.M., Fogg, G.E., Eweis, J.B., Gravner, J., Leaist, D.G., 2008. Isotopic fractionation by diffusion in groundwater. Water Resources Research, 44(7).

Lacks, D.J., 1995. Origins of molar volume isotope effects in hydrocarbon systems. The Journal of chemical physics, 103(12): 5085-5090.

Lemons, D.S., Gythiel, A., 1997. Paul Langevin's 1908 paper "On the Theory of Brownian Motion" [Sur la théorie du movement brownien," C.R. Acad. Sci. (Paris) 146, 530 - 533 (1908)]. Annalen der Physik, 65(11): 1079 - 1081.

Liu, X. et al., 2013. Diffusion Coefficients from Molecular Dynamics Simulations in Binary and Ternary Mixtures. International Journal of Thermophysics, 34(7): 1169-1196.

Maxwell, J.C., 1866. On the dynamical theory of gases. Philosophical Transactions of the Royal Society of London 15: 167 - 171.

McManus, J., Nägler, T.F., Siebert, C., Wheat, C.G., Hammond, D.E., 2002. Oceanic molybdenum isotope fractionation: Diagenesis and hydrothermal ridge-flank alteration. Geochemistry, Geophysics, Geosystems, 3(12): 1-9.

Peeters, F. et al., 2003. Improving noble gas based paleoclimate reconstruction and groundwater dating using Ne-20/Ne-22 ratios. Geochimica Et Cosmochimica Acta, 67(4): 587-600.

Pikal, M.J., 1972. Isotope effects in tracer diffusion. Comparison of the diffusion coefficients of $^{24}Na^{+}$ and $^{22}Na^{+}$ in aqueous electrolytes. J. Phys. Chem., 76: 3038 - 3040.

Rehfeldt, S., Stichlmair, J., 2007. Measurement and calculation of multicomponent diffusion coefficients in liquids. Fluid Phase Equilibria, 256(1-2): 99-104.

Rehfeldt, S., Stichlmair, J., 2010. Measurement and prediction of multicomponent diffusion coefficients in four ternary liquid systems. Fluid Phase Equilibria, 290(1-2): 1-14.

Richter, F.M. et al., 2006. Kinetic isotopic fractionation during diffusion of ionic species in water. Geochimica et Cosmochimica, 70: 277 - 289.

Schloemer, S., Krooss, B.M., 2004. Molecular transport of methane, ethane and nitrogen and the influence of diffusion on the chemical and isotopic composition of natural gas accumulations. Geofluids, 4(1): 81-108.

Senftle, F.E., Bracken, J.T., 1954. Theoretical effects of diffusion on isotopic abundance ratios in rocks and associated fluids. Geochimica et Cosmochimica, 7: 61 - 76.

Stefan, J., 1871. Über das Gleichgewicht und die Bewegung insbesondere die Diffusion von Gasgemengen. Sitzungsberichte der Kaiserlichen Akademie der Wissenschaften Wien, 2te Abteilung a, 63: 63-124.

Tempest, K.E., Emerson, S., 2013. Kinetic isotopic fractionation of argon and neon during air-water gas transfer. Marine Chemistry, 153: 39-47.

Tyrrell, H., Harris, K., 1984. Diffusion in Liquids: a Theoretical and Experimental Study. Butlerworth.

Wanner, P., Hunkeler, D., 2015. Carbon and chlorine isotopologue fractionation of chlorinated hydrocarbons during diffusion in water and low permeability sediments. Geochimica et Cosmochimica Acta, 157: 198-212.

Wilke, C.R., Chang, P., 1955. Correlation of Diffusion Coefficients in Dilute Solutions. Aiche Journal, 1(2): 264-270.

Wolynes, P.G., 1978. Molecular theory of solvated ion dynamics. The Journal of Chemical Physics, 68(2): 473-483.

Worch, E., 1993. Eine neue gleichung zur berechnung von diffusionskoeffizienten gelöster stoffe. Vom Wasser, 81: 289-297.

Zhang, T.W., Krooss, B.M., 2001. Experimental investigation on the carbon isotope fractionation of methane during gas migration by diffusion through sedimentary rocks at elevated temperature and pressure. Geochimica Et Cosmochimica Acta, 65(16): 2723-2742.

Chapter 3: Carbon and chlorine isotopologue fractionation of chlorinated hydrocarbons during diffusion in water and low permeability sediments

Published in Geochimica and Cosmochimica Acta

Philipp Wanner and Daniel Hunkeler (2015). *Geochim. et Cosmochim. Acta* **157**, 198 – 212

Abstract

To identify reactive processes in diffusion dominated water-saturated systems using compound-specific isotope analysis (CSIA), the effect of the diffusive transport process on isotope ratios needs to be known. This study aims to quantify the magnitude of carbon and chlorine isotopologue fractionation of two chlorinated hydrocarbons (trichloroethene (TCE) and 1,2-dichloroethane (1,2-DCA)) during diffusion in the aqueous phase and to relate for the first time laboratory with field results. Diffusion coefficient ratios in the aqueous phase were experimentally quantified with a modified Stokes diffusion cell. The experiment revealed a significant shift of carbon and chlorine isotopologue ratios of TCE and 1,2-DCA during diffusion. For both TCE and 1,2-DCA, the magnitude of the shift of chlorine isotopologue ratios was larger (TCE: D_{132}/D_{130}=0.99963±0.00003; 1,2-DCA: D_{102}/D_{100}=0.99939±0.00003) in comparison to carbon isotopologue ratios (TCE: D_{131}/D_{130}=0.99978±0.00006; 1,2-DCA: D_{101}/D_{100}=0.99977±0.00004), which is consistent with the larger mass difference between stable chlorine compared to carbon isotopes. Determined diffusion coefficients for carbon and chlorine isotopologues of TCE and 1,2 DCA follow an inverse power law form ($D \propto m^{-\beta}$) with $\beta<0.5$ revealing that the magnitude of isotopologue fractionation of TCE and 1,2-DCA is lower than in the previously postulated kinetic theory ($D \propto m^{-0.5}$). To relate laboratory with field results, a water-saturated clay core from a VOC contaminated site was retrieved and subsampled as a function of depth to assess possible shifts in isotopologue ratios during downward diffusion of VOCs into the low permeable clay. Observed small shifts of TCE carbon and chlorine isotopologue ratio profiles were consistent with laboratory determined diffusion coefficient ratios, demonstrated by a 1D-diffusion model. Further 1D-simulations for shorter diffusion periods (5-10 years) than observed in the retrieved clay core (45 years), revealed a larger effect on TCE chlorine and carbon isotopologue ratio profiles. Thus the diffusive transport process in water-saturated low permeability sediments only impairs the identification of reactive processes using compound-specific isotope analysis (CSIA) during short diffusion periods and for reactive processes with small enrichment factors.

3.1. Introduction

Due to industrial activities, groundwater contamination by chlorinated hydrocarbons is a widespread problem (Pankow and Cherry, 1996). When chlorinated hydrocarbons are released as dense non-aqueous phase liquid (DNAPL), vertical transportation through the unsaturated zone into aquifer systems usually occurs due to high density and low viscosity of DNAPLs (Cotel et al., 2011). During the further migration in aquifer systems, DNAPLs tend to accumulate on top of low permeability zones and diffuse into them (Falta, 2005; Feenstra et al., 1991; Johnson and Pankow, 1992; Parker et al., 2004; Seyedabbasi et al., 2012). In these zones, typically more reducing conditions are encountered and biodegradation of chlorinated hydrocarbons possibly occurs (Damgaard et al., 2013).

Compound-specific stable isotope analysis (CSIA) has been developed to track such (bio)chemical transformation processes and to associate contaminant sources to down gradient contamination. This method is generally based on the assumption, that only bond cleavage of organic molecules (i.e.(bio)chemical transformation processes) is associated with isotope effects (Elsner et al., 2005; Hunkeler et al., 2011; Hunkeler et al., 2005; Hunkeler et al., 1999; Lollar et al., 2001; Meckenstock et al., 2004). However, recent studies have shown that physical processes also can fractionate isotopes such as gas diffusion (Bouchard et al., 2008a; Bouchard et al., 2008b), vaporization and air water partitioning (Harrington et al., 1999; Huang et al., 1999; Hunkeler et al., 2011; Jeannottat and Hunkeler, 2013; Kuder et al., 2009; Poulson and Drever, 1999; Shin and Lee, 2010), which potentially complicates the identification of (bio)chemical transformation processes using CSIA. In contrast to these processes, the effect of diffusion in the aqueous phase and water-saturated low permeability materials on isotope ratios has received little attention so far. In particular, isotope fractionation during diffusion could impair the identification of reactive processes in diffusion dominated saturated low permeability sediments using CSIA. Consequently, the quantification of a potential isotopic effect during diffusion of chlorinated hydrocarbons is indispensable to track reactive processes in diffusion dominated low permeability sediments such as clays.

Most previous studies in groundwater hydrology assumed that isotope fractionation of dissolved ions and noble gases during diffusion in the aqueous phase follows either the hydrodynamic theory (Berkowitz and Wan, 1987; Biswas and Bagchi, 1997; Chernyavsky and

Wortmann, 2007; Chong and Hirata, 1998; McManus et al., 2002) or alternatively the kinetic theory, which was developed for gaseous mixtures (Appelo and Postma, 2005; Clark and Fritz, 1997; Desaulniers et al., 1985; Donahue et al., 2008; LaBolle et al., 2008; Peeters et al., 2003; Senftle and Bracken, 1954). The hydrodynamic theory assumes that a solute molecule moves through a continuum solvent with a specified viscosity and the diffusion coefficient is commonly described by the well-known Stokes-Einstein relation (Cussler, 2009):

$$D = \frac{k_B T}{6\pi\mu R_0} \tag{3-1}$$

where D (m^2/s) is the diffusion coefficient, k_B (J/K) is Boltzmann's constant, T (K) is the temperature, μ (kg/ms) refers to the viscosity of the solvent and R_0 (m) is the solute radius.

In the framework of the Stokes-Einstein relation, the diffusion coefficient of a dissolved species is radius but not mass dependent. Therefore, the hydrodynamic theory foresees no fractionation between isotopically distinct species differing in one or more neutrons, since an additional neutron increases the mass significantly but not necessarily the radius of the dissolved species. In contrary, in the framework of the kinetic theory, the diffusion coefficient of a dissolved species is mass dependent and the ratio between two diffusion coefficients of two isotopically distinct species is proportional to the inverse square root of their reduced masses:

$$\frac{D_H}{D_L} = \left(\frac{\mu_L}{\mu_H}\right)^{0.5} \tag{3-2}$$

where D_H (m^2/s) is the diffusion coefficient of the heavy isotope, D_L (m^2/s) is the diffusion coefficient of the light isotope and μ_L and μ_H refer to the reduced masses ($\mu_i = m_i M_i / m_i + M_i$) of the diffusing species, where m_i and M_i are solute and solvent masses.

For diffusing gases equation 3-2 can be simplified by assuming that the mass of the molecules of the medium (M_i) is infinitively large in comparison to the diffusing molecules ($M_i >> m_i$) (Ballentine et al., 2002; Bourg and Sposito, 2008; Klump et al., 2007; Lippmann et al., 2003; Peeters et al., 2003; Richter et al., 2006; Strassmann et al., 2005; Zhou et al., 2005).

Therefore, the reduced mass in equation 2 becomes to $\mu_i \rightarrow m_i$ since $m_i + M_i \rightarrow M_i$. This simplification leads to the kinetic "square root" relation:

$$\frac{D_H}{D_L} = \left(\frac{m_L}{m_H}\right)^{0.5} \tag{3-3}$$

where m_L and m_H refer to the molecular weights of the diffusing species.

Although the kinetic theory (eq. 3-3) was commonly used for estimating the magnitude of isotope fractionation during diffusion in the aqueous phase, it has been long known that this theory is not suitable, especially in liquid water, when a hydrodynamic behavior becomes more important (Alder et al., 1974; Nuevo et al., 1995). Recent studies emphasized this incorrect assumption by showing experimentally that the kinetic square root relation (eq. 3-3) overestimates the magnitude of isotope fractionation during diffusion in liquid water. Several studies (Richter et al., 2006; Eggenkamp and Coleman, 2009; Tempest and Emerson, 2013) demonstrated that the exponent in equation 3 ranges between 0 and 0.2 for diffusing ions (Li^+, Na^+, K^+, Mg^{2+}, Cl^-, Br^-) and noble gases (Ar, Ne) and that a more general power law model with an exponent $\beta<0.5$ is more suitable to quantify isotope fractionation due to aqueous phase diffusion:

$$\frac{D_H}{D_L} = \left(\frac{m_L}{m_H}\right)^{\beta} \tag{3-4}$$

Molecular dynamic simulations (Bourg and Sposito, 2007; Bourg and Sposito, 2008; Bourg et al., 2010) confirmed the validity of the general power law model (eq. 3-4) for quantifying isotope fractionation during diffusion in liquid water. Bourg and Sposito (2007) revealed an inverse proportionality between beta values and the residence time of nearest water molecules surrounding dissolved ions (Li^+, Cl^-, Mg^{2+}). Moreover, by expanding molecular dynamic simulations to noble gases (Ar, Ne) and metal cations (Na^+, K^+, Cs^+, Ca^{2+}), Bourg and Sposito (2008) and Bourg et al. (2010) confirmed the generality of the inverse power law (eq. 3-4) for a wider range of solutes. Due to the wider spectra of assessed species, Bourg et al. (2010) demonstrated, that the value of β (eq. 3-4) also depends, in addition to the residence time of

nearest water molecules, on solute radius and valence state. Thus, diffusive transport process in the aqueous phase can be considered as an intermediate between a hydrodynamic and a kinetic behavior. Furthermore, Beekmann et al. (2009), Lavastre et al. (2005) and Bourg and Sposito (2008) showed, that a general inverse power law form (eq. 3-4) is also valid at the field scale for assessing diffusive isotope fractionation of chlorine ($^{37}Cl/^{35}Cl$) and noble gases ($^{40}Ar/^{36}Ar$, $^{22}Ne/^{20}Ne$) in diffusion dominated saturated low permeable clays.

In contrast to ions, chlorinated hydrocarbons are dissolved as uncharged molecules in water. A given chlorinated hydrocarbon exists as species with different weight, denoted as isotopologues, as the elements (C, Cl, H) constituting the molecule have several stable isotopes. Compared to ions, less information is available in the literature regarding isotopologue fractionation during diffusive transport of organic compounds in water. Some studies used deuterated vs. non-deuterated compounds to determine isotopologue fractionation in ambient liquid water at the laboratory scale, as they are easy to measure. However, the results are conflicting, since some studies obtained beta values close to the kinetic theory (e.g. 0.455 for toluene and ethylbenzene isotopologue pairs) (Jin et al., 2014), while other studies received lower beta values close to the values obtained for diffusing ions (e.g. 0.063 for isopropanol (IPA) and 0.023 for tertiary butyl alcohol (TBA)) (LaBolle et al., 2008). This raises the question of the representativeness of the approach for natural abundance studies. In contrast, a few studies evaluated isotopologue fractionation of organic compounds at natural abundance under controlled laboratory conditions by addressing one type of isotopologue: Zhang and Krooss (2001) and Schloemer and Krooss (2004) assessed carbon isotopologue fractionation of methane and ethane, while Jin et al. (2014) assessed chlorine isotopologue fractionation of cis-1,2-dichloroethene (cDCE) and trichloroethene (TCE). These studies received beta values close to those for diffusing ions and clearly lower than 0.5, postulated in the kinetic theory (methane and ethane: 0.021 – 0.055, cDCE: 0.088 and TCE: 0.043). Furthermore, studies addressing isotopologue fractionation in saturated systems at the field scale are limited to modelling studies assuming a kinetic beta value of 0.5 (LaBolle et al., 2008; Rolle et al., 2010; Van Breukelen and Rolle, 2012). Thus, a study relating laboratory measured beta with measured field values and addressing more than one type of isotopologue pair of a specific organic compound (e.g. C and Cl types) is lacking.

In this study, diffusion coefficient ratios were for the first time determined for isotopes with distinct mass differences (C and Cl) within the same molecule and related to isotopologue

ratio profiles at a field site, where transport is likely diffusion dominated. At the laboratory scale, diffusion coefficient ratios of carbon and chlorine isotopologue pairs of two common chlorinated organic groundwater contaminants, 1,2-dichloroethane (1,2-DCA) and TCE, were determined using a modified Stokes diffusion cell. At the field scale, a water-saturated clay core was retrieved from the bottom of a contaminated site and subsampled as a function of depth to evaluate possible shifts of TCE carbon and chlorine isotopologue ratios during downward diffusion into the clay. To compare field and laboratory data, field isotopologue ratio profiles were simulated using a 1D-diffusion model based on the laboratory determined diffusion coefficient ratios. The new insight into isotopologue fractionation of chlorinated hydrocarbons during diffusion in the aqueous phase provides a basis for identifying reactive processes in diffusion dominated low permeability sediments using CSIA.

3.2. Experimental design of modified Stokes' diffusion cell

We used a modified Stokes' diffusion cell to quantify isotopologue fractionation during aqueous phase diffusion. Stokes' diffusion cell design (Stokes, 1950) is a well-accepted and commonly used method to determine diffusion coefficients of dissolved species in aqueous solutions (Asfour, 1983; Asfour and Dullien, 1983; Cussler, 2009; Lo, 1974; Mills et al., 1968; Vangeet and Adamson, 1964; Wedlake and Dullien, 1974). The concept relies on a horizontal separation of two, well-stirred compartments by a frit with small pore sizes (diameter: 5-7 μm). The lower compartment contains a dissolved species while the upper compartment is filled with pure water. Because of the concentration gradient between the two compartments and the small pore size of the frit, the dissolved species in the lower compartment are exclusively transported by diffusion through the frit into the upper compartment. Diffusion coefficients are determined using the concentration difference between the two compartments, diffusion time and the previously determined diffusion cell constant. The latter is derived from species with known diffusion coefficients and is a correction factor for tortuosity and porosity effects affecting the diffusing species in the frit (Asfour, 1983; Asfour and Dullien, 1983; Cussler, 2009; Lo, 1974; Mills et al., 1968; Vangeet and Adamson, 1964; Wedlake and Dullien, 1974).

For the present study, the classical Stokes' diffusion cell design was modified to determine diffusion coefficient ratios for carbon and chlorine isotopologue pairs differing in one

heavy isotope in ambient liquid water at constant temperature (22°C). The intention of the modification was to maintain a maximal concentration gradient between the two compartments over time, by keeping the concentration in the upper compartment close to zero. This provides the advantage, that a constant rate of isotopologue accumulation was achieved in the lower compartment, which corresponds to a typical Rayleigh type behavior. The prevention of an equilibration between the source and the sink compartment is also an improvement in comparison to earlier diffusion experiments (Richter et al., 2006). In the earlier experiments, diffusion occurs from a small source container into a large sink container (V_{sink}/V_{source} ~ 300), during which equilibration occurred at the latest stage of the experiment between the source and the sink container. The modification was implemented by continuously renewing the water in upper compartment. For this purpose, deionized water was passed at a rate of 10ml/min through the upper compartment, by connecting it to a clean water reservoir placed higher than the diffusion cell (see Fig. 3-1 for details).

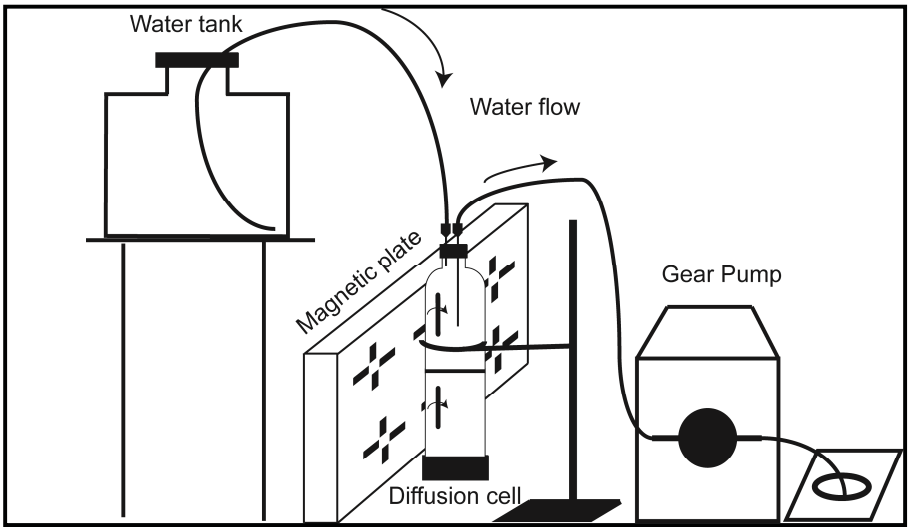

Figure 3-1. Set up of modified Stokes' diffusion cell experiment.

The lower compartment was filled with an aqueous solution, containing either TCE or 1,2-DCA. The solutions of the two compartments of the modified diffusion cell were stirred with the help of a magnetic plate set vertically on the side of the cell, to stir the magnetic bars inside the two compartments (Fig. 3-1). This prevented the formation of boundary layers above and below the

porous frit and ensured a homogenous concentration in the two compartments of the modified diffusion cell. To produce more data, two diffusion cells (named P2 and P3) were used simultaneously. The lower compartment of the diffusion cells used had volumes of 41.0 mL (P3) and 40.9 mL (P2), respectively and the upper compartments volumes of 34.0 mL (P3) and 35.0 ml (P2), respectively. The porous frit of both cells has the same pore size (1.0 – 1.6 μm diameter; data from manufacturer) (Fig. 3-1). Experiments of different duration were performed and samples were taken at the beginning and the end of each experiment from the lower compartment.

The governing equation for diffusive transport within the modified diffusion cells can be expressed according to Fick's law of diffusion:

$$V_{lower}\frac{dC_{lower}}{dt} = -Aj \tag{3-5}$$

where V_{lower} (L) is the volume of the lower compartment, dC_{lower}/dt (mg/L/s) corresponds to the temporal change in concentration, A is the area of the frit (m^2) and j (mg/m^2s) is the diffusive flux.

Within the frit a linear concentration gradient was assumed (quasi-steady-state), which has been proven as a reasonable assumption (Mills et al., 1968; Wedlake and Dullien, 1974). Thus, the diffusive flux across the porous frit is defined as follows according to the given geometric conditions of the diffusion cells:

$$j = \frac{D_e\left(C_{lower} - C_{upper}\right)}{L} \tag{3-6}$$

with

$$D_e = D_0 \Phi \tau \tag{3-7}$$

where D_0 (m^2/s) is the diffusion coefficient in free solution, Φ (-) is the porosity, τ (-) is the tortuosity factor, D_e (m^2/s) is the effective diffusion coefficient and C_{lower} (mg/L) and C_{upper} (mg/L) are the concentrations in the lower and upper compartment, respectively.

The tortuosity factor in equation 3-7 includes the lowering of the diffusive transport rate due to the curved diffusion paths in the porous media in comparison to the straight paths in free solutions. Commonly tortuosity factors are expressed as the squared ratio between the length of the diffusion path in porous media and the diffusion path in free solution (Bear, 1972; Steefel and Maher, 2009):

$$\tau = \left(\frac{L}{L_E} \right)^2 \tag{3-8}$$

where, L (m) is the diffusion path length in a free solution and L_E (m) is the diffusion path length in porous media.

Due to the continuous renewal of the water, the concentration in the upper compartment of the diffusion cell is close to zero. Inserting equation 3-6 and 3-7 with $C_{upper} = 0$ in equation 3-5 leads to:

$$V_{lower} \frac{dC_{lower}}{dt} = -\frac{D_0 \Phi \tau A C_{lower}}{L} \tag{3-9}$$

Rearranging and integrating formula 3-9 under the given boundary conditions, leads to the concentration evolution as function of time in the lower compartment:

$$C_t = C_0 e^{-\frac{D_0 \Phi \tau A t}{L V_{lower}}} \tag{3-10}$$

where C_0 (mg/L) is the initial concentration in the lower compartment at time zero and C_t (mg/L) is the final concentration in the lower compartment at time t.

Equation 3-10 can also be expressed for the temporal concentration evolution of one individual isotopologue, since the diffusion transport process in the diffusion cells acts on isotopologues. By formulating equation 3-10 for two isotopologues and dividing these equations by each other, the temporal evolution of the ratio of two isotopologues in the lower compartment of the diffusion cell can be expressed as follows:

$$\frac{C_{H,t}}{C_{L,t}} = \frac{C_{H,0}}{C_{L,0}} \frac{e^{-\frac{D_{0,H}\Phi\tau At}{LV_{lower}}}}{e^{-\frac{D_{0,L}\Phi\tau At}{LV_{lower}}}} = \frac{C_{H,0}}{C_{L,0}} e^{\frac{-\Phi\tau At\left(D_{0,H}-D_{0,L}\right)}{LV_{lower}}} \tag{3-11}$$

where $C_{H,0}$ (mg/L) is the initial concentration of the heavy isotopologue, $C_{L,0}$ (mg/L) is the initial concentration of the light isotopologue, $C_{H,t}$ (mg/L) is the concentration of the heavy isotopologue at time t, $C_{L,t}$ (mg/L) is the concentration of the light isotopologue at time t, $D_{0,H}$ (m^2/s) refers to the diffusion coefficient of the heavy isotopologue in free solution and $D_{0,L}$ (m^2/s) refers to the diffusion coefficient of the light isotopologue in free solution.

Expanding the right term of equation 3-11 by power to $D_{0,L}/D_{0,L}$ and expressing the isotopologue ratios at time t and time zero by R_t and R_0, respectively leads to the following equation:

$$R_t = R_0 e^{\left[\frac{-\Phi\tau At\left(D_{0,H}-D_{0,L}\right)}{LV_{lower}}\right]^{\frac{D_{0,L}}{D_{0,L}}}} = R_0 e^{\left(\frac{-\Phi\tau AtD_{0,L}}{LV_{lower}}\right)\left(\frac{D_{0,H}}{D_{0,L}}-1\right)} \tag{3-12}$$

Equation 3-12 corresponds to a typical Rayleigh type equation of the form $R_t = R_0 f^{(\alpha-1)}$, where the term $e^{\left(\frac{-\Phi\tau AtD_{0,L}}{LV_{lower}}\right)}$ equals the remaining fraction f of the species in the lower compartment and $D_{0,H}/D_{0,L}$ corresponds to the fractionation factor α. Therefore, equation 3-12 demonstrates that the fractionation between two isotopologues in the lower compartment of the diffusion cell follows a typical Rayleigh type behavior with a constant fractionation factor α and that the magnitude of fractionation depends only on the ratio between the diffusion coefficients in free solution of the two isotopologues. For convenience, equation 3-12 was multiplied by a factor of 1000 and the natural logarithm was taken, which results in the following equation:

$$\left[ln\left(R_t/R_0\right)\right]\times 1000 = \left(\frac{D_{0,H}}{D_{0,L}}-1\right)\times 1000\, ln\ f \tag{3-13}$$

Hence, by plotting $[\ln(R_t/R_0)]$x1000 vs. ln f, the ratio of the diffusion coefficients in free solution for heavy and light isotopologues can be obtained using linear regression. The usage of

isotopologue ratios in equation 3-13 instead of isotope ratios provides the advantage that the determined ratio of $D_{0,H}/D_{0,L}$ in equation 3-13 can be used to evaluate the β values (eq. 3-4) for the corresponding isotopologue pairs. To obtain the uncertainty of diffusion coefficient ratios ($D_{0,H}/D_{0,L}$) using the slope of the linear regression in the plotting space $\ln(R_t/R_0)]x1000$ vs. ln f (eq. 3-13), the 95% confidence interval of the slope of the regression line was calculated according to the following equation:

$$m = \pm t_{0.025,n-2} \times S_m \tag{3-14}$$

where m is the slope of the regression line, $t_{0.025,n-2}$ is the t-distribution for the 95% confidence interval, n is the degree of freedoms and S_m is the standard deviation of the regression line. The uncertainty of beta values was calculated according to Gauss' error propagation law including the uncertainty of the determined diffusion coefficient ratios.

3.3. Site description

For comparing laboratory with field results, samples were taken from a saturated clay unit, which underlies a chemical waste landfill. The clay consists mainly of Smectite, Illite and Kaolinite and has sandy layers showing a higher permeability than the clay. During the deposition period (~45 years), hazardous waste including organic contaminants was placed on top of the clay and remained in place until remediation of the site. During the period of waste storage, diffusion was expected to be the predominant process for transporting organic contaminants away from the waste landfill into the underlying clay. In April 2013, a clay core of 45cm length was retrieved from the saturated bottom of the waste landfill and subsampled as a function of depth to analyze concentrations and isotopic evolution with increasing distance from the source for the landfill age of about 45 years.

3.4. Sampling, analytical methods and data evaluation

3.4.1. VOC extraction from clay core

Volatile organic compounds (VOCs) were extracted from the clay core following the procedure described by Parker (1996): The retrieved clay core (diameter = 20 cm) was split longitudinally in two pieces of the same size. After splitting, the core was logged (photographs and description) for geological features. Logging was performed as fast as possible (~5 min) to prevent any loss of VOCs. Afterwards subsampling was carried out with a spacing of 5 cm to gain a satisfactory resolution of the concentration and isotopic data of the VOCs as a function of depth. Subsamples of about 3 cm length were taken from the clay core using a mini corer (inner diameter 16 mm, length 110 mm) and a plunger (diameter 15 mm, length of 125mm), both made of stainless steel. To prevent any loss of VOC during subsampling, the clay core was covered by aluminum foil except at the place, where subsampling took place. The subsamples were extruded by the plungers into 42 mL glass vials containing 20 mL high purity (>99.7%) methanol (MeOH). A high clay to MeOH ratio (typically 0.8) was chosen to maximize the amount of VOCs in the MeOH extracts. Subsequently the vials were sealed with a screw cap with a Teflon lined septum. The vials were weighed before and after the collection of the clay samples to determine the weight of the solid samples.

In the laboratory, the 42 mL vials were sonicated for 30 minutes followed by shaking for one hour in order to disperse the clay samples and to dissolve all VOC completely in the MeOH. Afterwards, the vials were centrifuged for 30 minutes at 1200 rpm to obtain a clear MeOH supernatant. The clear MeOH supernatant was then decanted in 4 mL vials, which were sealed with a screw cap with Teflon lined septum for storage prior to analysis.

3.4.2. VOC concentration analysis

VOC concentrations in water samples were analyzed using a Trace^{TM} GC-DSQII mass spectrometer (Thermo Fisher Scientific, Waltham, MA, US) operated in selected ion mode with a detection limit of 2.0 µg/L. Calibration curves for cDCE, TCE, Tetrachloroethene (PCE), 1,1,2,2-Tetrachloroethane (TCA) and 1,2-DCA were produced using external standards (purity ≥ 95.0%), which were prepared at seven different concentration levels: 5, 10, 25, 50, 75, 100, 150 µg/L.

Headspace samples from 20mL vials filled with 10ml sample were injected using a CombiPal auto sampler (CTC Analytics, Zwingen, Switzerland). Based on an initial screening of VOC concentrations, the samples were diluted to approximately identical concentrations (50µg/L) to fit the calibration interval and to maximize precision of the analysis. For samples containing cDCE, TCE, PCE and 1,1,2,2-TCA, the GC oven temperature was held at 40°C for 2 minutes, ramped at 15°C/min to 130°C and held for 2 minutes. For samples with 1,2-DCA, the oven temperature was held at 40°C for 2 minutes, ramped at 15°C/min to 90°C and held for 2 minutes. The carrier gas was helium with a flow rate of 1,2 ml/min. The analytical uncertainty (1σ) of the concentration measurements was determined by a repeated measurement of standards included in the sample sequence (standards/samples = 1/5) and corresponded to ±5% (n=10) for cDCE, TCE, PCE and 1,1,2,2-TCA and of ±4%, (n=5) for 1,2-DCA.

For analyzing VOC concentrations in the clay samples, aliquots of the MeOH extracts were diluted at least 10 times with pure water and analyzed analogously to water samples. The dilution was made because the polar MeOH is incompatible with the non-polar column of the gas chromatograph. The total soil concentrations were calculated according the following formula:

$$C_s = \frac{V_m C_m}{m_{ws}} \tag{3-15}$$

where, C_s (mg/kg) is the VOC concentration in the wet clay, V_m (L) is the total volume of methanol, C_m (mg/L) is the VOC concentration in the methanol and m_{WS} (kg) is the total mass of the wet clay. The detection limit for VOCs concentrations in the wet clay is approximately 0.05 mg/kg for typical clay to MeOH ratio of 0.8.

3.4.3. Carbon Isotopes

Compound-specific carbon isotope measurements of TCE and 1,2-DCA were performed using a purge-and-trap concentrator (Tekmar Velocity XPT, USA) coupled to a TRACE^{TM} gas chromatograph (GC) and a DeltaPlus XP isotope mass spectrometer (IRMS) via a combustion III interface (Thermo Finnigan, Germany). Water samples were diluted to identical concentrations of 30µg/L in 42 mL glass vials with PTFE-lined screw cap to maximize precision of the measurements. The MeOH extracts from the field samples were also diluted to identical

concentrations of 30µg/L but the dilution had to be at least 100 times due to the incompatibility of the MeOH with the purge-and-trap concentrator and the column of the GC. Prior analysis, pre-concentration of samples was performed with the purge-and-trap system by purging 25 ml for ten minutes with N_2 (40 mL/min) and trapping the VOCs on a Vocarb 3000 trap. After desorption, the compounds were transferred to a cryogenic trap (Tekmar Dohrmann) in the GC oven set to -80°C. The trap was heated to 180°C to release the compounds to the GC column (DB-VRX, 60m, 0.25mm, 1,2 µm) for chromatographic separation. The GC oven temperature for TCE analysis was held at 50°C for 2 minutes, then ramped at 5°C/min to 135°C and held for 2 minutes. For 1,2-DCA the temperature was held at 60°C and then ramped at 5°C/min to 135°C and held for 2 minutes. The carrier gas was helium with a constant flow of 1.2 ml/min. Carbon isotope signatures of TCE and 1,2-DCA were analyzed relative to a standard and expressed in the delta notation (VPDB $\delta = (R/R_{std} - 1)*1000$ (‰), where R and R_{std} are the isotope ratios of the sample and the standard, respectively. The analytical uncertainty for experimental water samples (standard deviation of the mean: $SDM = 1\sigma/(n)^{1/2}$, σ: standard deviation, n: sample number) of each TCE and 1,2-DCA measurements was determined based on triplicate measurements. In contrast, field samples were analyzed twice due to the limited samples volume. Thus, the standard deviation of the mean (±SDM) of the field samples was determined based on the standard deviation (1σ) of standards included in the samples sequence (σ=0.30‰, n=15).

3.4.4. Chlorine Isotopes

Compound-specific chlorine isotope measurement of TCE and 1,2 DCA was performed using a gas chromatograph coupled to a quadrapole mass spectrometer (GC-qMS; Agilent 7890A, Agilent 5975C). Samples were injected by a headspeace method from 20 mL vials filled with 15 mL solution using a CompiPal Autosampler (CTC Analytics, Zwingen, Switzerland). For chromatographic separation a DB-5 column (30m, 0.25mm, 0.25µm, Agilent) with a constant helium flow of 1,2 mL/min was used. Water samples and MeOH extracts were diluted to identical concentrations of 30µg/L to maximize precision of the measurements. For the MeOH extracts from the field, the dilution had to be at least 10 times due to the incompatibility of the MeOH with the column of the GC. The analytical uncertainty (±SDM) of each TCE and 1,2-

DCA measurements was based on a tenfold measurement of each sample from two different vials (5 replicates from each vial).

The TCE samples and standards were diluted to identical concentrations of 100µg/L to obtain identical peak areas and thus to maximize precision of the measurements. The temperature program of the GC for TCE was started at 35°C for 2 minutes and then ramped at 10°C/min to 50°C and held for 0.2 minutes. All four chlorine isotopologues intensities of TCE (mass 130, 132, 134, 136) were quantified using the GC-qMS. Thus, raw chlorine isotopic ratios were calculated with the method developed by Sakaguchi-Soder et al. (2007) and further improved by Aeppli et al. (2010), which takes all chlorine isotopologue of TCE (130, 132, 134 and 136) into account. The raw chlorine isotopic ratios of TCE were then calculated using the following equation:

$$R_{TCE} = \frac{I_{132} + 2I_{134} + 3I_{136}}{3I_{130} + 2I_{132} + I_{134}} \tag{3-16}$$

where I is the corresponding molecular ion abundance at different m/z values.

A calibration of raw isotope ratio (eq. 3-16) was performed with two external TCE standards having different chlorine isotope ratios (EIL1 = 3.05‰ and EIL2 = -2.70‰). The standards were previously determined by an IRMS after conversion to methyl chloride using the Holt method (Holt et al., 1997) at the University of Waterloo. Calibration with external standards was performed to receive delta values on the SMOC scale. A recent inter laboratory comparison for different GC-qMS equipment, demonstrated that a lack of calibration of raw GC-qMS chlorine isotope ratios potentially leads to variation of the difference in isotope ratios between two samples by as much as a factor of 1.3 (Bernstein et al., 2011).

The 1,2-DCA samples and standards were also diluted to identical concentrations of 2000µg/L to obtain identical peak areas and thus to maximize precision of the analysis. The temperature program of the GC for 1,2-DCA was held at 40°C for 1.8 minutes and then ramped at 25°C/min to 120°C and held for 0.2 minutes. Chlorine isotopic raw ratios of 1,2-DCA were determined from the two most abundant fragment ion peaks (m/z 64 and 62) in combination with the general equation for the chlorine isotopic ratios for symmetric molecules developed by Elsner and Hunkeler (2008). For 1,2-DCA this equation corresponds to:

$$R_{1,2-DCA} = \frac{I_{64}}{I_{62}} \quad (3\text{-}17)$$

where I is the corresponding fragment ion abundance of 1,2-DCA at different m/z values.

As for TCE, received raw chlorine isotope ratios from 1,2-DCA fragments (eq. 3-17) were calibrated against two external standards having different chlorine isotopic ratios (CHYN1 = 6.30‰ and CHYN2 = -0.84‰) to obtain delta values on the SMOC scale.. The standards were characterized by the Holt method (Holt et al., 1997) at the Helmholtz Centre in Munich.

3.4.5. Isotope and isotopologue data evaluation

Since fractionation of isotopically distinct species of chlorinated hydrocarbons occurs between isotopologues and not between isotopes, isotope effects associated with diffusion are characterized by considering isotopologue rather than isotope ratios as justified in more detail for carbon and chlorine in the following paragraph.

3.4.5.1. Carbon isotopes vs. carbon isotopologues

As demonstrated in the Supplementary Information at the end of this chapter (section 3.10.), carbon isotope ratios ($^{13}C/^{12}C$), measured in the delta notation, fractionate proportionally to carbon isotopologue pairs differing in one heavy carbon isotope ($^{13}C/^{12}C \propto C_{HL}/C_{LL}$ and C_{HH}/C_{HL}). This proportionality implies no information loss when considering only one of the two proportional isotopologue pairs. Due to the low abundance of the heavy carbon isotope (^{13}C 1.07% vs. ^{12}C 98.93%), in the present study only the most abundant TCE and 1,2-DCA carbon isotopologue pairs containing one and zero heavy carbon isotope, respectively ($^{131}TCE/^{130}TCE$ and ^{101}1,2DCA/^{100}1,2DCA) are considered, which is coherent with previous studies (Elsner and Hunkeler, 2008; Jin et al., 2013; Neumann et al., 2009).

3.4.5.2. Chlorine isotopes vs. chlorine isotopologues

In contrast to carbon, both chlorine isotopes are present at high abundance (^{37}Cl 24.22% vs. ^{35}Cl 75.78%) therefore, also several chlorine isotopologues are present at high abundance. As shown theoretically and experimentally by previous studies (Elsner and Hunkeler, 2008;

Jeannottat and Hunkeler, 2012), TCE chlorine isotope ratios ($^{37}Cl/^{35}Cl$) behave proportional to TCE isotopologue pairs differing in one heavy chlorine isotope analogously to carbon. The possibility of tracking TCE chlorine isotopologues directly (eq. 3-16) permits verification of this proportionality. This study confirmed that TCE chlorine isotope ratios ($^{37}Cl/^{35}Cl$) are proportional to TCE chlorine isotopologue pairs differing in one heavy chlorine isotope ($^{132}TCE/^{130}TCE$ and $^{134}TCE/^{132}TCE$) (Fig. 3-2). For 1,2-DCA, chlorine isotope ratios are also expected to fractionate proportionally to isotopologue pairs differing in one heavy chlorine isotope ($^{37}Cl/^{35}Cl \propto {}^{102}1,2DCA/^{100}1,2DCA$ and $^{100}1,2DCA/^{98}1,2DCA$) as demonstrated in the Supplementary Information at the end of this chapter (section 3.10.) for 1,2-DCA and more generally for symmetric molecules by Elsner and Hunkeler (2008). The proportionality among TCE and 1,2-DCA chlorine isotopologue pairs differing in one heavy chlorine isotope also results in equal beta values (eqs. 3-13 and 3-4), since the change of mass ratios between isotopologue pairs differing by one heavy chlorine isotope affects the beta value only within the uncertainty. Therefore, the present study considers only the most abundant TCE and 1,2-DCA chlorine isotopologue pairs differing by one heavy chlorine isotope ($^{132}TCE/^{130}TCE$ and for 1,2-DCA $^{102}1,2DCA/^{100}1,2DCA$).

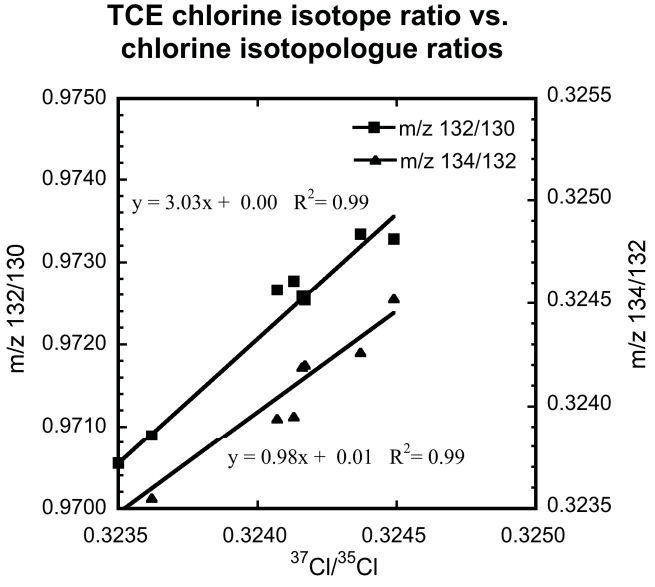

Figure 3-2. Relation between TCE chlorine isotope ratios ($^{37}Cl/^{35}Cl$) and TCE chlorine isotopologue pairs differing in one heavy chlorine isotope ($^{132}TCE/^{130}TCE$ and $^{134}TCE/^{132}TCE$). The chlorine isotopologue pairs differing by one heavy chlorine isotope correlate ($R^2 = 0.99$) with the chlorine isotope ratios with a slope of three and one, respectively and intercept the origin.

3.5. Results

3.5.1. Diffusion cell experiment

Initial concentrations of TCE and 1,2-DCA in the lower compartment of the diffusion cell ranged between 22.6 and 901 mg/L (Tab. 3-1), while final concentrations after performance of different time series of the diffusion cell experiments were between 8.2 and 199 mg/L (Tab. 3-1). Initial and final concentrations of each time series of the experiment were used to determine diffusive transport rates acting on TCE and 1,2-DCA in both diffusion cells by calculating effective diffusion coefficients (eqs. 3-7 and 3-10). Effective diffusion coefficients for TCE and 1,2-DCA in both diffusion cells ranged from 1.28×10^{-10} to 2.20×10^{-10} m^2/s (TCE; Tab. 3-1) and from 1.75×10^{-10} to 8.96×10^{-11} m^2/s (1,2-DCA; Tab. 3-1), respectively. The effective diffusion coefficients are lower than published diffusion coefficients in free aqueous solutions of TCE (1.01×10^{-9} m^2/s) (Pankow and Cherry, 1996) and 1,2 DCA (9.70×10^{-10} m^2/s) (Gordon, 1999) due to tortuosity and porosity effects affecting the diffusing species in the frit. The average tortuosity and porosity effects in the two used diffusion cells were quantified by dividing the determined effective diffusion coefficient by published diffusion coefficients in free solution (eq. 3-7). Different D_e/D_0 ratios were obtained for the two cells with values of 0.19±0.02 (1σ=±0.03, n=3) for P2 and 0.13±0.02 (1σ=±0.03, n=5) for P3 (Tab. 3-1). Both ratios lie within the range of values obtained in previous studies using the classical Stokes diffusion cell (e.g. 0.10 – 0.49 in Mills et al. (1968)).

Table 3-1. Effective diffusion coefficients and D_e/D_0 ratios of diffusion cells P2 and P3. Uncertainty of D_e/D_0 (±SDM) was determined by a triplicate measurement of cell P2 and a quintuple measurement of cell P3.

Compound	Initial (mg/L)	Final (mg/L)	Fraction	Time (d)	Effective diffusion coefficient D_e (m^2/s)	D_e/D_0	Diffusion cell	D_e/D_0 Average
TCE	22.6	8.2	0.364	0.9	2.20E-10	0.22	P2	
1,2-DCA	96.3	33.2	0.345	11.9	1.75E-10	0.18	P2	
1,2-DCA	211	20.4	0.097	26.9	1.69E-10	0.17	P2	0.19±0.02[a]
TCE	84.0	63.1	0.751	4.3	1.28E-10	0.13	P3	
TCE	608	28.8	0.047	42.1	1.41E-10	0.14	P3	
TCE	608	114	0.188	18.2	1.79E-10	0.18	P3	
1,2-DCA	88.4	69.1	0.782	4.0	1.19E-10	0.12	P3	
1,2-DCA	901	199	0.221	32.8	8.96E-11	0.09	P3	0.13±0.02[b]

[a]Average for cell P2
[b]Average for cell P3

With increasing experimental duration, an accumulation of heavy carbon and chlorine isotopologues of TCE and 1,2-DCA in the lower compartment of the diffusion cells was observed (Figs. 3-3 and 3-4). Thus, the light carbon and chlorine isotopologues diffused faster than heavy isotopologues through the frit into the upper compartment. The accumulation was stronger for heavy chlorine isotopologues in comparison to heavy carbon isotopologues of TCE and 1,2-DCA. The accumulation of both isotopologue types (carbon and chlorine) followed a Rayleigh trend (Figs. 3-3 and 3-4), which is expected given that the Stokes' diffusion cell was modified to a Rayleigh type experiment. The magnitude of isotopologue fractionation was quantified from the slope of the regression line using the Rayleigh equation (eq. 3-13). The diffusion coefficient ratios for TCE isotopologue pairs differing in one heavy isotope gave values of D_{132}/D_{130}=0.99963±0.00003 for chlorine D_{131}/D_{130}=0.99978±0.00006 for carbon (Tab. 3-1).

For 1,2-DCA, the isotopologue fractionation was stronger for chlorine (D_{102}/D_{100}=0.99939±0.00003) than for carbon (D_{101}/D_{100}=0.99977±0.00006) similarly as for TCE. But when comparing the two compounds, a stronger chlorine isotopologue fractionation was observed for 1,2 DCA relative to TCE, while similar carbon isotopologue fractionation occurred for both compounds (Tab. 3-2).

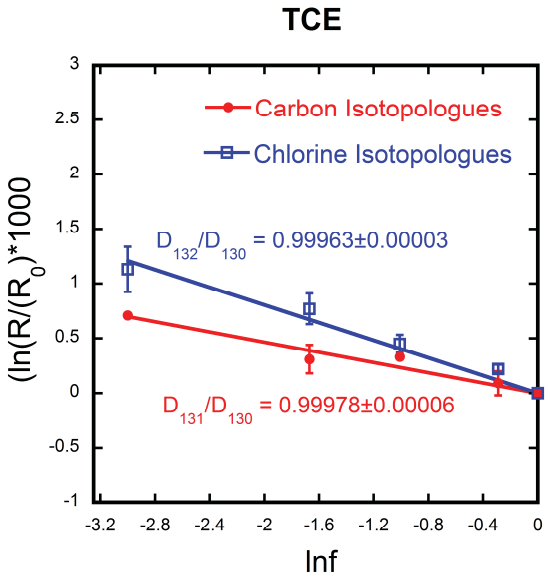

Figure 3-3. Rayleigh plot for TCE carbon (red) and chlorine (blue) isotopologue fractionation in the lower compartment of the diffusion cell. Error bars indicate analytical uncertainty (±SDM) of measurements. Uncertainty of diffusion coefficient ratios of TCE carbon and chlorine isotopologue pairs was calculated based on the 95% confidence interval of the regression line.

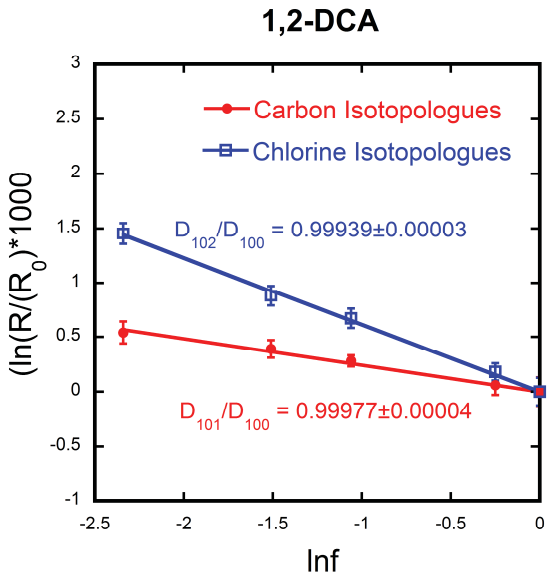

Figure 3-4. Rayleigh plot for 1,2-DCA carbon (red) and chlorine (blue) isotopologue fractionation in the lower compartment of the diffusion cell. Error bars indicate analytical uncertainty (±SDM) of measurements. Uncertainty of diffusion coefficient ratios of 1,2-DCA carbon and chlorine isotopologue pairs was calculated based on the 95% confidence interval of the regression line.

Table 3-2. Diffusion coefficient ratios and beta values of carbon and chlorine isotopologues of TCE and 1,2-DCA. Uncertainty of diffusion coefficient ratio was calculated based on the 95% confidence interval of regression line (eqs. 3-13 and 3-14). Uncertainty of beta values was calculated according to Gauss' error propagation law by including the uncertainty of the diffusion coefficient ratios.

Compound	**Isotopologue type**	**D_i/D_j**	**β in eq. 3-4**
TCE	Carbon	D_{131}/D_{130} = 0.99978±0.00006	0.029±0.008
	Chlorine	D_{132}/D_{130} = 0.99963±0.00003	0.024±0.002
	Carbon	D_{101}/D_{100} = 0.99977±0.00004	0.023±0.004
1,2-DCA	Chlorine	D_{102}/D_{100} = 0.99939±0.00003	0.031±0.002

3.5.2. Diffusion profiles in retrieved core

Four different organic contaminants were found in the clay core from the chemical waste landfill: cDCE, TCE, PCE and 1,1,2,2-TCA (Figs. 3-5A-D). All four contaminants showed the highest concentration at the top of the clay core reaching values of 2.27 mg/kg (cDCE), 5.69 mg/kg (TCE), 0.11 mg/kg (PCE) and of 0.12 mg/kg (1,1,2,2,-TCA), while with increasing depth

the concentrations gradually decreased (Figs. 3-5A-D). Only concentrations of TCE were high enough to measure isotopologue ratios. Chlorine and carbon isotopologue ratios of TCE displayed a small but significant shift towards smaller values with increasing depth within the clay core (Figs. 3-6A and B). Carbon isotopologue ratios of TCE (^{131}TCE/^{130}TCE) showed a value of 0.010903 ($\delta^{13}C_{VPDB}$ = -29.72‰) at the top of the clay core before the ratio decreased to 0.010898 ($\delta^{13}C_{VPDB}$= -30.18‰) at 40 cm depth ($\Delta\delta^{13}C_{VPDB}$ = 0.46‰) (Fig. 3-6A). The same pattern was observed for the TCE chlorine isotopologue ratios differing in one heavy isotope (^{132}TCE/^{130}TCE): The ratio showed values of 0.97374 ($\delta^{37}Cl_{SMOC}$ = 1.79‰) at the top of the clay core decreasing to 0.97324 ($\delta^{37}Cl_{SMOC}$ = 1.28‰) at 40cm depth ($\Delta\delta^{37}Cl_{SMOC}$ = 0.51‰) (Fig. 3-6B).

3.6. Discussion

3.6.1. Diffusion cell experiment

The observed stronger accumulation of heavy chlorine isotopologues in comparison to heavy carbon isotopologues of TCE and 1,2-DCA is consistent with the mass differences between the stable isotopes of carbon and chlorine. Chlorine isotopologue pairs differ by two mass units in molecular weight, while carbon isotopologue differ only by one. Consequently the fractionation is larger for chlorine than carbon isotopologues. Furthermore, the larger chlorine isotopologue fractionation for 1,2-DCA compared to TCE (Tab. 3-2) is most likely due to the larger relative mass difference caused by an additional heavy chlorine isotope for 1,2-DCA (2.0%) compared to TCE (1.5%). However, a larger fractionation is not observable for the carbon isotopologues pairs of 1,2-DCA in comparison to TCE. Most likely for carbon, the difference is hidden in the uncertainty, given the relatively small mass difference of an additional heavy carbon isotope in comparison to the whole organic molecule (TCE: 0.8% vs. 1,2-DCA: 1%). To evaluate whether chlorine and carbon isotopologue fractionation of TCE and 1,2-DCA shows a similar mass dependence, beta values were calculated (eq. 3-4, Tab. 3-2). The beta value for the chlorine (0.024±0.002) and carbon (0.029±0.008) isotopologue pairs of TCE agree within the range of uncertainty. The equal beta values indicate that the diffusion coefficient ratios for carbon and chlorine isotopologues of TCE follow the same proportionality on a logarithmic scale with respect to their mass ratios.

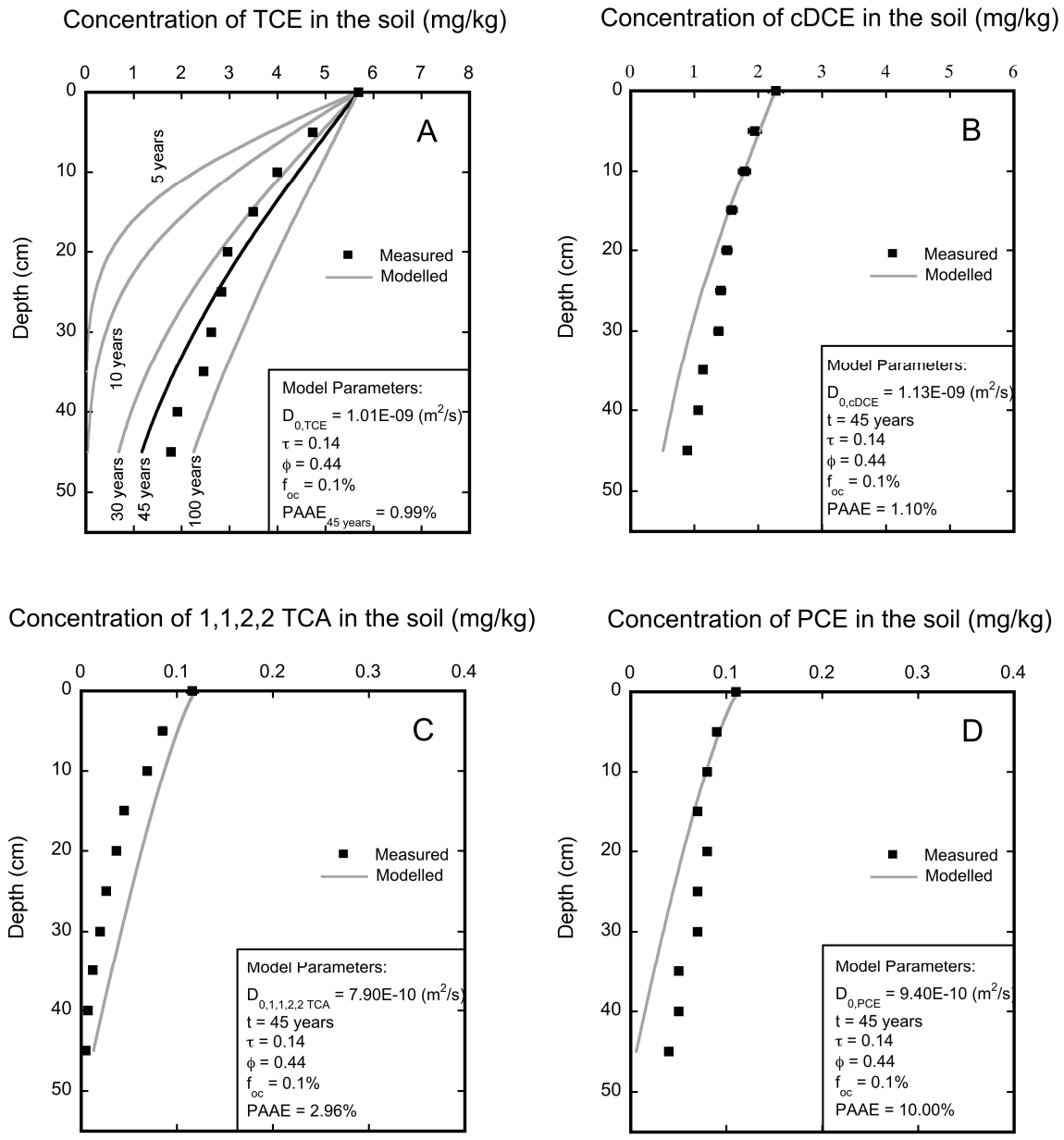

Figure 3-5. Concentration profiles of TCE (A), cDCE (B), 1,1,2,2-TCA (C) and PCE (D) in the retrieved clay core beneath the chemical waste landfill. Error bars indicate analytical uncertainty of (±1σ). Where no error bars are visible the analyitical uncertainty was smaller than the size of the symbols. Grey lines indicate simulated concentration evolution in a 1D-diffusion model for a time period of 45 years and additionally in figure 3-5A for time periods of 5, 10, 30 and 100 years. A tortuosity factor of 0.14, a clay porosity of 0.44 and fraction of 0.1% of organic carbon in the clay were used as parameters in the 1D-diffusion model, whereby the tortuosity factor was used as the fitting parameter. A percent average absolute error (PAAE) of 0.99% for TCE (A), of 1.10% for cDCE (B), of 2.96% for 1,1,2,2 TCA (C) and of 10.00% (D) for PCE was determined for quantifying the goodness of the fit between measured and modelled data for the time period of 45 years.

For 1,2-DCA, the determined beta value for the carbon isotopologue pair (Tab. 3-2) agrees within the uncertainty with the value obtained for the TCE carbon isotopologue pair. In contrast, the determined beta value for the 1,2-DCA chlorine isotopologue pair (0.031±0.002) is slightly higher than the value for the carbon isotopologue pair (0.023±0.004). This indicates that the magnitude of carbon and chlorine isotopologue fractionation of 1,2-DCA is not equally proportional on a logarithmic scale in relation to the different mass ratios of the isotopologue pairs. This behavior is not yet fully understood and thus the fractionation of 1,2-DCA chlorine and carbon isotopologues is most likely influenced by other properties in addition to the mass ratios.

Generally, the determined beta values for carbon and chlorine isotopologue pairs of 1,2-DCA and TCE are more than one order of magnitude smaller than 0.5, indicating that the kinetic theory (eq. 3-3) overestimates the magnitude of isotopologue fractionation of 1,2-DCA and TCE during diffusion in the aqueous phase. For the chlorine isotopologues of TCE, Jin et al. (2014) also observed a more than one order of magnitude smaller beta value (0.043) than the value (0.5) postulated by the kinetic theory. Although the beta value obtained by Jin et al. (2014) falls in the same range as the value of the present study (0.024±0.002), the two results differ significantly possibly due to a different analytical approach. In our study, we maximized the accuracy and precision by using a two point calibration, equal concentrations for all samples and standards and 10 repeats for each chlorine sample (cf. section 3.4.). The determined beta values of the present study for carbon and chlorine isotopologue pairs of TCE and 1,2-DCA (Tab. 3-2) are consistent with recent experimentally determined range of beta values ($0 \leq \beta < 0.2$) for diffusing ions in ambient liquid water (Richter et al., 2006), in polyacrylamide gel (Eggenkamp and Coleman, 2009) and in silicate melts (Watkins et al., 2011). Furthermore, obtained beta values are in the same range as values quantified by molecular dynamic simulations for metal ions and noble gases (0.000 – 0.171) (Bourg et al., 2008; Bourg et al., 2010). Moreover, the determined beta values fall in the same range as observed for carbon isotopologues of methane (0.024 – 0.055) and ethane (0.021 – 0.046) (Schloemer and Krooss, 2004; Zhang and Krooss, 2001) and are close to the beta values for deuterated and non-deuterated isotopologues of TBA (0.063) and IPA (0.023) (LaBolle et al., 2008). This confirms the hypothesis, that the kinetic theory (eq. 3-3) overestimates not only the magnitude of isotope fractionation for ions diffusing in water but also for organic compounds. Furthermore, previous kinetic-theory based models of MTBE and TBA

transport in a thin high permeability layer bordered by two low permeability zones likely overestimate the magnitude of isotopologue fractionation due to aqueous phase diffusion (LaBolle et al., 2008).

Moreover, the coherence of the determined beta values with a wide range of other studies also suggests that the experimental determined beta values for perdeuterated and non-deuterated isotopologues of toluene and ethylbenzene (0.433) by Jin et al. (2014) are also not representative for molecules with isotope ratios at natural abundance.

3.6.2. Diffusion profiles in clay core

The concentration profiles of cDCE, TCE, PCE and 1,1,2,2-TCA in the clay core, were fitted using a 1D analytical solution of Fick's second law for a homogeneous, semi-finite porous medium (Crank, 1975; Cussler, 2009) assuming a constant concentration on the top of the clay:

$$C_s(z) = C_{s,0}\,erfc\left(\frac{z}{2\sqrt{\Phi\tau D_0 / R}}\right) \tag{3-18}$$

where $C_{s,0}$ (mg/kg) is the initial concentration at the top of the clay unit, z refers to the depth (m), C_s (z) (mg/kg) is the concentration at depth z, and R is the retardation factor, which includes the adsorbed mass of the organic contaminants on organic matter in the clay layer. The retardation factor was determined using the well-known relationship:

$$R = 1 + \left(\frac{\rho_b}{\Phi}\right)K_d \tag{3-19}$$

where ρ_b (g/cm^3) is the dry soil bulk density, Φ (-) is the soil porosity and K_d (ml/g) is the distribution coefficient. The value of K_d was calculated using the well-known relationship Kd = $K_{OC} \cdot f_{OC}$, where K_{OC} is the soil organic carbon-water partitioning coefficient and f_{OC} is the organic matter content in the clay. K_{OC} values of 126 ml/g for TCE, 364 ml/g for PCE, 86 ml/g for cDCE and 118 ml/g for 1,1,2,2-TCA were taken from Pankow and Cherry (1996). Clay porosity (0.44), clay dry bulk density (1.560 g/cm^3), organic matter content in the clay (0.1%), were taken from

previous consultant studies. For diffusion coefficients in free solution (D_0), published diffusion coefficients of 9.40E-10 m^2/s for PCE, 1.01E-9 m^2/s for TCE (Pankow and Cherry, 1996), 7.90E-10 m^2/s for cDCE and 7.90E-10 m^2/s for 1,1,2,2-TCA (GSI, 2013) were used.

The tortuosity factor (eq. 3-18) was used as the fitting parameter as it is common for such VOC diffusion profiles in clay units (Parker et al., 2004). The goodness of the fit between measured and modeled data was quantified using the percent average absolute error (PAAE). The best fit of the concentration profiles for the landfill age of 45 years was obtained with a tortuosity factor of 0.14 (Figs. 3-5A-D) with PAAE values ≤ 10% for all four VOCs. Determined low tortuosity factor is in a plausible range, since Schloemer and Krooss (2004) showed, that in low permeability sediments tortuosity factors are potentially up to three orders of magnitude lower than in free aqueous solutions.

The fact that all four VOC diffusion profiles within the clay core were satisfactorily reproduced with equation 3-18 for the age landfill age of 45 years (PAAE<10%) indicates, that diffusion is likely the predominant transport process and that advection and biodegradation plays a minor role within the clay core. Furthermore, the advective flow velocity was previously estimated to be less than one mm per year using Darcy's law (unpublished consultant study) confirming that diffusion is the predominant transport process in the clay layer. Therefore, the small shift of carbon and chlorine isotopologue ratios towards smaller values with increasing depth in the clay unit likely also originates from the diffusive transport. To explore this explanation in more detail, chlorine and carbon isotopologue ratios of TCE were simulated using the experimentally determined diffusion coefficient ratios for TCE carbon and chlorine isotopologue pairs differing in one heavy isotope and the same tortuosity factor (0.14) as for fitting the TCE concentration profile. For this purpose equation 3-18 was expressed for individual isotopologues of TCE and divided by each other:

$$R(z)=\left(\frac{C_H}{C_L}\right)_{Sample}=\frac{C_{H,0}\,erfc\left(\frac{z}{2\sqrt{\Phi\pi D_{0,H}/R}}\right)}{C_{L,0}\,erfc\left(\frac{z}{2\sqrt{\Phi\pi D_{0,L}/R}}\right)} \qquad (3\text{-}20)$$

where R(z) is the evolution of the isotopologue ratio as function of depth in the clay core, $(C_H/C_L)_{Sample}$ is the ratio between the heavy and the light isotopologue pair of the sample, $C_{H,0}$ and $C_{L,0}$ are the initial concentrations of the heavy and the light isotopologue at the top of the clay, z (m) is the depth, t (s) is the time, $D_{0,H}$ (m^2/s) and $D_{0,L}$ (m^2/s) are diffusion coefficients in free solution of the heavy and the light isotopologue of TCE, respectively taken from the diffusion cell experiment (D_{131}/D_{130}=0.99978 and D_{132}/D_{130}=0.99963, cf. section. 3.5.1.)

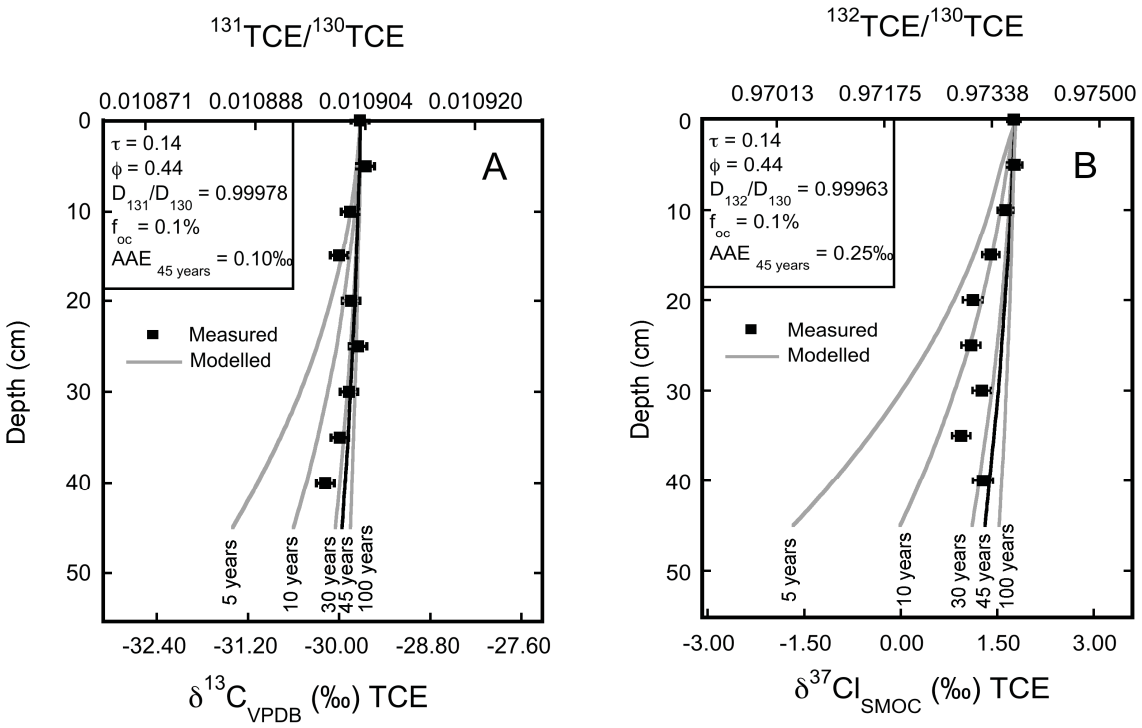

Figure 3-6. Profiles of TCE carbon (A) and chlorine (B) isotopologues ratios measured in the retrieved clay core beneath the chemical waste landfill. Grey lines indicate simulated isotopic evolution with a 1D-diffusion model for 5, 10, 30, 45 and 100 years. Error bars of TCE carbon and chlorine isotopologue ratio measurements indicate standard error of the mean (±SDM). The same tortuosity factor of 0.14 as for the concentration profile, a clay porosity of 0.44 and an organic carbon fraction of 0.1% in the clay was used in the 1D diffusion model. An absolute average error (AAE) of 0.25‰ for chlorine and of 0.10‰ for carbon isotopologue ratios was determined for quantifying the goodness of the fit between measured and modelled ratios for the time period of 45 years.

Simulated carbon and chlorine isotopologue profiles for the landfill age of 45 years, fitted well with measured carbon and chlorine isotopologue ratio profiles showing absolute average errors of 0.10‰ for carbon and of 0.25‰ for chlorine isotopologues, which are in the range of

the measurement uncertainty (Fig. 3-6A and B). This indicates that the magnitude of isotopologue fractionation observed in the clay unit of the field site is consistent with laboratory determined ratios of diffusion coefficients especially for the carbon isotopologue pairs of TCE (Figs. 3-6A and B). This also suggests that sorption likely has a relatively small influence on isotopologue fractionation, which is consistent with previous findings (Harrington et al., 1999; Slater et al., 2000). Furthermore, simulations for different diffusion periods in the clay unit (5, 10, 30, 45 and 100 years) show how TCE concentrations and carbon and chlorine isotopologue ratio profiles evolve over time in diffusion dominated systems. In the initial stage (5 years), when the concentration gradient is steep (Fig. 3-5A), a much larger isotopologue effect is observed than in later times (Figs. 3-6A and B). The difference between the ratios at the top of the clay core and the value at 45 cm depth is almost 0.00275 ($\Delta\delta^{37}Cl_{SMOC}$ = 2.83‰) for chlorine isotopologues and 0.000015 ($\Delta\delta^{13}C_{VPDB}$ = 1.35‰) for carbon isotopologues. In contrast with increasing time, when the TCE concentration gradient becomes more flat (Fig. 3-5A), the heavier isotopologues catch up and the isotopologue shift towards lighter isotopologue signatures with increasing depth becomes smaller and almost disappears during long diffusion periods (100 years, Figs. 3-6A and B). Therefore, although there is a significant isotopologue fractionation during the diffusive transport process, during long diffusion periods, shifts in isotopologue ratios almost completely disappear.

3.7. Conclusions and implications for environmental studies

The results of the present study demonstrate that the kinetic theory (eq. 3-3) overestimates the magnitude of carbon and chlorine isotopologue fractionation of TCE and 1,2-DCA during diffusion in the aqueous phase. This outcome is consistent with experimentally determined beta values for the fractionation of diffusing ions (Eggenkamp and Coleman, 2009; Richter et al., 2006), noble gases (Tempest and Emerson, 2013; Tyroller et al., 2014) and different isotopologue types of organic compounds (Jin et al., 2014; LaBolle et al., 2008; Schloemer and Krooss, 2004; Zhang and Krooss, 2001). Furthermore, the results of the present study are consistent with molecular dynamic simulations addressing metal cations and noble gases (Bourg and Sposito, 2008; Bourg et al. 2010). Thus, our results confirm that the kinetic theory not only fails for the

prediction of isotope fractionation of diffusing ions and noble gases in the aqueous phase, but also for organic compounds. Furthermore, by including the laboratory determined diffusion coefficients in a 1D-diffusion model, the present study relates for the first time consistently laboratory with field values for chlorinated hydrocarbons. Thus, the measurements and simulations demonstrate that the kinetic theory is also not suitable for assessing isotopologue fractionation in diffusion dominated low permeable systems at the field scale. Therefore, previous kinetic theory based modeling studies have overestimated isotope effects during diffusive transport of organic compounds into low permeability units (LaBolle 2008; Rolle et al., 2010; Van Breukelen and Rolle, 2012). Furthermore, simulations for different time periods showed that large shifts in isotopologue ratios will only occur during short diffusion periods. Consequently, diffusion-caused isotopologue fractionation in water-saturated low permeability sediment only impairs the identification of reactive processes using CSIA during short diffusion periods, when diffusion-rated shifts in isotopologue ratios are largest and shifts related to reactive processes might still be small. The diffusion coefficient ratios for carbon and chlorine isotopologues of TCE and 1,2-DCA from this study can help to improve models that incorporate isotope data to identify reactive processes.

3.8. Acknowledgment

The authors acknowledge the Swiss National Science Foundation (SNSF) for their financial support. Furthermore, the authors thank Prof. Ian Bourg and two anonymous reviewers for their constructive comments, which greatly helped to improve the quality of the manuscript.

3.9. References

Aeppli, C., Holmstrand, H., Andersson, P., Gustafsson, O., 2010. Direct Compound-Specific Stable Chlorine Isotope Analysis of Organic Compounds with Quadrupole GC/MS Using Standard Isotope Bracketing. Analytical Chemistry, 82: 420-426.

Alder, B.J., Alley, W.E., Dymond, J.H., 1974. Studies In Molecular-Dynamics.14. Mass and Size Dependence of Binary Diffusion Coefficients. Journal of Chemical Physics, 61: 1415-1420.

Appelo, C.A.J., Postma, D., 2005. Geochemistry, groundwater and pollution. CRC Press Amsterdam.

Asfour, A.F.A., 1983. Improved and Simplified Diaphragm Cell Design and Analysis Technique for Calibration. Review of Scientifc Instruments, 54: 1394-1396

Asfour, A.F.A., Dullien, F.A.L.,1983. Diaphragm Diffusion Cell - Simpler Cell Design and New Equation to Calculate Diffusivities. AIChE Journal, 29: 347-349.

Ballentine, C.J., Burgess, R., Marty, B., 2002. Tracing fluid origin, transport and interaction in the crust. In Noble Gases in Geochemistry and Cosmochemistry (eds. D. Porcelli, C.J. Ballentine and R. Wieler). Mineralogical Society of America, pp. 539-614.

Bear, J., 1972. Dynamics of Fluids in Porous Media, Dover, New York.

Beekmann, H.E., Eggenkamp, H.G.M., Appelo, C.A.J., 2011. An integrated modelling approach to reconstruct complex solute transport mechanism – Cl and δ^{37}Cl in pore water of sediments from a former brackish lagoon in The Netherlands. Applied Geochemistry, 26: 257 - 268.

Berkowitz, M., Wan W., 1987. The Limiting Ionic Conductivity of Na^+ and Cl^- Ions in Aqueous Soluttions - Molecular Dynamics Simulation. J Journal of Chemical Physics, 86: 376-382.

Bernstein, A., Shouakar-Stash O., Ebert, K., Laskov, C., Hunkeler, D., Jeannottat, S., Sakaguchi-Soder, K., Laaks, J., Jochmann, M.A., Cretnik, S., Jager, J., Haderlein, S.B., Schmidt, T.C., Aravena, R., Elsner, M., 2011. Compound-Specific Chlorine Isotope Analysis: A Comparison of Gas Chromatography/Isotope Ratio Mass Spectrometry and Gas Chromatography/Quadrupole Mass Spectrometry Methods in an Interlaboratory Study. Analytical Chemistry, 83: 7624-7634.

Biswas, R., Bagchi, B., 1997. Limiting ionic conductance of symmetrical, rigid ions in aqueous solutions: Temperature dependence and solvent isotope effects. Journal of the American Chemical Society, 119: 5946-5953.

Bouchard, D., Hohener, P., Hunkeler, D., 2008a. Carbon Isotope Fractionation During Volatilization of Petroleum Hydrocarbons and Diffusion Across a Porous Medium: A Column Experiment. Environ. Science and Technology, 42: 7801-7806.

Bouchard, D., Hunkeler, D., Gaganis, P., Aravena, R., Hohener, P., Broholm, M.M., Kjeldsen, P., 2008b. Carbon isotope fractionation during diffusion and biodegradation of petroleum hydrocarbons in the unsaturated zone: Field experiment at Vaerlose airbase, Denmark, and modeling. Environmental Science and Technology, 42: 596-601.

Bourg, I. C., Richter, F. M., Christensen J. N., Sposito, G., 2010. Isotopic mass dependence of metal cation diffusion coefficient in liquid water. Geochimica et Cosmochimica Acta, 74: 2249 - 2256.

Bourg, I.C., Sposito, G., 2007. Molecular dynamics simulations of kinetic isotope fractionation during the diffusion of ionic species in liquid water. Geochimica et Cosmochimica Acta, 71: 5583-5589.

Bourg, I. C., Sposito, G. (2008) Isotopic fractionation of noble gases by diffusion in liquid water: Molecular dynamics simulations and hydrologic applications. Geochimica et Cosmochimica Acta, 72: 2237-2247.

Chernyavsky, B. M., Wortmann, U.G., 2007. REMAP: A reaction transport model for isotope ratio calculations in porous media. Geochemistry, Geophysics, Geosystems, 8: Q02009.

Chong, S. H., Hirata, F., 1998. Dynamics of solvated ion in polar liquids: An interaction-site-model description. Journal of Chemical Physics, 108: 7339-7349.

Clark, I. D., Fritz, P., 1997. Environmental Isotopes in Hydrogeology. CRC Press, New York.

Cotel, S., Schafer, G., Barthes, V., Baussan, P., 2011. Effect of Density-Driven Advection on Trichloroethylene Vapor Diffusion in a Porous Medium. Vadose Zone Journal, 10: 565-581.

Crank, J., 1975. The Mathematics of Diffuison. Oxford University Press, New York.

Cussler, E.L., 2009. Diffusion Mass transfer in Fluid Systems. Cambridge University Press, New York.

Damgaard, I., Bjerg, P.L., Baelum, J., Scheutz, C., Hunkeler, D., Jacobsen, C.S., Tuxen, N., Broholm, M.M., 2013. Identification of chlorinated solvents degradation zones in clay till by high resolution chemical, microbial and compound specific isotope analysis. Journal of Contaminant Hydrology, 146: 37-50.

Desaulniers, D.E., Kaufmann, R.S., Cherry, J.A., Bentley, H.W., 1985. ^{37}Cl - ^{35}Cl variations in a diffusion-controlled groundwater system. Geochimica et Cosmochimica Acta, 50: 1757 - 1764.

Donahue, M.A., Werne, J.P., Meile, C., Lyons, T.W., 2008. Modeling sulfur isotope fractionation and differential diffusion during sulfate reduction in sediments of the Cariaco Basin. Geochimica et Cosmochimica Acta, 72: 2287-2297.

Eggenkamp, H.G.M., Coleman, M.L., 2009. The effect of aqueous diffusion on the fractionation of chlorine and bromine stable isotopes. Geochimica et Cosmochimica Acta, 73: 3539-3548.

Elsner, M., Hunkeler, D., 2008. Evaluating chlorine isotope effects from isotope ratios and mass spectra of polychlorinated molecules. Analytical Chemistry 80: 4731-4740.

Elsner, M., Zwank, L., Hunkeler, D., Schwarzenbach, R.P., 2005. A new concept linking observable stable isotope fractionation to transformation pathways of organic pollutants. Environmental Science and Technology, 39: 6896-6916.

Falta, R.W., 2005. Dissolved chemical discharge from fractured clay aquitards contaminated by DNAPLs. In American Geophysical Union (eds. B. Faybishenko., P.A. Witherspoon, J. Gale). Dynamics of Fluids and Transport in Fractured Rock, pp. 165-174.

Feenstra, S., Mackay, D.M., Cherry, J.A., 1991. A Method for Assessing Residual NAPL Based on Organic-Chemical Concentraions in Soil Samples. Ground Water Monititoring and Remediation, 11: 128-136.

Gordon, S.L., 1999. A Labaratory Method for Investigations of Diffusion and Transformation of Volatile Organic Compounds in Low Permeability Media. PhD Thesis, University of Waterloo.

GSI, 2013. GSI Environmental Inc. Chemical Properties Database, Houston.

Harrington, R.R., Poulson, S.R., Drever, J.I., Colber, P.J.S., Kelly, E.F., 1999. Carbon isotope systematics of monoaromatic hydrocarbons: vaporization and adsorption experiments. Organic Geochemistry, 30: 765-775.

Holt, B.D., Sturchio, N.C., Abrajano, T.A., Heraty, L.J., 1997. Conversion of chlorinated volatile organic compounds to carbon dioxide and methyl chloride for isotopic analysis of carbon and chlorine. Analytical Chemistry, 69: 2727-2733.

Huang, L., Sturchio, N.C., Abrajano, T., Heraty, L.J., Holt, B.D., 1999. Carbon and chlorine isotope fractionation of chlorinated aliphatic hydrocarbons by evaporation. Organic Geochemistry, 30: 777-785.

Hunkeler, D., Abe Y., Broholm, M.M., Jeannottat, S., Westergaard, C., Jacobsen C.S., Aravena, R., Bjerg P.L., 2011. Assessing chlorinated ethene degradation in a large scale contaminant plume by dual carbon-chlorine isotope analysis and quantitative PCR. Journla of Contaminant Hydrology, 119: 69-79.

Hunkeler, D., Aravena R., Berry-Spark, K., Cox, E., 2005. Assessment of degradation pathways in an aquifer with mixed chlorinated hydrocarbon contamination using stable isotope analysis. Environmental Science and Technology, 39: 5975-5981.

Hunkeler, D., Aravena, R., Butler, B.J., (1999). Monitoring microbial dechlorination of tetrachloroethene (PCE) in groundwater using compound-specific stable carbon isotope ratios: Microcosm and field studies. Environmental Science and Technology, 33: 2733-2738.

Jeannottat, S., Hunkeler, D., 2012. Chlorine and Carbon Isotopes Fractionation during Volatilization and Diffusive Transport of Trichloroethene in the Unsaturated Zone. Environmental and Science and Technology, 46: 3169-3176.

Jeannottat, S., Hunkeler D., 2013. Can Soil Gas VOCs be Related to Groundwater Plumes Based on Their Isotope Signature? Environmental Science and Technology, 47: 12115-12122.

Jin, B. Haderlein, S.B., Rolle, M., 2013. Integrated Carbon and Chlorine Isotope Modeling: Applications to Chlorinated Aliphatic Hydrocarbons Dechlorination. Environmental Science and Technology, 47: 1443-1451.

Jin, B., Rolle, M., Li, T., Haderlein, S.B., 2014. Diffusive Fractionation of BTEX and Chlorinated Ethenes in Aqueous Solution: Quantification of Spatial Isotope Gradients. Environmental Science and Technology, 48: 6141-6150.

Johnson, R.L., Pankow, J.F., 1992. Dissolution of Dense Chlorinated Solvents Into Groundwater. 2. Source Functions for Pools of Solvent. Environmental Science and Technology, 26: 896-901.

Klump, S., Tomonaga, Y., Kienzler, P., Kinzelbach, W., Baumann, T., Imboden, D.M., Kipfer, R., 2007. Field experiments yield new insights into gas exchange and excess air formation in natural porous media. Geochimica et Cosmochimica Acta, 71: 1385-1397.

Kuder, T., Philp, P., Allen, J., 2009. Effects of Volatilization on Carbon and Hydrogen Isotope Ratios of MTBE. Environmental Science and Technology 43: 1763-1768.

LaBolle, E.M., Fogg, G.E., Eweis, J.B., Gravner, J., Leaist, D.G., 2008. Isotopic fractionation by diffusion in groundwater. Water Resources Research, 44: W07405.

Lavastre, V., Jendrzejewski, N., Agrinier, P., Javoy, M., and Evrard, M., 2005. Chlorine transfer out of a very low permeability clay sequence (Paris Basin, France): ^{37}Cl and ^{35}Cl evidence. Geochimica et Cosmochimica Acta, 69: 4949-4961.

Lippmann, J., Stute, M., Torgersen, T., Moser, D.P., Hal, J.A., Lin, L., Borcsik, M., Bellamy, R.E.S., Onstott T.C., 2003. Dating ultra-deep mine waters with noble gases and Cl-36, Witwatersrand Basin, South Africa. Geochimica et Cosmochimica Acta, 67: 4597-4619.

Lo, H.Y., 1974. Diffusion Coefficients in Binary-Liquid Alkane Systems. Journal of Chemical & Engineering Data, 19: 236-241.

Lollar, B.S., Slater, G.F., Slee, B., Witt, M., Klecka, G.M., Harkness, M., Spivack J., 2001. Stable carbon isotope evidence for intrinsic bioremediation of tetrachloroethene and trichloroethene at area 6, Dover Air Force Base. Environmental Science and Technology, 35: 261-269.

McManus, J., Nägler, T.F., Sieber,t C., Wheat, C.G., Hammond, D.E., 2002. Oceanic molybdenum isotope fractionation: Diagenesis and hydrothermal ridge-flank alteration. Geochemistry, Geophysics, Geosystems, 3: 1-9.

Meckenstock, R.U., Morasch, B., Griebler, C., Richnow, H.H., 2004. Stable isotope fractionation analysis as a tool to monitor biodegradation in contaminated acquifers. Journal of Contaminant Hydrology, 75: 215-255.

Mills, R., Woolf, L.A., Watts, R.O., 1968. Simplified Procedures for Diaphragm - Cell Diffusion Studies. AIChE Journal, 14: 671-673.

Neumann, A., Hofstetter, T.B., Skarpeli-Liati, M., Schwarzenbach, R.P., 2009. Reduction of Polychlorinated Ethanes and Carbon Tetrachloride by Structural Fe(II) in Smectites. Environmental Science and Technology, 43: 4082-4089.

Nuevo, M.J., Morales, J.J., Heyes, D.M., 1995. Mass Dependence of Isotope Self-Diffusion by Molecular-Dynamics. Physical Review, 51: 2026-2032.

Pankow, J.F., Cherry J.A., 1996. Dense Chlorinated Solvents and Other DNAPLs in Groundwater. Waterloo Press, Portland.

Parker, B.L., 1996. Effect of Molecular Diffusion on the Persistence of Dense Immiscible Phase Organic Liquids in Fractured Porous Geologic Media. PhD Thesis, University of Waterloo.

Parker, B.L., Cherry, J.A., Chapman, S.W., 2004. Field study of TCE diffusion profiles below DNAPL to assess aquitard integrity. Journal of Contaminant Hydrology, 74: 197-230.

Peeters, F., Beyerle, U., Aeschbach-Hertig, W., Holocher, J., Brennwald, M.S., Kipfer, R., 2003. Improving noble gas based paleoclimate reconstruction and groundwater dating using Ne-20/Ne-22 ratios. Geochimica et Cosmochimica Acta, 67: 587-600.

Poulson S.R., Drever J.I. (1999) Stable isotope (C, Cl, and H) fractionation during vaporization of trichloroethylene. Environ. Sci. Technol. 33, 3689-3694.

Richter, F.M., Mendybaev, R.A., Christensen, J.N., Hutcheon, I.D., Williams, R.W., Sturchio, N.C., Beloso, Jr., A.D., 2006. Kinetic isotopic fractionation during diffusion of ionic species in water. Geochimica et Cosmochimica Acta, 70: 277 - 289.

Rolle, M., Chiogna, G., Bauer, R., Griebler, C., Grathwohl, P., 2010. Isotopic Fractionation by Transverse Dispersion: Flow-through Microcosms and Reactive Transport Modeling Study. Environmental Science and Technology, 44: 6167-6173.

Sakaguchi-Soder, K., Jager, J., Grund, H., Matthaus, F., Schuth, C., 2007. Monitoring and evaluation of dechlorination processes using compound-specific chlorine isotope analysis. Rapid Communication in Mass Spectrometry, 21: 3077-3084.

Schloemer, S., Krooss, B.M., 2004. Molecular transport of methane, ethane and nitrogen and the influence of diffusion on the chemical and isotopic composition of natural gas accumulations. Geofluids, 4: 81-108.

Senftle, F.E., Bracken, J.T., 1954. Theoretical effects of diffusion on isotopic abundance ratios in rocks and associated fluids. Geochimica et Cosmochimica Acta, 7: 61 - 76.

Seyedabbasi, M.A., Newell, C.J., Adamso, D.T., Sale, T.C., 2012. Relative contribution of DNAPL dissolution and matrix diffusion to the long-term persistence of chlorinated solvent source zones. Journal of Contaminant Hydrology, 134: 69-81.

Shin, W.J., Lee, K.S., 2010. Carbon isotope fractionation of benzene and toluene by progressive evaporation. Rapid Communication in Mass Spectrometry, 24: 1636-1640.

Slater, G.F., Ahad, J.M.E., Lollar, B.S., Allen-King, R., Sleep, B., 2000. Carbon isotope effects resulting from equilibrium sorption of dissolved VOCs. Analytical Chemistry, 72: 5669-5672.

Steefel, C.I., Maher, K., 2009. Fluid-Rock Interaction: A Reactive Transport Approach. In: Thermodynamics and Kinetics of Water-Rock Interaction. (eds. E.H. Oelkers and J. Schott). Mineralogical Society of America, pp. 485-532.

Stokes, R.H., 1950. An Improved Diaphragm-Cell for Diffusion Studies, and Some Test of the Method. Journal of American Chemical Society, 72: 763-767.

Strassmann, K.M., Brennwald, M.S., Peeters, F., Kipfer, R., 2005. Dissolved noble gases in the porewater of lacustrine sediments as palaeolimnological proxies. Geochimica et Cosmochimica Acta, 69: 1665-1674.

Tempest, K., Emerson, S., 2013. Kinetic isotope fractionation of argon and neon in during air-water transfer. Marine Chemistry, 153: 39 -47.

Tyroller, L., Brennwald, M.S., Mächler, L., Livingston, D.M., Kipfer R., 2014. Fractionation of Ne and Ar isotopes by molecular diffusion in water. Geochimica et Cosmochimica Acta, 126: 60-66.

Van Breukelen, B.M., Rolle, M., 2012. Transverse Hydrodynamic Dispersion Effects on Isotope Signals in Groundwater Chlorinated Solvents' Plumes. Environmental Science and Technology, 46: 7700-7708.

Vangeet, A.L., Adamson, A.W., 1964. Diffusion in Liquid Hydrocarbon Mixtures. Journal of Physical Chemistry, 68: 238-246.

Watkins, J.M., DePaolo, D.J., Ryerson, F.J., Peterson, T.P., 2011. Influence of liquid structure on diffusive isotope separation in molten silicates and aqueous solutions. Geochimica et Cosmochimica Acta, 75: 3103-3118.

Wedlake, G.D., Dullie, F.A.L., 1974. Interdiffusion and Density-Measurements in some Binary-Liquid Mixtures. Journal of Chemical & Engineering Data, 19: 229-236.

Zhang, T.W., Krooss, B.M., 2001. Experimental investigation on the carbon isotope fractionation of methane during gas migration by diffusion through sedimentary rocks at elevated temperature and pressure. Geochimica et Cosmochimica Acta, 65: 2723-2742.

Zhou, Z., Ballentine, C.J., Kipfer, R., Schoell, M., Thibodeaux, S., 2005. Noble gas tracing of groundwater/coalbed methane interaction in the San Juan Basin, USA. Geochimica et Cosmochimca Acta, 69: 5413-5428.

3.10. Supplementary Information to Chapter 3

In the diffusion cell, fractionation occurs according to the Rayleigh equation. In the following, we consider a symmetric compound consisting of two atoms that occurs as three different isotopologues, HH, HL and LL representing TCE and 1,2-DCA carbon and 1,2-DCA chlorine isotopologues.

Fractionation between isotopologues containing no and one heavy isotopes can be described following the Rayleigh fractionation by:

$$\frac{C_{HL}}{C_{HL,0}} = \left(\frac{C_{LL}}{C_{LL,0}} \right)^{(\alpha_1)} \qquad \text{(S3-1)}$$

dividing both sides by $C_{LL}/C_{LL,0}$ yields:

$$\frac{C_{HL}/C_{LL}}{C_{HL,0}/C_{LL,0}} = \frac{C_{HL}/C_{HL,0}}{C_{LL}/C_{LL,0}} = \left(\frac{C_{LL}}{C_{LL,0}}\right)^{(\alpha_1-1)} \quad \text{(S3-2)}$$

Fractionation between isotopologues with one or two heavy isotopes is given by:

$$\frac{C_{HH}/C_{HL}}{C_{HH,0}/C_{HL,0}} = \frac{C_{HH}/C_{HH,0}}{C_{HL}/C_{HL,0}} = \left(\frac{C_{HL}}{C_{HL,0}}\right)^{(\alpha_2-1)} \quad \text{(S3-3)}$$

Inserting equation S3-1 into equation S3-3 leads to:

$$\frac{C_{HH}/C_{HL}}{C_{HH,0}/C_{HL,0}} = \frac{C_{HH}/C_{HH,0}}{C_{HL}/C_{HL,0}} = \left(\frac{C_{LL}}{C_{LL,0}}\right)^{\alpha_1\cdot(\alpha_2-1)} \quad \text{(S3-4)}$$

In good approximation:

$$\left(\frac{C_{LL}}{C_{LL,0}}\right)^{(\alpha_1-1)} \approx \left(\frac{C_{LL}}{C_{LL,0}}\right)^{\alpha_1\cdot(\alpha_2-1)} \quad \text{(S3-5)}$$

The validity of this approximation can be illustrated by calculating an example. The calculation is made for a typical α value of 0.998 for diffusive fractionation and assuming that $\alpha_1 = \alpha_2$ given that mass ratios between isotopologue pair differing by one isotope is nearly equal. A value of -0.002000 for the term (α_1-1) and a value of -0.001996 is obtained for the term $\alpha_1\cdot(\alpha_2-1)$, which is not significantly different.

Consequently:

$$\frac{C_{HL}/C_{HL,0}}{C_{LL}/C_{LL,0}} = \frac{C_{HH}/C_{HH,0}}{C_{HL}/C_{HL,0}} \quad \text{(S3-6)}$$

or

$$\frac{C_{HL}/C_{LL}}{C_{HH}/C_{HL}} = \frac{C_{HL,0}/C_{LL,0}}{C_{HH,0}/C_{HL,0}} \quad \text{(S3-7)}$$

Equation S3-7 demonstrates that the isotopologue containing two heavy isotopes C_{HH} is enriched relative to the isotopologue containing only one heavy isotope C_{HL} in the same way as C_{HL} is enriched relative to the isotopologue containing no heavy isotope C_{LL}. Therefore, isotopologue pairs that differ in one heavy isotope behave proportional. Furthermore, initial proportional isotopologue pairs differing by one heavy isotope can be related to the initial isotope ratio assuming an non-selective distribution of isotopes over isotopologue, which was proven to be a valid assumption by Elsner and Hunkeler (2008). For the initial isotope and isotopologue ratios, respectively the following equation was used:

$$R_0 = \frac{C_{H,0}}{C_{L,0}} = \frac{H_{p,0}}{L_{p,0}} = \frac{1}{2} \times \frac{C_{HL,0}}{C_{LL,0}} = 2 \times \frac{C_{HH,0}}{C_{HL,0}} \quad \text{(S3-8)}$$

where R_0 is the initial isotope ratio, $H_{P,0}$ and $L_{p,0}$ are the probabilities of encountering heavy and light isotopes, respectively.

Combining equation S3-7 and S3-8:

$$\frac{C_{HL}/C_{LL}}{C_{HH}/C_{HL}} = \frac{C_{HL,0}/C_{LL,0}}{C_{HH,0}/C_{HL,0}} = 4 \quad \text{(S3-9)}$$

To relate isotope ratios to isotopologue ratios, isotope ratio can be expressed in terms of isotopologue abundance.

$$\frac{C_H}{C_L} = \frac{2 \cdot C_{HH} + C_{HL}}{2 \cdot C_{LL} + C_{HL}} \tag{S-10}$$

Rearrangement of equation S3-10 and insertion of equation S3-9 leads to

$$\frac{C_H}{C_L} = \frac{2 \cdot C_{HH} + C_{HL}}{2 \cdot C_{LL} + C_{HL}} = \frac{\frac{2 \cdot C_{HH}}{C_{HL}} + 1}{\frac{2 \cdot C_{LL}}{C_{HL}} + 1} = \frac{\frac{2 \cdot C_{HL}}{4 \cdot C_{LL}} + 1}{\frac{2 \cdot C_{LL}}{C_{HL}} + 1} = \frac{\frac{C_{HL} + 2 \cdot C_{LL}}{2 \cdot C_{LL}}}{\frac{C_{HL} + 2 \cdot C_{LL}}{C_{HL}}} = \frac{C_{HL}}{2 \cdot C_{LL}} \tag{S3-11}$$

Equation S3-11 shows that the assumption of a non-selective distribution of equation S3-11 isotopes over isotopologues is generally true regardless the degree of fractionation thus:

$$R = \frac{C_H}{C_L} = \frac{H_p}{L_p} = \frac{1}{2} \times \frac{C_{HL}}{C_{LL}} = 2 \times \frac{C_{HH}}{C_{HL}} \tag{S3-12}$$

Dividing equation S3-12 by equation S3-8 leads to:

$$\frac{R}{R_0} = \frac{C_{HL} / C_{HL,0}}{C_{LL} / C_{LL,0}} = \frac{C_{HH} / C_{HH,0}}{C_{HL} / C_{HL,0}} \tag{S3-13}$$

Equations S3-12 and S3-13 demonstrate that for symmetric molecules having three possible isotopologues (HH, HL, LL), isotope ratios behave proportionally to isotopologue ratios differing by one heavy isotope. Therefore, measured carbon isotope ratios of TCE and 1,2-DCA and measured chlorine isotope ratios of 1,2-DCA are proportional to isotopologue pairs differing in one heavy isotope. The proportionality between isotope ratios and isotopologue ratios also demonstrates that there is no information loss, when considering only the TCE and 1,2-DCA carbon isotopologue pair containing one and zero heavy carbon isotope

Reference for Supplementary Information

Elsner, M., Hunkeler, D., 2008. Evaluating chlorine isotope effects from isotope ratios and mass spectra of polychlorinated molecules. Analytical Chemistry, 80(12): 4731-4740

Chapter 4: Molecular Dynamic Simulations of Carbon and Chlorine Isotopocule Fractionation of Chlorinated Hydrocarbons During Diffusion in Liquid Water

4.1. Introduction

Molecular dynamic (MD) simulations have been increasingly used as a computational tool to gain molecular-scale insight into properties of liquids and solids (Abraham, 1986; Allen and Tildesley, 1989; Hansson et al., 2002; Plimpton, 1995; Rapaport, 2004). In contrast to experimental and field studies, which investigate the average behavior of atoms and molecules, MD simulations provide the advantage of assessing the behavior of individual atoms and molecules. This is especially important for the study of liquid and solid properties, which originate from the atomistic or molecular scale such as sorption, partitioning mechanism, interfacial tension or diffusive transport rates. Furthermore, MD simulations open the possibility to examine systems under different conditions such as homogeneous pore sizes or hypothetical isotope masses, which is challenging to impose in laboratory or field studies.

Despite the widespread application of MD simulations, only a few studies investigated the mass dependency of the diffusive transport rate in the aqueous phase using MD simulations so far. The main constraint was that determined diffusion coefficients for isotopes at natural abundance remained within the uncertainty of MD simulations results, prohibiting the assessment of a relationship between the diffusive transport rate and the mass of the diffusing species. In contrast, Wilson et al. (1985) revealed for the first time that diffusion coefficients obtained from MD simulations are different for isotopes at natural abundances (e.g. $^{23}Na^{+}$) and having an infinitively large mass (e.g. $^{\infty}Na^{+}$). More recent MD simulation studies (Bourg et al., 2010; Bourg and Sposito, 2007; Bourg and Sposito, 2008) addressing a wider spectra of diffusing ions and noble gases, also observed significantly different diffusion coefficients for hypothetical isotopes having large mass differences (mass range: 2 – 133) confirming the results by Wilson et al. (1985). Despite the use of hypothetical isotopes, Bourg and Sposito (2007), Bourg and Sposito (2008) and Bourg et al. (2010) demonstrated that MD simulation results can be compared with experimental natural abundance studies by using beta values embedded in the general power law model (eq. 1-6, chp. 1). The beta value is non-sensitive to mass differences between isotope pairs and hence, fractionation between hypothetical isotopes having large mass differences and isotopes at natural abundance can be related. The beta values for hypothetical isotope pairs of dissolved ions and noble gases calculated via MD simulations were consistent with the values determined by experimental natural abundance studies (Bourg et al., 2010; Bourg and Sposito,

2007; Bourg and Sposito, 2008). Therefore, as mentioned in chapter 2, the MD simulations performed by Bourg and Sposito (2007), Bourg and Sposito (2008) and Bourg et al. (2010) provided for the first time a theoretical basis for the general power law model with exponent beta and reinforced its validity for estimating the magnitude of isotope fractionation due to aqueous phase diffusion for dissolved ions and noble gases (eq. 1-6, chp. 1).

In contrast to dissolved inorganic species MD simulation addressing isotope fractionation due to aqueous phase diffusion of organic compounds such as chlorinated hydrocarbons are lacking. Hence, all experimental studies, which investigated the magnitude of isotope fractionation due to aqueous phase diffusion of organic compounds have no theoretical basis and remain on a phenomenological level so far (Jin et al., 2014; LaBolle et al., 2008; Schloemer and Krooss, 2004; Wanner and Hunkeler, 2015; Zhang and Krooss, 2001). To address this gap of knowledge MD simulations for hypothetical carbon and chlorine isotopocules of trichloroethene (TCE) and 1,2-dichloroethane (1,2-DCA) having large mass differences are performed in this chapter and compared with experimental results determined in chapter 3 by using beta values. Hence, this chapter provides for the first time a theoretical basis for the experimental results of aqueous phase diffusion induced isotope fractionation of organic compounds and thus, opens the possibility to predict diffusion isotope effects for a wider spectra of organic compounds.

4.2. Molecular dynamic simulation methods

In MD simulations, the trajectories of atoms and molecules within liquids and solids are simulated by integrating Newton's differential equations of motions, which are given as follows:

$$m_i \frac{d\vec{v}_i}{dt} = \sum_j F_2\left(\vec{r}_i, \vec{r}_j\right) + \sum_j \sum_k F_3\left(\vec{r}_i, \vec{r}_j, \vec{r}_k\right) + \ldots \quad (4\text{-}1)$$

$$\frac{d\vec{r}_i}{dt} = \vec{v}_i \quad (4\text{-}2)$$

where m_i is the mass of the atom i, $\vec{r}_i$ and $\vec{v}_i$ are its position and velocity vectors, F_2 is a force function for the pairwise interactions between atoms, F_3 describes three-body interactions and additional body interactions can be added.

The force terms in equation 4-1 are derivate expressions in which the energy of an atom is expressed as a function of the position of itself or other atoms including both long- and short range interactions between atoms. The long-range interactions are commonly included in the MD simulations by assigning partial charges to each atom resulting in coulombic interactions, while short-range interactions are described by the 6-12 Lennard-Jones (LJ) potential:

$$\phi_{ij}\left(r_{ij}\right) = 4 \in_{ij} \left[\left(\frac{\sigma_{ij}}{r_{ij}} \right)^{6} - \left(\frac{\sigma_{ij}}{r_{ij}} \right)^{12} \right] \qquad (4\text{-}3)$$

where, ϕ (kcal/mol) refers to the potential energy of the Lennard Jones potential, r_{ij} (Å) is the interatomic distance, σ_{ij} (Å) and $\in_{ij}$ (kcal/mol) correspond the to the LJ parameters, while $2^{1/6}\sigma_{ij}$ and $\in_{ij}$ define the location, where the LJ potential has its minimum.

To minimize the computational demand, a cut-off distance is defined for calculation of the long- and short-range interactions i.e. the summation in equation 4-1 is restricted to the distance r_c around atom i, whereas outside of r_c all interactions between atoms are ignored.

For performing MD simulations for isotopically distinct TCE and 1,2-DCA molecules (denominated as isotopocules) in liquid water, a simulation box with a volume of 58360 $Å^3$ (x=32Å, y=32Å, z=57Å) was created containing 1884 water and one TCE or 1,2-DCA molecule. The size of the box was chosen to minimize computation time, while avoiding boundary effects. Liquid water was described using the extended simple point charge (SPCE/E) model (Berendsen et al., 1987), whereas the water molecules were treated as rigid and non-polarizable. It has been demonstrated that the SPCE/E model predicts accurately the properties (density, surface tension, static dielectric constant) of liquid water at different temperatures (Alejandre et al., 1995; Berendsen et al., 1987; Hura et al., 2003; Wasserman et al., 1995). For the water molecules a O-H bond length of 1 Å and an H-O-H angle of 109.47 degrees was defined. Furthermore, long-range coulombic interactions were taken into account by assigning discrete atomic charges of q_O = -0.8476 e and of q_H = 0.4238 e to the oxygen and hydrogen atoms of the water molecules. The short-range interactions of the oxygen atoms in the water molecules were described by using Lennard Jones parameters of $\in_{OO}$ = 0.15527 kcal/mol and σ_{OO} = 3.169 Å (eq. 4-3) taken from

previous MD simulation studies (Bourg et al., 2010; Bourg and Sposito, 2007; Bourg and Sposito, 2008).

The long- and short-range interactions for the atoms constituting the TCE and 1,2-DCA molecules were defined according to Jorgensen (2009). Partial discrete charges resulting in long-range coulomb interactions were assigned to each atom in the TCE (C_1 = 0.005, C_2 = 0.120, Cl and Cl_2 = -0.06, Cl_3 = -0.120 and H = 0.115 (Fig. 4-1A)) and in the 1,2-DCA molecule (-0.006 for C_1 and C_2, -0.200 for Cl_1 and Cl_2 and 0.103 for H_1, H_2, H_3 and H_4 (Fig. 4-1B)).

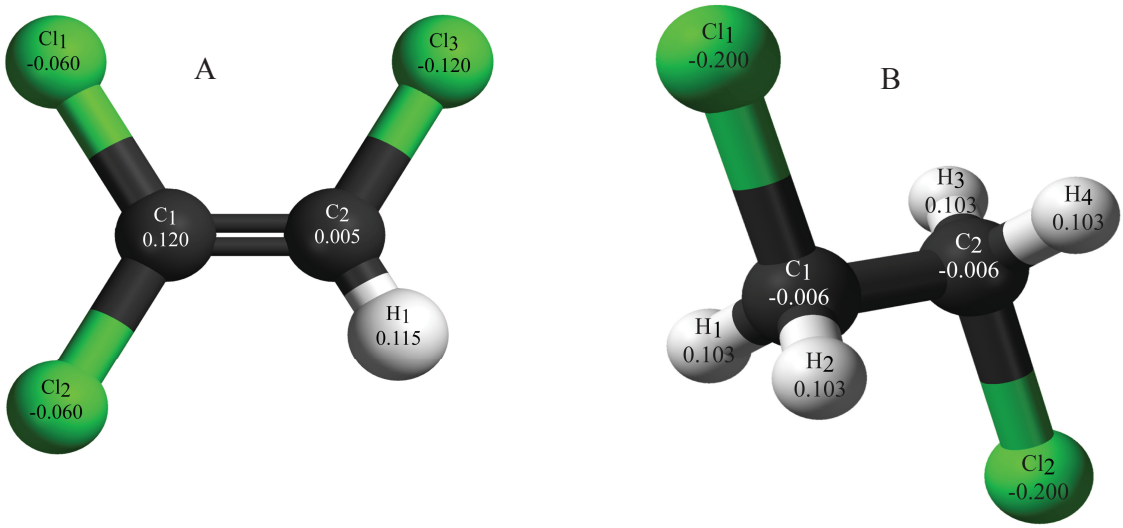

Figure 4-1. Molecular structure of A) TCE modified after ChemLibrarian (2015) and B) 1,2-DCA modified after Mills (2009) with assigned partial atomic charges.

Short-range interactions were described by defining LJ parameters for each atom type in the TCE and 1,2-DCA molecules (Tabs. 4-1A and 4-1B). LJ parameters for the interactions between the different atom types in the TCE and 1,2-DCA molecule and the O atom in the water molecules were calculated using the following rules (Plimpton, 2005):

$$\epsilon_{ij} = \sqrt{\epsilon_i + \epsilon_j} \tag{4-4}$$

$$\sigma_{ij} = \left(\sigma_i + \sigma_j\right)/2 \tag{4-5}$$

In contrast to the water molecules, TCE and 1,2-DCA molecules were treated as non-rigid molecules in the MD simulations. Hence, energy potentials for the bond length (eq. 4-6), the angles between three atoms in the TCE and 1,2-DCA molecule (eq. 4-7) and for the torsional angle defined by the quadruplet of atoms in the same plane (dihedrals) (eq. 4-8) were defined as follows (Tabs. 4-1A and 4-1B) (Plimpton, 2005):

$$E_B = K_B\left(r - r_0\right)^2 \tag{4-6}$$

$$E_A = K_A\left(\theta - \theta_0\right)^2 \tag{4-7}$$

$$E_D = \frac{1}{2}K_{D,1}\left[1 + cos\left(\phi\right)\right] + \frac{1}{2}K_{D,2}\left[1 - cos\left(2\phi\right)\right] + \frac{1}{2}K_{D,3}\left[1 + cos\left(3\phi\right)\right] + \frac{1}{2}K_{D,4}\left[1 - cos\left(4\phi\right)\right] \tag{4-8}$$

where E_B, E_A and E_D (kcal/mol) refer to the energy potentials of the bonds, angles and dihedrals respectively, K_B (kcal/mol/Å), refers to the bond coefficient, K_A (kcal/mol/rad) is the angle coefficients and $K_{D,1}$, $K_{D,2}$, $K_{D,3}$ and $K_{D,4}$ (kcal) are the dihedral coefficients. Furthermore r and r_o (Å) refer to the bond length and the equilibrium bond length, respectively, θ and θ_0 (degrees) refer to the angle and to the equilibrium angle defined by three atoms in the molecule, respectively and ϕ (degrees) refers to the dihedral angle.

Table 4-1A. Lennard Jones and bond parameters for TCE and 1,2-DCA molecules used in the MD simulations according to Jorgensen (2009).

Molecule	Atom	σ_{ij}(Å)	$\in$ (kcal/mol)	Bond	Length(Å)	K (kcal/mol/Å^2)
TCE	C	3.55	0.076	C-C	1.340	549.00
	Cl	3.40	0.300	C-Cl	1.725	300.00
	H	2.42	0.030	C-H	1.080	340.00
1,2-DCA	C	3.50	0.060	C-C	1.529	268.00
	Cl	3.40	0.300	C-Cl	1.781	245.00
	H	2.50	0.030	C-H	1.090	340.00

Table 4-1B. Angle and dihedral parameters for TCE and 1,2-DCA molecules used in MD simulations according to Jorgensen (2009).

Molecule	Angle type	Angle (°)	K (kcal/mol/rad^2)	Dihedrals	K_1, K_2, K_3, K_4 (kcal)
TCE	Cl-C-C	121.50	75.00		
	H-C-C	120.00	35.00	Cl-C-C-Cl	-1.60, 14.00, 0.00, 0.00
	Cl-C-H	121.50	75.00	Cl-C-C-H	0.00, 14.00, 0.00, 0.00
1,2-DCA	Cl-C-C	109.90	69.00		
	H-C-C	110.70	37.50		
	Cl-C-H	107.60	51.00		
	H-C-H	107.80	33.00	Cl-C-C-Cl	-0.25, 0.00, 0.00, 0.00

To avoid that obtained diffusion coefficient from MD simulations for 1,2-DCA and TCE carbon and chlorine isotopocules remain within the uncertainty of the MD simulations, hypothetical masses were assigned to carbon and chlorine atoms ranging between 1.65 – 301.65 for C and between 2.00 -178.50 for Cl, respectively (Tabs. 4-2 and 4-3). The range of hypothetical isotope mass variations was chosen similar to previous MD simulations studies (2 – 133), which assessed the mass dependency of the diffusive transport rate of diffusing ions and noble gasses in the aqueous phase (Bourg, 2008; Bourg et al., 2010; Bourg and Sposito, 2007). As both stable chlorine isotopes are present at high abundance (^{35}Cl = 75.76%; ^{37}Cl = 24.24%) isotopic substitution occurs for all chlorine atoms in the TCE and 1,2-DCA molecules at natural abundance. Hence, the hypothetical masses of all chlorine isotopes were varied in the TCE and 1,2-DCA chlorine isotopocules in the MD simulations for being consistent with natural abundance conditions. In contrast, for the TCE and 1,2-DCA carbon isotopocules the

hypothetical mass of only one carbon isotope was varied in the MD simulations (C_1 in Fig. 4-1B) as at natural abundance isotopic substitution occurs only for one carbon isotope due to the low abundance of the heavy carbon compared to the light isotope (^{12}C = 98.93% ;^{13}C = 1.07%). MD simulations of TCE and 1,2-DCA carbon and chlorine isotopocules in liquid water were carried out with the software Lammps (Plimpton, 1995) on the "Cori" Supercomputer at the US National Energy Research Scientific Computing Center (NERSC) located at the University of Berkeley. For performing MD simulations, Newton's equations of motions (eqs. 4-1 and 4-2) were integrated by using the SHAKE algorithm (Ryckaert et al., 1977) with a cut-off distance of 10 Å. MD simulation production runs for TCE and 1,2-DCA isotopocules were performed in the NVT ensemble (constant volume of simulation box) at 298 K for 50 nanoseconds with a one femtosecond time step. The production runs were anteceded by 5 picoseconds of simulations in the NPT ensemble (constant pressure in simulation box) at 1 bar and at 298 K and a 30 picoseconds simulation in the NVT ensemble at 298 K to fully equilibrate the system (see Appendix for used input files). For assessing the random trajectories of the TCE and 1,2-DCA isotopocules its position was saved every picosecond. Diffusion coefficient for the TCE and 1,2-DCA isotopocules were calculated from their mean square displacement using the well-known Einstein relation:

$$D = \frac{1}{2n} \lim_{t \to \infty} \frac{d\left\langle l^2 \right\rangle}{dt} \qquad \text{(n=order of dimension)} \tag{4-9}$$

The uncertainty of the determined diffusion coefficient was estimated by dividing each 50 ns production run into 5 blocks of 10 ns, whereas for each block the average diffusion coefficients for TCE and 1,2-DCA isotopocules was calculated from the slope of $\left\langle l^2 \right\rangle$ (eq. 4-9) from several 100 ps time intervals. Afterwards, the uncertainty of the diffusion coefficient was indicated as the standard error of the mean (SDM) based on the standard deviation of the block-averaged diffusion coefficients: SDM = $1\sigma(Di_{,Total})/(n_B)^{0.5}$($\sigma$: standard deviation of block-averaged diffusion coefficients, n_B: numbers of block).

To investigate the mass dependency of the obtained diffusion coefficients for the hypothetical TCE and 1,2-DCA carbon and chlorine isotopocules from equation 4-9, log (D)

versus log (m) plots were used, in which the slope of the regression line corresponds to the beta value (eq. 1-6 chp. 1) as illustrated with the following equation:

$$log(D_i) = A - \beta log(m_i) \quad (4\text{-}10)$$

The uncertainty of the beta value was determined based on the 95% confidence interval of the regression line in the log (D) - log (m) plots. To compare experimental beta values from isotopes at natural abundance inferred in chapter 3 with MD simulations for hypothetical isotopes, the experimentally determined beta values were plotted as solid lines in the log (D) – log (m) plots, while the A values (eq. 4-10) were used to minimize the deviation between experimental and MD simulation results.

4.3. Results and Discussion

For the TCE and 1,2-DCA isotopocules at natural abundance (^{130}TCE and ^{99}1,2-DCA; Tabs. 4-2 and 4-3) obtained free solution diffusion coefficients from MD simulations are comparable with published "bulk" diffusion coefficient. The detected faster diffusive transport rate for TCE (1.39E-09 m^2/s) compared to 1,2-DCA (1.36E-09 m^2/s) (Tabs. 4-2 and 4-3) is in agreement with published diffusion coefficients (TCE: 1.01E-09 m^2/s (Pankow and Cherry, 1996) and 1,2.DCA: 9.9E-10 m^2/s (Wiedemeier, 1999)). The observed faster absolute diffusive transport rates during MD simulations compared to the published rates for TCE and 1,2-DCA can be likely attributed to the higher temperature applied in the MD simulations (25°C) than for the determination of diffusion coefficients found in literature (20°C). When the temperature dependence of the diffusion coefficients is taken into account (11% faster at 25°C compared to 20°C (Mills, 1973)), published and calculated values agree well.

Table 4-2. Results of MD simulations for TCE carbon and chlorine isotopocules at 298K. All chlorine atoms were isotopically substituted, while for carbon the mass was varied only for one C atom.

Isotopocule	**Mass of hypothetical C or Cl isotopes in the TCE molecule (m_i)**	**Diffusion coefficient (10^{-9} m^2s^{-1})**
Carbon isotopocules		
^{121}TCE	1.65	1.33± 0.01
^{181}TCE	61.65	1.28± 0.02
^{271}TCE	151.65	1.29±0.08
^{331}TCE	211.65	1.28±0.02
^{421}TCE	301.65	1.25±0.04
Chlorine isotopocules		
^{31}TCE	2.00	1.44±0.07
^{91}TCE	22.00	1.36±0.04
^{130}TCE	35.00	1.39±0.07
^{235}TCE	70.00	1.31±0.03
^{421}TCE	132.00	1.26±0.04

Table 4-3. Results of MD simulations for 1,2-DCA carbon and chlorine isotopocules at 298K. All chlorine atoms were isotopically substituted, while for carbon the mass was varied only for one C atom.

Isotopocule	**Mass of hypothetical C or Cl isotope in the 1,2-DCA molecule (m_i)**	**Diffusion coefficient (10^{-9} m^2s^{-1})**
Carbon isotopocules		
^{90}1,2-DCA	3.10	1.34±0.09
^{99}1,2-DCA	12.00	1.36±0.09
^{178}1,2-DCA	91.10	1.30±0.09
^{223}1,2-DCA	136.10	1.31±0.06
^{283}1,2-DCA	196.10	1.30±0.12
^{353}1,2-DCA	266.10	1.27±0.06
Chlorine isotopocules		
^{35}1,2-DCA	3.50	1.36± 0.10
^{55}1,2-DCA	13.50	1.42± 0.10
^{99}1,2-DCA	12.00	1.36±0.09
^{145}1,2-DCA	58.50	1.28±0.08
^{235}1,2-DCA	103.50	1.33±0.08
^{385}1,2-DCA	178.50	1.32±0.13

For the hypothetical TCE and 1,2-DCA isotopocules diffusive transport rates in the range between 1.25E-09 m^2/s and 1.34E-09 m^2/s for the carbon and between 1.26E-09 m^2/s and 1.44E-09 m^2/s for chlorine isotopocules were obtained from the MD simulations (Tabs. 4-2 and 4-3). The log(D)-log(m) plots, for the hypothetical TCE and 1,2-DCA isotopocules revealed a trend towards slower diffusive transport rates with increasing mass (Figs. 4-2 and 4-3). The slope of the regression lines (eq. 4-10) revealed beta values in the range between 0.025 and 0.049 for the TCE and 1,2-DCA isotopocules.

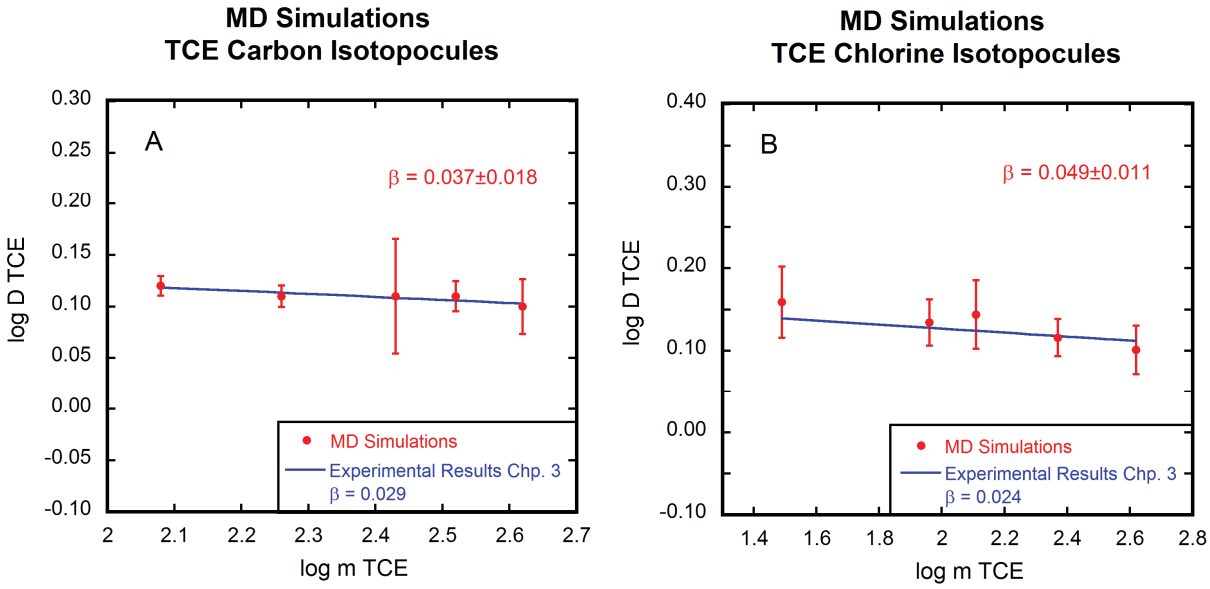

Figure 4-2. Log-log plots of diffusion coefficients of TCE carbon (A) and chlorine (B) isotopocules in liquid water at 298K obtained from MD simulations as a function of the hypothetical mass. The β-values inferred from the experimental results in chapter 3 are represented by the solid blue lines.

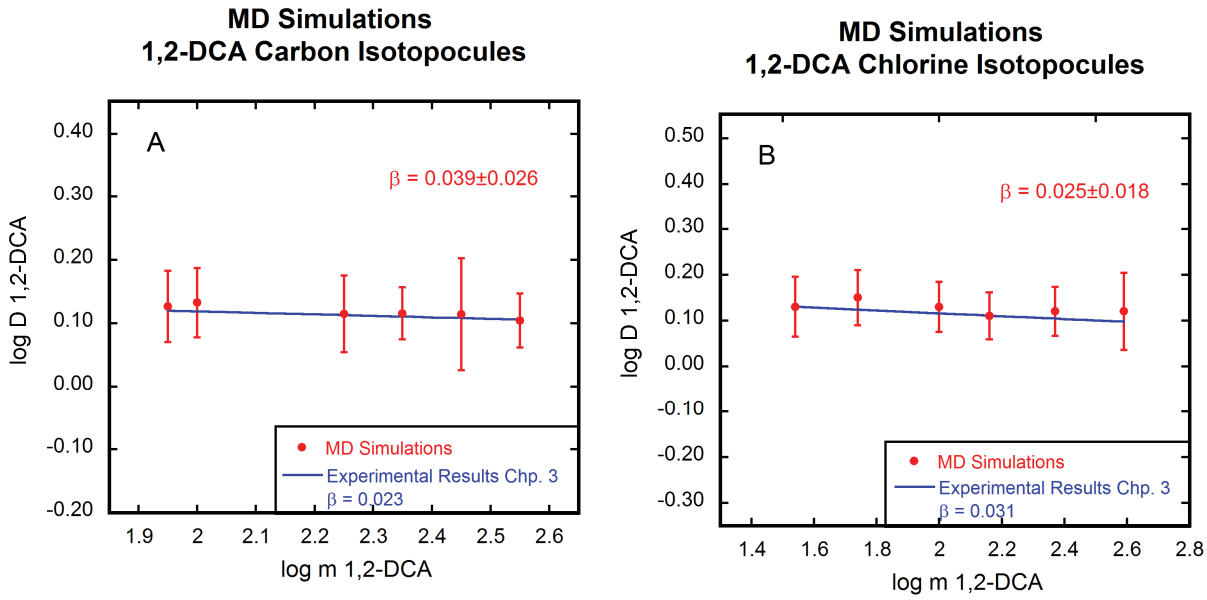

Figure 4-3. Log-log plots of diffusion coefficients of 1,2-DCA carbon (A) and chlorine (B) isotopocules in liquid water at 298K obtained from MD simulations as a function of the hypothetical mass. The β-values inferred from the experimental results in chapter 3 are represented by the solid blue lines.

By plotting the experimentally determined beta values derived in chapter 3 for TCE and 1,2-DCA carbon and chlorine isotopocules in figures 4-2 and 4-3 (solid blues lines) a coherency between experimental and MD simulation results was revealed. Hence, the performed MD simulations provided for the first time a theoretical basis for the experimentally determined lower beta values for diffusing organic compounds in chapter 3 than predicted by the kinetic theory (0.5). The simulated beta values were also consistent with previous MD simulations ($0 \leq \beta < 0.2$) addressing isotope fractionation of inorganic species (Bourg et al., 2010; Bourg and Sposito, 2007; Bourg and Sposito, 2008). This indicates that the mass dependency of diffusive transport rate in the aqueous phase for organic compounds is likely governed by similar molecular scale mechanisms as for inorganic species.

For inorganic species some studies attributed the failure of the kinetic theory for estimating the mass dependency of the diffusive transport rate in the aqueous phase to the formation of solvation shells around the diffusing solutes (Gussone et al., 2003; Pernaton et al., 1996). They argued that the magnitude of isotope fractionation due to aqueous phase diffusion is

consistent with the kinetic theory when replacing the solute mass (eq. 1-5, chp. 1) by an assembly composed of solute and several solvent molecules ($m_i + n \cdot m_0$), where m_i is the solute and m_0 is the solvent mass and n can be treated as fitting parameter to obtain a beta value of 0.5. However, Richter et al. (2006) revealed that an impossible large amount of solvent molecules (e.g. n = 900 for Mg^{2+} isotopes) would be required to obtain a beta value of 0.5. A similar unrealistic number of surrounding solvent molecules (n = 86 – 143) was also observed for the TCE and 1,2-DCA carbon and chlorine isotopocules for obtaining a beta value 0.5. This shows that the simple consideration of a diffusing assembly is also not valid to explain the weak power law mass dependency of the diffusive transport rate for carbon and chlorine TCE and 1,2-DCA isotopocules. Hence, a more sophisticated model is required to explain the observed lower beta values for the carbon and chlorine TCE and 1,2-DCA isotopocules compared to the kinetic theory. Bhattacharyya and Bagchi (2000) demonstrated that the weak power law mass dependency of diffusing species can be more accurately described by a mode-coupling theory, assuming that isotope fractionation in the aqueous phase is a result of a competition between long-term hydrodynamic and short-term binary collision modes of motion. The hydrodynamic modes of motion describe the movement of solute molecules through a continuum solvent following the Stokes-Einstein relation (eq. 2-5. chp. 2). Hence, the hydrodynamic modes of motion foresee no mass dependency of the diffusing transport rate. In contrast the binary collision modes of motion, which occur at much shorter timescales, originate from collisions between the solute and the surrounding solvent molecules and show a strong mass dependency following the kinetic theory (eq. 1-5, chp. 1). The relative contribution of the hydrodynamic and binary collision modes of motion to the overall mass dependency of the diffusive transport rates can be identified by considering a memory function of the friction affecting a diffusing solute (Bourg et al., 2010). The friction memory can be decomposed in short-time binary collision component and in a long-time hydrodynamic component (Chong and Hirata, 1999; Yamaguchi et al., 2005). The decomposition showed that the contribution of the mass dependent short-time binary collision mode is 30 – 40% to the total diffusive motion of the solute (Bhattacharyya and Bagchi, 2000) causing likely the weaker power law mass dependency of the diffusing TCE and 1,2-DCA carbon and chlorine isotopocules compared to the kinetic theory.

4.4. Conclusions

In this chapter, MD simulations results were conducted for the first time to investigate the mass dependency of the diffusive transport rate for isotopocially distinct organic compounds. The results revealed a weaker power-law mass dependency of the diffusive transport rate than in the previously postulated by kinetic theory, which was consistent with the experimental results obtained in chapter 3. Hence, conducted MD simulations provided for the first time a theoretical rationale for the experimentally determined lower beta values compared to the kinetic theory for isotopically distinct organic compounds. The weak mass dependency of the diffusive transport rate of organic compounds can be explained by the mode-coupling theory showing that the overall isotope effect due to aqueous phase diffusion is a result of a competition between mass independent hydrodynamic and strongly mass dependent kinetic modes of motion.

4.5. References

Abraham, F.F., 1986. Computational statistical mechanics methodology, applications and supercomputing. Advances in Physics, 35(1): 1-111.

Alejandre, J., Tildesley, D.J., Chapela, G.A., 1995. Molecular dynamics simulation of the orthobaric densities and surface tension of water. The Journal of chemical physics, 102(11): 4574-4583.

Allen, M.P., Tildesley, D.J., 1989. Computer simulation of liquids. Oxford university press.

Berendsen, H.J.C., Grigera, J.R., Straatsma, T.P., 1987. THE MISSING TERM IN EFFECTIVE PAIR POTENTIALS. Journal of Physical Chemistry, 91(24): 6269-6271.

Bhattacharyya, S., Bagchi, B., 2000. Power law mass dependence of diffusion: A mode coupling theory analysis. Physical Review E, 61(4): 3850-3856.

Bourg, I.C., 2008. Comment on "Modeling sulfur isotope fractionation and differential diffusion during sulfate reduction in sediments of the Cariaco Basin" by MA Donahue, JP Werne, C. Meile and TW Lyons. Geochimica Et Cosmochimica Acta, 72(23): 5852-5854.

Bourg, I.C., Richter, F.M., Christensen, J.N., Sposito, G., 2010. Isotopic mass dependence of metal cation diffusion coefficient in liquid water. Geochimica et Cosmochimica, 74: 2249 - 2256.

Bourg, I.C., Sposito, G., 2007. Molecular dynamics simulations of kinetic isotope fractionation during the diffusion of ionic species in liquid water. Geochimica et Cosmochimica Acta, 71(23): 5583-5589.

Bourg, I.C., Sposito, G., 2008. Isotopic fractionation of noble gases by diffusion in liquid water: Molecular dynamics simulations and hydrologic applications. Geochimica Et Cosmochimica Acta, 72(9): 2237-2247.

ChemLibrarian, 2015. A 3D ball and stick model of Trichloroethylene (published on wikimedia.org).
Chong, S.H., Hirata, F., 1999. Dynamics of ions in liquid water: An interaction-site-model description. Journal of Chemical Physics, 111(8): 3654-3667.
Gussone, N. et al., 2003. Model for kinetic effects on calcium isotope fractionation (delta Ca-44) in inorganic aragonite and cultured planktonic foraminifera. Geochimica Et Cosmochimica Acta, 67(7): 1375-1382.
Hansson, T., Oostenbrink, C., van Gunsteren, W., 2002. Molecular dynamics simulations. Current opinion in structural biology, 12(2): 190-196.
Hura, G. et al., 2003. Water structure as a function of temperature from X-ray scattering experiments and ab initio molecular dynamics. Physical Chemistry Chemical Physics, 5(10): 1981-1991.
Jin, B., Rolle, M., Li, T., Haderlein, S.B., 2014. Diffusive Fractionation of BTEX and Chlorinated Ethenes in Aqueous Solution: Quantification of Spatial Isotope Gradients. Environmental Science & Technology, 48(11): 6141-6150.
Jorgensen, W.L., 2009. OPLS All-Atom Parameters for Organic Molecules, Ions, Peptides & Nucleic Acids. User Manual Boss 4.8.
LaBolle, E.M., Fogg, G.E., Eweis, J.B., Gravner, J., Leaist, D.G., 2008. Isotopic fractionation by diffusion in groundwater. Water Resources Research, 44(7).
Mills, B., 2009. Ball and stick model of the 1,2-dichloroethane molecule (published on wikimedia.org).
Mills, R., 1973. Self-diffusion in normal and heavy water in the range 1-45. deg. The Journal of Physical Chemistry, 77(5): 685-688.
Pankow, J.F., Cherry, J.A., 1996. Dense Chlorinated Solvents and Other DNAPLs in Groundwater Waterloo. Press. Portland, OR., 522 pp.
Pernaton, E., Prinzhofer, A., Schneider, F., 1996. Reconsideration of methane isotope signature as a criterion for the genesis of natural gas - Influence of migration on isotopic signatures. Revue De L Institut Francais Du Petrole, 51(5): 635-651.
Plimpton, S., 1995. Fast parallel algorithms for short-range molecular dynamics. Journal of computational physics, 117(1): 1-19.
Plimpton, S., 2005. LAMMPS user's manual. Sandia National Laboratory.
Rapaport, D.C., 2004. The art of molecular dynamics simulation. Cambridge university press.
Richter, F.M. et al., 2006. Kinetic isotopic fractionation during diffusion of ionic species in water. Geochimica et Cosmochimica, 70: 277 - 289.
Ryckaert, J.-P., Ciccotti, G., Berendsen, H.J., 1977. Numerical integration of the cartesian equations of motion of a system with constraints: molecular dynamics of n-alkanes. Journal of Computational Physics, 23(3): 327-341.
Schloemer, S., Krooss, B.M., 2004. Molecular transport of methane, ethane and nitrogen and the influence of diffusion on the chemical and isotopic composition of natural gas accumulations. Geofluids, 4(1): 81-108.
Wanner, P., Hunkeler, D., 2015. Carbon and chlorine isotopologue fractionation of chlorinated hydrocarbons during diffusion in water and low permeability sediments. Geochimica et Cosmochimica Acta, 157: 198-212.
Wasserman, E., Wood, B., Brodhol, J., 1995. The static dielectric constant of water at pressures up to 20 kbar and temperatures to 1273 K: Experiment, simulations, and empirical equations. Geochimica et cosmochimica acta, 59(1): 1-6.

Wiedemeier, T.H., 1999. Natural attenuation of fuels and chlorinated solvents in the subsurface. John Wiley & Sons.
Wilson, M.A., Pohorille, A., Pratt, L.R., 1985. Molecular dynamics test of the Brownian description of Na+ motion in water. The Journal of chemical physics, 83(11): 5832-5836.
Yamaguchi, T., Matsuoka, T., Koda, S., 2005. Molecular dynamics simulation study on the transient response of solvation structure during the translational diffusion of solute. Journal of Chemical Physics, 122(1).
Zhang, T.W., Krooss, B.M., 2001. Experimental investigation on the carbon isotope fractionation of methane during gas migration by diffusion through sedimentary rocks at elevated temperature and pressure. Geochimica Et Cosmochimica Acta, 65(16): 2723-2742.

Chapter 5: Investigations of sorption effects on isotope ratios during diffusion of chlorinated hydrocarbons in low permeability sediments

To be submitted to Geochimica and Cosmochimica Acta

Philipp Wanner, Beth L. Parker, Steven W. Chapman, Ramon Aravena and Daniel Hunkeler

Abstract

This study aims to investigate the effect of sorption on isotope ratios of chlorinated hydrocarbons migrating through the subsurface under field conditions. For that purpose concentration and isotope (carbon and chlorine) ratio profiles were determined in saturated low permeability sediments below two DNAPL sources (1,2-DCA and DCM), which were emplaced artificially as a part of a long-term controlled release field experiment 15.5 years (5672 days) ago. Low permeable units are superior to aquifers for investigating sorption induced isotope fractionation under field conditions as the advancing concentration front, where isotope fractionation due to sorption is predicted, can be localized precisely and sampled at a high spatial resolution. Isotope trends in opposite directions were observed below the DNAPL sources, whereby carbon isotope ratios of 1,2-DCA and DCM became heavier ($\Delta\delta 13C$=2.0‰ and 2.4‰, respectively) and chlorine isotope ratios of 1,2-DCA became lighter with depth ($\Delta\delta 37Cl$=1.3‰). A simulation scenario considering only diffusive isotope fractionation failed to reproduce the opposite isotope trends. When sorption induced isotope fractionation was also considered based on laboratory-derived isotope fractionation factors, the model reproduced the data well. Hence, the observed isotope trends reflect a superposition between competing isotope effects due to sorption and diffusion. For chlorine the diffusive isotope effect is larger than for carbon due to the mass difference of two between the stable isotopes overruling the sorption effect, while for carbon the sorption effect dominates. The observed shifts of isotope ratios due to sorption are in the range of the threshold value of 2‰ set by the US EPA for identifying reactive processes. Numerical modelling showed that under specific conditions (strong sorption behavior, early transient diffusion) even higher shifts of isotope ratios can occur. Hence, when shifts of isotope ratios in the range of 2‰ are observed under field conditions their attribution to reactive processes should be made with caution. This is especially crucial for slow reactive processes associated with small isotope fractionation factor as for instance the degradation of BTEX.

5.1. Introduction

Chlorinated hydrocarbons are frequent subsurface contaminants at many polluted sites throughout the world (Aelion et al., 2010; Pankow and Cherry, 1996). As a result of improper disposal and accidental spills, chlorinated hydrocarbons are often released at the surface as dense non-aqueous phase liquid (DNAPL) and migrate downwards into aquifer systems due to their high mobility (high density, low viscosity) (Pankow and Cherry, 1996; Schwille, 1988). Chlorinated hydrocarbons tend to accumulate on top of low permeability layers (e.g. aquitards) and are slowly dissolved creating a persistent contaminant plume (Hwang et al., 2008; Kueper et al., 1993). With increasing time, the accumulated chlorinated hydrocarbons are transported by diffusion into the underlying low permeability layer (Chapman and Parker, 2005; Parker et al., 2008). During the migration in aquifers and low permeable units, chlorinated hydrocarbons are retarded due to sorption, which affect the migration rate and spreading of the contaminants (Allen-King et al., 1996; Parker et al., 1994; Rivett and Allen-King, 2003).

Stable isotope methods have been widely applied to gain insight into the origin and fate of organic compounds in the subsurface (Elsner et al., 2005; Harrington et al., 1999; Huang et al., 1999; Hunkeler et al., 2011; Hunkeler et al., 2005; Hunkeler et al., 1999; Jeannottat and Hunkeler, 2012; Jeannottat and Hunkeler, 2013; Lollar et al., 1999; Meckenstock et al., 2004; Wanner and Hunkeler, 2015; Wanner et al., 2016). Researchers have shown that aqueous phase diffusion can cause isotopic fractionation in aquifer – aquitard systems (Wanner and Hunkeler, 2015). However, there is currently no consensus on whether sorption results in significant isotope fractionation under field conditions, partly due to the lack of field data at sufficiently high spatial resolution. In analytical chemistry it is known that liquid chromatographic separation of organic compounds is associated with an isotope effect, whereas light isotopes are preferentially sorbed on the stationary phase leading to an enrichment of heavy isotopes in the mobile phase (Caimi and Brenna, 1993; Caimi and Brenna, 1997; Filer, 1999; Klein et al., 1964; Poulson et al., 1997). In contrast, less is known about isotope effects of chlorinated hydrocarbons during sorption processes in natural systems. Some laboratory studies suggested that sorption might not significantly change isotope ratios (Schüth et al., 2003; Slater et al., 2000), while others provided evidence that sorption induced isotope fractionation is significant (Höhener and Yu, 2012; Imfeld et al., 2014; Kopinke et al., 2005). To extrapolate the magnitude of isotope fractionation due to

sorption from laboratory to field studies, modeling studies have been used so far (Höhener and Atteia, 2010; Liu et al., 2016; Van Breukelen and Prommer, 2008). The simulations revealed a significant isotope effect due sorption, especially at the fringe of contaminant plumes, which potentially complicates the assessment of reactive processes using isotope methods (Van Breukelen and Prommer, 2008). However, verification of the modelling results is challenging, as it is difficult to localize and to sample the plume fringe, where isotope fractionation is predicted, at sufficient high spatial resolution. Furthermore, at the plume fringe, isotope fractionation might also occur due to mixing enhanced degradation and diffusion across the steep concentration gradient, which complicates an unequivocal attribution of isotope patterns to sorption. In contrast to aquifers, low permeability aquitards offer several advantages for investigating sorption induced isotope fractionation, since: a) the diffusion front can be targeted very precisely and at a very high spatial resolution, b) the retardation due to sorption is expected to be stronger due to the higher organic carbon content typical of fine-grained clay-rich sediments (i.e. clayey aquitards) compared to granular aquifers, and c) the transport mechanisms are well constrained, while in case of dispersion in sandy aquifers, the diffusion contribution often remains unclear, which introduces greater uncertainty in the data evaluation.

This study aims to investigate, whether sorption has a significant influence on isotope ratios of chlorinated hydrocarbons under field conditions. The study was done as part of a long-term release field experiment on diffusion transport over a range of time-scales to evaluate variability of effects of various natural processes on transport in fate in natural clay rich sediments. The field experiment was created by emplacing between 1.5 and 2.0 liters of different chlorinated solvents (PCE, TCE, DCM, 1,2-DCA and TCE/DCM mixture) as DNAPL, into a well characterized (Johnson et al., 1989; Parker, 1996) low-permeability, clay-rich sediment, where significant sorption occurs due to high organic carbon content (Allen-King et al., 1995; Allen-King et al., 1996; Allen-King et al., 1997). The DNAPL sources were emplaced at the bottom of drilled boreholes at 10 – 12 m depth below ground surface (bgs), below the water table, where no visible fractures were present. For the present study cores are retrieved 15.5 years (5672 days) after DNAPL emplacement beneath the 1,2-DCA and the DCM DNAPL sources and subsampled at depth-specific points for detailed concentration and carbon and chlorine isotope ratios to assess changes due to sorption during the diffusive migration of the chlorinated hydrocarbons. For field data interpretation, isotope fractionation factors for sorption and diffusion

are determined on uncontaminated samples of the sediment in the laboratory and included in a numerical model to simulate observed isotope ratio profiles. Finally, conclusions are drawn as to what extent isotope fractionation due to sorption impairs the identification of reactive processes using stable isotope methods.

5.2. Materials and Methods

5.2.1. Multistep sorption experiment

In the laboratory, isotope fractionation due to sorption was quantified using a multistep approach, which leads to a higher shift of isotope ratios and thus, to a higher precision of the determined isotope fractionation factor compared to a single step batch experiment. Two replicates of multistep sorption experiments were performed for 1,2-DCA and DCM with initial concentrations of 7226 mg/L and 5983 mg/L for 1,2-DCA and of 572 mg/L and 745 mg/L for DCM, respectively. The experiment included five sorption steps until the concentration in the solution was too low to determine the concentration and isotope ratios. In a 42 mL vial, 30 mL of solution with 1,2-DCA or DCM were mixed with 15 g of dry uncontaminated clay from the field site (see site description below). The vials were shaken on a rotary shaker for 24 hours. After each sorption step, an aliquot (4 mL) of the solution was removed from the vials for concentration and isotope ratio analyses and 10 mL of the solution removed from the vial to be added to the subsequent 42 mL vial containing a new 15 g dry sample of clay for the next sorption step. The solution in the following vial was topped up to 30 mL with deionized water in order to keep a constant volume of solution during each step. The isotope fractionation factor due to sorption was determined using the equation for multistep experiments derived by Kopinke et al. (2005), Voskamp (2004) and Imfeld et al. (2014):

$$\alpha_{sorption} = \frac{{}^{H}K_d}{{}^{L}K_d} \approx 1 + \Delta\delta_i / \left[1000m(1 - X_{dissovled})\right] \quad (5\text{-}1)$$

where ${}^{H}K_d$ and ${}^{L}K_d$ are the carbon-pore water partitioning coefficients for the heavy and light isotope, respectively, $\alpha_{sorption}$ refers to the fractionation factor due to sorption, $\Delta\delta_i = \delta_{i,final} - \delta_{i,intial}$ refers to the total shift of isotope ratios during the multistep experiment, m corresponds to the

number of identical sorption steps and ($1 - X_{dissolved}$) is the average amount adsorbed after each sorption step.

5.2.2. Diffusion cell experiment

In addition to sorption, the isotope effect due to aqueous phase diffusion was also quantified, which is required for interpretation of the field profile isotope data given the simultaneous occurrence of diffusion and sorption in saturated low permeability sediments. The magnitude of isotope fractionation due to aqueous phase diffusion was quantified using a modified Stokes' diffusion cell as described by Wanner and Hunkeler (2015). For the present study the diffusion cell experiment was performed for DCM, while for 1,2-DCA the previously reported value was used (Wanner and Hunkeler, 2015). The modified Stokes' diffusion cell corresponds to a Rayleigh type experiment, where isotopically heavy and light species are transported by diffusion out of a source reservoir through a small pore sized frit at different diffusive transport rates. The magnitude of isotope fractionation due to differential rates of aqueous phase diffusion was quantified by determining the diffusion coefficient ratios between isotopically distinct species using the Rayleigh equation:

$$\left[ln\left(R_t/R_0\right)\right]\times 1000 = \left(\frac{D_{0,H}}{D_{0,L}} - 1\right)\times 1000\, ln\, f \qquad (5\text{-}2)$$

where R_t is the isotope ratio at time t in the source reservoir, R_0 refers to the initial isotope ratio in the source reservoir, $D_{0,H}/D_{0,L}$ is the ratio between diffusion coefficient of the heavy and the light isotope, respectively in free solution and f corresponds to the remaining fraction in the source reservoir.

5.2.3. Site description and emplaced source field experimental procedure

A detailed description of the controlled release field experiment is provided in section S1.1. of the Supporting Information at the end of this chapter. In brief, the controlled release field experiment was carried out at a permitted hazardous waste disposal site, 15 km southeast from Sarnia and 300 km west of the city of Toronto in Ontario, Canada in the St. Clair clay plain (Fig. 5-1A).

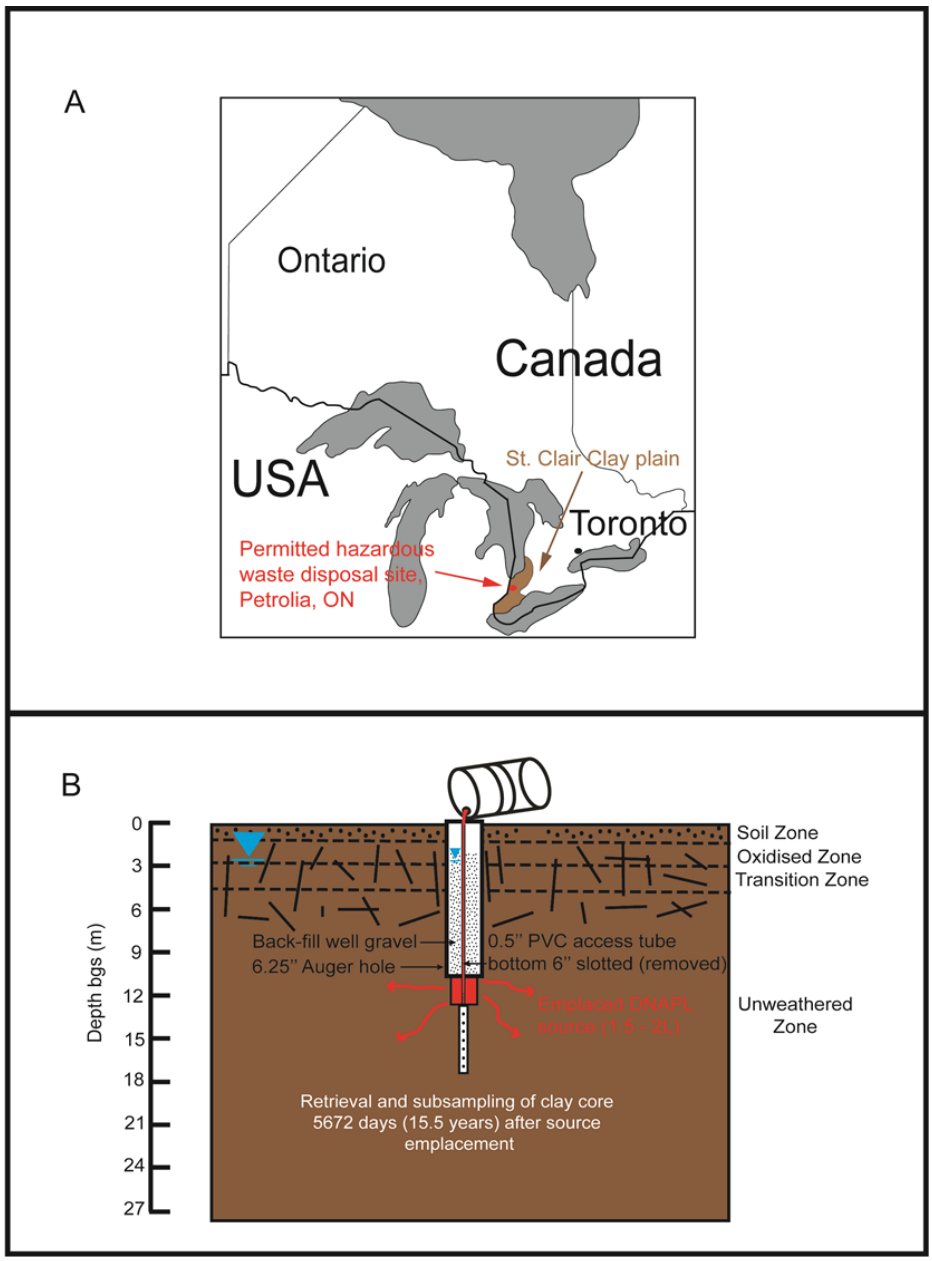

Figure 5-1. Location of emplaced source field experiment at the permitted hazardous waste disposal site in Petrolia, Ontario (Fig. 5-1A) in the St. Clair clay plaine (outlined based on Johnson et al., 1989). (Fig, 5-1B), A across section of the experimental setup for multiple-year solute diffusion from a constant source concentration (with DNAPL present to ensure aqueous solubility in the adjacent pore water) (Fig. 5-1B).

At the site, an experimental area was established outside of the active disposal area, with the goal of conducting long-term emplaced source experiments in saturated low permeability sediments of the St. Clair clay plain (Fig. 5-1A). The well-characterized, regionally extensive saturated clay unit of the St. Clair Clay Plain underlying this area (Allen-King et al., 1996; Desaulniers et al., 1985; Johnson et al., 1989; McKay and Fredericia, 1995; Myrand et al., 1992; Parker, 1996) can be divided into a weathered upper clay unit with a thickness of about 2.5 to 3.5 meters, transitioning to unoxidized clay with oxidation staining along fractures to a depth of 6 to 7 m blow ground surface (bgs), underlain by a non-weathered, unfractured lower unit with a thickness of about 30 meters in which the experiment was carried out (Fig. 5-1B). The high organic matter content of the aquitard unit (0.534% ± 0.241%; n=36) strongly retards the migration of organic contaminants due to sorption processes, with no evidence of degradation occurring over the time-scales of previous studies (Allen-King et al., 1996; Parker, 1996). To perform the field experiment, different DNAPL sources (PCE, TCE, DCM, 1,2-DCA and TCE/DCM mixture) with a volume of between 1.5 and 2.0 liters were emplaced approximately 5 m apart in November 1998 in the non-weathered clay at depths of 10 to 12 meters bgs (Fig. 5-1B) in holes created with large diameter Shelby tubes for minimal disturbance.

5.2.4. Core retrieval, subsampling and VOC extractions

A detailed description of core retrieval, core subsampling and VOC extraction from core subsamples is provided in sections S1.2. and S1.3. of the Supporting Information at the end of this chapter. Briefly, continuous cores were collected from the unweathered clay below the 1,2-DCA and DCM DNAPL – sediment interface from the boreholes in June 2014, 15.5 years (5672 days) after source emplacement. The cores were retrieved using a direct push rig using the Envirocore dual tube continuous coring system described by Einarson et al. (1998). After bringing the cores to the surface, the percent recovery was recorded and core tubes were split in half longitudinally and subsampled in the field as a function of depth with narrow spaced sampling points (~5 cm) to gain highly resolved depth discrete chlorinated hydrocarbon concentration and isotope profiles. Subsequently, chlorinated hydrocarbons were extracted into the methanol following the description by Parker (1996) and White et al. (2008). The DCM and 1,2-DCA pore water concentrations were determined based on the measured total concentration using the following partitioning equation (Parker et al., 2004):

$$C_e = C_{tot} \frac{\rho_{wet}}{R \cdot \Phi} \quad (5\text{-}3)$$

where C_e (mg/L) is the pore water concentration, C_{tot} (mg/kg) corresponds to the measured total (sorbed and dissolved) concentration in the clay derived directly from the laboratory extraction, ρ_{wet} (g/cm^3) refers to the sediment wet bulk density, ϕ (–) refers to the clay porosity, R (-) corresponds to the non-linear retardation factor (eq. S5-5, Supporting Information) as justified by our multistep sorption experiment (see below in section 5.4.1.) and ρ_{dry} (g/cm^3) refers to the dry bulk density. Parameter values used to estimate pore water concentrations were taken from a previous study at the site (Parker, 1996) (Tab. 5-1, Supporting Information).

5.2.5 Concentration and compound-specific isotope analysis (CSIA)

Detailed descriptions of analytical methods are available in section S1.4. of the Supporting Information at the end of this chapter. In brief, chlorinated hydrocarbon concentrations in laboratory samples (multistep sorption and diffusion experiment) and in the methanol extracts of the field samples were analyzed by a gas chromatograph coupled to a mass spectrometer (GC-MS). Compound-specific carbon isotope ratios of 1,2-DCA and DCM were analyzed relative to a CO_2 standard by a gas chromatograph coupled to an isotope mass spectrometer (GC-IRMS) and expressed in the delta notation (VPDB $\delta = (R/R_{std} - 1)*1000$ (‰), where R and R_{std} are the isotope ratios of the sample and the standard, respectively. The analytical uncertainty for samples from the laboratory multistep sorption and diffusion experiment (standard deviation of the mean: $SDM=1\sigma/(n)^{1/2}$ σ: standard deviation n: sample number) was determined based on a triplicate measurement. In contrast, field samples were analyzed only twice due to the limited sample volume. Thus, the standard deviation of the mean (±SDM) for the field samples was estimated based on the standard deviation (1σ) of standards included in the samples sequence (σ=0.32‰, n=12). Compound-specific chlorine isotope ratios were analyzed using a gas chromatograph coupled to a quadrupole mass spectrometer (GC-qMS). Compound-specific chlorine isotope ratios were exclusively determined for 1,2-DCA, since no standards referenced to the SMOC scale (standard mean ocean water) are available for DCM. The 1,2-DCA chlorine isotopic raw ratios were determined from the two most abundant fragment ion peaks (m/z 64 and 62) (Palau et al., 2014; Wanner and Hunkeler, 2015) using an equation that

relates fragment ratios to isotope ratios for symmetric molecules developed by Elsner and Hunkeler (2008):

$$\left(\frac{^{37}Cl}{^{35}Cl}\right)_{1,2-DCA} = \frac{I_{64}}{I_{62}} \quad (5\text{-}4)$$

where I is the corresponding fragment ion abundance of 1,2-DCA at different m/z values.
The raw chlorine isotope ratios from 1,2-DCA fragments (eq. 5-4) were calibrated against two external standards having different chlorine isotopic ratios (CHYN1 = 6.30‰ and CHYN2 = -0.84‰) to obtain delta values on the SMOC scale. The standards were characterized by the Holt method (Holt et al., 1997) at the Helmholtz Centre in Munich. The analytical uncertainty (±SDM) of each 1,2-DCA measurement was based on a tenfold measurement of each sample from two different vials (5 replicates from each vial).

5.3. Numerical modelling

The migration of chlorinated hydrocarbons in the clayey unit was simulated in 3 dimensions by rotating a 2D numerical modeling domain around a vertical axis (Fig. S5-1, Supporting Information). A detailed description of such a 2D axisymmetrical numerical model is provided by Jin et al. (2012). The aim of the simulation was to assess a) how isotope fractionation due to sorption and diffusion are reflected in isotope ratio profiles in saturated low permeability sediments, and b) whether observed shifts of carbon and chlorine isotope ratios are reproducible with laboratory determined isotope fractionation factors for diffusion and sorption. A detailed description of the 2D axisymmetrical model is available in section S2. of the Supporting Information at the end of this chapter. Briefly, it has been assumed that the transport is diffusion dominated and that advective transport can be neglected, consistent with previous studies of organic contaminant transport at the site (Johnson et al., 1989; Myrand et al., 1992; Parker, 1996). Sorption was represented by the non-linear Freundlich isotherm as justified by our multistep sorption experiment (see below in section 5.4.1.) and by previous studies at the site for

similar chlorinated hydrocarbon compounds (Allen-King et al., 1996; Allen-King et al., 1997; Johnson et al., 1989; Myrand et al., 1992).

To simulate isotope ratio profiles of 1,2-DCA and DCM, isotopocules were considered as fractionation occurs between species of chlorinated hydrocarbon that differ in their isotopic composition and not between isolated isotopes. The term isotopocules encompasses isotopologues (molecules differing in isotopic composition) as well as isotopomers (molecules having the same number of isotopes but at different positions). Each 1,2-DCA and DCM carbon and 1,2-DCA chlorine isotopocules differing by one heavy isotope was defined as individual species in the model database (Tabs. S5-2 and S5-3 in Supporting Information). To account for isotopocule fractionation due to aqueous phase diffusion and sorption during the migration in the water-saturated clay, different Freundlich constants (K_{Fr}) and diffusion coefficients were assigned to each carbon and chlorine isotopocule differing in one heavy isotope (see section S2.1. in Supporting Information). The different Freundlich constants and diffusion coefficients were determined based on experimentally derived isotope fractionation factors for sorption and diffusion, which are proportional to the ratio of diffusion coefficients and Freundlich constants for isotopocules differing by one heavy isotope (Wanner and Hunkeler, 2015) (Tab. 5-2). To compare modelled isotopocule ratios with measured isotope ratio profiles, carbon and chlorine isotopocules differing by one heavy isotope were simulated in separate runs and converted to isotope ratios by making use of the proportional behavior during the migration in low permeability sediments between isotopes and isotopocule pairs differing in one heavy isotope (Wanner and Hunkeler, 2015):

$$\delta^{37}Cl_{1,2-DCA}(z) = \left(\frac{\frac{I_{100}(z) + 2I_{102}(z)}{2I_{98}(z) + I_{100}(z)}}{R_{SMOC}} - 1 \right) \cdot 1000 \tag{5-5}$$

$$\delta^{13}C_{1,2-DCA}(z) = \left(\frac{\frac{I_{100}(z) + 2I_{101}(z)}{2I_{99}(z) + I_{100}(z)}}{R_{VPDB}} - 1 \right) \cdot 1000 \tag{5-6}$$

$$\delta^{13}C_{DCM}(z) = \left(\frac{\frac{I_{88}(z)}{I_{87}(z)}}{R_{VPDB}} - 1 \right) \cdot 1000 \qquad (5\text{-}7)$$

where $\delta^{13}C$ and $\delta^{37}Cl$ are the carbon and chlorine delta values as a function of depth, I_x refers to the isotopocule abundance as a function of depth and R_{VPDB} and R_{SMOC} correspond to the international reference standard for carbon ($^{13}C/^{12}C$=0.011237) and chlorine ($^{37}Cl/^{35}Cl$=0.32) isotope ratios, respectively (Aelion et al., 2010).

To prevent boundary effects, the size of the rotating 2D numerical model domain was built sufficiently large (5 meters length and 1 meter width) (Fig. S5-1, Supporting Information). The initial concentration boundary condition at the location, where the DNAPL was present corresponded to the literature reported solubility limits for 1,2-DCA (8,690 mg/L (Wiedemeier, 1999)) and DCM (15,400 mg/L (Wiedemeier, 1999)), respectively; while at the other end and on the vertical side of the modeling domain the boundary concentration was set to zero. The abundance of carbon and chlorine isotopocules differing by one heavy isotope of 1,2-DCA and DCM used in the boundary conditions, was determined based on the measured isotope ratios adjacent to the source zone using a binominal distribution combining the occurrence of both C and Cl isotopes as proposed by Jin et al. (2013) (Tabs. 5-2 and 5-3, Supporting Information). Model calibration was conducted against measured concentration profiles, while the isotope ratio profiles were predicted based on the laboratory derived enrichment factors for diffusion and sorption without further calibration. Calibration of concentration profiles was conducted by varying the tortuosity factor, by setting the point in time when the boundary concentrations started to decrease (due to DNAPL exhaustion) and by the extent of the boundary concentration decrease at the location, where the DNAPL was present. To quantify the quality of the fit between measured and modeled data, the Nash Sutcliff efficiency (NSE) was used. NSE values range between -∞ and 1, while 1 indicates a perfect fit between measured and modelled data.

5.4. Results

5.4.1. Multistep sorption experiment

During the performance of the multistep sorption experiment the aqueous-phase concentration dropped by about six orders of magnitude compared to the initial concentration due to the sorbed mass on the clay after each sorption step (Figs. 5-2A and 5-2B). The mass distribution between the clay sediment and aqueous solution for both 1,2-DCA and DCM agreed well with the Freundlich isotherm (Freundlich, 1909) (Figs. 5-2A and 5-2B):

$$\log q_e = \log K_{Fr} + \frac{1}{N} C_e \qquad (5\text{-}8)$$

where q_e (mg/kg-dry) and C_e (mg/L) are the equilibrium sorbed and solution concentrations, respectively, K_{Fr} ($mg^{1-1/n}\ kg^{-1}\ L^{1/n}$) refers to the Freundlich sorption coefficient and 1/N (-) is an empirical exponent indicating the degree of non-linearity.

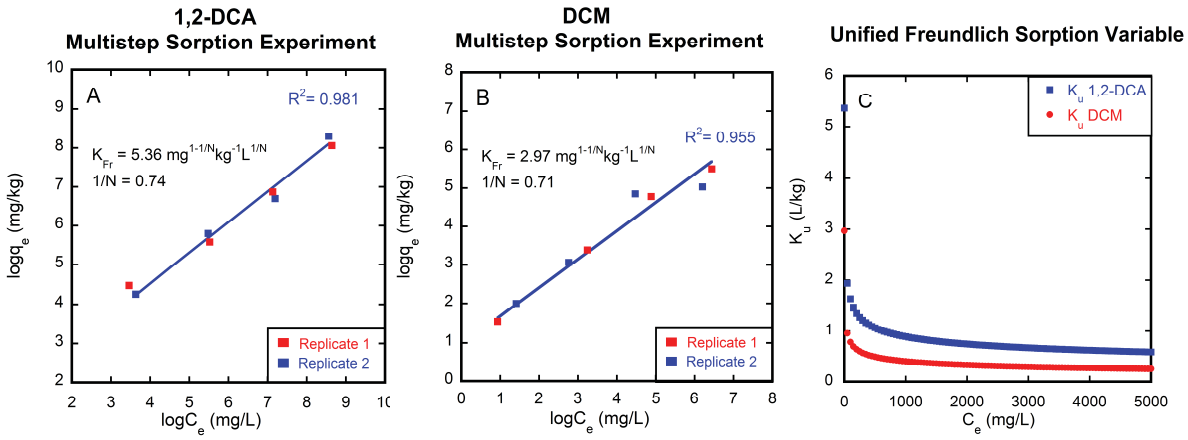

Figure 5-2. Concentration in solution Ce (mg/L) vs. the sorbed concentration on the clay qe (mg/kg-dry) for 1,2-DCA (Fig. 5-2A) and for DCM (Fig. 5-2B). Freundlich isotherm parameter (K_{Fr} and 1/N) for 1,2-DCA and DCM were determined by using linear regression. Comparison of the sorption behavior of 1,2-DCA and DCM using the unified Freundlich variable K_u (eq. 5-9) as a function of the concentration in solution (Ce) (Fig. 5-2C).

This indicates that the sorption behavior of 1,2-DCA and DCM behaves non-linearly at the site i.e. is stronger at low compared to high pore water concentrations. The determination of the Freundlich isotherm parameters (K_{FR} and 1/N; eq. 5-8) exhibited values of 5.36±0.35 $mg^{1-1/n}\,kg^{-1}\,L^{1/n}$ for 1,2-DCA and of 2.97±0.33 $mg^{1-1/n}\,kg^{-1}\,L^{1/n}$ for DCM (Tab. 5-1) for the Freundlich constant and a slightly stronger non-linear behavior for DCM (1/N=0.71±0.08) compared to 1,2-DCA (1/N=0.74±0.05) (Tab. 5-1). It has been demonstrated that Freundlich constants (K_{Fr}) with different 1/N values are not comparable as its value is directly dependent on 1/N. (Chen et al., 1999). Hence, to compare the sorption behavior of 1,2-DCA and DCM, the unified Freundlich sorption variable (K_u) was determined (Chen et al., 1999), which corresponds to the slope of the Freundlich isotherm:

$$K_u = \frac{K_{Fr}}{C_e^{(N-1)/N}} \tag{5-9}$$

where K_u (L/kg) is the unified sorption variable for Freundlich isotherms. and 1/N (-) is the empirical exponent indicating the degree of non-linearity.

The calculated K_u values (eq. 5-9) for concentrations between 0 and 5000 mg/L indicate that 1,2-DCA sorbs stronger than DCM on the clay at the Laidlaw hazardous waste disposal site (Fig. 5-2C), which is consistent with the higher value of the carbon-pore water partitioning coefficient (K_{OC}) for 1,2-DCA compared to DCM (Mabey et al., 1982).

Table 5-1. Determined parameters for the Freundlich isotherm for the clay unit at the Sarnia site. Uncertainty of Freundlich constant (K_{Fr}) and exponent (1/N) was determined based on the 95% confidence interval of the regression line (eq. 5-8).

Compound	**K_{Fr} ($mg^{1-1/N}\,kg^{-1}\,L^{1/n}$)**	**1/N (-)**
1,2-DCA	5.36±0.35	0.74±0.05
DCM	2.97±0.33	0.71±0.08

During the multistep sorption experiment 1,2-DCA and DCM became increasingly enriched in heavy carbon and chlorine isotopes after each sorption step (Figs. 5-3A-C) showing that 1,2-DCA and DCM isotopocules with light isotopes are preferentially sorbed compared to isotopocules with heavy isotopes. To quantify the isotope fractionation factor for sorption

following the Freundlich isotherm, the term $^{H}K_d/^{L}K_d$ in equation 5-1 was replaced by the ratio of the unified Freundlich sorption variable $^{H}K_u/^{L}K_u$ for the heavy and the light isotope, respectively:

$$\alpha_{sorption} = \frac{^{H}K_u}{^{L}K_u} = \frac{\frac{^{H}K_{Fr}}{C_e^{(N-1)/N}}}{\frac{^{L}K_{Fr}}{C_e^{(N-1)/N}}} = \frac{^{H}K_{Fr}}{^{L}K_{Fr}} \approx 1 + \Delta\delta_i / [1000m(1 - X_{dissovled})] \qquad (5\text{-}10)$$

where $^{H}K_{Fr}$ and $^{L}K_{Fr}$ ($mg^{1-1/N}\ kg^{-1}\ L^{1/N}$) are the Freundlich constants for the heavy and light isotope, respectively.

Equation 5-10 shows that the isotope fractionation factor for sorption according to the Freundlich isotherm reduces to the ratio of the Freundlich constants $^{H}K_{Fr}/^{L}K_{Fr}$ of the heavy and light isotope, respectively.

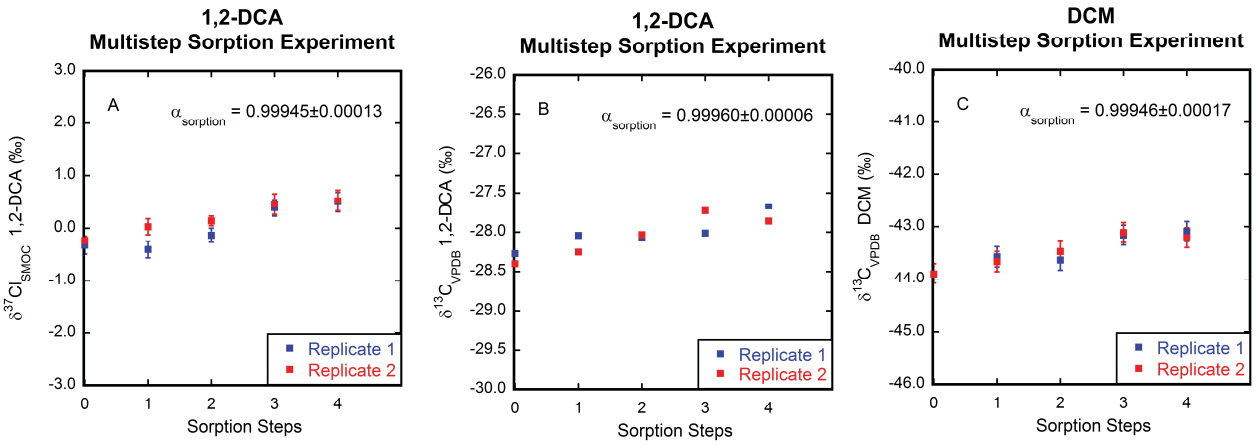

Figure 5-3. Determination of the fractionation factor due to sorption for chlorine (Fig. 5-3A) and carbon (Fig. 5-3B) isotopes of 1,2-DCA and for DCM carbon isotopes (Fig. 5-3C). Error bars indicate analytical measurement uncertainty (standard error of the mean: SDM=1σ/(n)1/2 σ: standard deviation n: sample number). For 1,2-DCA carbon isotopes (Fig. 5-3B) the error was smaller than the size of the symbols in the plot. The uncertainty of the sorption fractionation factor was determined using the Gaussian error propagation law in equation 5-8 by including the uncertainty (±SDM) of the isotope ratio and the remaining fraction measurements after each sorption step.

For 1,2-DCA a lager enrichment of heavy chlorine compared to carbon isotopes was observed during the multistep sorption experiment resulting in isotope fractionation factors of $\alpha_{Cl,sorption}$ = 0.99945±0.00006 (eq. 5-10) ($\varepsilon_{Cl,sorption}$ = -0.55‰; whereas $\varepsilon = (\alpha - 1) \cdot 1000$) and $\alpha_{C,sorption}$ = 0.99960±0.00014 ($\varepsilon_{C,sorption}$ = -0.40‰), respectively (Tab. 5-2). For DCM the enrichment of heavy carbon isotope was larger compared to 1,2-DCA with a fractionation factors of $\alpha_{C,sorption}$ = 0.99946±0.00017 ($\varepsilon_{C,sorption}$ = -0.54‰) (Tab. 5-2).

Table 5-2. Carbon and chlorine isotope fractionation factors for diffusion and sorption for 1,2-DCA and DCM. Uncertainty of determined diffusion induced isotope fractiationation factor was calculated based on the 95% confidence interval of the regression line (eq. 5-2). Uncertainty of the isotope fractionation factors due to sorption was calculated based on the twofold performance of the sorption experiment and by including the uncertainty (standard error of the mean) of the isotope ratio and the remaining fraction measurements after each sorption step (eq. 5-10).

Compound	**Isotopocule type**	**Fractionation factor diffusion ($\alpha_{Diffusion}=D_i/D_j$)**	**Fractionation factor sorption ($\alpha_{Sorption}=K_{Fr,i}/K_{Fr,j}$)**
1,2-DCA	Carbon	$\alpha_{Diffusion}$= 0.99977±0.00004[1]	$\alpha_{Sorption}$ = 0.99960±0.00014[2]
	Chlorine	$\alpha_{Diffusion}$= 0.99939±0.00003[1]	$\alpha_{Sorption}$==0.99945±0.00006[2]
DCM	Carbon	$\alpha_{Diffusion}$=0.99972±0.00009[2]	$\alpha_{Sorption}$= 0.99946±0.00017[2]

[1]Determined in chapter 3.
[2]Determined in this chapter.

5.4.2. Diffusion cell experiment

The initial and final concentration after each time series of the diffusion cell experiment was used to determine the effective diffusion coefficient (D_e) according to equations 3-7 and 3-10 in chapter 3. The ratio between initial and final DCM aqueous concentration ranged between 0.19 and 0.86 for the different time series of the diffusion cell experiments (Tab. 5-3). The average effective diffusion coefficient for DCM of the different time series was 1.06E-10 ± 1.78E-12 (m^2/s) (Tab. 5-3), which is lower than the diffusion coefficients in free solution (1.17E-09 m^2/s (USEPA, 1989)) as the frit reduces the diffusive transport rate due to porosity and tortuosity effects (eq. S5-4, Supporting Information). During the performance of the experiment an enrichment of heavy DCM carbon isotopes in the source reservoir was observed. This indicates that the DCM carbon isotopocules with light isotopes diffuses faster out of the source reservoir than isotopocules with heavy carbon isotopes. The magnitude of DCM carbon isotope fractionation due to diffusion was quantified from the slope of the regression line using the

Rayleigh equation (eq. 5-2), resulting in an isotope fractionation factor of $\alpha_{C,diffusion}$ = 0.99972±0.00009 ($\varepsilon_{C,diffusion}$ = -0.28‰) (Fig. 5-4).

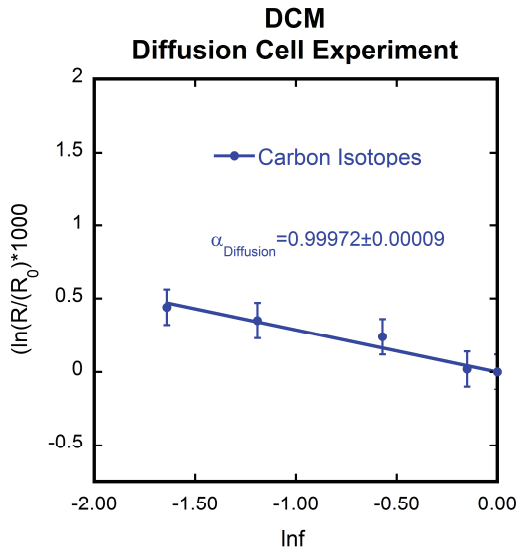

Figure 5-4. Rayleigh plot for DCM carbon isotope fractionation in the source reservoir of the diffusion cell experiment. Error bars indicate analytical uncertainty (standard error of the mean: SDM=1σ/(n)1/2 σ: standard deviation n: sample number) of measurements. Uncertainty of diffusion induced isotope fractionation factor was calculated based on the 95% confidence interval of the regression line.

Table 5-3. Effective diffusion coefficients and De/D_0 ratios of DCM for the diffusion cell experiment. Uncertainty of average diffusion coefficient was calculated using the standard error of the mean (±SDM).

Initial (mg/L)	Final (mg/L)	Fraction	Time (d)	Effective diffusion coefficient (m^2/s)	Average effective diffusion coefficient (m^2/s)	De/D_0	De/D_0 Average
15.5	8.8	0.566	10.1	1.10E-10		0.09	
58.8	50.7	0.862	3.3	8.86E-11		0.08	
324	98.4	0.303	22.3	1.04E-10		0.09	
416	80.4	0.193	25.9	1.23E-10	1.06E-10±1.78E-12	0.11	0.09

5.4.3. Concentration and compound-specific isotope profiles beneath the emplaced DNAPL sources

The determined 1,2-DCA and DCM pore water concentration profiles in the clay unit below the emplaced DNAPL sources, which were determined based on the measured total (sorbed and dissolved) concentration (eq. 5-3), showed typical transient-diffusion profiles (Fig. 5-5A). The highest 1,2-DCA pore water concentration (917 mg/L) was determined at 18 cm vertical distance from the emplaced DNAPL source in the clay unit, while the pore water concentration decreased below detection limit (<2µg/L) at 100 cm below the bottom of the emplaced source (Fig. 5-5A). The 1,2-DCA carbon and chlorine isotope ratio profiles showed trends in opposite directions, whereby ^{37}Cl in 1,2-DCA became depleted ($\Delta\delta^{37}Cl$=1.3‰; Fig. 5-5B) and ^{13}C enriched ($\Delta\delta^{13}C$ = 2.4‰; Fig. 5-5C) with increasing depth. The DCM pore water concentration was highest adjacent to the DNAPL source and declined below the detection limit (<2µg/L) at 160 cm distance below the bottom of the emplaced source (Fig. 5-6A). DCM became enriched in ^{13}C with depth to the same extent ($\Delta\delta^{13}C$ = 2.4‰) as 1,2-DCA ($\Delta\delta^{13}C$ = 2.0‰) (Fig. 5-6B).

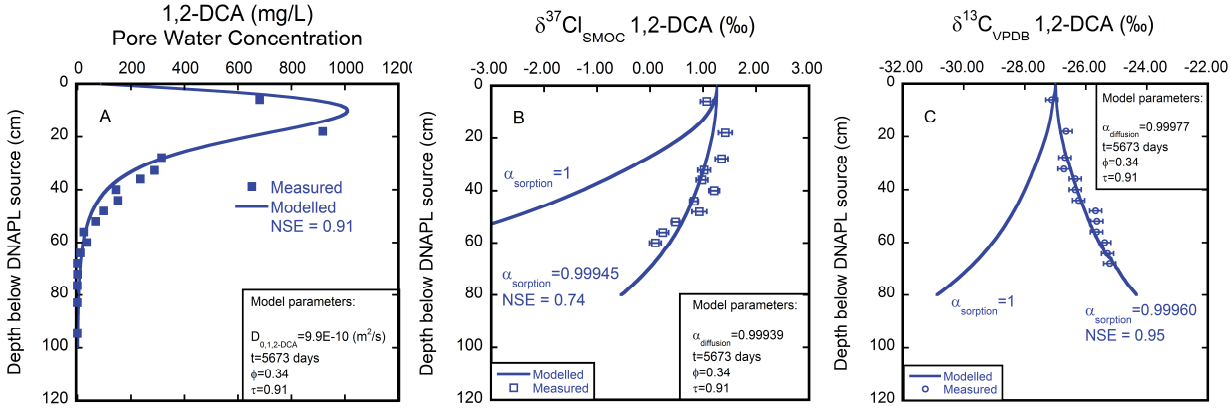

Figure 5-5. Measured and modelled 1,2-DCA pore water concentrations (Fig. 5-5A) and 1,2-DCA chlorine (Fig. 5-5B) and carbon (Fig. 5-5C) isotope ratio profiles vs. vertical distance from the 1,2-DCA DNAPL source in the clay core retrieved 5281 days after emplacement of the 1,2-DCA DNAPL source. The continuous lines represent the modelled concentration and isotope ratio profiles, while the filled squares (Fig. 5-5A), the open squares (Fig. 5-5B) and the open circles (Fig. 5-5C) represent the measured concentrations on depth-discrete samples. For the 1,2-DCA chlorine and carbon isotopes two scenarios were simulated: Diffusion only ($\alpha_{sorption}$ = 1) and a combined scenario that includes diffusion and sorption induced isotope fractionation for 1,2-DCA chlorine ($\alpha_{sorption}$ = 0.99945) and carbon ($\alpha_{sorption}$ = 0.99960) isotopes. The Nash-Sutcliff efficiency (NSE) was used to quantify the quality of the fit between measured and modelled data.

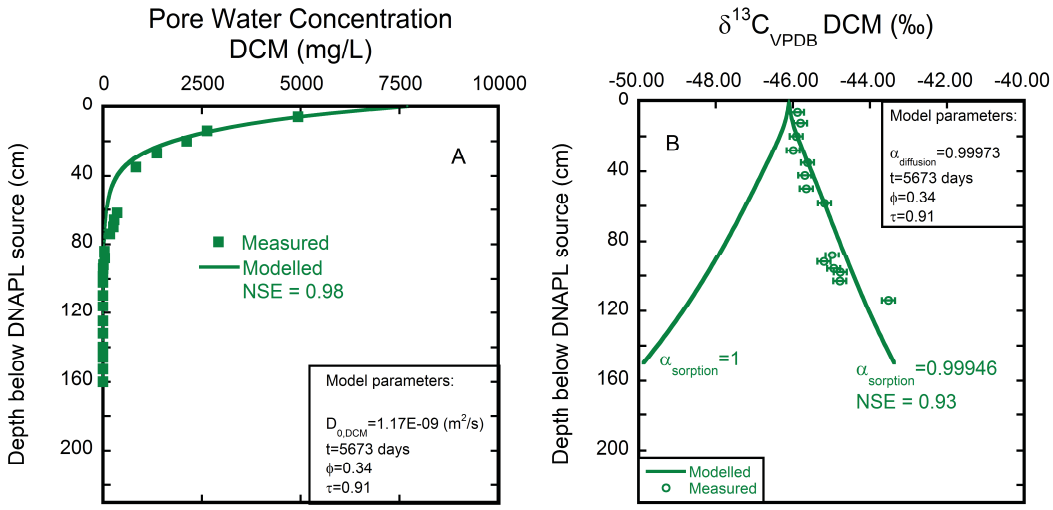

Figure 5-6. Measured and modelled pore water DCM concentration (Fig. 6A) and DCM carbon isotope ratio profiles (Fig. 6B) vs. vertical distance from the DCM DNAPL source in the retrieved clay core 5281 days after emplacement of the DCM DNAPL source. The continuous lines indicate the modelled concentration and isotope ratios profiles, while the filled squares (Fig. 6A) and the open circles (Fig. 6B) represent the measured concentrations for depth-discrete samples. For the DCM carbon isotopes two scenarios were simulated: Diffusion only ($\alpha_{sorption}$ = 1) and a combined scenario, which includes diffusion and sorption induced isotope fractionation ($\alpha_{sorption}$ = 0.99946). The Nash-Sutcliff efficiency (NSE) was used to quantify the quality of the fit between measured and combined simulation scenario

5.5. Discussion

5.5.1. Multistep sorption and diffusion cell experiment

The non-linear sorption behavior in the multistep sorption experiment is consistent with previous studies at the site, which also observed a Freundlich sorption trend with a similar degree of non-linearity (Allen-King et al., 1996; Allen-King et al., 1997). Furthermore, the multistep sorption experiment showed for the first time that isotope fractionation due to sorption occurs not only for carbon but also for chlorine isotopes for organic compounds.

The observed preferential sorption of isotopocules with light isotopes compared to isotopocules with heavy isotopes and the detected magnitude of isotope fractionation

(αCl,Sorption = 0.99960 - 0.99945; Cl,Sorption = -0.40‰ - -0.55‰) for 1,2-DCA and DCM is coherent with previous experimental studies (αSorption = 0.99987 - 0.99896; Sorption = -0.13‰ - -1.04‰) conducted for carbon and hydrogen isotopes of benzene, toluene, trichloroethene (Höhener and Yu, 2012; Imfeld et al., 2014; Kopinke et al., 2005). Furthermore, as after the first sorption step the shifts of isotope ratios remained within the analytical uncertainty of about 0.5‰, our multistep sorption experiment shows that single step experiment is not sufficient to detect sorption induced isotope fractionation. This is agreement with the studies conducted by Slater et al. (2000) and Schüth et al. (2003), which observed no significant sorption induced isotope effect by performing a single step sorption experiment.

Isotope effects due to phase transition of hydrophobic compounds mainly occur due to changes of vibrational frequencies of the solute molecules caused by changing nonbonding interactions (Aelion et al., 2010; Jancso and Van Hook, 1974; Jeannottat and Hunkeler, 2012; Jeannottat and Hunkeler, 2013; Turowski et al., 2003). Accordingly, the detected preferential sorption of isotopocules with light compared to isotopocules with heavy isotopes can be likely explained by changes of vibrational frequencies due to changing nonbonding interactions during the transition between the aqueous solution and the sorbent material. In the sorbent material vibrational frequencies of the chlorinated hydrocarbon molecules are reduced compared to the aqueous solution due to the stronger interactions of the molecules with sorbent material (Turowski et al., 2003). Consequently, the zero point energy levels of the light and heavy isotopocules are lower and closer together in the sorbent material than in the aqueous solution. As a result, the difference of zero point energies between sorbed and dissolved compounds in the aqueous solution is lower for heavy than for light isotopocules and thus, it takes slightly less energy for the heavy isotopocule to go into the aqueous phase than for the light isotopocules leading to a depletion of heavy isotopocules in the sorbent material. This isotope effect is similar as observed for air – water partitioning and DNAPL – vapor equilibration, during which also the reduction of vibrational frequencies in the water phase or in the DNAPL lead to a preferential transition of heavy carbon isotopocules to the gas phase compared to light isotopocules (Jeannottat and Hunkeler, 2012; Jeannottat and Hunkeler, 2013). For the diffusion cell experiment, the observed faster diffusive transport rate for isotopocules with light compared to the heavy DCM carbon isotopes is in agreement with previous studies, which investigated isotope fractionation due to aqueous phase diffusion (Eggenkamp and Coleman, 2009; Richter et al.,

2006; Wanner and Hunkeler, 2015). Furthermore, the determined magnitude of DCM carbon isotope fractionation due to diffusion is consistent with an earlier study (Wanner and Hunkeler, 2015), which investigated carbon and chlorine isotope fractionation of TCE and 1,2-DCA due to aqueous phase diffusion and obtained isotope fractionation factors in the same range ($\alpha_{Diffusion}$ = 0.99939 - 0.99978; $\varepsilon_{Diffusion}$ = -0.61‰ - -0.22‰) as the present study ($\alpha_{Diffusion}$ = 0.99972; $\varepsilon_{Diffusion}$ = -0.28‰). Moreover, the mass dependency of the diffusive transport rate (D) of the carbon isotopes of DCM showed a weaker power mass dependency ($D = m^{-0.025}$) than previously postulated by the kinetic theory ($D = m^{-0.5}$). This is in agreement with previous experiments (Eggenkamp and Coleman, 2009; Pikal, 1972; Richter et al., 2006; Rodushkin et al., 2004; Schloemer and Krooss, 2004; Tyroller et al., 2014; Wanner and Hunkeler, 2015; Zhang and Krooss, 2001) and molecular dynamic simulation studies (Bourg et al., 2010; Bourg and Sposito, 2007; Bourg and Sposito, 2008). Hence, the results of the diffusion cell experiment emphasized the failure of the kinetic theory for estimating the magnitude of isotope fractionation due to aqueous phase diffusion.

5.5.2. Concentration and compound-specific isotope diffusion profiles beneath the emplaced DNAPL sources

The presence of the highest 1,2-DCA concentration below and not adjacent to the contamination source in the clay unit indicates that upward diffusion (i.e. back-diffusion) occurred due to the depletion of the contamination source, as it has been observed at other contaminated sites (Chapman and Parker, 2005). In contrast, the highest DCM concentration was detected adjacent to the emplaced source, suggesting the DCM DNAPL mass in the source zone had not decreased sufficiently to initiate back-diffusion. This can be explained by the slower DCM mass flux out the source zone due to the flatter concentration gradient between the source zone and the surrounding clay caused by the weaker sorption behavior and the higher solubility of DCM compared to 1,2-DCA. The greater migration distance for DCM (160 cm) compared to 1,2-DCA (100 cm) is in agreement with the results of the multistep sorption experiment, which revealed stronger sorption of 1,2-DCA compared to DCM (Fig. 5-2C).

The enrichment of heavy carbon isotopes in 1,2-DCA and DCM with depth (Figs. 5-5C and 5-6B) are contrary to the trend expected for diffusion (Wanner and Hunkeler, 2015). Moreover, the small enrichment of heavy 1,2-DCA and DCM carbon isotopes can also not be

likely related to degradation, as the decrease in concentration with depth would be associated with a large isotope effect due the large degradation induced carbon isotope enrichment factors for 1,2-DCA (-3.5 to -32.0‰ (Palau et al., 2014)) and DCM ((-41.2 to -66.3‰ (Nikolausz et al., 2006)), respectively. Moreover, neither the present nor previous studies (Allen-King et al., 1996; Parker, 1996) found evidence for reactive processes at the site, supporting inferences that degradation is not responsible for enrichment of 1,2-DCA and DCM carbon isotopes with depth. This suggests that an isotope effect due to sorption might govern the 1,2-DCA and DCM carbon isotope trends towards heavy signatures with depth, as the clay unit is known for its strong sorption due to high organic matter content (Allen-King et al., 1996; Allen-King et al., 1997; Myrand et al., 1992; Parker, 1996). This hypothesis is supported by the results of the multistep sorption experiment, which showed that the sorbed compounds are depleted in heavy isotopes, enhancing the mobility of isotopocules with heavy isotopes in the clay unit and leading to an enrichment of heavy isotopes with depth (Figs. 5-3). However, in contrast to carbon isotopes, the 1,2-DCA chlorine isotopes show an opposite isotope trend towards lighter signatures with depth. As the mass difference is two between stable chlorine isotopes compared to one for carbon, the diffusive isotope effect is stronger for the chlorine compared to carbon isotopes. Hence, the trend towards lighter signatures with depth for 1,2-DCA chlorine isotopes could be explained by the interaction between sorption and diffusion, whereby the diffusion isotope effect overrules the sorption effect. To analyze the relative contribution of sorption and diffusion in more detail, numerical modeling was used as discussed in the following section.

5.5.3. Simulation of field site-derived concentration and compound-specific isotope profiles

The 2D axisymmetrical numerical model was used to: a) assess if measured 1,2-DCA and DCM concentration profiles can be reproduced with the experimentally determined parameters for the non-linear Freundlich isotherm (Tab. 5-1, Figs. 5-2A-B); and b) investigate if and how isotope fractionation due to diffusion and sorption processes are superimposed in saturated low permeability sediments.

Simulated 1,2-DCA and DCM concentration profiles agreed well with measured concentration profiles. The best fit for the 1,2-DCA (NSE=0.91) and for the DCM (NSE=0.98) concentration profiles was obtained with a tortuosity factor of 0.91 (eq. S5-4, Supporting Information) and with a start of the concentration decrease at the source zone at 9.5 (1,2-DCA) and 10 years (DCM) after source emplacement to concentrations of 86.9 mg/L for 1,2-DCA and

of 7700 mg/L for DCM, respectively (Figs. 5-5A and 5-6A). The consistency between measured and modelled 1,2-DCA and DCM concentration data shows that non-linear sorption occurs, consistently with the laboratory experiments and with previous studies at the site (Allen-King et al., 1996; Allen-King et al., 1997).

To assess the relative contribution of isotope fractionation due sorption and diffusion on isotope ratio profiles in the clay unit, two scenarios were simulated and compared with measured isotope ratio profiles: Isotope fractionation by a) diffusion only ($\alpha_{Sorption}$=1), and b) by a combination of diffusion and sorption. The diffusion only scenario showing a shift towards lighter isotope signatures with depth was inconsistent with measured isotope ratio profiles (Fig. 5-5B-C and Fig. 5-6B). For the 1,2-DCA chlorine isotopes, the simulated shift with depth was larger than the measured, while for the 1,2-DCA and DCM carbon isotopes the simulated profiles showed an opposite trend compared to measured isotope profiles, suggesting that isotope fractionation occurs not only due to the diffusion. In contrast, for the simulation scenario including both sorption and diffusion induced isotope fractionation, the simulated 1,2-DCA and DCM isotope profiles agreed well with the measured profiles (NSE = 0.74 – 0.95) (Fig. 5-5B-C and Fig. 5-6B). This further substantiates that sorption induced isotope fractionation causes an enrichment of heavy 1,2-DCA and DCM carbon isotopes, and that for 1,2-DCA chlorine isotopes the stronger diffusion isotope effect overrides the sorption effect causing a trend towards lighter isotopes with depth.

The magnitude of isotope fractionation due to sorption might not only depend on the sorption isotope effect but also on the extent of sorption. To investigate how the extent of sorption impacts the magnitude of isotope fractionation the migration of 1,2-DCA in saturated low permeability sediments was simulated for different Freundlich constants (K_{Fr}) ranging between 2 and 10 for the same time period as for the field experiment. By plotting simulated 1,2-DCA carbon and chlorine isotope profiles for different K_{Fr} values against 1,2-DCA concentrations normalized to the initial concentration (C/C_0), it is shown that higher sorption amplifies the isotope trend going in opposite directions (Fig. 5-7A and 5-7B). For the 1,2-DCA chlorine isotopes, for which diffusion is the predominate fractionation process, an increased extent of sorption results in a slower diffusive transport rate causing a steeper concentration gradient enlarging the shift of isotope ratios towards lighter isotope signatures with depth (Fig. 5-7A). This is consistent with previous detections by Wanner and Hunkeler (2015). In contrast, for

the 1,2-DCA carbon isotopes, for which sorption dominates isotope fractionation, an augmentation of the extent of sorption leads to larger a shift towards heavier isotope signatures with depth (Fig. 5-7B). The effect of increased sorption is more pronounced when sorption is the predominant fractionation process (Fig. 5-7B) compared to the scenario when diffusion caused isotope fractionation is prevalent (Fig. 5-7A).

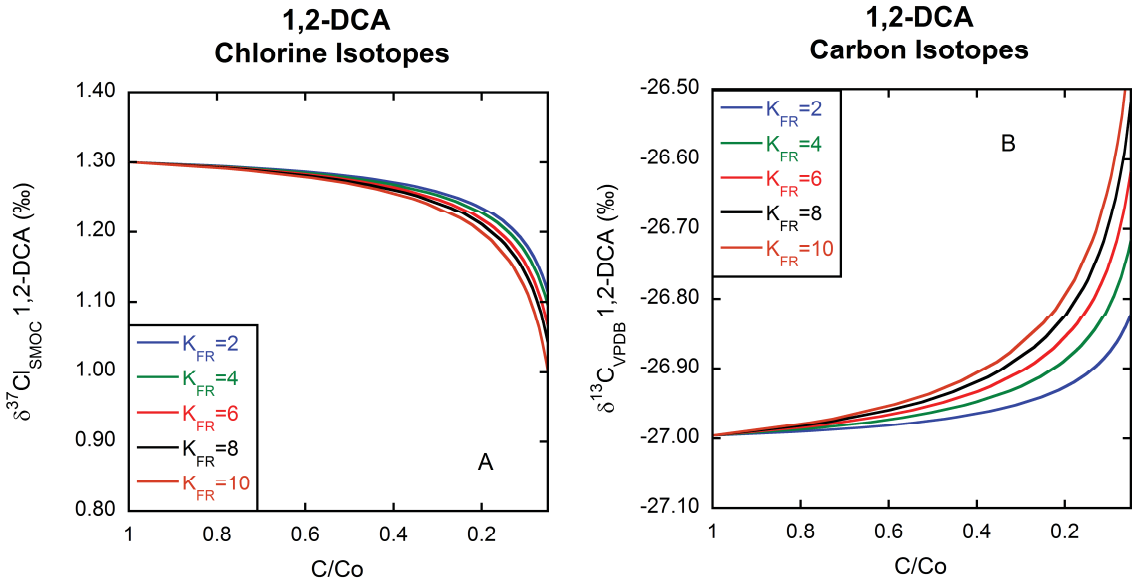

Figure 5-7.1,2-DCA chlorine (Fig. 5-7A) and carbon (Fig. 5-7B) isotope fractionation as function of concentration normalized to the initial concentration for a typical diffusion profile in saturated low permeability sediments for different Freundlich constants (K_{Fr}) ranging between 2 and 10.

Sorption induced isotope fractionation might impair the identification of reactive processes using stable isotope methods, especially for carbon isotopes as sorption shifts carbon isotope ratios towards the same direction as reactive (degradation) processes (towards heavier isotope signatures with depth). The impairment might especially occur for organic compounds having small degradation induced carbon isotope enrichment factors (e.g. for BTEX compounds (benzene, toluene, ethylbenzene, xylenes)). To investigate the extent of impairment, a degradation scenario was simulated with a relatively slow degradation rate (half-life = 506 days) associated with isotope fractionation factors ranging between 0.999 and 0.995. Furthermore, the

degradation scenario was simulated without and with taking into account sorption induced isotope fractionation. The degradation scenario was compared with measured 1,2-DCA and DCM carbon isotope ratio profiles as the observed magnitude of isotope fractionation due to sorption for 1,2-DCA and DCM carbon isotopes is expected to be representative for other organic compounds such as BTEX. In the degradation scenario with the smallest isotope fractionation factor (0.999) a similar shift of carbon isotope ratios with depth was observed as in the scenario without degradation (Figs 5-8A and 5-8B). This indicates that for carbon isotope ratio profiles with shifts of about $\Delta\delta^{13}C$=2.0‰ with depth, it remains ambiguous whether or not degradation occurs in high organic content (high sorption capacity) sediments. Furthermore, the simulated profiles in the degradation scenario revealed that if sorption induced isotope fractionation is ignored (considered negligible), the enrichment of heavy isotopes with depth is less strong (Figs. 5-8A and 5-8B). Hence, when fitting a reactive transport model to measured carbon isotope ratio profiles by ignoring sorption induced isotope fractionation, the total enrichment of heavy isotope with depth will be assigned to degradation processes, which leads to an overestimation of the degradation rates. Therefore, isotope effects due to sorption processes should be considered for the identification and quantification of reactive processes using stable isotope methods, especially for slow reactions with small fractionation factors. The impairment of isotope fractionation due sorption for the identification of reactive processes using stable isotope methods could be even more important for hydrogen isotopes as the sorption induced isotope effect is more distinct for hydrogen compared to carbon and chlorine isotopes (Höhener and Yu, 2012; Imfeld et al., 2014).

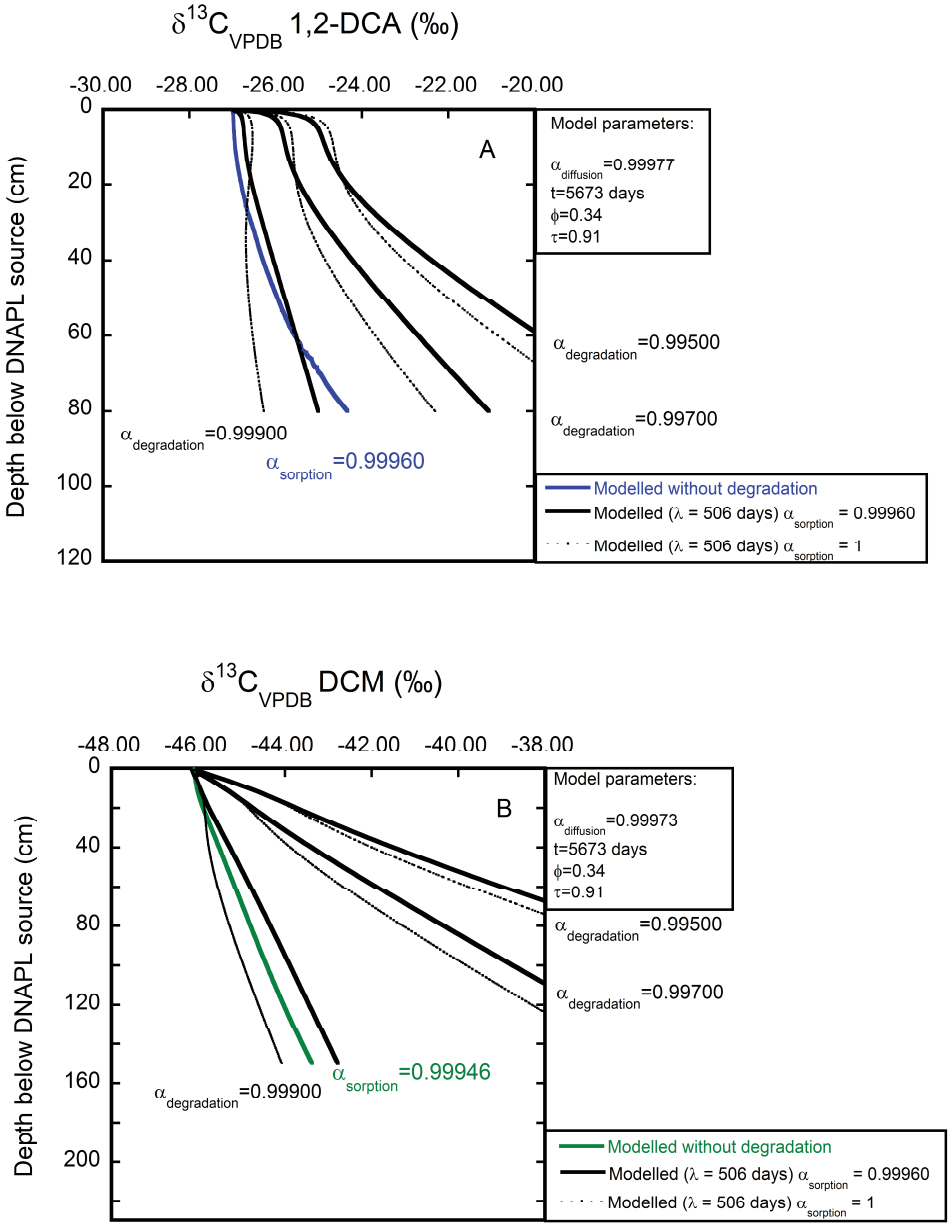

Figure 5-8. Simulated 1,2-DCA (Fig. 5-8A) and DCM (Fig. 5-8B) carbon isotope ratio profiles by including reactive processes (black lines) with fraction factors ranging between 0.999 – 0.995 and a half-life (λ) of 506 days. The continuous black lines represent the reactive scenario in which sorption induced fractionation was included, while the black-dashed lines represent the reactive scenario in which sorption induced isotope fractionation was neglected. The continuous blue (Fig. 5-8A) and green lines (Fig. 5-8B) correspond to the non-reactive scenario, which considers isotope fractionation due to sorption and diffusion only.

5.6. Conclusions

This study provides for the first time clear evidence that isotope fractionation due to sorption has a measurable effect on carbon and chlorine isotope patterns of chlorinated hydrocarbons under field conditions. By including laboratory determined enrichment factors for sorption and diffusion in a numerical model, laboratory and field observations were for the first time consistently related. The results of the numerical model demonstrated that under field conditions sorption and diffusion are superimposed and compensate each other to some degree as the fractionate isotopes in opposite directions. Hence, depending on whether sorption or diffusion shows the larger isotope fractionation factor, isotope trends go towards opposite directions. Moreover, an increased sorption extent of organic compounds leads to an amplification of the isotope trends in opposite directions. The amplification is larger when sorption is the dominant fractionation process (enrichment of heavy isotopes with depth) compared to the case when diffusion is the predominant fractionation process (enrichment of light isotopes with depth) during migration in low permeability sediments.

Furthermore this study shows that under field conditions sorption induced isotope fractionation can cause shifts of isotope ratios of around 2‰, which is considered by the US EPA (Hunkeler et al., 2008) as a threshold for identifying reactive processes affecting organic compounds. Numerical modelling showed that specific conditions (high sorption capacity, early transient diffusion state) can cause even larger shifts of isotope ratios due to sorption. Therefore, shifts of isotope ratios of around 2‰ at the field scale are not unequivocally attributable to reactive processes. This is especially important for the identification of slow reactive processes associated with small degradation induced isotope fraction factors as for the degradation of BTEX. Furthermore, the consideration of sorption induced isotope fractionation might even be more important for the identification of slow reactive processes with small fractionation factors in aquifers (granular sands and gravels) as sorption induced isotope fractionation is compensated to a lower degree by diffusion in aquifers compared to clayey sediments.

5.7. Acknowledgment

The authors acknowledge the Swiss National Science Foundation (SNFS) for financial support for this isotope focused study, as well as the University Consortium for Field-Focused Groundwater Contamination Research and the Natural Sciences and Engineering Research Council of Canada (NSERC) including a Discovery Grant to Dr. Parker for funding of the larger research effort. Furthermore, the authors thank Robert Ingleton and Paul Johnson from the University of Waterloo, who operated the Geoprobe rig and also supported the initial emplaced source installations. Several people from the University of Guelph, notably Ryan Kroeker, Dan Elliot and Keelin Scully also provided field support and Maria Gorecka and Rashmi Jadeja provided analytical support. The site operator Clean Harbors is also acknowledged for providing site access and field support for the research.

5.8. References

Aelion, C.M., Höhener, P., Hunkeler, D., Aravena, R., 2010. Environmental Isotopes in Biodegradation and Bioremediation CRC Press, USA, 450 pp.

Allen-King, R.M., Groenevelt, H., Mackay, D.M., 1995. Analytical method for the sorption of hydrophobic organic pollutants in clay-rich materials. Environmental science & technology, 29(1): 148-153.

Allen-King, R.M., Groenevelt, H., Warren, C.J., Mackay, D.M., 1996. Non-linear chlorinated-solvent sorption in four aquitards. Journal of contaminant hydrology, 22(3): 203-221.

Allen-King, R.M., McKay, L.D., Trudell, M.R., 1997. Organic Carbon Dominated Trichloroethene Sorption in a Clay-Rich Glacial Deposit. Groundwater, 35(1): 124-130.

Bourg, I.C., Richter, F.M., Christensen, J.N., Sposito, G., 2010. Isotopic mass dependence of metal cation diffusion coefficient in liquid water. Geochimica et Cosmochimica, 74: 2249 - 2256.

Bourg, I.C., Sposito, G., 2007. Molecular dynamics simulations of kinetic isotope fractionation during the diffusion of ionic species in liquid water. Geochimica et Cosmochimica Acta, 71(23): 5583-5589.

Bourg, I.C., Sposito, G., 2008. Isotopic fractionation of noble gases by diffusion in liquid water: Molecular dynamics simulations and hydrologic applications. Geochimica Et Cosmochimica Acta, 72(9): 2237-2247.

Caimi, R.J., Brenna, J.T., 1993. High-precision liquid chromatography-combustion isotope ratio mass spectrometry. Analytical chemistry, 65(23): 3497-3500.

Caimi, R.J., Brenna, J.T., 1997. Quantitative evaluation of carbon isotopic fractionation during reversed-phase high-performance liquid chromatography. Journal of Chromatography A, 757(1): 307-310.

Chapman, S.W., Parker, B.L., 2005. Plume persistence due to aquitard back diffusion following dense nonaqueous phase liquid source removal or isolation. Water Resources Research, 41(12).

Chen, Z., Xing, B., McGill, W., 1999. A unified sorption variable for environmental applications of the Freundlich equation. Journal of environmental quality, 28(5): 1422-1428.

Desaulniers, D.E., Kaufmann, R.S., Cherry, J.A., Bentley, H.W., 1985. ^{37}Cl - ^{35}Cl variations in a diffusion-controlled groundwater system. Geochimica et Cosmochimica, 50: 1757 - 1764.

Eggenkamp, H.G.M., Coleman, M.L., 2009. The effect of aqueous diffusion on the fractionation of chlorine and bromine stable isotopes. Geochimica et Cosmochimica Acta, 73(12): 3539-3548.

Einarson, M.D., Casey, M.B., Winglewich, D.L., Morkin, M.I., 1998. Enviro-core - A dual-tube direct push system for rapid site characterization. Proceedings of the Symposium on the Application of Geophysics to Environmental and Engineering Problems. Environmental & Engineering Geophysical Society, Wheat Ridge, 1-10 pp.

Elsner, M., Zwank, L., Hunkeler, D., Schwarzenbach, R.P., 2005. A new concept linking observable stable isotope fractionation to transformation pathways of organic pollutants. Environmental Science & Technology, 39(18): 6896-6916.

Filer, C.N., 1999. Isotopic fractionation of organic compounds in chromatography. Journal of Labelled Compounds and Radiopharmaceuticals, 42(2): 169-197.

Freundlich, H., 1909. Kappilarchemie. Leipzig.

Harrington, R.R., Poulson, S.R., Drever, J.I., Colberg, P.J.S., Kelly, E.F., 1999. Carbon isotope systematics of monoaromatic hydrocarbons: vaporization and adsorption experiments. Organic Geochemistry, 30(8A): 765-775.

Höhener, P., Atteia, O., 2010. Multidimensional analytical models for isotope ratios in groundwater pollutant plumes of organic contaminants undergoing different biodegradation kinetics. Advances in Water Resources, 33(7): 740-751.

Höhener, P., Yu, X., 2012. Stable carbon and hydrogen isotope fractionation of dissolved organic groundwater pollutants by equilibrium sorption. Journal of contaminant hydrology, 129: 54-61.

Huang, L., Sturchio, N.C., Abrajano, T., Heraty, L.J., Holt, B.D., 1999. Carbon and chlorine isotope fractionation of chlorinated aliphatic hydrocarbons by evaporation. Organic Geochemistry, 30(8A): 777-785.

Hunkeler, D. et al., 2011. Assessing chlorinated ethene degradation in a large scale contaminant plume by dual carbon-chlorine isotope analysis and quantitative PCR. Journal of Contaminant Hydrology, 119(1-4): 69-79.

Hunkeler, D., Aravena, R., Berry-Spark, K., Cox, E., 2005. Assessment of degradation pathways in an aquifer with mixed chlorinated hydrocarbon contamination using stable isotope analysis. Environmental Science & Technology, 39(16): 5975-5981.

Hunkeler, D., Aravena, R., Butler, B.J., 1999. Monitoring microbial dechlorination of tetrachloroethene (PCE) in groundwater using compound-specific stable carbon isotope ratios: Microcosm and field studies. Environmental Science & Technology, 33(16): 2733-2738.

Hwang, Y.K., Endres, A.L., Piggott, S.D., Parker, B.L., 2008. Long-term ground penetrating radar monitoring of a small volume DNAPL release in a natural groundwater flow field. Journal of contaminant hydrology, 97(1): 1-12.

Imfeld, G., Kopinke, F.D., Fischer, A., Richnow, H.H., 2014. Carbon and hydrogen isotope fractionation of benzene and toluene during hydrophobic sorption in multistep batch experiments. Chemosphere, 107: 454-461.

Jeannottat, S., Hunkeler, D., 2012. Chlorine and Carbon Isotopes Fractionation during Volatilization and Diffusive Transport of Trichloroethene in the Unsaturated Zone. Environmental Science & Technology, 46(6): 3169-3176.

Jeannottat, S., Hunkeler, D., 2013. Can Soil Gas VOCs be Related to Groundwater Plumes Based on Their Isotope Signature? Environmental Science & Technology, 47(21): 12115-12122.

Jin, B., Haderlein, S.B., Rolle, M., 2013. Integrated carbon and chlorine isotope modeling: applications to chlorinated aliphatic hydrocarbons dechlorination. Environmental science & technology, 47(3): 1443-1451.

Jin, Y., Holzbecher, E., Ebneth, S., 2012. Simulation of pumping induced groundwater flow in unconfined aquifer using arbitrary Lagrangian-Eulerian method, COMSOL Conference, Milan (Italy).

Johnson, R.L., Cherry, J.A., Pankow, J.F., 1989. Diffusive contaminant transport in natural clay: a field example and implications for clay-lined waste disposal sites. Environmental Science & Technology, 23(3): 340-349.

Klein, P., Simborg, D., Szczepanik, P.A., 1964. Detection and computation of isotope fractionation in the adsorption chromatography of dual-labelled compounds. Pure and Applied Chemistry, 8(3-4): 357-370.

Kopinke, F.D., Georgi, A., Voskamp, M., Richnow, H.H., 2005. Carbon isotope fractionation of organic contaminants due to retardation on humic substances: Implications for natural attenuation studies in aquifers. Environmental Science & Technology, 39(16): 6052-6062.

Kueper, B.H., Redman, D., Starr, R.C., Reitsma, S., Mah, M., 1993. A field experiment to study the behavior of Tetrachloroethylene below the water-table - Spatial - distribution of residual and pooled DNAPL. Ground Water, 31(5): 756-766.

Liu, H. et al., 2016. Compound-specific carbon isotopic fractionation during transport of phthalate esters in sandy aquifer. Chemosphere, 144: 1831-1836.

Lollar, B.S. et al., 1999. Contrasting carbon isotope fractionation during biodegradation of trichloroethylene and toluene: Implications for intrinsic bioremediation. Organic Geochemistry, 30(8): 813-820.

Mabey, W. et al., 1982. Aquatic fate process data for organic priority pollutants. US Environmental Protection Agency, Office of Water Regulations and Standards, Washington, DC EPA, 440: 4-81.

McKay, L., Fredericia, J., 1995. Distribution, origin, and hydraulic influence of fractures in a clay-rich glacial deposit. Canadian Geotechnical Journal, 32(6): 957-975.

Meckenstock, R.U., Morasch, B., Griebler, C., Richnow, H.H., 2004. Stable isotope fractionation analysis as a tool to monitor biodegradation in contaminated acquifers. Journal of Contaminant Hydrology, 75(3-4): 215-255.

Myrand, D., Gillham, R., Sudicky, E., O'Hannesin, S., Johnson, R., 1992. Diffusion of volatile organic compounds in natural clay deposits: Laboratory tests. Journal of Contaminant Hydrology, 10(2): 159-177.

Nikolausz, M., Nijenhuis, I., Ziller, K., Richnow, H.H., Kästner, M., 2006. Stable carbon isotope fractionation during degradation of dichloromethane by methylotrophic bacteria. Environmental Microbiology, 8(1): 156-164.

Palau, J. et al., 2014. C and Cl isotope fractionation of 1,2-dichloroethane displays unique δ13C/δ37Cl patterns for pathway identification and reveals surprising C-Cl bond involvement during microbial oxidation. Environmental Science & Technology.

Pankow, J.F., Cherry, J.A., 1996. Dense Chlorinated Solvents and Other DNAPLs in Groundwater Waterloo. Press. Portland, OR., 522 pp.

Parker, B.L., 1996. Effect of Molecular Diffusion on the Persistence of Dense Immiscible Phase Organic Liquids in Fractured Porous Geologic Media. PhD Thesis Thesis, University of Waterloo, Waterloo, Ontario, Canada, 191 pp.

Parker, B.L., Chapman, S.W., Guilbeault, M.A., 2008. Plume persistence caused by back diffusion from thin clay layers in a sand aquifer following TCE source-zone hydraulic isolation. Journal of Contaminant Hydrology, 102(1-2): 86-104.

Parker, B.L., Cherry, J.A., Chapman, S.W., 2004. Field study of TCE diffusion profiles below DNAPL to assess aquitard integrity. Journal of Contaminant Hydrology, 74(1-4): 197-230.

Parker, B.L., Gillham, R.W., Cherry, J.A., 1994. Diffusive Disappearance of Immiscible-Phase Organic Liquids in Fractured Geologic Media. Groundwater, 32(5): 805-820.

Pikal, M.J., 1972. Isotope effects in tracer diffusion. Comparison of the diffusion coefficients of $^{24}Na^{+}$ and $^{22}Na^{+}$ in aqueous electrolytes. J. Phys. Chem., 76: 3038 - 3040.

Poulson, S.R., Drever, J.I., Colberg, P.J., 1997. Estimation of K oc values for deuterated benzene, toluene, and ethylbenzene, and application to ground water contamination studies. Chemosphere, 35(10): 2215-2224.

Richter, F.M. et al., 2006. Kinetic isotopic fractionation during diffusion of ionic species in water. Geochimica et Cosmochimica, 70: 277 - 289.

Rivett, M.O., Allen-King, R.M., 2003. A controlled field experiment on groundwater contamination by a multicomponent DNAPL: dissolved-plume retardation. Journal of contaminant hydrology, 66(1): 117-146.

Rodushkin, I., Stenberg, A., Andrén, H., Malinovsky, D., Baxter, D.C., 2004. Isotopic fractionation during diffusion of transition metal ions in solution. Analytical Chemistry, 76: 2148 - 2151.

Schloemer, S., Krooss, B.M., 2004. Molecular transport of methane, ethane and nitrogen and the influence of diffusion on the chemical and isotopic composition of natural gas accumulations. Geofluids, 4(1): 81-108.

Schüth, C., Taubald, H., Bolaño, N., Maciejczyk, K., 2003. Carbon and hydrogen isotope effects during sorption of organic contaminants on carbonaceous materials. Journal of Contaminant Hydrology, 64(3): 269-281.

Schwille, F., 1988. Dense chlorinated solvents in porous and fractured media: model experiments. Boca Raton, FL, USA.

Slater, G.F., Ahad, J.M.E., Lollar, B.S., Allen-King, R., Sleep, B., 2000. Carbon isotope effects resulting from equilibrium sorption of dissolved VOCs. Analytical Chemistry, 72(22): 5669-5672.

Tyroller, L., Brennwald, M.S., Mächler, L., Livingstone, D.M., Kipfer, R., 2014. Fractionation of Ne and Ar isotopes by molecular diffusion in water. Geochimica et Cosmochimica Acta, 136: 60-66.

USEPA, 1989. Hazardous Waste Treatment, Storage, and Disposal Facilities (TSDF)-USEPA, OAQPS, Air Emission Models. (EPA-450/3-87-026).

Van Breukelen, B.M., Prommer, H., 2008. Beyond the Rayleigh equation: Reactive transport modeling of isotope fractionation effects to improve quantification of biodegradation. Environmental Science & Technology, 42(7): 2457-2463.

Voskamp, M., 2004. Untersuchungen zur Sorption an Huminstoffen: Molekulargewicht und Kohlenstoff-Isotopenfraktionierung, UFZ.

Wanner, P., Hunkeler, D., 2015. Carbon and chlorine isotopologue fractionation of chlorinated hydrocarbons during diffusion in water and low permeability sediments. Geochimica et Cosmochimica Acta, 157: 198-212.

Wanner, P., Parker, B., Chapman, S.W., Aravena, R., Hunkeler, D., 2016. Quantification of Degradation of Chlorinated Hydrocarbons in Saturated Low Permeability Sediments Using Compound-Specific Isotope Analysis (CSIA). Environmental science & technology.

White, R.A., Rivett, M.O., Tellam, J.H., 2008. Paleo-roothole facilitated transport of aromatic hydrocarbons through a Holocene clay bed. Environmental science & technology, 42(19): 7118-7124.

Wiedemeier, T.H., 1999. Natural attenuation of fuels and chlorinated solvents in the subsurface. John Wiley & Sons.

Zhang, T.W., Krooss, B.M., 2001. Experimental investigation on the carbon isotope fractionation of methane during gas migration by diffusion through sedimentary rocks at elevated temperature and pressure. Geochimica Et Cosmochimica Acta, 65(16): 2723-2742.

5.9. Supporting Information to Chapter 5

S1. Materials and Methods

S1.1. DNAPL source emplacement procedure

First a 6.25” whole was augered into the undisturbed clay of the St. Clair clay plain to a depth of 10 m below ground surface (bgs) slightly higher than the desired depth for emplacing the chlorinated solvent DNAPL sources. Following the removal of the augers, a 6’’ PVC casing was pushed to the bottom of the augered hole to get access to the zone, where the DNAPLs were intended to emplace. During advancement of the casing, a slurry of Quik-Gel (high yield bentonite) was poured around the casing to provide lubrication, which allowed easier pushing of the casing and to help sealing the annular space between the casing and the borehole. Afterwards the casing was cleaned before installing the source zone by pushing a 4.5’’ Shelby Tube through the casing down to the bottom of the augered hole a few centimetres into the undisturbed clay. Afterwards the Shelby Tube was turned by 360° to shear the clay at the bottom and retrieved to complete the cleaning of the casing. After cleaning at the surface, the Shelby tube was placed back in the casing in a centralized position and advanced about 60 centimetres into the clay beneath the augered hole and removed full of clay to clear space for the emplacement of the chlorinated solvent DNAPL sources. Subsequently, an access tube was placed to the bottom of the Shelby tube hole for emplacing the different chlorinated solvent DNAPL sources. The access tube consisted of a 0.5’’ PVC, while the bottom 6’’ were slotted. After installing the access tube the casing was back-filled with coarse silica sand (well gravel) to about 2.5 bgs. Afterwards, the back-filled casing was filled with water to a level of about 3 meters bgs corresponding to the water level at the site. To install the DNAPL sources 1.5 – 2 litres of different chlorinated solvent DNAPL single phase and mixtures (TCE, DCM, 1,2-DCA TCE/DCM mixture) were poured into the access tube in five different wholes 5 m apart from each other. Subsequently, the access tube was pulled up about 60 cm and 2 L of water was poured into the access tube to flush out the remaining solvents, followed by removal of the access tube.

S1.2. Core retrieval

To retrieve the cores below the emplaced 1,2-DCA and DCM DNAPL sources a Geoprobe 7720DT direct-push rig and the Envirocore dual tube sampling system was used as described by Einarson et al. (1998). An outer casing and an inner sample barrel containing a plastic liner of about 60 centimetres were, depending on the clay properties, pushed, pounded or vibrated simultaneously into the ground. During advancement, the clay cores were collected within the plastic liner inside the sample barrel. As soon as the sample barrel and the plastic line were filled with clay, it was withdrawn to the surface, while the casing was left in place to avoid a collapse of the borehole during further core retrieval.

S1.3. Subsampling and VOC extractions from cores

The collected cores were split lengthwise on-site in two equal pieces. After splitting, the cores were logged (photographs and description) as fast as possible (~5 minutes) for geological features to prevent any loss of chlorinated hydrocarbons by volatilization. Afterwards the cores were subsamples and chlorinated hydrocarbons were extracted from core subsamples following the procedure described by Parker (1996) to obtain highly resolved concentration and compound-specific isotope profiles. Initially the cores were covered by aluminum foil except at the place, where subsampling took place to minimize the loss of chlorinated hydrocarbons. Subsampling of the clay cores as a function of depth was performed using a cut plastic syringe as a mini corer. The subsamples were taken by the cut plastic syringe and expelled into 42 mL glass vials containing 20 mL high purity VWR methanol. The vials were sealed with a screw cap with a Teflon lined septum and weighted before and after the collection of the clay samples to determine the weight of the solid samples. A high clay to methanol ratio (average: 0.8 with some variation among the samples) was chosen to maximize the amount of chlorinated solvents in the methanol extraction.

In the laboratory the 42 mL vials were sonicated for 30 minutes followed by shaking for one hour in order to disperse the clay samples and to dissolve all chlorinated solvents completely in the methanol. Afterwards the vials were centrifuged for 30 minutes at 1200 rpm to obtain a clear methanol supernatant. The clear methanol supernatant was then decanted and stored prior to analysis.

S1.4. Concentration and compound-specific isotope analysis (CISA)

S1.4.1. Concentration analysis

VOC concentrations in the experimental water samples were analyzed using a TraceTM GC-DSQII mass spectrometer (Thermo Fisher Scientific, Waltham, MA, US) using the selected ion mode with a detection limit of 2.0 μg/L at the University of Neuchâtel. Calibration curves for 1,2-DCA and DCM were produced using external standards (purity ≥ 95.0%), which were prepared at seven different concentration levels: 5, 10, 25, 50, 75, 100, 150 μg/L. Headspace samples from 20mL vials filled with 10ml sample were injected using a CombiPal auto sampler (CTC Analytics, Zwingen, Switzerland). The samples were diluted to approximately identical concentrations (50μg/L), based on an initial screening of VOC concentrations, to fit the calibration interval and to maximize precision of the analysis. For samples containing 1,2-DCA, the oven temperature was held at 40°C for 2 minutes, ramped at 15°C/min to 90°C and held for 2 minutes. For samples with DCM the oven temperature was held at 40°C for 2 minutes at 15°C/min to 130°C and held for 2 minutes. The carrier gas was helium with a flow rate of 1,2 ml/min. The analytical uncertainty (±1σ) of the concentration measurements was determined by a repeated measurement of standards included in the sample sequence (standards/samples = 1/5) and corresponded to ±4%, (n=5) for 1,2-DCA and to ±5% (n=6) for DCM.

For analysing VOC concentrations in the clay samples, aliquots of the methanol extracts were diluted at least 10 times with pure water and analyzed analogously to water samples. The dilution was made because the polar methanol is incompatible with the non-polar column of the gas chromatograph. The total soil concentrations were calculated according the following formula:

$$C_s = \frac{V_m C_m}{m_{ws}} \qquad \text{(S5-1)}$$

where, (mg/kg) is the VOC concentration in the wet clay, (L) is the total volume of methanol, (mg/L) is the VOC concentration in the methanol and (kg) is the total mass of the wet clay. The detection limit for VOCs concentrations in the wet clay is approximately 0.05 mg/kg for the average clay to methanol ratio of 0.8.

S1.4.2. Compound-specific carbon isotope analysis

Compound-specific carbon isotope ratios of 1,2-DCA and DCM in methanol extractions from clay core subsamples were performed using a TRACE^{TM} gas chromatograph (GC) coupled to a DeltaPlus XP isotope mass spectrometer (IRMS) via a combustion III interface (Thermo Finnigan, Germany) at the University of Neuchâtel, Switzerland. The methanol extractions were diluted to identical concentrations of 30µg/L in 42 mL glass vials with PTFE-lined screw cap, whereas the dilution had to be at least 100 times due to the incompatibility between the polar methanol extractions the column of the GC. Prior analysis with the GC-IRMS, samples were pre-concentrated with a purge-and-trap concentrator (Tekmar Velocity XPT, USA) by purging a sample volume of 25 mL from the 42 mL glass vial for ten minutes with N_2 (40mL/min) and by detaining the degassed VOCs on a Vocarb 3000 trap. After purging, the samples were desorbed from the trap and transferred to a cryogenic trap (Tekmar Dohrmann) installed in the GC oven having a temperature of -80°C for 1,2-DCA and of -150°C for DCM. Subsequently, the temperature was increased to 180°C and the samples were release to the column of the GC (DB-VRX, 60m, 0.25mm, 1,2 µm) for chromatographic separation. The GC oven temperature for 1,2-DCA analysis was held at 60°C for 2 minutes, then ramped at 5°C/min to 135°C and held for two minutes. The GC oven temperature for DCM was held at 60°C for two minutes, then ramped at 10°C/min to 135°C and held for two minutes.

S1.4.3. Compound-specific chlorine isotope analysis

Compound-specific chlorine isotope measurement of 1,2-DCA was performed using a gas chromatograph coupled to a quadrapole mass spectrometer (GC-qMS; Agilent 7890A, Agilent 5975C). Samples were injected using a headspeace method from 20 mL vials filled with 15mL solution using a CompiPal Autosampler (CTC Analytics, Zwingen, Switzerland). For chromatographic separation a DB-5 column (30m, 0.25mm, 0.25µm, Agilent) with a constant helium flow of 1,2 mL/min was used. methanol extraction from the clay cores and 1,2-DCA standards were diluted to identical concentrations of 2000µg/L to maximize precision of the measurements whereas, the dilution of the methanol extractions had to be at least 10 times due to the incompatibility of the methanol with the column of the GC. The temperature program of the GC for 1,2-DCA was held at 40°C for 1.8 minutes and then ramped at 25°C/min to 120°C and held for 0.2 minutes.

S2. Modelling Approach

S2.1. Model description

The migration of chlorinated hydrocarbons in the clay unit around the emplaced 1,2-DCA and DCM DNAPL sources was simulated using the finite element computer code Comsol Multiphysics®. A 2D axisymmetric transport model domain was created with a vertical depth of 5 meters and with 1 meter width. By rotating the model domain around the vertical axis a 3D domain was produced representing the clay unit around the emplaced source zone (Fig. S5-1). The modelling domain contains a highly resolved mesh, especially refined at the boundary between the source zone and the clay unit. To simulate solute transport of chlorinated hydrocarbons in the clay unit next to the emplaced sources, the advection-dispersion equation for porous saturated systems was used:

$$\frac{\partial}{\partial t}\left(\phi R_n C_n\right) = \nabla\left(D_n \nabla c - vc\right) \qquad \text{(S5-2)}$$

where z (m) is the vertical depth, C_n (µg/kg) is the concentration of species n, v (cm/y) is the vertical flow velocity in the clayey aquitard, D_n (m^2/s) is the dispersion coefficient and R_n (-) refers to the retardation factor and ϕ (-) is the porosity.

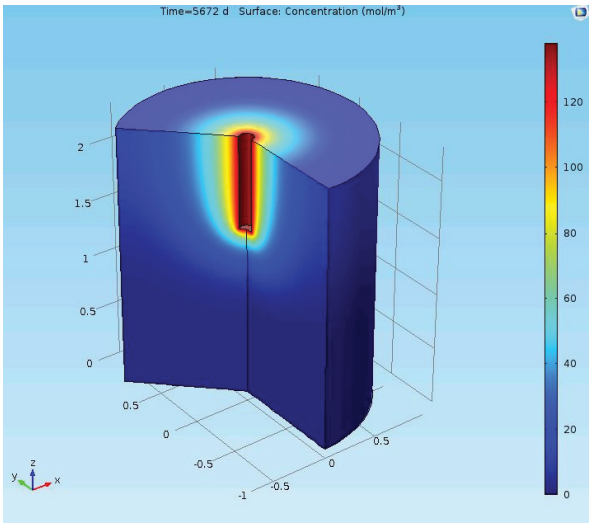

Figure S5-1. 3D numerical diffusion model of the DCM concentration in the clay unit around the emplaced DNAPL source, 5672 days after the emplacement of the source.

The vertical dispersion coefficient (eq. S5-1) is determined using the relationship:

$$D_n = D_e + \alpha v \tag{S5-3}$$

where D_n (m^2/s) is the dispersion coefficient, D_e (m^2/s) is the effective diffusion coefficient, α (m) refers to the dispersivity and v (m/s) is the 1D linear flow velocity. In saturated low permeability sediments the advective velocity is often negligible (v~0 m/s) and the dispersion coefficient reduces to the diffusion coefficient.

The effective diffusion coefficient (eq. S5-3) includes the lowering of the diffusive transport rate in porous media due porosity and tortuosity effects and is defined as follows:

$$D_e = D_0 \phi \tau \tag{S5-4}$$

where D_0 (m^2/s) is the diffusion coefficient in free solution and τ (-) refers to the tortuosity factor The retardation factor was calculated assuming non- linear equilibrium sorption following the Freundlich isotherm:

$$R = 1 + \left(\frac{\rho_{bdry}}{\Phi} \right) \frac{K_{Fr}}{C_e^{(N-1)/N}} \tag{S5-5}$$

where ρ_{bdry} (g/cm^3) is the dry soil bulk density, K_{Fr} ($mg^{1-1/n}\ kg^{-1}\ L^{1/n}$) refers to the Freundlich sorption constant ,C_e (mg/L) is the pore water concentration and N (-) corresponds to the non-linearity factor.

For modelling isotopocule fractionation during migration into the clay DCM and 1,2-DCA carbon (^{99}1,2-DCA, ^{100}1,2-DCA, ^{101}1,2-DCA and ^{87}DCM, ^{88}DCM) and 1,2-DCA chlorine isotopocules (^{98}1,2-DCA, ^{100}1,2-DCA, ^{102}1,2-DCA) differing by one heavy isotope were defined as separate species in the model database. The initial abundances of the defined 1,2-DCA and DCM carbon and 1,2-DCA chlorine isotopocules were determined out of all possible isotopocules (Tabs. S5-2 and S5-3) applying the binominal distribution combining the occurrence of both C and Cl isotopes as proposed by Jin et al. (2013) and using the measured 1,2-DCA and DCM carbon and 1,2.-DCA chlorine isotope ratio adjacent to the DNAPL source zone:

$$A_j = \binom{u}{v} \cdot P_{^{13}C}^{v} \cdot P_{^{12}C}^{u-v} \cdot \binom{h}{i} \cdot P_{^{37}Cl}^{i} \cdot P_{^{35}Cl}^{h-i} \qquad \text{(S5-6)}$$

where A_j is the relative abundance of an isotopocule j having v ^{13}C out of total u carbon atoms and i ^{37}Cl out of total h chlorine atoms and P is the abundance of the corresponding carbon and chlorine isotopes.

Table S5-1. Model parameters for simulating the migration of chlorinated hydrocarbons in the clay unit at the permitted hazardous waste disposal site in Petrolia, Ontario.

Parameter	**Unit**	**Value**	**Reference**
Porosity:	-	0.34	(Parker, 1996)
Soil dry bulk density: ρ_{bdry}	g/cm^3	1.71	(Parker, 1996)
Soil wet bulk density: ρ_{bwet}	g/cm^3	2.02	(Parker, 1996)
Tortuosity[b]	-	0.91	Present study
Diffusion coefficient in free solution 1,2-DCA: $D_{0,1,2\text{-DCA}}$	m^2/s	9.90E-10	(USEPA, 1989)
Diffusion coefficient in free solution DCM: $D_{0,DCM}$	m^2/s	1.17E-09	(USEPA, 1989)
Freundlich sorption constant $K_{Fr,1,2\text{-DCA}}$[a]	$mg^{1-1/n} kg^{-1} L^{1/n}$	5.36	Present study
Freundlich sorption constant K_{DCM}[a]	$mg^{1-1/n} kg^{-1} L^{1/n}$	2.97	Present study
Freundlich exponent 1/N 1,2-DCA[a]	-	0.74	Present study
Freundlich exponent 1/N DCM[a]	-	0.71	Present study

[a]Experimentally determined
[b]Calibrated

Table S5-2. Initial abundances of 1,2-DCA carbon and chlorine isotopocules differing by one heavy isotope.

Isotopocule 1,2-DCA	Carbon ^{13}C	Carbon ^{12}C	Chlorine ^{37}Cl	Chlorine ^{35}Cl	Abundance	Mass	Abundance carbon isotopocules differing by one heavy isotope	Average mass carbon isotopocules differing by one heavy isotope	Abundance chlorine isotopocules differing by one heavy isotope	Average mass chlorine isotopocules differing by one heavy isotope
1	0	2	0	2	0.55786	98				
2	0	2	1	1	0.36192	100				
3	0	2	2	0	0.05870	102	0.97848	99	0.57012	98
4	1	1	0	2	0.01220	99				
5	1	1	1	1	0.00792	101				
6	1	1	2	0	0.00128	103	0.02140	100	0.36988	100
7	2	0	0	2	0.00007	100				
8	2	0	1	1	0.00004	102				
9	2	0	2	0	0.00001	104	0.00012	101	0.05999	102
Sum					1.00000		1.00000		1.00000	

Table S5-3. Initial abundances of DCM carbon and chlorine isotopocules differing by one heavy isotope.

Isotopocule DCM	Carbon ^{13}C	Carbon ^{12}C	Chlorine ^{37}Cl	Chlorine ^{35}Cl	Abundance	Mass	Abundance carbon isotopocules differing by one heavy isotope	Average mass carbon isotopocules differing by one heavy isotope
1	0	1	0	2	0.56418	86		
2	0	1	1	1	0.36559	88		
3	0	1	2	0	0.05923	90	0.98900	87
4	1	0	0	2	0.00628	87		
5	1	0	1	1	0.00407	89		
6	1	0	2	0	0.00066	91	0.01100	88
Sum					1.00000		1.00000	

Thus, the initial abundance of 1,2-DCA and DCM carbon and 1,2-DCA chlorine isotopocules differing by one heavy isotope corresponds to (Tabs. S5-2 and S5-3):

Initial abundances of 1,2-DCA carbon isotopocules differing by one heavy carbon isotope:

^{99}1,2-DCA= $I_{98(1)}+I_{100(2)}+I_{102(3)}$ (S5-7)

^{100}1,2-DCA= $I_{99(4)}+I_{101(5)}+I_{103(6)}$ (S5-8)

^{101}1,2-DCA= $I_{100(4)}+I_{102(5)}+I_{104(6)}$ (S5-9)

Initial abundances of 1,2-DCA chlorine isotopocules differing by one heavy chlorine isotope:

^{98}1,2-DCA= $I_{98(1)}+I_{99(4)}+I_{100(7)}$ (S5-10)

^{100}1,2-DCA= $I_{100(2)}+I_{101(5)}+I_{102(8)}$ (S5-11)

^{102}1,2-DCA= $I_{100(2)}+I_{101(5)}+I_{102(8)}$ (S5-12)

Initial abundances of DCM carbon isotopocules differing by one heavy carbon isotope:

^{87}DCM= $I_{86(1)}+I_{88(2)}+I_{90(3)}$ (S5-13)

^{88}DCM= $I_{87(4)}+I_{89(5)}+I_{91(6)}$ (S5-14)

where I is the isotopocule abundance and the number of in brackets corresponds to the isotopocule ID in tables 2 and 3.

To simulate isotopocule fractionation due to sorption during the migration in the clayey unit, different Freundlich constants were assigned to each defined 1,2-DCA and DCM isotopocule differing in one heavy isotope. The different Freundlich were determined based on experimentally derived isotope fractionation factors for sorption (eq. 10), which are proportional to the ratio of the Freundlich constants for isotopocules differing by one heavy isotope.

For 1,2-DCA:

$$\alpha_{Sorption,Carbon} = \frac{^{13C}K_{Fr}}{^{12C}K_{Fr}} = \frac{^{100}1,2\text{–}DCA K_{Fr}}{^{99}1,2\text{–}DCA K_{Fr}} = \frac{^{101}1,2\text{–}DCA K_{Fr}}{^{100}1,2\text{–}DCA K_{Fr}} \quad \text{(S5-15)}$$

$$\alpha_{Sorption,Chlorine} \frac{^{37Cl}K_{Fr}}{^{37Cl}K_{Fr}} = \frac{^{100}1,2\text{–}DCA K_{Fr}}{^{98}1,2\text{–}DCA K_{Fr}} = \frac{^{102}1,2\text{–}DCA K_{Fr}}{^{100}1,2\text{–}DCA K_{Fr}} \quad \text{(S5-16)}$$

For DCM:

$$\alpha_{Sorption,Carbon}\frac{^{13C}K_{Fr}}{^{12C}K_{Fr}}=\frac{^{88DCM}K_{Fr}}{^{87DCM}K_{Fr}} \quad \text{(S5-17)}$$

Expecting that the Freundlich constant of the 1,2-DCA carbon and chlorine isotopocules with the mass 100 (Tab. 2) correspond to the Freundlich constant of the total 1,2-DCA concentrations ($K_{Fr,1,2\text{-}DCA,total} \approx K_{Fr,100,1,2\text{-}DCA}$), the Freundlich constant for each individual 1,2-DCA isotopocules becomes to:

$$K_{Fr,99_{1,2-DCA}} = K_{Fr,1,2-DCA,total} \big/ \alpha_{Sorption,Carbon} \quad \text{(S5-18)}$$

$$K_{Fr,100_{1,2-DCA}} = K_{Fr,1,2-DCA,total} \quad \text{(S5-19)}$$

$$K_{Fr,101_{1,2-DCA}} = \alpha_{Sorption,Carbon} \cdot K_{Fr,1,2-DCA,total} \quad \text{(S5-20)}$$

$$K_{Fr,98_{1,2-DCA}} = K_{Fr,1,2-DCA,total} \big/ \alpha_{Sorption,Chlorine} \quad \text{(S5-21)}$$

$$K_{Fr,100_{1,2-DCA}} = K_{Fr,1,2-DCA} \quad \text{(S5-22)}$$

$$K_{Fr,102_{1,2-DCA}} = \alpha_{Sorption,Chlorine} \cdot K_{Fr,1,2-DCA} \quad \text{(S5-23)}$$

For DCM it was assumed that the unified Freundlich sorption variable of the DCM carbon isotopocules with the mass 87 (Tab. 2) correspond to the unified Freundlich sorption variable of the total DCM concentration ($K_{u,DCM,total} \approx K_{u,87,DCM}$). Hence, the diffusion coefficients for each individual DCM carbon isotopocules corresponds to:

$$K_{Fr,87_{DCM}} = K_{Fr,DCM} \quad \text{(S5-24)}$$

$$K_{Fr,87_{DCM}} = \alpha_{Sorption,Carbon} \cdot K_{Fr,DCM} \quad \text{(S5-25)}$$

To simulate isotopocule fractionation due to diffusion during the migration in the clayey unit, different diffusion coefficients were assigned to each defined 1,2-DCA and DCM isotopocule differing in one heavy isotope. The different diffusion coefficients were determined based on experimentally derived isotope fractionation factors for diffusion (eq. 5-2), which are proportional to the ratio of diffusion coefficients for isotopocules differing by one heavy isotope (Wanner and Hunkeler, 2015):

For 1,2-DCA:

$$\alpha_{Diffusion,Carbon} = \frac{D_{13C}}{D_{12C}} = \frac{D_{100_{1,2-DCA}}}{D_{99_{1,2-DCA}}} = \frac{D_{101_{1,2-DCA}}}{D_{100_{1,2-DCA}}} \quad \text{(S5-26)}$$

$$\alpha_{Diffusion,Chlorine} = \frac{D_{37Cl}}{D_{37Cl}} = \frac{D_{100_{1,2-DCA}}}{D_{98_{1,2-DCA}}} = \frac{D_{102_{1,2-DCA}}}{D_{100_{1,2-DCA}}} \quad \text{(S5-27)}$$

For DCM:

$$\alpha_{Diffusion,Carbon} = \frac{D_{13C}}{D_{12C}} = \frac{D_{88_{DCM}}}{D_{87_{DCM}}} \quad \text{(S5-28)}$$

Assuming that the diffusion coefficients in free solution of the 1,2-DCA carbon and chlorine isotopocules with the mass 100 (Tab. 1) correspond to the diffusion coefficient in free solution of the total 1,2-DCA concentrations ($D_{0,1,2\text{-DCA,total}} \approx D_{0,100,1,2\text{-DCA}}$) the diffusion coefficients for each individual 1,2-DCA isotopocules becomes to:

$$D_{0,99_{1,2-DCA}} = D_{0,1,2-DCA,total} / \alpha_{Diffusion,Carbon} \quad \text{(S5-29)}$$

$$D_{0,100_{1,2-DCA}} = D_{0,1,2-DCA,total} \quad \text{(S5-30)}$$

$$D_{0,101_{1,2-DCA}} = \alpha_{Diffusion,Carbon} \cdot D_{0,1,2-DCA,total} \quad \text{(S5-31)}$$

$$D_{0,98_{1,2-DCA}} = D_{0,1,2-DCA,total} / \alpha_{Diffusion,Chlorine} \quad \text{(S5-32)}$$

$$D_{0,100_{1,2-DCA}} = D_{0,1,2-DCA,total} \quad \text{(S5-33)}$$

$$D_{0,102_{1,2-DCA}} = \alpha_{Diffusion,Chlorine} \cdot D_{0,1,2-DCA,total} \quad \text{(S5-34)}$$

For DCM it was assumed that the diffusion coefficients in free solution of the DCM carbon isotopocules with the mass 87 (Tab. 2) correspond to the diffusion coefficient in free solution of the total DCM concentration ($D_{0,DCM,total} \approx D_{0,87,DCM}$). Hence, the diffusion coefficients for each individual DCM carbon isotopocules corresponds to:

$$D_{0,87_{DCM}} = D_{0,DCM} \quad \text{(S5-35)}$$

$$D_{0,88_{DCM}} = \alpha_{Diffusion,Carbon} \cdot D_{0,DCM} \quad \text{(S5-36)}$$

S4. References

Einarson, M.D., Casey, M.B., Winglewich, D.L., Morkin, M.I., 1998. Enviro-core - A dual-tube direct push system for rapid site characterization. Proceedings of the Symposium on the Application of Geophysics to Environmental and Engineering Problems. Environmental & Engineering Geophysical Society, Wheat Ridge, 1-10 pp.

Jin, B., Haderlein, S.B., Rolle, M., 2013. Integrated carbon and chlorine isotope modeling: applications to chlorinated aliphatic hydrocarbons dechlorination. Environmental science & technology, 47(3): 1443-1451.

Parker, B.L., 1996. Effect of Molecular Diffusion on the Persistence of Dense Immiscible Phase Organic Liquids in Fractured Porous Geologic Media. PhD Thesis Thesis, University of Waterloo, Waterloo, Ontario, Canada, 191 pp.

USEPA, 1989. Hazardous Waste Treatment, Storage, and Disposal Facilities (TSDF)-USEPA, OAQPS, Air Emission Models. (EPA-450/3-87-026).

Wanner, P., Hunkeler, D., 2015. Carbon and chlorine isotopologue fractionation of chlorinated hydrocarbons during diffusion in water and low permeability sediments. Geochimica et Cosmochimica Acta, 157: 198-212.

Chapter 6: Quantification of Degradation of Chlorinated Hydrocarbons in Saturated Low Permeability Sediments Using Compound-Specific Isotope Analysis (CSIA)

Published in Environmental Science and Technology

Philipp Wanner, Beth Parker, Steven Chapman, Ramon Aravena and Daniel Hunkeler (2016). *Environ. Sci. Technol.* **50(11)**, 5622–5630

Abstract

This field and modelling study aims to reveal if degradation of chlorinated hydrocarbons in low permeability sediments can be quantified using compound-specific isotope analysis (CSIA). For that purpose, the well-characterized Borden research site was selected, where an aquifer-aquitard system was artificially contaminated by a three component chlorinated solvent mixture (Tetrachloroethene (PCE) 45 vol%, Trichloroethene (TCE) 45 vol%, and Chloroform (TCM) 10 vol%). Nearly 15 years after the contaminant release, several high-resolution concentration and CSIA profiles were determined for the chlorinated hydrocarbons that had diffused into the clayey aquitard. The CSIA profiles showed large shifts of carbon isotope ratios with depth (up to 24‰) suggesting that degradation occurs in the aquitard despite the small pore sizes. Simulated scenarios without or with uniform degradation failed to reproduce the isotope data, while a scenario with decreasing degradation with depth fit the data well. This suggests that nutrients had diffused into the aquitard favoring stronger degradation close to the aquifer – aquitard interface than with increasing depth. Moreover, the different simulation scenarios showed that CSIA profiles are more sensitive to different degradation conditions compared to concentration profiles in aquitards highlighting the power of CSIA to constrain degradation activities in aquitards.

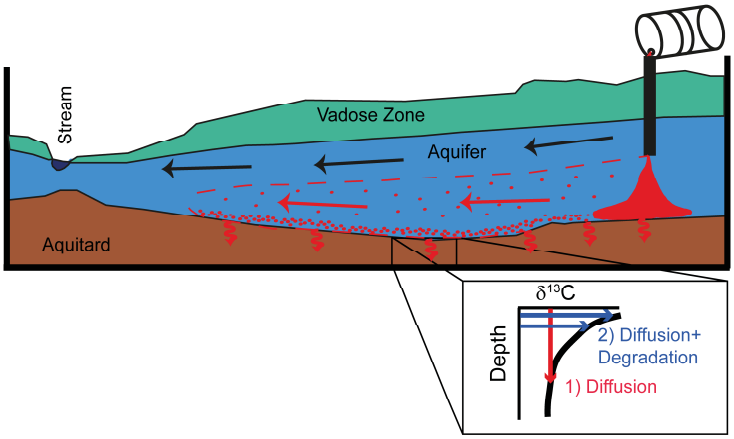

Graphical Abstract

6.1. Introduction

Due to improper disposal and accidents, chlorinated hydrocarbons are major subsurface contaminants at many industrial sites. After releasing at the surface, chlorinated hydrocarbons migrate vertically as dense non-aqueous phase liquid (DNAPL) into aquifer systems and tend to form pools on top of low permeability sediments. With time the accumulated DNAPL phase is dissolved and transported by advection in the aquifer and by diffusion into the underlying low permeability sediments (Chapman and Parker, 2005; Parker et al., 2008). After reduction of the strength of the chlorinated hydrocarbon plume in the aquifer, back-diffusion occurs from low permeability sediments towards the aquifer due to the reversal of the concentration gradient, forming a long-term contamination source (Adamson et al., 2015; Johnson and Pankow, 1992; Liu and Ball, 2002; Parker et al., 2008). Most previous studies assumed that chlorinated hydrocarbons are not affected by degradation in low permeability sediments (Chapman and Parker, 2005; Johnson and Pankow, 1992; Liu and Ball, 2002; Seyedabbasi et al., 2012). It was commonly hypothesized that microbial growth is very limited in the small pores of low permeability sediments and that degradation of chlorinated hydrocarbons is thus unlikely to occur (Fredrickson et al., 1989; Lima and Sleep, 2007; Stotzky, 1986; White et al., 2008). In contrast, Manoli et al. (2012) and Scheutz et al. (2010) stimulated artificial microbial growth in a clayey till and demonstrated that degradation can also occur in low permeability sediments despite the small pore sizes. By injecting electron donors and nutrients into fractures and sandy stringer in a low permeable clay unit, Manoli et al. (2012) and Scheutz et al. (2010) revealed that the electron donors and nutrients diffuse into the low permeable zones stimulating degradation activities in the surrounding clay unit. The degradation activities in the clay were strongest adjacent to the high permeability zone and decreased within a few centimeters distance. Moreover, recent studies (Damgaard et al., 2013; Takeuchi et al., 2011) found evidence for degradation of chlorinated hydrocarbons in low permeability sediments without stimulating microbial growth. However, the natural occurrence of degradation activities in aquitards has not yet been well constrained. In general most degradation studies have been done at sites, where the contamination occurred accidentally (Damgaard et al., 2013; Takeuchi et al., 2011) such that the initial conditions of the contamination source (composition, spill time, volume) were not well known. This complicates the identification of degradation activities and hampers the quantification of degradation rates.

Compound-specific isotope analysis (CSIA) has been successfully used as a tool to assess degradation occurring in aquifer systems. This method makes use of the more rapid cleavage of bonds between light compared to heavy isotopes during degradation.(Elsner et al., 2005; Hunkeler et al., 2011; Hunkeler et al., 2005; Hunkeler et al., 1999; Kuder et al., 2005; Lollar et al., 2001; Meckenstock et al., 2004) In contrast to aquifers, it is not yet clear as to what extent CSIA can also be used to quantify degradation of chlorinated hydrocarbons in saturated low permeability sediments. Recent studies (Jin et al., 2014; Wanner and Hunkeler, 2015) quantified for the first time isotope fractionation of organic contaminants due to aqueous phase diffusion and showed that it is associated with only a small isotope effect. Therefore, isotope fractionation associated with diffusion is not expected to impair identification of degradation in low permeability sediments using CSIA.

In this study, we investigate if CSIA can be used to identify and quantify reactive processes in saturated low permeability sediments. For this purpose, an area of the well-characterized aquifer-aquitard system at the Borden research site was selected. At this site a prior chlorinated hydrocarbon DNAPL infiltration experiment was conducted, resulting in formation of a plume in the aquifer and contamination of the underlying aquitard via diffusion below the plume. Multiple high-resolution concentration and compound-specific carbon isotope ratio profiles were determined using cores collected from the aquitard along groundwater monitoring transects at varying distances downgradient from the contamination source at about 14.5 years (5281 days) after the DNAPL release. Three different degradation scenarios were simulated for the aquitard to assess how vertically varying degradation conditions affect CSIA profiles and to identify which scenario is most consistent with measured field data. The present study provides new insight into degradation activities in a clayey aquitard from an aged controlled release experiment, which improves the understanding of the fate of chlorinated hydrocarbons in saturated low permeability sediments. Moreover, the study provides a basis for estimating the longevity of secondary contamination sources in low permeability sediments affecting adjacent aquifers.

6.2. Materials and Methods

6.2.1. Site description and controlled release experiment procedure

The controlled release experiment was performed in an aquifer overlying a clayey aquitard in the forested area of the Borden research (BDI) site, Ontario, Canada approximately 100 kilometers north of the city of Toronto (Fig. 6-1). Both the aquifer as well as the aquitard is well characterized by previous studies (Brewster et al., 1995; Freyberg, 1986; Hartog et al., 2010; Hwang et al., 2008; Laukonen, 2001; Mackay et al., 1986; Morrison, 1998; Sudicky, 1986; Sudicky and Illman, 2011; Vargas, 2005). The sandy aquifer and the clayey aquitard were formed during the sedimentary deposition in the proglacial lake Algonquin 12,000 years B.P. (Brewster et al., 1995) and consists of primarily horizontal, discontinuous lenses of medium grained, fine-grained, and silty fine grained sand (Sudicky, 1986) with a mean porosity of 0.33 (standard deviation (SD) of 0.017) (Mackay et al., 1986). Despite the observed variability, the sandy aquifer is considered as relatively homogeneous (Freyberg, 1986). At the study site the water table varies seasonally between 0.5 and 1.5 m below ground surface (bgs) and the groundwater velocity varies over the year with an average of 12±8 cm/day (Hartog et al., 2010). The lateral flow direction also changes seasonally within an angle range of about 58° (Laukonen, 2001) (Fig. 6-1). The aquifer thickness is about 3 m (Hartog et al., 2010) containing a thin transition zone with occasional cobbles at the aquifer-aquitard interface (Fig. 6-1). The underlying aquitard consist mainly of dioctahedral mica (likely muscovite) and chlorite with detectable amounts of kaolinite and smectite (Allen-King et al., 1996) with a mean porosity of 0.40 (standard deviation (SD) of 0.09) (Parker, 1996). The aquitard thickness is about 8 m and is subdivided into upper and lower aquitard units (Morrison, 1998). The upper aquitard is about 3 m thick with a hydraulic gradient of 0.1 (Meldrum, 1999) and a hydraulic conductivity ranging between 2.0E-7 and 1.80E-9 m/s (Morrison, 1998), while the lower aquitard is 5 m thick with a hydraulic gradient of 0.7 (Meldrum, 1999) and a hydraulic conductivity of 1.0E-8 m/s (Foley, 1992).

The controlled release experiment was initiated by Laukonen (2001) on April 8, 1999 by injecting a 50-liter three component DNAPL mixture of Tetrachloroethene (PCE, 45 vol%), Trichloroethene (TCE, 45 vol%) and Chloroform (TCM, 10 vol%) into the sandy aquifer, through an open-ended pipe 0.5 m below the groundwater table (Fig. 6-1). After injection, the

DNAPL served as a source for a natural gradient, dissolved phase plume that was monitored in detail with sixteen rows of multilevel wells located perpendicular to groundwater flow direction over a distance of 95 m downgradient of the injection point by Laukonen (2001), Klein (2002), Vargas (2005) and the present study. Each multilevel row has between 8 and 30 multilevel wells containing between 7 and 16 sample points each, with a maximum 0.15 m vertical spacing, resulting in more than 3200 sampling ports total.

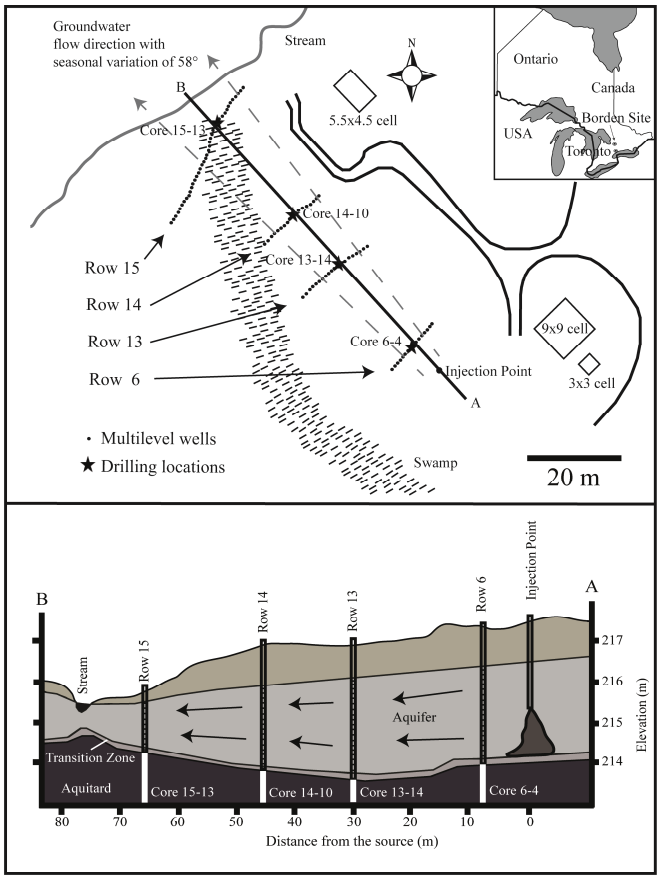

Figure 6-1. Locations of multilevel wells along transects (only selected transects shown), drilling locations for determination of aquitard concentration and compound-specific carbon isotope ratio profiles, and injection point at the forested area at the Borden research site (Fig. 6-1A), and cross-section along the groundwater flow direction showing multilevel system depths in the aquifer and core intervals in the aquitard (Fig. 6-1B).

6.2.2. Groundwater sampling, core retrieval and VOC extractions

A detailed description of groundwater sampling, core retrieval, core subsampling and VOC extraction from core subsamples can be found in section S1. of the Supporting Information (SI), which can be found at the end of this chapter. In brief, groundwater from multilevel wells in the aquifer was sampled using Geopump® peristaltic pumps with dedicated 0.32 cm OD diameter Teflon® tubing. For the present study, multilevel well rows 6, 13, 14 and 15, located at 8, 30, 45, 65 m distance downgradient from DNAPL injection point, were sampled in summer 2008 and 2013 (Fig. 6-1). In contrast to the aquifer, water sampling in the aquitard was not possible as not enough water can be obtained from the aquitard. Hence, to assess chlorinated hydrocarbon concentration and compound-specific carbon isotope ratio profiles in the aquitard, continuous cores were collected adjacent to selected multilevel wells (ca. 20 cm distance) along four transects at rows 6, 13, 14 and 15 downstream of the injection point (cores referred to as 6-4, 13-14, 14-10 and 15-13, corresponding to the nearest multilevel well designation) on November 15, 2013, at about 14.5 years (5281 days) after the DNAPL release occurred (Fig. 6-1). Continuous cores were collected from the aquitard beginning just above the interface using a Geoprobe 7720DT direct-push rig and the Envirocore dual tube sampling system described by Einarson et al. (1998). To obtain high resolution chlorinated hydrocarbon concentration CSIA profiles, retrieved cores were photographed, logged and subsampled with a narrow spacing (~5cm) as a function of depth and chlorinated hydrocarbons were subsequently extracted from the subsamples in methanol as described by Parker (1996) and White et al. (2008)

6.2.3. Concentration, compound-specific carbon isotope and organic carbon content analysis

Detail descriptions of analytical methods are available in section S1. of the SI at the end of this chapter. Briefly, chlorinated hydrocarbon concentrations in groundwater samples and in the MeOH extracts of core subsamples were analyzed by a gas chromatograph coupled to a mass spectrometer (GC-MS). Compound-specific carbon isotope ratios of PCE, TCE and cDCE were determined by a gas chromatograph coupled to an isotope mass spectrometer (GC-IRMS). The organic carbon content in the cores was measured using a G4 Icarus combustion analyzer.

6.3. Numerical Modelling

A 1D numerical reactive transport model was developed to simulate the migration of chlorinated hydrocarbons in the aquitard at the BDI site under various degradation conditions. The aim of the simulations was to assess how different degradation scenarios are reflected in concentration and CSIA profiles and to explore if degradation activities lead to unique concentration and isotope ratio patterns compared to a diffusion/back-diffusion scenario without degradation. The modelling approach is described in detail in section S2. of the SI at the end of this chapter. Briefly, it was assumed that transport is diffusion dominated in the clayey aquitard and that sorption occurs linearly and non-competitive for the observed VOC concentration range, which is consistent with previous studies (Allen-King et al., 1995; Allen-King et al., 1996; Parker, 1996). Model calibration was performed against measured field data (see section S2.3. in SI for details). The known time series of chlorinated hydrocarbon concentrations at the aquifer interface from the bottommost port on the adjacent multilevel well (ca. 20 cm distance) were used as a boundary condition (Figs. S6-1A-D, SI). The degradation scenarios were modelled for 5281 days (~14.5 years), which corresponds to the time period between contaminant infiltration and the retrieval of the cores from the aquitard. For simulating the scenarios, initial compound-specific carbon isotope ratios ($\delta^{13}C_{VPDB}$) at the aquifer – aquitard interface in a range between -25.0‰ and -26.0‰ for PCE, between -28.0‰ and -30.0‰ for TCE and between -33.0‰ and -37.0‰ for cDCE were used. These values correspond to groundwater CSIA measurements conducted by Vargas (2005) at the aquifer-aquitard interface. Degradation activities affecting chlorinated hydrocarbons in the aquitard were taken into account in the model by considering the sequential dechlorination of PCE (Tab. S6-1, SI). Carbon isotope fractionation during the sequential dechlorination of PCE was simulated as described by Van Breukelen et al. (2005) using calibrated enrichment factors of ε_{PCE}= -2.0‰, ε_{TCE}=-18.2‰ and ε_{cDCE}=-24.0‰ (Tab. S6-4a). These values are within the ±1σ range of the average of all published enrichment factors for the sequential dechlorination of PCE (Tab. S6-2a-c, SI). Beside reactive processes, it was assumed that the diffusive transport process is also associated with an isotope effect. Fractionation factors due to diffusion were defined according to Wanner and Hunkeler (2015). The calibration of the model revealed that degradation is non-uniformly distributed in the aquitard (stronger close to the aquifer – aquitard interface than with increasing depth), which will

be discussed in more detail in the "Results and Discussion" section. To quantify the quality of the fit between measured and modeled concentration and isotope data, the root mean squared error was used (RMSE; see equation S6-5 in SI). After model calibration, two additional degradation scenarios were simulated for the aquitard: No-degradation and uniform degradation with depth and compared with field data to investigate the sensitivity of concentration and CSIA profiles to different degradation conditions.

6.4. Results and Discussion

6.4.1. Concentration data

The groundwater concentration analysis of the present study in combination with data from previous studies (Klein, 2002; Laukonen, 2001; Vargas, 2005) provides a detailed spatial and temporal data set of the long-term chlorinated hydrocarbon plume evolution in the aquifer at the BDI site (see section S3. in SI for details). In this study, the chlorinated hydrocarbon concentration evolution is of interest in the bottom most sampling points in the aquifer at about 20 cm distance from the aquifer - aquitard interface, adjacent to the locations, where the clay cores were retrieved (Fig. 6-1A). At these locations, the chlorinated hydrocarbon plume arrived between 100 and 700 days after DNAPL infiltration (Figs. S6-1A-D, SI). During the migration in the aquifer, a separation of the different compounds was observed. PCE was detected later than TCE and TCM (Figs. S6-1A-D, SI), which is attributed to different sorption behavior. PCE sorbs more strongly on the sandy aquifer material and hence, migrates more slowly in the aquifer compared to TCE and TCM (Rivett et al., 2001). At all four coring locations, TCE shows the highest peak concentration (range: 16,000 - 210,000 μg/L = 0.015 - 0.191 $Solubility_{TCE}$) followed by PCE (range: 10,000 - 100,000 μg/L = 0.050 - 0.500 $Solubility_{PCE}$) and TCM (range: 800 - 50,000 μg/L = 9.76E-05 – 6.10E-03 $Solubility_{TCM}$ (Figs. S6-1A-D, SI). In contrast, significant cDCE concentrations (maximum of 1400 μg/L = 2.84E-05 $Solubility_{cDCE}$) were detected only at the interface at the farthest downgradient core location 15-13, with the peak occurring 3300 days after injection.

Concentration analysis in the clay cores revealed that three different contaminants are present in the aquitard: PCE, TCE and cDCE (TCM was only detected at low concentrations <0.05 μg/g, likely due to its rapid depletion from the DNAPL source and rapid flushing through

the aquifer, hence, the results are not presented here) (Figs. 6-2A-D). The penetration depth of the organic contaminations into the aquitard varied among the cores between 30 and 50 centimeters (Figs. 6-2A-D). In the cores 6-4, 13-14 and 15-13 PCE shows the highest concentrations within 10 centimeter distance from the aquifer - aquitard interface ranging between 2.3 and 6.4 μg/g (Figs. 6-2A,B and D), while in core 14-10 PCE shows the lowest concentration (<0.2 μg/g) compared to TCE and cDCE (Fig. 6-2C). The TCE concentrations reach their maximum deeper than PCE (12-20 cm depth) ranging between 1.7 and 2.1 μg/g and declined with increasing depth (Figs. 6-2A-D). The cDCE concentrations showed a similar distribution as for TCE. However, compared to TCE, an increase of cDCE concentrations with increasing distance from the contaminant injection point is observed reaching concentrations up to 1.4 μg/g in the farthest downgradient core 15-13 (Figs. 6-2A-D). Fractions of organic carbon content ranging between 0.59 and 0.78% were measured in the retrieved cores (Tab. S6-4b, SI).

The low chlorinated hydrocarbon concentrations (<7.0 μg/g) in the retrieved clay cores indicate that no DNAPL phase was present at the aquifer-aquitard interface as otherwise the aquitard concentrations would be at least one order of magnitude higher (Parker et al., 2004). The shape of the concentration profiles with the peak occurring below the interface and decreasing concentrations both with depth and towards the interface in combination with the temporal concentration evolution in the overlying aquifer is characteristic for a diffusion/back-diffusion scenario in the aquitard as observed in previous studies (Chapman and Parker, 2005; Johnson and Pankow, 1992; Liu and Ball, 2002; Parker et al., 2008; Seyedabbasi et al., 2012). The concentration profiles suggest that chlorinated hydrocarbons were initially diffusing into the clay as the plume arrived. After the peak concentrations passed through each location, concentrations at the interface diminished initiating back-diffusion towards the aquifer due to the reversal of the concentration gradient. However, the presence of cDCE in all four cores indicates that degradation is occurring in the aquifer and/or aquitard, since this compound is a degradation product of TCE and was not part of the injection mixture. The observed aerobic conditions in the aquifer between the contamination source and multilevel row 15 (Vargas, 2005) in 2004 and 2005 suggest that degradation of the chlorinated hydrocarbons is mainly occurring in the aquitard. Furthermore, the integration of the time series of chlorinated hydrocarbon concentrations at the aquifer interface and of the aquitard concentration profiles, show that cDCE represents a larger mass portion (5-75%) of the total VOC mass in the aquitard than in the aquifer

(0.05-15%) (Figs. 6-2A-D). This indicates that cDCE is mainly produced in the aquitard and confirms the hypothesis that degradation is taking place mainly in the aquitard.

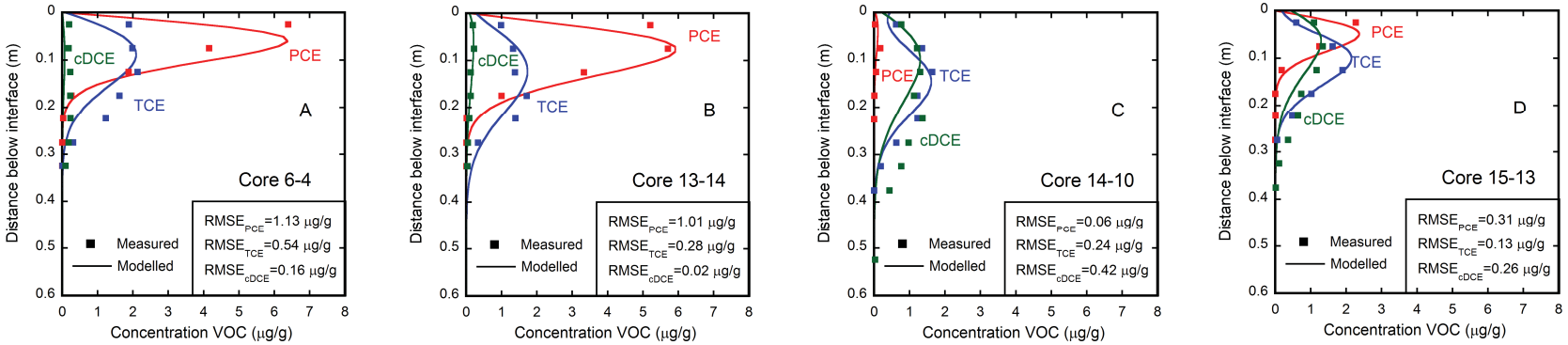

Figures 6-2A-D. Measured and modelled chlorinated hydrocarbon concentrations in the retrieved clay cores 5281 days after infiltrating the organic contaminants into aquifer. The continuous lines indicate the modelled concentration profiles of PCE (red), TCE (blue) and cDCE (green), while the squares represent the measuring points. The technical details of the modelling approach are provided in section S2. of the Supporting Information at the end of this chapter. The root-mean squared error (RMSE) was used to quantify the quality of the fit between measured modelled concentration profiles.

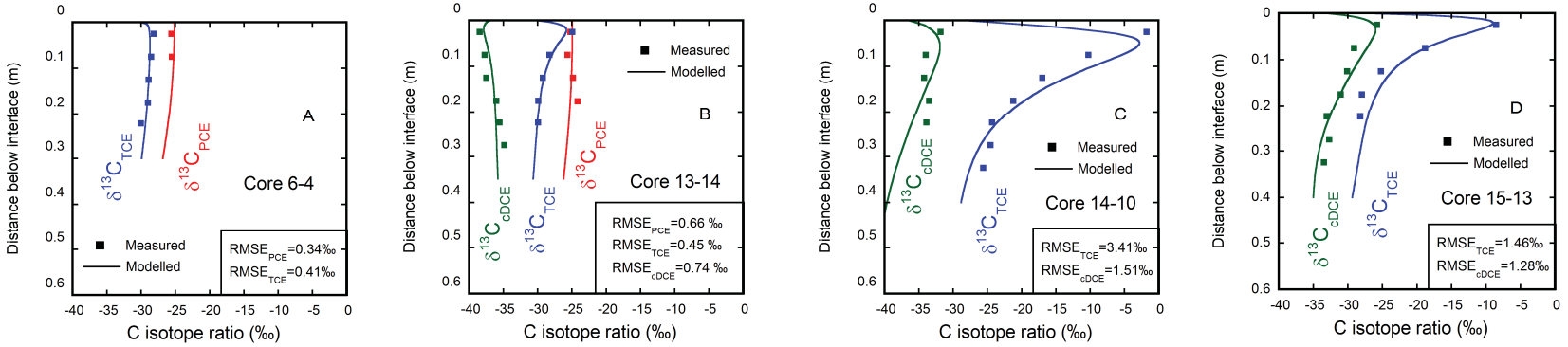

Figures 6-3A-D. Measured and modelled compound-specific carbon isotope profiles in the retrieved clay cores 5281 days after infiltrating the organic contaminants into aquifer. The continuous lines indicate the modelled isotope profiles of PCE (red), TCE (blue) and cDCE (green), while the squares represent the measuring points. The technical details of the modelling approach are provided in section S2. of the Supporting Information at the end of this chapter. The root-mean squared error (RMSE) was used to quantify the quality of the fit between measured modelled carbon isotope profiles.

6.4.2. Compound-specific carbon isotope ratios in the aquitard

The magnitude of the shift of compound-specific carbon isotope ratios with depth varied among the retrieved cores (Figs. 6-3A–D). In core 6-4, located closest to the injection point (Fig. 6-1), small shifts of PCE and TCE carbon isotope ratios in a range of $\Delta\delta^{13}C_{VPDB}$=2‰ were observed with increasing depth (Fig. 6-3A). In contrast, larger shifts of carbon isotope ratios with depth were observed in cores 13-14, 14-10 and 15-13 (Figs. 6-3B-D), which are located further downgradient from the injection point (Fig. 6-1). In core 13-14, PCE and cDCE became enriched, while TCE was depleted in heavy isotopes with increasing depth (Fig. 6-3B) with the magnitude of the shift of carbon isotope ratios for TCE up to $\Delta\delta^{13}C_{VPDB}$=4.8‰. In core 14-10, the largest shift ($\Delta\delta^{13}C_{VPDB}$ = 23.9‰) of TCE carbon isotope ratios was observed, whereas for cDCE carbon isotope ratios were only slightly shifted towards lighter signatures with depth (Fig. 6-3C). In core 15-13 (Fig. 6-3D) similar TCE and cDCE carbon isotope ratio profiles were observed compared to core 14-10 (Fig. 6-3C). However, the magnitude of the shift of carbon isotope ratios of TCE in core 15-13 was smaller than in core 14-10 ($\Delta\delta^{13}C_{VPDB}$=19.7‰) but larger for cDCE ($\Delta\delta^{13}C_{VPDB}$=7.7‰).

The observed shifts primarily towards lighter carbon isotope signatures with depth in the retrieved clay cores (Figs. 6-3A-D) are consistent with what is expected for diffusive transport in saturated low permeability sediments without degradation (Wanner and Hunkeler, 2015). However, the magnitude of the shifts of carbon isotope ratios is much larger (up to 23.9‰) mainly in clay cores 13-14, 14-10 and 15-13 (Figs. 6-3B–D) than what is expected due to diffusion only (~2‰) (Wanner and Hunkeler, 2015). Earlier CSIA aquifer measurements performed by Vargas (2005) showed that five and six years after contaminant injection isotope signatures had not changed significantly upgradient of multitlevel row 15 within the zone where clay cores were retrieved. This suggests minor degradation in the aquifer upgradient of multilevel row 15 within the first six years after the contaminants were released. After the isotope measurements performed by Vargas (2005) back diffusion occurred as most of the plume had passed the sampling locations (Figs. S6-1A-D and S6-2A-D, SI). This indicates that the isotope ratios in the aquitard are no longer influenced by isotope signatures in the aquifer after the study performed by Vargas (2005). Hence, even if degradation had occurred in the aquitard after the isotope measurements performed by Vargas (2005), increasingly heavier carbon isotope

signatures in the aquifer due to degradation followed by diffusive transport into the aquitard is not a plausible explanantion for the observed shifts of carbon isotope ratios in the aquitard. This shows consistently with the concentration data that observed larger shifts of isotope ratios with depth can only be explained by degradation in the aquitard. Furthermore, the lack of observation of degradation beyond cDCE is also frequently observed at other contaminated sites, where degradation of chlorinated hydrocarbons occurs (Wiedemeier, 1999).

However, most of the carbon isotope patterns especially in cores 13-14, 14-10 and 15-13 are opposite to what is expected when degradation occurs uniformly with depth in the aquitard (Figs. 6-3B-D). In a uniform degradation scenario, carbon isotope ratios would be shifted towards heavier isotopes with increasing depth, which does not agree with the measured isotope ratio profiles. However, it was striking that carbon isotope ratios at the bottom of the core profiles corresponded to the ratios measured by Vargas (2005) at the aquifer-aquitard interface (Figs. 6-3A-D). This is an indication that chlorinated hydrocarbons were likely initially diffusing from the aquifer into the aquitard unaffected by degradation and only slightly fractionated due to diffusion. Afterwards, degradation appears to have become more active and shifted carbon isotope ratios more strongly close to the interface than with increasing depth. Thus, the scenario of non-uniformly distributed degradation activities with depth starting with a time lag could be the reason for the opposite carbon isotope ratio profiles to what is expected when degradation is uniformly distributed with depth in the aquitard.

6.4.3. Simulation of different degradation scenarios in the aquitard

In order to investigate the processes that produced the observed unique carbon isotope ratio pattern and to assess how different degradation conditions are reflected in carbon isotope ratio profiles, three different scenarios were simulated: A) no-degradation, B) uniform degradation and C) non-uniform degradation with depth in the aquitard starting with a time lag. In the no-degradation scenario, typical diffusion/back-diffusion concentration patterns were observed and carbon isotope ratios are only slightly shifted with depth due the diffusive transport process (Figs. 6-4A-D and Figs. S6-7A-D, SI). Comparing measured and modelled concentration profiles in the no-degradation scenario shows that measured PCE, TCE and cDCE concentration profiles are in agreement (except for core 14-10) with modelled data (Figs. S6-7A-D, SI). In contrast the large shifts of isotope ratios with depth especially in cores 13-14, 14-10 and 15-13 are clearly different than simulated profiles in the no-degradation scenario (Figs. 6-4A-D). Thus,

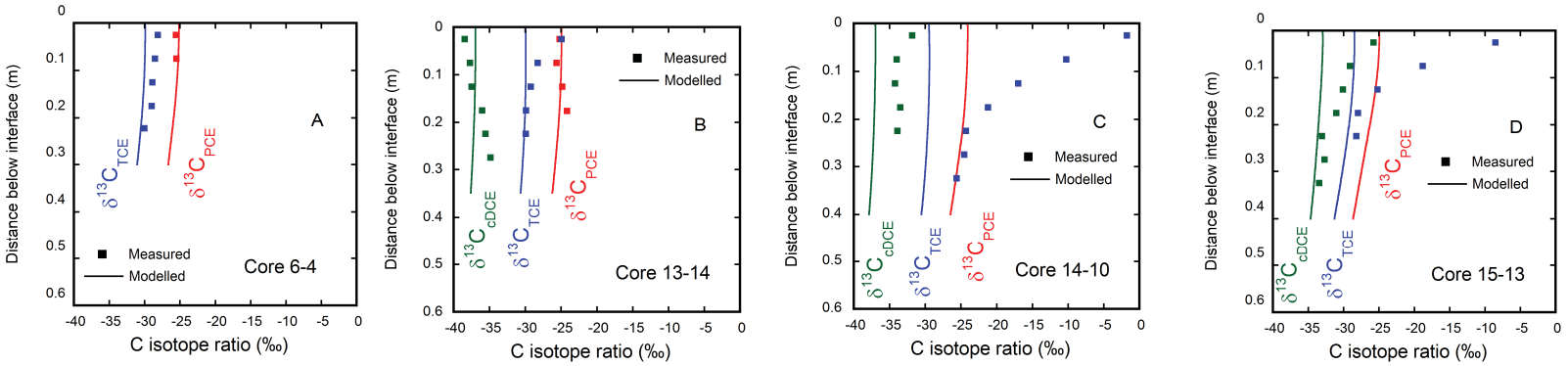

Figures 6-4A-D. Comparison between measured and modelled compound-specific carbon isotope ratio profiles in the retrieved clay cores for the no-degradation scenario 5281 days after injecting the organic contaminants into aquifer. The continuous lines indicate the modelled isotope profiles of PCE (red), TCE (blue) and cDCE (green), while the squares represent the measuring points. Technical details of the modelling approach are provided in section S2. of the Supporting Information at the end of this chapter.

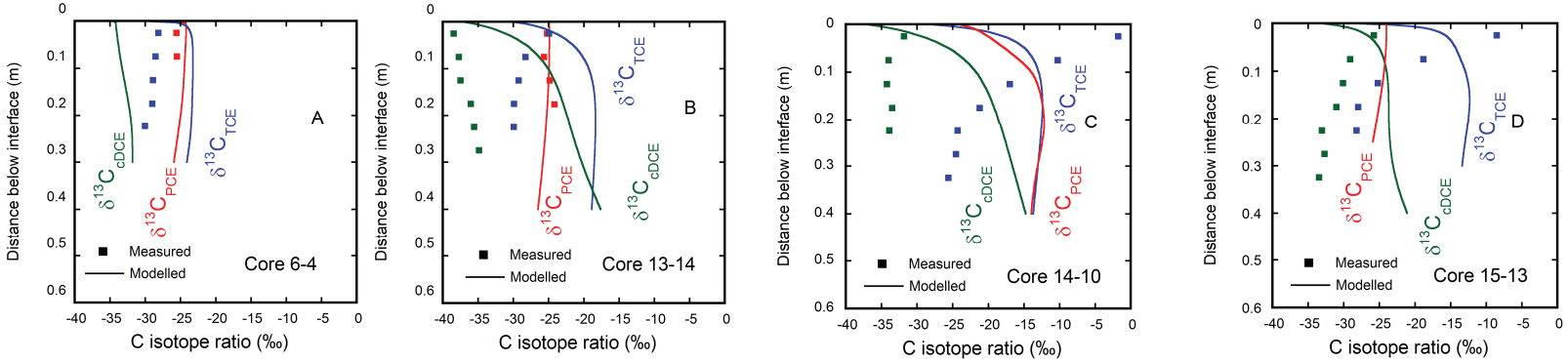

Figures 6-5A-D. Comparison between measured and modelled compound-specific carbon isotope ratio profiles in the retrieved clay cores for the uniform degradation scenario 5281 days after injection of the organic contaminants into aquifer. The continuous lines indicate the modelled isotope profiles of PCE (red), TCE (blue) and cDCE (green), while the squares represent the measuring points. The technical details of the modelling approach are provided in section S2. of the Supporting Information at the end of this chapter.

the comparison between measured data and the no-degradation scenario confirms the hypothesis that degradation is minimal in core 6-4 but takes place more strongly in the lower part of the aquitard downgradient of multilevel row 6 in cores 13-14, 14-10 and 15-13 (Fig. 6-1).

In order to evaluate the dynamics of degradation with depth in the aquitard, measured concentration and carbon isotope profiles were compared with the uniform (B) and the non-uniform (C) degradation simulation scenario starting with a time lag. In the uniform degradation scenario, carbon isotope ratios are primarily shifted towards heavier signatures with increasing depth as soon as degradation is active (Figs. 6-5A-D). The magnitude of carbon isotope fractionation for PCE is smaller than for TCE and cDCE due to the smaller fractionation factor (Tab. S6-4a, SI). Although the shape of the concentration profiles is in agreement with modelled concentration profiles for the uniform degradation scenario (Figs. S6-8A-D, SI), modelled carbon isotope ratio profiles are clearly different than measured ratio profiles (Figs. 6-5A-D). This demonstrates that chlorinated hydrocarbons are most likely not affected by uniform degradation in the aquitard. In contrast, in the non-uniform degradation scenario, chlorinated hydrocarbons are affected more strongly by degradation close to the aquifer-aquitard interface than with increasing depth. The non-uniformly distributed degradation activities were described by first order degradation rates following an inverse error function dependent on the depth (Tab. 6-1) i.e. degradation activities decreased exponentially with increasing depth (Figs. S6-6A and S6-6B, SI). The measured concentration and carbon isotope ratio profiles are both consistent with the non-uniform degradation scenario in all four cores (Figs. 6-2A-D and 6-3A-D). This confirms the hypothesis that chlorinated hydrocarbons are influenced by non-uniform degradation in the aquitard starting with a time lag after contaminant release and arrival. The best fit between measured and modelled data (RMSE: 0.06 – 1.30 μg/g for concentration profiles and 0.35 – 3.72‰ for carbon isotope profiles) was achieved by setting the starting point for the degradation activities at 2300 – 2800 days after the contaminant release (Tab. 6-1). The simulated non-uniform degradation scenario showed that the largest enrichment of heavy isotopes occurs slightly below the aquifer – aquitard interface despite the occurrence of the strongest degradation activities at the interface. This can be explained with the slight vertical displacement of the largest enrichment of heavy isotopes due to diffusive transport as degradation and diffusion occur simultaneously in the Borden aquitard.

Table 6-1. Selected model parameters for concentration and carbon isotope ratio profiles simulations in the retrieved cores. The shape of the degradation function and the start of the degradation for each clay core were determined by means of model calibration.

Parameters	Unit	Core 6-4	Core 13-14	Core 14-10	Core 15-13
Distance from injection point	m	8	30	45	65
Degradation rate PCE: k_{PCE}[2]	1/s	3.3E-11·erfc(0.1z)[1]	9.8E-10·erfc(20.z)[1]	9.8E-8·erfc(0.1z)[1]	3.3E-8·erfc(8.0z)1
Degradation rate TCE: k_{TCE}[2]	1/s	9.2E-10·erfc(0.5z)[1]	7.6E-8·erfc(34z)[1]	8.5E-8·erfc(11.0z)[1]	2.7E-7·erfc(20.0z)[1]
Degradation rate cDCE: k_{cDCE}[2]	1/s	3.3E-10·erfc(0.1z)[1]	2.0E-9·erfc(0.1z)[1]	4.6E-10·erfc(0.1z)[1]	6.2E-8·erfc(17.0z)[1]
Start (bio)degradation after injection[2]	days	2300	2800	2500	2600

[1]z corresponds to vertical depth in the cores
[2]Calibrated

The successful reproduction of the measured concentrations and carbon isotope ratio profiles with the non-uniform degradation scenario by means of model calibration opened the possibility to quantify degradation rates (Tab. 6-1). Chlorinated hydrocarbons were affected most faintly by degradation close to the contamination source (core 6-4), while with increasing distance degradation activities become stronger in cores 13-14, 14-10 and 15-13 (Tab. 6-1). The variation in degradation rates might be related to spatial variations in organic carbon composition.

In core 13-14 determined degradation rates revealed that TCE is degraded more rapidly than cDCE and PCE (Tab. 6-1). Due to the faster degradation of TCE compared to cDCE and PCE, the preferential degradation of light TCE carbon isotopes in comparison to heavy isotopes is the predominant fractionation process close to the interface. This explains the accumulation of the remaining isotopically heavy TCE and the produced light cDCE carbon isotope with respect to the interface values originating from TCE degradation close to the interface. In contrast, with increasing depth TCE, PCE and cDCE are less affected by degradation (Tab. 6-1) and carbon isotope ratios are approaching similar values as before degradation activities commenced (Fig. 6-3B).

In contrast to core 13-14, determined degradation rates for core 14-10 showed that PCE was strongly affected by degradation (Tab. 6-1). Due to strong degradation, PCE concentrations decreased below 0.2 μg/g (Fig. 6-2C). Furthermore, in clay core 14-10, TCE is degraded two orders of magnitude faster than cDCE (Tab. 6-1) shifting the TCE carbon isotope ratios more

strongly towards heavier signatures than cDCE carbon isotope signatures with respect to the interface signatures. In core 15-13, both TCE and cDCE are degraded to a similar extent in the upper part of the core (Tab. 6-1), generating the more enriched isotope values for both compounds close to the interface compared to the interface carbon isotope ratios. Furthermore, as observed for cores 13-14 and 14-10, TCE and cDCE carbon isotope ratios are approaching original values before degradation activities started due to the decrease in degradation activities with depth (Tab. 6-1).

Variable and larger porosity close to the aquitard-aquifer interface as a possible explanation of the occurrence of the non- uniform degradation scenario can be likely excluded as previous porosity measurements at different depths in the upper 15cm of the Borden aquitard revealed that the porosity is fairly constant (0.40±0.09) (Parker, 1996). A more plausible explanation for the observed gradual decrease in degradation activity with increasing distance from the aquifer – aquitard interface, is the availability of nutrients diffusing from the overlying aquifer into the aquitard. Although on the larger scale this is similar to what Manoli et al. (2012) and Scheutz et al. (2010) observed around small fractures and stringers in low permeable units. These studies suggested that electron donors and nutrients diffuse from high into low permeability zones causing graduated degradation activities with increasing distance from the high permeability zones. Hence, analogously at the Borden site, it is likely that nutrients are transported by diffusion from the aquifer into the underlying aquitard and favor, combined with the high organic matter content in the aquitard, stronger degradation activities close the aquifer – aquitard interface than with depth. The rationale of diffusing nutrients causing the non-uniform degradation occurrence is supported by the fact that the distribution of the degradation activities with depth in the aquitard was best fitted by an inverse error function, which corresponds to the shape of diffusion profiles. Furthermore, the time lag between the degradation activities and the presence of the chlorinated hydrocarbons in the aquitard might be related with the fact that the establishment of microbial activities in the aquitard takes time and that chlorinated hydrocarbons are not compulsory immediately degraded when coming in contact with microbes (Ellis et al., 2000; Kao and Lei, 2000; Lendvay et al., 2003; Scheutz et al., 2008).

6.4.4. Advances in understanding degradation processes in saturated low permeability sediments

The present study has demonstrated for the first time that compound-specific isotope analysis (CSIA), measured in depth discrete profiles can be used for the quantification of reactive processes affecting chlorinated hydrocarbons in saturated low permeability sediments. Furthermore, the present study revealed that degradation of chlorinated hydrocarbon is possible to occur in saturated low permeability sediments despite the small pore sizes. The simulation of three different scenarios, (no-degradation, uniform degradation and non-uniform degradation) for the clayey aquitard at the Borden BDI research site showed that in contrast to concentration profiles, various degradation conditions produce characteristic carbon isotope ratio profiles. This indicates that carbon isotope ratio profiles are more sensitive to degradation activities than concentration profiles can be in aquitards. Hence, CSIA is an important complement in addition to concentration data to identify and quantify degradation activities and has the potential to become a standard tool to reveal degradation activities including spatial variability in saturated low permeability sediments. Furthermore, our study showed that the combination of aquitard isotope and concentration profiles provides more insight into the temporal dynamics of an aquifer/aquitard system and degradation processes in the aquitard. Understanding degradation processes in aquitards and low-permeability zones has important implications towards understanding long-term contaminant fate and potential magnitude and longevity of back-diffusion processes. This might have major impacts on the choice of the appropriate remediation approach for contaminated aquifer – aquitard systems. By improving the understanding of degradation processes in contaminated aquitards using CSIA, an excavation might become unnecessary and can be replaced by a monitored natural attenuation approach to remediate contaminated aquifer – aquitard systems. Thus, CSIA applications in aquitards potentially help to reduce costs for the remediation of contaminated sites.

6.5. Acknowledgement

The authors acknowledge the Swiss National Science Foundation (SNFS) for financial support. Furthermore, the authors thank Robert Ingleton from the University of Waterloo who

operated the Geoprobe rig, and several people from the University of Guelph: Ryan Kroeker, Dan Elliot and Keelin Scully for their skillful help in the field and Maria Gorecka and Rashmi Jadeja for their analytical support.

6.6. References

Adamson, D.T. et al., 2015. Characterization and Source History Modeling Using Low-k Zone Profiles at Two Source Areas. Groundwater Monitoring & Remediation, 35(2): 52-69.

Allen-King, R.M., Groenevelt, H., Mackay, D.M., 1995. Analytical method for the sorption of hydrophobic organic pollutants in clay-rich materials. Environmental science & technology, 29(1): 148-153.

Allen-King, R.M., Groenevelt, H., Warren, C.J., Mackay, D.M., 1996. Non-linear chlorinated-solvent sorption in four aquitards. Journal of contaminant hydrology, 22(3): 203-221.

Brewster, M.L. et al., 1995. Observed migration of a controlled DNAPL release by geophysical methods. Ground Water, 33(6): 977-987.

Chapman, S.W., Parker, B.L., 2005. Plume persistence due to aquitard back diffusion following dense nonaqueous phase liquid source removal or isolation. Water Resources Research, 41(12).

Damgaard, I. et al., 2013. Identification of chlorinated solvents degradation zones in clay till by high resolution chemical, microbial and compound specific isotope analysis. Journal of Contaminant Hydrology, 146: 37-50.

Einarson, M.D., Casey, M.B., Winglewich, D.L., Morkin, M.I., 1998. Enviro-core - A dual-tube direct push system for rapid site characterization. Proceedings of the Symposium on the Application of Geophysics to Environmental and Engineering Problems. Environmental & Engineering Geophysical Society, Wheat Ridge, 1-10 pp.

Ellis, D.E. et al., 2000. Bioaugmentation for accelerated in situ anaerobic bioremediation. Environmental science & technology, 34(11): 2254-2260.

Elsner, M., Zwank, L., Hunkeler, D., Schwarzenbach, R.P., 2005. A new concept linking observable stable isotope fractionation to transformation pathways of organic pollutants. Environmental Science & Technology, 39(18): 6896-6916.

Foley, S., 1992. Influcence of sand microbeds on hydraulic response of an unconfined clay aquitard. MSc Thesis Thesis, University of Waterloo, Waterloo, 277 pp.

Fredrickson, J. et al., 1989. Lithotrophic and heterotrophic bacteria in deep subsurface sediments and their relation to sediment properties. Geomicrobiology Journal, 7(1-2): 53-66.

Freyberg, D.L., 1986. A natural gradient experiment on solute transport in a sand aquifer .2. spatial moments and the advection and dispersion of nonreactive tracers. Water Resources Research, 22(13): 2031-2046.

Hartog, N., Cho, J., Parker, B.L., Annable, M.D., 2010. Characterization of a heterogeneous DNAPL source zone in the Borden aquifer using partitioning and interfacial tracers: Residual morphologies and background sorption. Journal of Contaminant Hydrology, 115(1-4): 79-89.

Hunkeler, D. et al., 2011. Assessing chlorinated ethene degradation in a large scale contaminant plume by dual carbon-chlorine isotope analysis and quantitative PCR. Journal of Contaminant Hydrology, 119(1-4): 69-79.

Hunkeler, D., Aravena, R., Berry-Spark, K., Cox, E., 2005. Assessment of degradation pathways in an aquifer with mixed chlorinated hydrocarbon contamination using stable isotope analysis. Environmental Science & Technology, 39(16): 5975-5981.

Hunkeler, D., Aravena, R., Butler, B.J., 1999. Monitoring microbial dechlorination of tetrachloroethene (PCE) in groundwater using compound-specific stable carbon isotope ratios: Microcosm and field studies. Environmental Science & Technology, 33(16): 2733-2738.

Hwang, Y.K., Endres, A.L., Piggott, S.D., Parker, B.L., 2008. Long-term ground penetrating radar monitoring of a small volume DNAPL release in a natural groundwater flow field. Journal of contaminant hydrology, 97(1): 1-12.

Jin, B., Rolle, M., Li, T., Haderlein, S.B., 2014. Diffusive Fractionation of BTEX and Chlorinated Ethenes in Aqueous Solution: Quantification of Spatial Isotope Gradients. Environmental Science & Technology, 48(11): 6141-6150.

Johnson, R.L., Pankow, J.F., 1992. Dissolution of dense chlorinated solvents into groundwater .2. source functions for pools of solvent. Environmental Science & Technology, 26(5): 896-901.

Kao, C., Lei, S., 2000. Using a peat biobarrier to remediate PCE/TCE contaminated aquifers. Water Research, 34(3): 835-845.

Klein, J.J.P., 2002. Comparison of Groundwater VOC Concentration Profiles From Different Sampling Scales and Techniques in The Borden Sand Aquifer. Bachelor Thesis, University of Waterloo, 69 pp.

Kuder, T. et al., 2005. Enrichment of stable carbon and hydrogen isotopes during anaerobic biodegradation of MTBE: microcosm and field evidence. Environmental Science & Technology, 39(1): 213-220.

Laukonen, K.A., 2001. Long-Term Natural Gradient Experiments in the Borden Sand Auqifer: A Bromide Slug and a Chloroform Plume from a Three-Component DNAPL Source. Master Thesis, University of Waterloo, 156 pp.

Lendvay, J. et al., 2003. Bioreactive barriers: a comparison of bioaugmentation and biostimulation for chlorinated solvent remediation. Environmental Science & Technology, 37(7): 1422-1431.

Lima, G.d.P., Sleep, B.E., 2007. The spatial distribution of eubacteria and archaea in sand–clay columns degrading carbon tetrachloride and methanol. Journal of contaminant hydrology, 94(1): 34-48.

Liu, C.X., Ball, W.P., 2002. Back diffusion of chlorinated solvent contaminants from a natural aquitard to a remediated aquifer under well-controlled field conditions: Predictions and measurements. Ground Water, 40(2): 175-184.

Lollar, B.S. et al., 2001. Stable carbon isotope evidence for intrinsic bioremediation of tetrachloroethene and trichloroethene at area 6, Dover Air Force Base. Environmental Science & Technology, 35(2): 261-269.

Mackay, D.M., Freyberg, D.L., Roberts, P.V., 1986. A natural gradient experiment on solute transport in a sand aquifer .1. approach and overview of plume movement. Water Resources Research, 22(13): 2017-2029.

Manoli, G. et al., 2012. A remediation performance model for enhanced metabolic reductive dechlorination of chloroethenes in fractured clay till. Journal of contaminant hydrology, 131(1): 64-78.

Meckenstock, R.U., Morasch, B., Griebler, C., Richnow, H.H., 2004. Stable isotope fractionation analysis as a tool to monitor biodegradation in contaminated acquifers. Journal of Contaminant Hydrology, 75(3-4): 215-255.

Meldrum, C.I., 1999. Use of a New Multi-Level Monitoring System for Determining Hydraulic Head Distribution in the Borden Aquitard, University of Waterloo, 52 pp.

Morrison, W.E., 1998. Hydrogeological Controls on Flow and Fate of PCE DNAPL in a Fractured and Layered Clayey Aquitard: A Borden Experiment. Master Thesis, Universitiy of Waterloo, 356 pp.

Parker, B.L., 1996. Effect of Molecular Diffusion on the Persistence of Dense Immiscible Phase Organic Liquids in Fractured Porous Geologic Media. PhD Thesis Thesis, University of Waterloo, Waterloo, Ontario, Canada, 191 pp.

Parker, B.L., Chapman, S.W., Guilbeault, M.A., 2008. Plume persistence caused by back diffusion from thin clay layers in a sand aquifer following TCE source-zone hydraulic isolation. Journal of Contaminant Hydrology, 102(1-2): 86-104.

Parker, B.L., Cherry, J.A., Chapman, S.W., 2004. Field study of TCE diffusion profiles below DNAPL to assess aquitard integrity. Journal of Contaminant Hydrology, 74(1-4): 197-230.

Rivett, M.O., Feenstra, S., Cherry, J.A., 2001. A controlled field experiment on groundwater contamination by a multicomponent DNAPL: creation of the emplaced-source and overview of dissolved plume development. Journal of Contaminant Hydrology, 49(1): 111-149.

Scheutz, C. et al., 2010. Field evaluation of biological enhanced reductive dechlorination of chloroethenes in clayey till. Environmental science & technology, 44(13): 5134-5141.

Scheutz, C. et al., 2008. Concurrent ethene generation and growth of Dehalococcoides containing vinyl chloride reductive dehalogenase genes during an enhanced reductive dechlorination field demonstration. Environmental science & technology, 42(24): 9302-9309.

Seyedabbasi, M.A., Newell, C.J., Adamson, D.T., Sale, T.C., 2012. Relative contribution of DNAPL dissolution and matrix diffusion to the long-term persistence of chlorinated solvent source zones. Journal of Contaminant Hydrology, 134: 69-81.

Stotzky, G., 1986. 10 Influence of Soil Mineral Colloids on Metabolic Processes, Growth, Adhesion, and Ecology of Microbes and Viruses1.

Sudicky, E.A., 1986. A natural gradient experiment on solute transport in a sand aquifer - spatial variability of hydraulic conductivity and its role in the dispersion process. Water Resources Research, 22(13): 2069-2082.

Sudicky, E.A., Illman, W., 2011. Lessons learned from a suite of CFB Borden experiments. Groundwater, 49(5): 630-648.

Takeuchi, M. et al., 2011. Comparative study of microbial dechlorination of chlorinated ethenes in an aquifer and a clayey aquitard. Journal of Contaminant Hydrology, 124(1-4): 14-24.

Van Breukelen, B.M., Hunkeler, D., Volkering, F., 2005. Quantification of sequential chlorinated ethene degradation by use of a reactive transport model incorporating isotope fractionation. Environmental science & technology, 39(11): 4189-4197.

Vargas, I., 2005. Assessment of the Fate of a Tetrachloroethene (PCE) and Trichloroethene (TCE) Plume at the Borden Aquifer. Master Thesis, Waterloo, 52 pp.

Wanner, P., Hunkeler, D., 2015. Carbon and chlorine isotopologue fractionation of chlorinated hydrocarbons during diffusion in water and low permeability sediments. Geochimica et Cosmochimica Acta, 157: 198-212.
White, R.A., Rivett, M.O., Tellam, J.H., 2008. Paleo-roothole facilitated transport of aromatic hydrocarbons through a Holocene clay bed. Environmental science & technology, 42(19): 7118-7124.
Wiedemeier, T.H., 1999. Natural attenuation of fuels and chlorinated solvents in the subsurface. John Wiley & Sons.

6.7. Supporting Information to Chapter 6

S1. Materials and Methods

S1.1. Groundwater sampling

For the present study the groundwater from the Borden aquifer was sampled from multilevel rows 6, 13 14 and 15 using Geopump® peristaltic pumps with 0.32 cm OD diameter Teflon® tubing in summer 2008 and 2013. Initially, a volume of about 60 mL was purged from each sampling port to remove the stagnant groundwater. Afterwards, the Teflon® tubing was connected to a stainless steel multiport manifold with which eight multilevel ports could be sampled simultaneously. Groundwater was collected in 8 mL glass vials without headspace. The sample vials were stored upside down at 4°C prior to concentration analysis.

S1.2. Clay core retrieval

To retrieve cores from the Borden aquitard a Geoprobe 7720DT direct-push rig and the Envirocore dual tube sampling system as described by Einarson et al. (1998) was used. An outer casing and an inner sample barrel containing a plastic liner of about 90 cm were, depending on the soil properties, pushed, pounded or vibrated simultaneously into the ground. During advancement, the cores were collected within the plastic liner inside the sample barrel. After each core run, the sample barrel containing the core was withdrawn to the surface, while the casing was left in place to avoid collapse of the borehole allowing collection of additional runs. Cores were collected in mostly 61 cm run lengths, except for a shorter initial run across the aquifer-

aquitard interface extending a short distance into the aquitard to total depths ranging from 2.2 to 2.9 m into the aquitard.

S1.3. Subsampling and VOC extractions from clay cores

After retrieval, cores were split longitudinally in two sections of about the same size, first using a rotary tool to cut along the liner and then large stainless steel scrapers to split the soil, which were decontaminated between depths. After splitting, half of the core was logged (photographs and description) for geological features, while the other half to be sampled was immediately covered by aluminum foil to prevent any loss of chlorinated hydrocarbons due to volatilization. Subsequently, the core was subsampled as a function of depth with a narrow spacing (~5cm) to obtain high resolution chlorinated hydrocarbon concentration and compound-specific carbon isotope ratio profiles. Subsampling of the cores was performed using a cut plastic syringe as a mini corer by peeling back the foil at the depths to be sampled and then inserting the cut syringe into the core taking care to avoid the outer edge of the core. The subsamples were extruded into 42 mL glass vials containing 20 mL high purity VWR methanol (MeOH). The vials were sealed with a screw cap with a Teflon lined septum and were weighed before and after the collection of the clay samples to determine the weight of the solid samples. A high clay to MeOH ratio (typically 0.8 by mass with some variability between samples) was chosen to maximize the amount of chlorinated hydrocarbons in the MeOH extraction. In the laboratory, the 42 mL vials were sonicated for 30 minutes followed by shaking for one hour in order to disperse the subsamples and to dissolve all chlorinated hydrocarbons completely in the MeOH. Afterwards the vials were centrifuged for 30 minutes at 1200 rpm to obtain a clear MeOH supernatant. The clear MeOH supernatant was then decanted and stored prior to analysis.

S1.4. VOC concentration analysis

Chlorinated hydrocarbon concentration analysis of MeOH extractions from core sub- and groundwater samples were performed at the University of Guelph, Ontario, Canada. For the MeOH extraction analysis, an aliquot of 1µL was injected on a HP 6890 gas chromatograph (GC in splitless mode at 225° and 3 mL/min helium carrier gas flow) equipped with a HP column (30m, 0.32mm ID, 5µm film thickness) and an electron capture detector (ECD). The temperature program of the GC was held for 0.5 min at 55°C and then ramped to 150°C at a rate of 10°C/min

and then to 210°C at 35°C/min and held for 8 min. Concentrations were quantified using calibration curves produced form seven standards prepared at different concentration levels by diluting MeOH stock solutions into water. The detection limits in the MeOH extractions were 0.1 µg/L for Trichloroethene (TCE) and Tetrachloroethene (PCE) and 3.5 µg/L for cis-dichloroethene (cDCE), which corresponds to detection limits of about 0.0001µg/g soil for PCE and TCE and 0.0035µg/g soil for cDCE in the subsamples for the average clay to MeOH ratio of 0.8. Chlorinated hydrocarbon concentrations in groundwater samples were analysed using an Agilent 7890C gas chromatograph coupled to an Agilent 5975C mass spectrometer. Samples were pre-concentrated using a purge and trap system by purging a volume of 5 mL for ten minutes with N_2 (40ml/min) and trapping the VOCs on Vocarb 3000 trap. After desorption the compounds were separated using a DB-VRX capillary column (20m, 0.18 mm ID, 1 µm film thickness) and subsequently conveyed to the mass spectrometer for detection. The calibration range was between 1 and 200µg/L and the detection limits were 0.1µg/L for TCE and c-DCE and 0.15µg/L for PCE.

S1.5. Compound-specific carbon isotope analysis

Compound-specific carbon isotope ratios in MeOH extractions from core subsamples were analysed using a TRACE^{TM} gas chromatograph (GC) coupled to a DeltaPlus XP isotope mass spectrometer (IRMS) via a combustion III interface (Thermo Finnigan, Germany) at the University of Neuchâtel, Switzerland. The MeOH extractions were diluted to identical concentrations of 30 µg/L in 42 mL glass vials with PTFE-lined screw cap, whereas the dilution had to be at least 100 times due to the incompatibility between the polar MeOH extractions and the column of the GC. Prior to analysis with the GC-IRMS, samples were pre-concentrated with a purge-and-trap concentrator (Tekmar Velocity XPT, USA) by purging a sample volume of 25 mL from the 42 mL glass vial for ten minutes with N_2 (40mL/min) and by detaining the degassed VOCs on a Vocarb 3000 trap. After purging, the samples were desorbed from the trap and transferred to a cryogenic trap (Tekmar Dohrmann) installed in the GC oven having a temperature of -80°C. Subsequently, the temperature was increased to 180°C and the samples were release to the column of the GC (DB-VRX, 60m, 0.25mm, 1,2 µm) for chromatographic separation. The GC oven temperature for cDCE and TCE analysis was held at 50°C for 2 minutes, then ramped at 5°C/min to 135°C and held for two minutes. The GC oven temperature

for PCE was held at 60°C for two minutes, then ramped at 5°C/min to 145°C and held for two minutes. Carbon isotope ratios of cDCE, TCE and PCE were analyzed relative to a CO_2 standard and expressed in the delta notation (VPDB $\delta = (R/R_{std} - 1)*1000$ (‰), where R and R_{std} are the isotope ratios of the sample and the standard, respectively. The standard deviation of the mean (±SDM) of the samples was estimated based on the standard deviation (1σ) of measured standards in the samples sequence (σ=0.33‰, n=15) and the twofold measurement of each sample.

S1.6. Organic carbon content measurements in clay cores

The organic content in the clay cores was measured at the Institute of Geological Sciences at the University of Bern, Switzerland using a G4 Icarus combustion analyzer. Solid samples were combusted to CO_2 and measured by a solid-state IR (infrared) detector. For total carbon content measurements, solid samples were combusted with O_2, while for total inorganic carbon content measurements solid samples were combusted with N_2. The organic carbon content in the solid samples was determined by the difference between measured total inorganic carbon and total carbon content.

S2. Modelling Approach

S2.1. Transport processes

The migration of chlorinated hydrocarbons in the clayey aquitard affected by reactive processes was simulated using the finite element computer code Comsol Multiphysics®. A 1D reactive transport model was developed using a modelling domain of 0.6 meter representing the retrieved cores. The modelling domain contains a highly resolved mesh, especially refined at the top end of the model domain representing the aquifer – aquitard interface. The used parameters in the numerical model are listed in tables S6-1 and S6-4a-b. To simulate reactive solute transport of chlorinated hydrocarbons in the retrieved cores the advection-dispersion equation for porous saturated systems was used:

$$R_n \frac{\partial(\phi C_n)}{\partial t} = \frac{\partial}{\partial z}\left[D_n \frac{\partial C_n}{\partial z} \right] - v\frac{\partial C_n}{\partial z} + \left(\frac{\partial C_n}{\partial t} \right)_{deg} \qquad \text{(S6-1)}$$

where z (m) is the vertical depth, C_n (µg/kg) is the concentration of species n, v (cm/y) is the vertical flow velocity in the clayey aquitard, D_n (m^2/s) is the dispersion coefficient and R_n (-) refers to the retardation factor and ϕ (-) is the porosity. The retardation factor is calculated assuming linear equilibrium sorption and is given by:

$$R = 1 + \left(\frac{\rho_{bdry}}{\Phi} \right) K_d \qquad \text{(S6-2)}$$

where ρ_{bdry} (g/cm^3) is the dry soil bulk density and K_d (L/kg) is the sorption equilibrium partition coefficient. The K_d values were estimated using the relationship $K_d = K_{OC} \cdot f_{OC}$, where K_{OC} is the soil organic carbon-water portioning coefficient and f_{OC} is the organic matter content in the clay (Tab. S6-4b).

The vertical dispersion coefficient (eq. S6-1) is determined using the relationship:

$$D_n = D_e + \alpha v \qquad \text{(S6-3)}$$

where D_n (m^2/s) is the dispersion coefficient, D_e (m^2/s) is the effective diffusion coefficient, α (m) refers to the dispersivity and v (m/s) is the 1D linear flow velocity. In saturated low permeability sediments the advective velocity is often very low (v~0 m/s) and the dispersion coefficient reduces to the diffusion coefficient.

The effective diffusion coefficient (eq. S6-3) includes the lowering of the diffusive transport rate in porous media due porosity and tortuosity effects and is defined as follows (Dykhuizen and Casey, 1989; Epstein, 1989):

$$D_e = D_0 \phi \tau \qquad \text{(S6-4)}$$

where D_0 (m^2/s) is the diffusion coefficient in free solution and τ (-) refers to the tortuosity factor

S2.2. Reactive Processes

The degradation term (rightmost in eq. S6-1) takes into account the temporal change of chlorinated hydrocarbon concentrations due to degradation caused by the sequential reductive dechlorination process. The 1D reactive transport model includes the sequential reductive dechlorination of PCE to VC via TCE and cDCE (PCE → TCE → cDCE → VC). Therefore, four different species (PCE_{tot}, TCE_{tot}, $cDCE_{tot,}$ VC_{tot}) and according degradation rates (k_{PCE}, k_{TCE}, k_{cDCE}) were defined for each dechlorination step in the model data base for simulating chlorinated hydrocarbon concentration profiles in the clayey aquitard (Tab. S6-1). For modelling concentration profiles, the measured temporal concentration evolution of the organic contaminants at the interface between aquifer and aquitard was used as boundary condition at the top end of the 1D model domain (Figs. S6-1A-D).

For modelling carbon isotope fractionation in the clayey aquitard using the developed 1D reactive transport model, species containing one heavy (^{13}C) and only light (^{12}C) carbon isotopes, respectively, were defined in the model database for PCE, TCE and cDCE (^{13}PCE, ^{12}PCE, ^{13}TCE, ^{12}TCE, ^{13}cDCE, ^{12}cDCE, ^{13}VC, ^{12}VC) (Tab. S6-1). Moreover, to simulate the magnitude of carbon isotope fractionation an enrichment factor for each dechlorination step ($\varepsilon_{PCE\text{-}TCE}$, $\varepsilon_{TCE\text{-}cDCE}$, $\varepsilon_{cDCE\text{-}VC}$) was defined (Tab. S6-1). However, the choice of the enrichment factor is challenging as a large variation of carbon isotope enrichment factors for describing carbon isotope fractionation during the sequential dechlorination can be found in literature (Tab.S6-2a-c). To reason the choice of the enrichment factors for modelling the sequential dechlorination in the present study, it was first investigated how the published enrichment factors are distributed using Q-Q plots. The Q-Q plots compare a theoretical normal distribution with the sample (published enrichment factors) distribution. To produce the Q-Q plots, the published enrichment factors were initially sorted in ascending order and the cumulative distribution factors (CDF) were determined and assigned to each enrichment factor. Afterwards, the theoretical normally distributed enrichment factors were calculated by inserting the CDF factors and the calculated average and standard deviation of the published enrichment factors into the inverse normal distribution function. The theoretical normal distributed enrichment factors were then compared with the distribution of the published enrichment factors by first standardizing both the theoretical and published enrichment factors and plotting against the CDF factors, which were transformed to Z values (x-axis in distribution plot) using the inverse normal probability distribution function.. A linear correlation

between the theoretical and the sample distribution indicates that the samples are normally distributed around an average. The Q-Q plots show that the published enrichment factors for each dechlorination step are normally distributed except for some outliers for PCE (Figs. S6-3A-C). Therefore, it is reasonable to assume that the standard deviation (±1σ) is equal in plus and minus direction with respect to the average value of the published enrichment factors. After revealing that the enrichment factors are normally distributed, the sensitivity of the carbon isotope ratio profiles to enrichment factors within the ±1σ range was investigated. The sensitivity analysis demonstrated that the carbon isotope profiles are different when varying the enrichment factors between +1σ and -1σ. However, the general shape of the carbon isotope ratio profiles remains equal (Fig. S6-4 e.g cores 13-14 and 14-10). Thus, for model calibration the enrichment factors were varied within the ±1σ interval to find the best-fit carbon isotope fractionation factor for each dechlorination step.

Beside reactive processes it was assumed that the diffusive transport process has also an influence on carbon isotope ratios. The magnitude of carbon isotope fractionation due to diffusion was defined according to determined enrichment factors for PCE (-0.15‰), TCE (-0.22‰) and cDCE (-0.30‰) by Wanner and Hunkeler (2015).

Table S6-1. Reactive processes included in the numerical model for simulating the sequential dechlorination of PCE via TCE to cDCE for total concentrations and for carbon isotopes in the clayey aquitard.

Species	Chemical reaction	Degradation rate (k_n)	
PCE_{tot}	$PCE_{tot} + H^2 \rightarrow TCE_{tot} + H^+ + Cl^-$	$\left(\frac{\partial C_{PCE_{tot}}}{\partial t}\right)_{deg} = -k_{PCE}$	(a)
TCE_{tot}	$TCE_{tot} + H^2 \rightarrow cDCE_{tot} + H^+ + Cl^-$	$\left(\frac{\partial C_{TCE_{tot}}}{\partial t}\right)_{deg} = +k_{PCE} - k_{TCE}$	(b)
$cDCE_{tot}$	$cDCE_{tot} + H^2 \rightarrow VC_{tot} + H^+ + Cl^-$	$\left(\frac{\partial C_{cDCE_{tot}}}{\partial t}\right)_{deg} = +k_{TCE} - k_{cDCE}$	(c)
^{12}PCE	$^{12}PCE + H^2 \rightarrow {}^{12}TCE + H^+ + Cl^-$	$\left(\frac{\partial C_{12\,PCE}}{\partial t}\right)_{deg} = -k_{PCE} \times f^{12}PCE$	(d)
^{13}PCE	$^{13}PCE + H^2 \rightarrow {}^{13}TCE + H^+ + Cl^-$	$\left(\frac{\partial C_{13\,PCE}}{\partial t}\right)_{deg} = -k_{PCE} \times \left(\frac{\varepsilon}{1000}+1\right)_{PCE-TCE} \times f^{13}PCE$	(e)
^{12}TCE	$^{12}TCE + H^2 \rightarrow {}^{12}cDCE + H^+ + Cl^-$	$\left(\frac{\partial C_{12\,TCE}}{\partial t}\right)_{deg} = +k_{PCE} \times f^{12}PCE - k_{TCE} \times f^{12}TCE$	(f)
^{13}TCE	$^{13}TCE + H^2 \rightarrow {}^{13}cDCE + H^+ + Cl^-$	$\left(\frac{\partial C_{13\,TCE}}{\partial t}\right)_{deg} = +k_{PCE} \times \left(\frac{\varepsilon}{1000}+1\right)_{PCE-TCE} \times f^{13}PCE - k_{TCE} \times \left(\frac{\varepsilon}{1000}+1\right)_{TCE-cDCE} \times f^{13}TCE$	(g)
$^{12}cDCE$	$^{12}cDCE + H^2 \rightarrow {}^{12}VC + H^+ + Cl^-$	$\left(\frac{\partial C_{12\,cDCE}}{\partial t}\right)_{deg} = +k_{TCE} \times f^{12}TCE - k_{cDCE} \times f^{12}cDCE$	(h)
$^{13}cDCE$	$^{13}cDCE + H^2 \rightarrow {}^{13}VC + H^+ + Cl^-$	$\left(\frac{\partial C_{13\,cDCE}}{\partial t}\right)_{deg} = +k_{TCE} \times \left(\frac{\varepsilon}{1000}+1\right)_{TCE-cDCE} \times f^{13}TCE - k_{cDCE} \times \left(\frac{\varepsilon}{1000}+1\right)_{cDCE-VC} \times f^{13}cDCE$	(i)

f corresponds to the abundance of carbon isotopes (^{13}C 1.07% vs. ^{12}C 98.93%) and ε corresponds to the enrichment factor

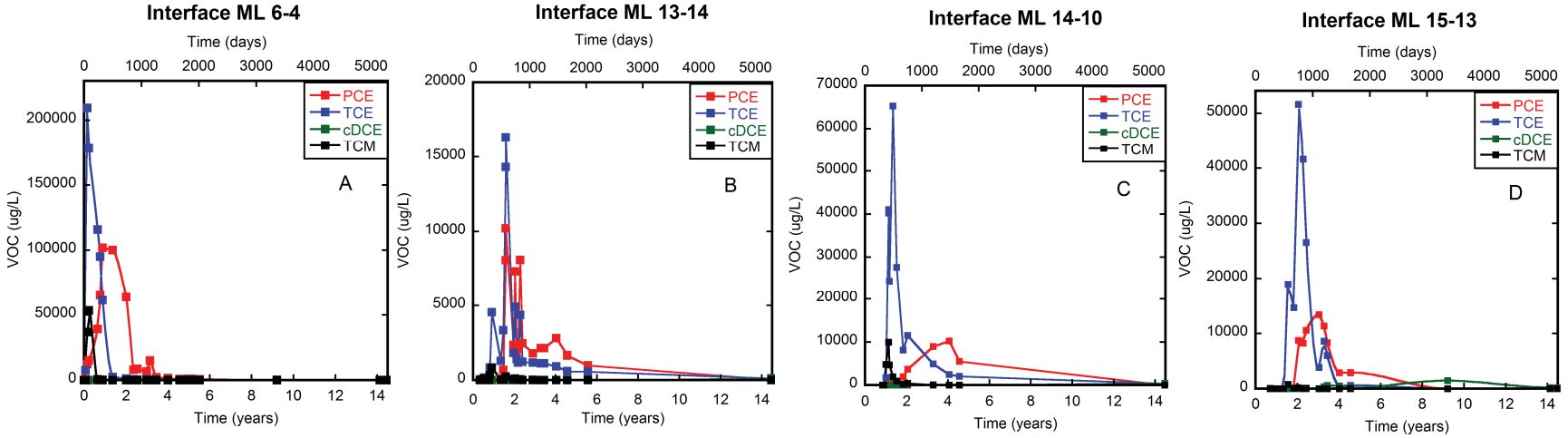

Figures S6-1 A-D. Concentration evolution at the aquifer – aquitard interface of PCE (red), TCE (blue), cDCE (green) and TCM (black) at the locations, where the cores were retrieved.

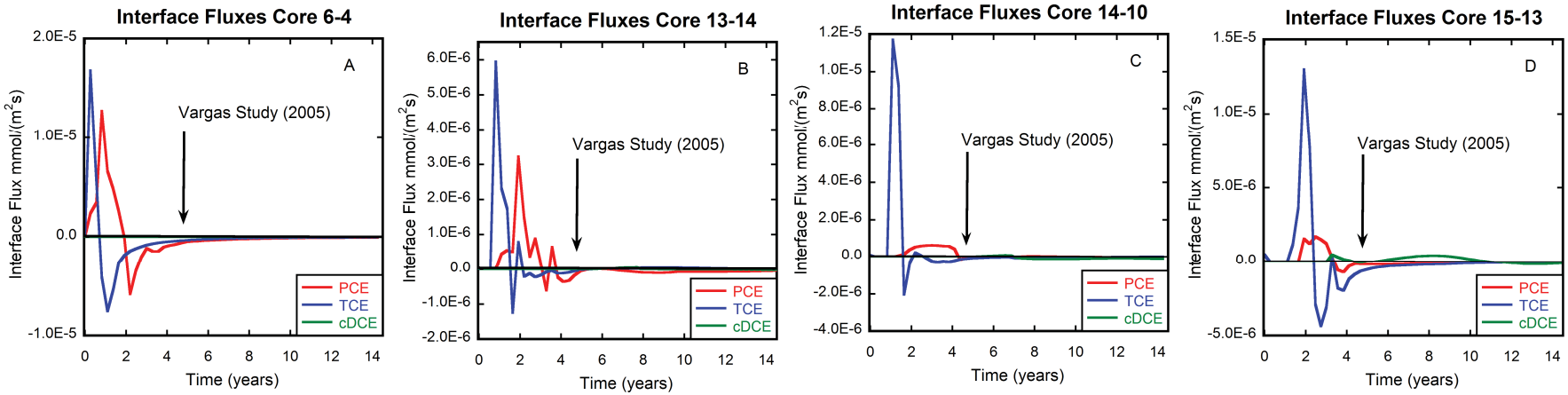

Figures S6-2A-D. Aquifer – aquitard interface mass fluxes of PCE (red), TCE (blue) and cDCE (green) at the locations, where the cores were retrieved. Positive values indicate forward diffusion, while negative values represent back-diffusion.

Table S6-2a. Compilation of carbon enrichment factors for performing a sensitivity analysis of the variation of carbon isotope enrichment factors during the anaerobic transformation from PCE to TCE. This table expands the overview of Aelion et al. (2010).

Pathway	**ε_C (‰)**	**Comment**	**Reference**
Biotic reductive dechlorination	-5.5	Mixed culture KB-1	(Slater et al., 2001)
Biotic reductive dechlorination	-5.3	Enrichment culture	(Slater et al., 2001)
Biotic reductive dechlorination	-0.42	Sulfurospirillum multivorans	(Nijenhuis et al., 2005)
Biotic reductive dechlorination	-5.2	Desulfitobacterium sp. PCE-S	(Nijenhuis et al., 2005)
Biotic reductive dechlorination	-0.5	Sulfurospirillum halorespirans	(Cichocka et al., 2007)
Biotic reductive dechlorination	-16.4	Desulfitobacterium sp. Viet 1	(Cichocka et al., 2008)
Biotic reductive dechlorination	-6.0	Dehalococcoides ethenogenes 195	(Cichocka et al., 2008)
Biotic reductive dechlorination	-3.6	Sulfurospirillum	(Badin et al., 2014)
Biotic reductive dechlorination	-5.6		(Wiegert et al., 2013)
Biotic reductive dechlorination	-19.0	Desulfitobacterium sp. Viet 1	(Cretnik et al., 2014)
Biotic reductive dechlorination	-11.9	DPF consortia	(Dong et al., 2011)
Biotic reductive dechlorination	-1.6	Dehalococcoides sp. Strain CBDB1	(Marco-Urrea et al., 2011)
Abiotic reductive dechlorination	-25.3	Corrinoid borpseudo-B12	(Renpenning et al., 2014)
Abiotic reductive dechlorination	-23.7	Corrinoid nor-B12	(Renpenning et al., 2014)
Abiotic reductive dechlorination	-22.4	Corrinoid cyano-B12	(Renpenning et al., 2014)
Abiotic reductive dechlorination	-25.2	Corrinoid dicyanocobinamid	(Renpenning et al., 2014)
Enzymatic reductive dechlorination	-1.4	S. multivorans Norpseudo-B12 type	(Renpenning et al., 2014)
Enzymatic reductive dechlorination	-1.3	S. multivorans Nor-B12 type	(Renpenning et al., 2014)
Dechlorination by Fe(0)	-25.3		(Dayan et al., 1999)
Dechlorination by Fe(0)	-7.5	Perless iron	(VanStone et al., 2004)
Dechlorination by Fe(0)	-12.6	Connelly iron	(VanStone et al., 2004)
Reduction by canocobalamin	-13.0		(Nijenhuis et al., 2005)
Average (N=22)	**-10.8**		
Standard deviation (±1σ)	**9.1**		
+1σ	**-19.9**		
-1σ	**-1.7**		

Table S6-2b. Compilation of carbon enrichment factors for performing a sensitivity analysis of the variation of carbon isotope enrichment factors during the anaerobic transformation from TCE to cDCE. This table expands the overview of Aelion et al. (2010).

Pathway	ε_C (‰)	Comment	Reference
Biotic reductive dechlorination	-7.1	Mixed culture (Pinellas)	(Lollar et al., 1999)
Biotic reductive dechlorination	-4.5	Mixed culture KB-1	(Bloom et al., 2000)
Biotic reductive dechlorination	-14.2	Mixed culture KB-1	(Slater et al., 2001)
Biotic reductive dechlorination	-9.6	Dehalococcoides ethenogenes 195	(Lee et al., 2007)
Biotic reductive dechlorination	-16.4	Sulfurospirillum multivorans	(Lee et al., 2007)
Biotic reductive dechlorination	-16.0	Dehalococcoides restrictus PER-K23	(Lee et al., 2007)
Biotic reductive dechlorination	-18.5	Sulfurospirillum halorespirans	(Cichocka et al., 2007)
Biotic reductive dechlorination	-18.4	Sulfurospirillum multivorans	(Cichocka et al., 2007)
Biotic reductive dechlorination	-12.1	Desulfitobacterium sp. PCE-S	(Cichocka et al., 2007)
Biotic reductive dechlorination	-3.5	Desulfuromonas michiganensis	(Cichocka et al., 2008)
Biotic reductive dechlorination	-8.4	Geobacter lovleyi SZ	(Cichocka et al., 2008)
Biotic reductive dechlorination	-3.3	Dehalobacter restrictus PER-L23	(Cichocka et al., 2008)
Biotic reductive dechlorination	-13.5	Dehalococcoides ethenogenes 195	(Cichocka et al., 2008)
Biotic reductive dechlorination	-11.2	Dehalococcoides sp. Strain CBDB1	(Marco-Urrea et al., 2011)
Biotic reductive dechlorination	-8.8		(Wiegert et al., 2013)
Biotic reductive dechlorination	-12.2	Geobacter lovleyi strain SZ	(Cretnik et al., 2013)
Biotic reductive dechlorination	-9.1	Desulfitobacterium hafniense Y51	(Cretnik et al., 2013)
Biotic reductive dechlorination	-12.2	Geobacter lovleyi strain SZ	(Cretnik et al., 2014)
Biotic reductive dechlorination	-15.9	Mixed Dehalococcoides culture	(Kuder et al., 2013)
Abiotic dechlorination by Fe(0)	-8.6		(Dayan et al., 1999)
Abiotic dechlorination by Fe(0)	-10.1		(Schüth et al., 2003)
Abiotic dechlorination by Fe(0)	-13.5	Peerless iron	(VanStone et al., 2004)
Abiotic dechlorination by Fe(0)	-9.0	Connelly iron	(VanStone et al., 2004)
Reduction by cyanocobalamin	-15.1		(Nijenhuis et al., 2005)
Reduction by cobalamin	-16.1		(Cretnik et al., 2013)
Reduction by cabaloxime	-21.3		(Cretnik et al., 2013)
Abiotic reductive dechlorination	-23.0	Chloride green rust (GR-Cl)	(Liang et al., 2009)
Abiotic reductive dechlorination	-21.7	Pyrite	(Liang et al., 2009)
Abiotic dechlorination by Fe(0)	-12.4		(Lojkasek‐Lima et al., 2012)
Abiotic dechlorination by Fe(0)	-14.9		(Audí-Miró et al., 2013)

Abiotic reductive dechlorination	-18.5	Corrinoid borpseudo-B12	(Renpenning et al., 2014)
Abiotic reductive dechlorination	-15.1	Corrinoid nor-B12	(Renpenning et al., 2014)
Abiotic reductive dechlorination	-15.0	Corrinoid cyano-B12	(Renpenning et al., 2014)
Abiotic reductive dechlorination	-16.5	Corrinoid dicyanocobinamid	(Renpenning et al., 2014)
Enzymatic reductive dechlorination	-20.1	S. multivorans Norpseudo-B12 type	(Renpenning et al., 2014)
Emzymatic reductive dechlorination	-20.2	S. multivorans Nor-B12 type	(Renpenning et al., 2014)
Average (N=36)	**-13.5**		
Standard deviation (±1σ)	**5.1**		
+1σ	**-18.6**		
-1σ	**-7.4**		

Table S6-2c. Compilation of carbon enrichment factors for performing a sensitivity analysis of the variation of carbon isotope enrichment factors during the anaerobic transformation from cDCE to VC. This table expands the overview of Aelion et al. (2010).

Pathway	**ε_C (‰)**	**Comment**	**Reference**
Biotic reductive dechlorination	-15.1	Mixed culture KB-1	(Bloom et al., 2000)
Biotic reductive dechlorination	-21.3	Enrichment culture	(Slater et al., 2001)
Reductive dechlorination	-19.2	Lab Microcosm	(Hunkeler et al., 2002)
Biotic reductive dechlorination	-21.1	Dehalococcoides ethenogenes 195	(Lee et al., 2007)
Biotic reductive dechlorination	-16.9	Dehalococcoides sp. BAV 1	(Lee et al., 2007)
Biotic reductive dechlorination	-29.7	Dehalococcoides - culture ANAS	(Lee et al., 2007)
Abiotic dechlorination by Fe(0)	-14.4		(Dayan et al., 1999)
Abiotic dechlorination by Fe(0)	-16.0	Peerless iron	(VanStone et al., 2004)
Abiotic dechlorination by Fe(0)	-9.4	Connelly iron	(VanStone et al., 2004)
Abiotic reductive dechlorination	-20.5		(Audí-Miró et al., 2013)
Biotic reductive dechlorination	-14.9	Dehalococcoides sp. strain BAV1	(Fletcher et al., 2011)
Biotic reductive dechlorination	-18.4	Dehalococcoides strains BAV1, FL2, GT, and VS	(Fletcher et al., 2011)
Biotic reductive dechlorination	-25.3	BDI consortium	(Fletcher et al., 2011)
Biotic reductive dechlorination	-26.8		(Kuder et al., 2013)
Average (N=14)	**-19.4**		
Standard deviation (±1σ)	**5.4**		
+1σ	**-24.8**		
-1σ	**-14.0**		

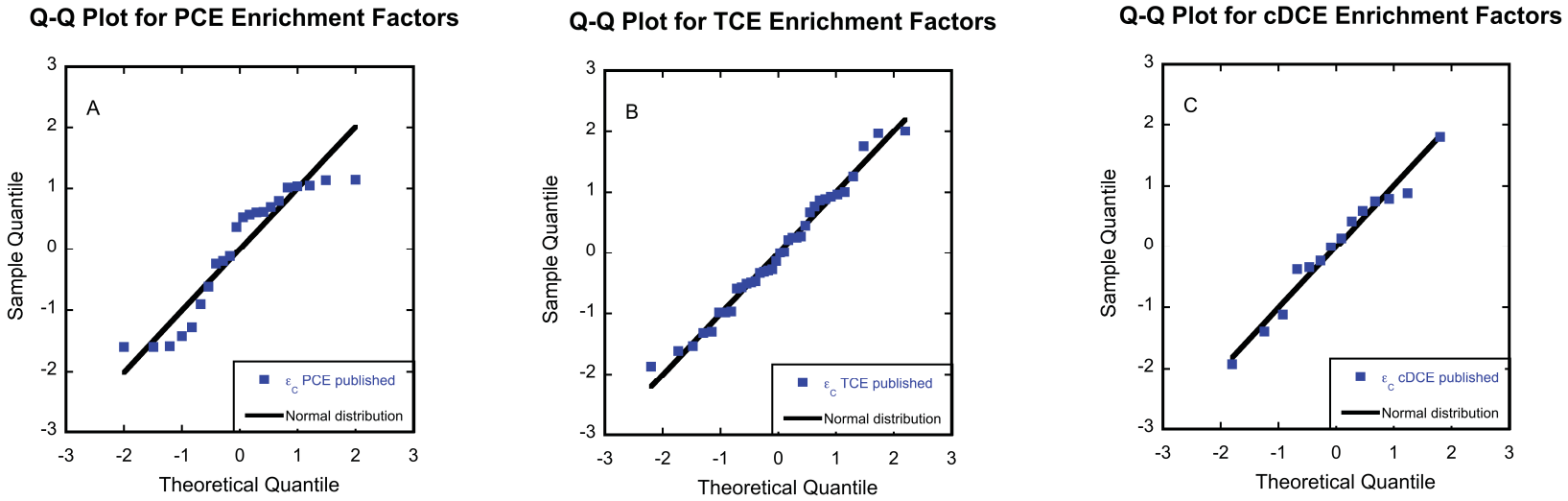

Figures S6-3A-C. Q-Q plot for published enrichments factors for the sequential dechlorination of PCE (Fig. S6-3A), TCE (Fig. S6-3B) and cDCE (Fig. S6-3C) (blue squares) and theoretical normally distributed values (black line).

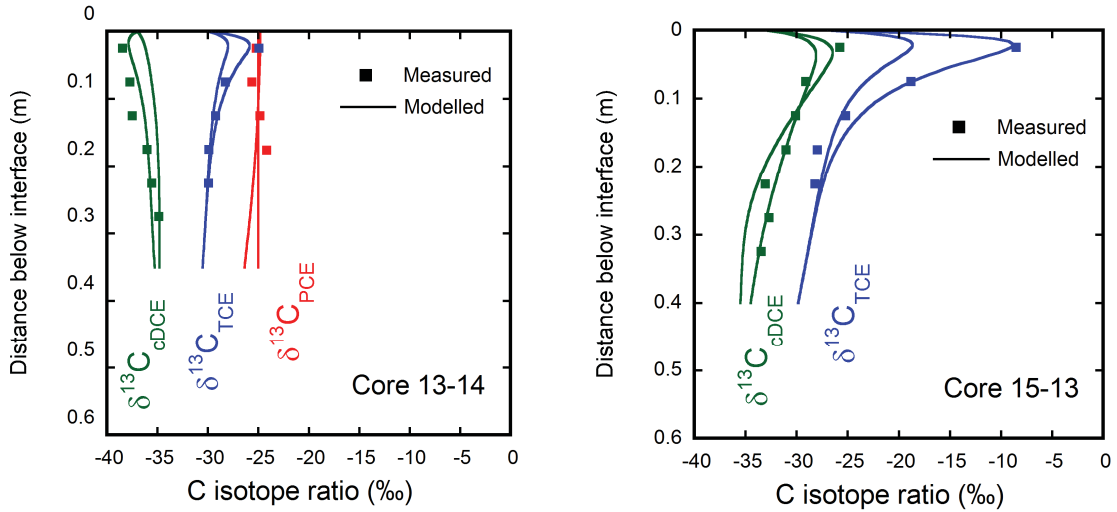

Figure S6-4. Modelled compound-specific carbon isotope ratios profiles for +1σ and -1σ of the published enrichment factors for PCE, TCE and cDCE for cores 13-14 and 15-13

S2.3. Model calibration

The 1D reactive transport model was calibrated against measured field data by varying all unknown parameters (Tab. S6-4a-b) in a predefined range (Tab. S6-3) until a minimal deviation (quantified by the root mean squared error (RMSE; eq.5)) between measured and modelled data was obtained.

$$RMSE = \left[\frac{\sum_{i=1}^{N} (S_i - Q_i)^2}{N} \right]^{1/2} \quad \text{(S6-5)}$$

where S_i is the modelled value Q_i is the measured value and N refers to the number of samples.

For the enrichment factors the same values were calibrated for all retrieved cores based on the ±1σ range of the published enrichment factors (Tabs. S6-2a-c and S6-3). The performance of a local sensitivity analysis of the most sensitive parameters confirmed that the calibrated parameters correspond to the minima of the objective function as exemplified for the TCE concentration and isotope profile in core 15-13. Moreover, the local sensitivity analysis showed that the isotope ratio profiles are more sensitive to the variation of the parameters compared to the concentration profiles (Fig. S6-5). Thus, small changes of the parameters lead to a large increase of the RMSE values for the isotope ratio profile, which supports the reasonableness of the obtained best-fit parameter set (Tab. S6-4a-b). Furthermore, an earlier study (Parker, 1996) compared measured and simulated PCE concentration profiles in the Borden aquitard and obtained parameters in the same range than in the present study indicating that the used parameters in the present study are in a plausible range.

Table S6-3. Range of model parameters for calibration.

Parameter	**Unit**	**Variation range**	**References for used parameter variation range**
Slope of degradation rate function (inverse error function)	-	0.01 – 100	Present study
Degradation rate (half-life) at aquifer - aquitard interface	days	10 – 1000	(Wiedemeier, 1999)
Degradation start after contaminant injection	days	0 – 5281	Present study (Time period between contaminant injection and retrieval of cores)
Advective flow velocity	cm/y	0 – 3	(Parker, 1996)
Tortuosity	-	0.05 – 0.5	(Parker, 1996)
K_{OC} PCE	L/kg	269 – 7244	Upper limit from Lu et al. (2011)
K_{OC} TCE	L/kg	18 – 3020	Lower limit from Wiedemeier (1999)
K_{OC} cDCE	L/kg	24 – 2042	
Enrichment factor PCE	‰	-1.7 – -19.9	Present study (Tab. S2a)
Enrichment factor TCE	‰	-17.4 – -18.6	Present study (Tab. S2b)
Enrichment factor cDCE	‰	-14.8 – -24.8	Present study (Tab. S2c)

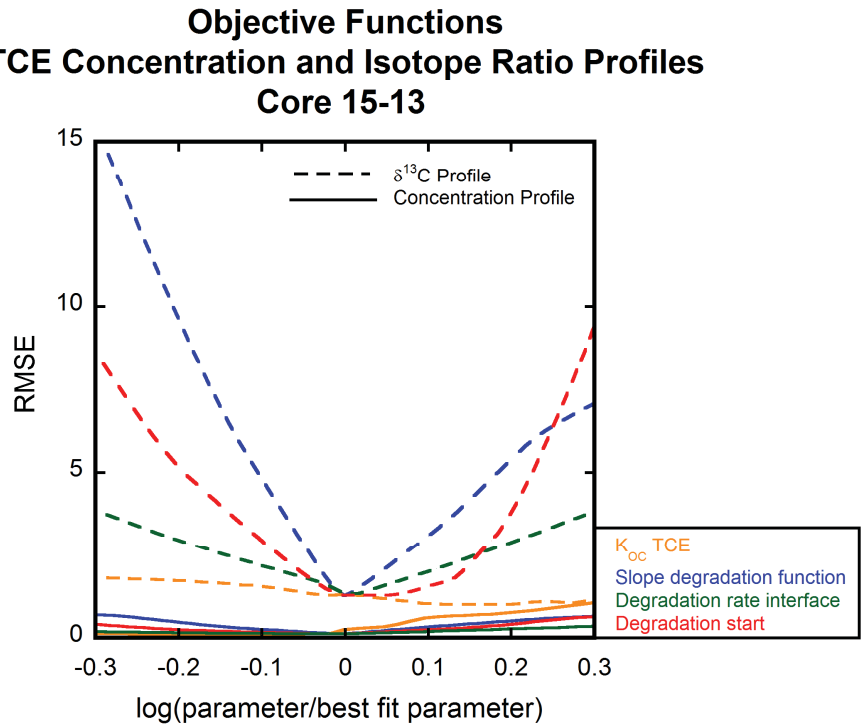

Figure S6-5. Objective functions for the most sensitive parameters (K_{OC} value, the slope of the degradation (inverse error) function, the degradation rate at the aquifer – aquitard interface, start of the degradation) for the TCE concentration and carbon isotope ratio profile in core 15-13.

Table S6-4a.General model parameters for simulating concentration and isotope ratio profiles in the retrieved cores.

Parameters	Unit	Value	Reference
Porosity: ϕ	-	0.40	(Parker, 1996)
Soil dry bulk density: ρ_{bdry}	g/cm^3	1.61	(Parker, 1996)
Soil wet bulk density: ρ_{bwet}	g/cm^3	2.04	(Parker, 1996)
Hydraulic conductivity: K	m/s	8.0E-09	(Morrison, 1998)
Diffusion coefficient in free solution PCE: $D_{0,PCE}$	m^2/s	9.40E-10	(Pankow and Cherry, 1996)
Diffusion coefficient in free solution TCE: $D_{0,TCE}$	m^2/s	1.01E-09	(Pankow and Cherry, 1996)
Diffusion coefficient in free solution cDCE: $D_{0,cDCE}$	m^2/s	1.13E-09	(Wiedemeier, 1999)
Enrichment factor PCE[1]	‰	-2.0	Present study
Enrichment factor TCE[1]	‰	-18.2	Present study
Enrichment factor cDCE[1]	‰	-24.0	Present study

[1]Calibrated by varying the values in the $\pm 1\sigma$ range (Tab. S6-3) of the published enrichment factors (Tabs.6-2a-c).

Table S6-4b. Clay core dependent model parameters for simulating concentration and carbon isotope ratio profiles in the retrieved cores.

Parameters	Unit	Core 6-4	Core 13-14	Core 14-10	Core 15-13
Organic content: f_{OC} [1]	%	0.59	0.75	0.54	0.78
Tortuosity: τ^2	-	0.07	0.12	0.08	0.20
Linear average flow velocity: v[2]	cm/y	0.00	2.50	1.50	0.35
K_{OC} PCE[2]	L/kg	470	450	500	750
K_{OC} TCE[2]	L/kg	220	230	260	400
K_{OC} cDCE[2]	L/kg	150	90	100	300
Retardation factor PCE: R_{PCE}[3]	-	12.16	14.58	11.87	24.54
Retardation factor TCE: R_{TCE}[3]	-	6.22	7.94	6.65	13.56
Retardation factor cDCE: R_{cDCE} [3]	-	4.56	3.72	3.17	10.42
Degradation rate PCE: k_{PCE}[2]	1/s	$3.3E\text{-}11 \cdot erfc(0.1z)^4$	$9.8E\text{-}10 \cdot erfc(20z)^4$	$9.8E\text{-}8 \cdot erfc(0.1z)^4$	$3.3E\text{-}8 \cdot erfc(8z)^4$
Degradation rate TCE: k_{TCE}[2]	1/s	$9.2E\text{-}10 \cdot erfc(0.5z)^4$	$7.6E\text{-}8 \cdot erfc(34z)^4$	$8.5E\text{-}8 \cdot erfc(11z)^4$	$2.7E\text{-}7 \cdot erfc(20.0z)^4$
Degradation rate cDCE: k_{cDCE}[2]	1/s	$3.3E\text{-}10 \cdot erfc(0.1z)^4$	$2.0E\text{-}9 \cdot erfc(0.1z)^4$	$4.6E\text{-}10 \cdot erfc(0.1z)^4$	$6.2E\text{-}8 \cdot erfc(17.0z)^4$
Start (bio)degradation after injection[2]	days	2300	2800	2500	2600

[1]Measured.
[2]Calibrated by varying the parameters in the range indicated in table S6-3.
[3]Determined by inserting the calibrated K_{OC} values in equation S6-2.
[4]z Corresponds to vertical depth.

S2.4. Simulation of different degradation scenarios

To investigate how concentration and carbon isotope ratio patterns are influenced by different degradation conditions in saturated low permeability sediments, three different degradation scenarios were simulated: A) no-degradation, B) uniform degradation and C) non-uniform degradation. In the uniform degradation scenario the degradation rates were assumed to be constant with depth, while in the non-uniform degradation scenario exponentially decreasing degradation rates were used, which follow an inverse error function (Fig. S6-6A-B). The simulation of the different scenarios showed that the concentration profiles are similar (Figs. 6-2A-D, S6-7A-D and S6-8A-D), while carbon isotope ratio profiles are clearly different among the different degradation scenarios (Figs. 6-3A-D, 6-4A-D, 6-5A-D).

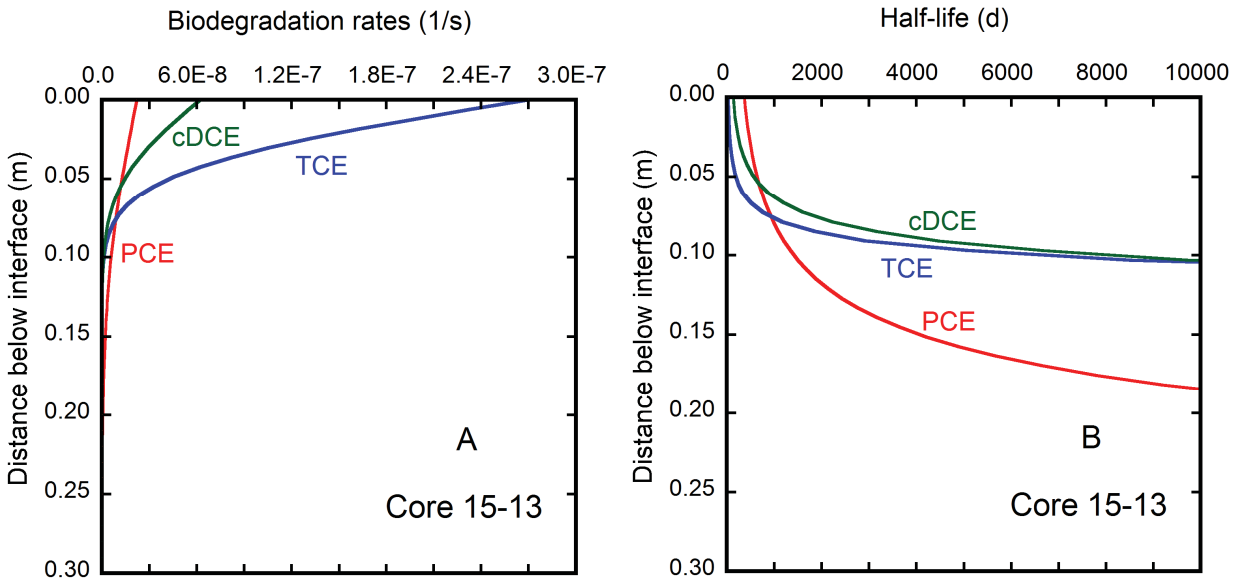

Figure S6-6. Degradation rates (Fig. S6-6A) and corresponding half-lifes for PCE, TCE and cDCE in clay core 15-13 (Fig. S6-6B).

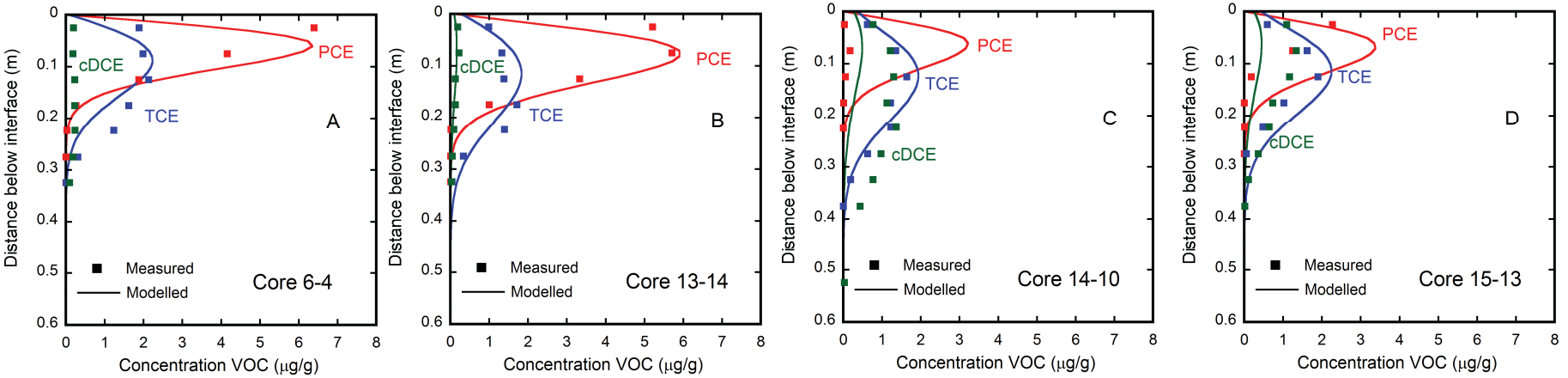

Figures S6-7A - D. Comparison between measured and modelled chlorinated hydrocarbon concentration profiles in the retrieved clay cores for the no-degradation scenario 5281 days after injecting the organic contaminants into aquifer. The continuous lines indicate the modelled isotope profiles of PCE (red), TCE (blue) and cDCE (green), while the squares represent the measuring points. The technical details of the modelling approach are provided in section S2. of the Supporting Information.

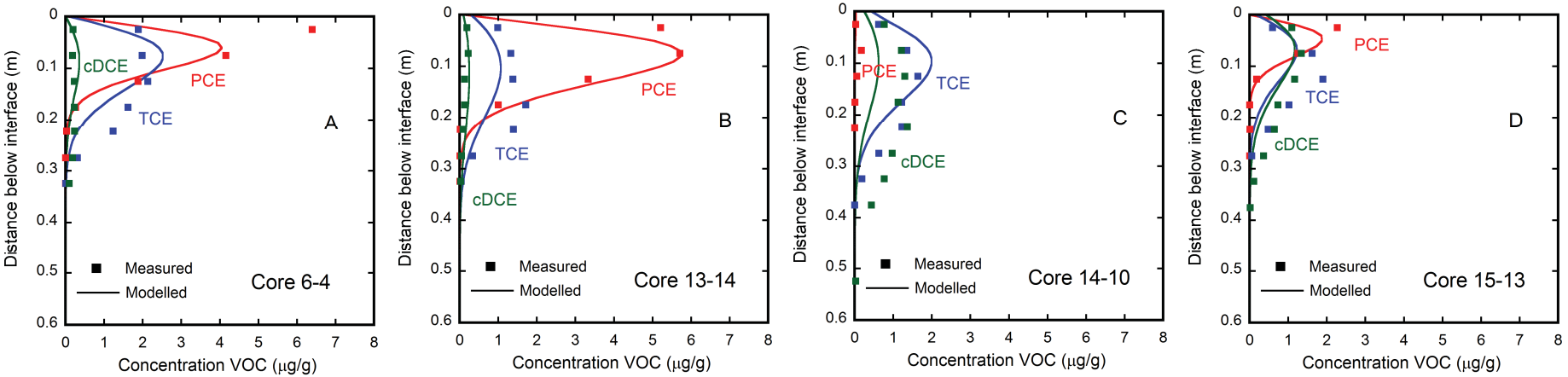

Figures S6-8A - D. Comparison between measured and modelled chlorinated hydrocarbon concentration profiles in the retrieved clay cores for the uniform degradation scenario 5281 days after injecting the organic contaminants into aquifer. The continuous lines indicate the modelled isotope profiles of PCE (red), TCE (blue) and cDCE (green), while the squares represent the measuring points. The technical details of the modelling approach are provided in section S2. of the Supporting Information.

S3. Detail description of plume evolution in sandy aquifer of the Borden site

Within the first two years after injection, Laukonen (2001) delineated the migration of the entire plume in three dimensions by sampling selected multilevel rows at eight different times. Due to the different solubilities of the three DNAPL components (PCE: 200 mg/L, TCE: 1300 mg/L, TCM: 8200 mg/L) the persistence time of the DNAPL phase varied for the injected contaminants at the source location. Two years after injection TCM was completely dissolved away from, while TCE and PCE DNAPLs were still present at the source location. After dissolution the TCM plume migrated ahead in the aquifer compared to the TCE and PCE plumes since TCM adsorbed less strongly on the aquifer material than TCE and PCE. The fringe of the TCM plume reached multilevel row 15 after 340 days, while the breakthroughs for TCE and PCE were observed after 450 and 700 days after injection, respectively. Five and six years (September 2004 and May 2005) after injection selected multilevel rows were sample again by Vargas (2005) to assess the further evolution of the TCE and PCE plume (TCM was not analysed). Although decreased by a factor of seven in comparison to 2001, the highest PCE concentration was still measured close to the source indicating that a remaining PCE DNAPL phase was still present at the source. In contrast, TCE seemed to be completely dissolved from the source but was still locally concentrated on the interface between the aquifer and the aquitard. Furthermore, Vargas (2005) revealed aerobic conditions in the aquifer between the injection point and multilevel row 15. Nine and 14 years (June 2008 and June 2013) after injection selected multilevel rows were sampled again in order to evaluate the long-term evolution of the TCE, PCE and cDCE plume (TCM was not analysed). In 2008 PCE concentrations showed no longer the highest concentration close to the source indicating that also PCE has been completely dissolved from the source. The highest PCE concentrations (over 2000 μg/L) were measured in multilevel row 13, which is about 40 times lower than the highest concentration measured in 2004. The highest TCE concentration was also observed in multilevel row 13 but lowered by a factor of six in comparison to the highest concentrations in 2004.

S4. References for Supporting Information

Aelion, C.M., Höhener, P., Hunkeler, D., Aravena, R., 2010. Environmental Isotopes in Biodegradation and Bioremediation CRC Press, USA, 450 pp.

Audí-Miró, C. et al., 2013. Cl and C isotope analysis to assess the effectiveness of chlorinated ethene degradation by zero-valent iron: Evidence from dual element and product isotope values. Applied Geochemistry, 32: 175-183.

Badin, A., Buttet, G., Maillard, J., Holliger, C., Hunkeler, D., 2014. Multiple Dual C-Cl Isotope Patterns Associated with Reductive Dechlorination of Tetrachloroethene. Environmental Science & Technology, 48(16): 9179-9186.

Bloom, Y., Aravena, R., Hunkeler, D., Edwards, E., Frape, S., 2000. Carbon isotope fractionation during microbial dechlorination of trichloroethene, cis-1, 2-dichloroethene, and vinyl chloride: implications for assessment of natural attenuation. Environmental science & technology, 34(13): 2768-2772.

Cichocka, D., Imfeld, G., Richnow, H.-H., Nijenhuis, I., 2008. Variability in microbial carbon isotope fractionation of tetra-and trichloroethene upon reductive dechlorination. Chemosphere, 71(4): 639-648.

Cichocka, D. et al., 2007. Factors controlling the carbon isotope fractionation of tetra-and trichloroethene during reductive dechlorination by Sulfurospirillum ssp. and Desulfitobacterium sp. strain PCE-S. FEMS microbiology ecology, 62(1): 98-107.

Cretnik, S., Bernstein, A., Shouakar-Stash, O., Löffler, F., Elsner, M., 2014. Chlorine isotope effects from isotope ratio mass spectrometry suggest intramolecular C-Cl bond competition in trichloroethene (TCE) reductive dehalogenation. Molecules, 19(5): 6450-6473.

Cretnik, S. et al., 2013. Reductive dechlorination of TCE by chemical model systems in comparison to dehalogenating bacteria: Insights from dual element isotope analysis (13C/12C, 37Cl/35Cl). Environmental science & technology, 47(13): 6855-6863.

Dayan, H., Abrajano, T., Sturchio, N., Winsor, L., 1999. Carbon isotopic fractionation during reductive dehalogenation of chlorinated ethenes by metallic iron. Organic Geochemistry, 30(8): 755-763.

Dong, Y., Butler, E.C., Philp, R.P., Krumholz, L.R., 2011. Impacts of microbial community composition on isotope fractionation during reductive dechlorination of tetrachloroethylene. Biodegradation, 22(2): 431-444.

Dykhuizen, R.C., Casey, W.H., 1989. An analysis of solute diffusion in rocks. Geochimica et Cosmochimica Acta, 53(11): 2797-2805.

Einarson, M.D., Casey, M.B., Winglewich, D.L., Morkin, M.I., 1998. Enviro-core - A dual-tube direct push system for rapid site characterization. Proceedings of the Symposium on the Application of Geophysics to Environmental and Engineering Problems. Environmental & Engineering Geophysical Society, Wheat Ridge, 1-10 pp.

Epstein, N., 1989. On Tortuosity and The Tortuosity Factor in Flow and Diffusion Through Porous-Media. Chemical Engineering Science, 44(3): 777-779.

Fletcher, K.E., Nijenhuis, I., Richnow, H.-H., Löffler, F.E., 2011. Stable carbon isotope enrichment factors for cis-1, 2-dichloroethene and vinyl chloride reductive dechlorination by Dehalococcoides. Environmental science & technology, 45(7): 2951-2957.

Hunkeler, D., Aravena, R., Cox, E., 2002. Carbon isotopes as a tool to evaluate the origin and fate of vinyl chloride: laboratory experiments and modeling of isotope evolution. Environmental science & technology, 36(15): 3378-3384.

Kuder, T., van Breukelen, B.M., Vanderford, M., Philp, P., 2013. 3D-CSIA: Carbon, chlorine, and hydrogen isotope fractionation in transformation of TCE to ethene by a Dehalococcoides culture. Environmental science & technology, 47(17): 9668-9677.

Laukonen, K.A., 2001. Long-Term Natural Gradient Experiments in the Borden Sand Auqifer: A Bromide Slug and a Chloroform Plume from a Three-Component DNAPL Source. Master Thesis, University of Waterloo, 156 pp.

Lee, P.K., Conrad, M.E., Alvarez-Cohen, L., 2007. Stable carbon isotope fractionation of chloroethenes by dehalorespiring isolates. Environmental science & technology, 41(12): 4277-4285.

Liang, X., Philp, R.P., Butler, E.C., 2009. Kinetic and isotope analyses of tetrachloroethylene and trichloroethylene degradation by model Fe (II)-bearing minerals. Chemosphere, 75(1): 63-69.

Lojkasek‐Lima, P. et al., 2012. Evaluating TCE abiotic and biotic degradation pathways in a permeable reactive barrier using compound specific isotope analysis. Groundwater Monitoring & Remediation, 32(4): 53-62.

Lollar, B.S. et al., 1999. Contrasting carbon isotope fractionation during biodegradation of trichloroethylene and toluene: Implications for intrinsic bioremediation. Organic Geochemistry, 30(8): 813-820.

Lu, C., Bjerg, P.L., Zhang, F., Broholm, M.M., 2011. Sorption of chlorinated solvents and degradation products on natural clayey tills. Chemosphere, 83(11): 1467-1474.

Marco-Urrea, E., Nijenhuis, I., Adrian, L., 2011. Transformation and carbon isotope fractionation of tetra-and trichloroethene to trans-dichloroethene by Dehalococcoides sp. strain CBDB1. Environmental science & technology, 45(4): 1555-1562.

Morrison, W.E., 1998. Hydrogeological Controls on Flow and Fate of PCE DNAPL in a Fractured and Layered Clayey Aquitard: A Borden Experiment. Master Thesis, Universitiy of Waterloo, 356 pp.

Nijenhuis, I. et al., 2005. Stable isotope fractionation of tetrachloroethene during reductive dechlorination by Sulfurospirillum multivorans and Desulfitobacterium sp. strain PCE-S and abiotic reactions with cyanocobalamin. Applied and Environmental Microbiology, 71(7): 3413-3419.

Pankow, J.F., Cherry, J.A., 1996. Dense Chlorinated Solvents and Other DNAPLs in Groundwater Waterloo. Press. Portland, OR., 522 pp.

Parker, B.L., 1996. Effect of Molecular Diffusion on the Persistence of Dense Immiscible Phase Organic Liquids in Fractured Porous Geologic Media. PhD Thesis Thesis, University of Waterloo, Waterloo, Ontario, Canada, 191 pp.

Renpenning, J. et al., 2014. Combined C and Cl isotope effects indicate differences between corrinoids and enzyme (Sulfurospirillum multivorans PceA) in reductive dehalogenation of tetrachloroethene, but not trichloroethene. Environmental science & technology, 48(20): 11837-11845.

Schüth, C., Bill, M., Barth, J.A., Slater, G.F., Kalin, R.M., 2003. Carbon isotope fractionation during reductive dechlorination of TCE in batch experiments with iron samples from reactive barriers. Journal of contaminant hydrology, 66(1): 25-37.

Slater, G.F., Sherwood Lollar, B., Sleep, B.E., Edwards, E.A., 2001. Variability in carbon isotopic fractionation during biodegradation of chlorinated ethenes: Implications for field applications. Environmental science & technology, 35(5): 901-907.

VanStone, N.A., Focht, R.M., Mabury, S.A., Lollar, B.S., 2004. Effect of iron type on kinetics and carbon isotopic enrichment of chlorinated ethylenes during abiotic reduction on Fe (0). Groundwater, 42(2): 268-276.

Vargas, I., 2005. Assessment of the Fate of a Tetrachloroethene (PCE) and Trichloroethene (TCE) Plume at the Borden Aquifer. Master Thesis, Waterloo, 52 pp.

Wanner, P., Hunkeler, D., 2015. Carbon and chlorine isotopologue fractionation of chlorinated hydrocarbons during diffusion in water and low permeability sediments. Geochimica et Cosmochimica Acta, 157: 198-212.

Wiedemeier, T.H., 1999. Natural attenuation of fuels and chlorinated solvents in the subsurface. John Wiley & Sons.

Wiegert, C. et al., 2013. Carbon and chlorine isotope fractionation during microbial degradation of tetra-and trichloroethene. Environmental science & technology, 47(12): 6449-6456.

Chapter 7: Assessing the effect of chlorinated hydrocarbon degradation in aquitards on plume persistence due to back-diffusion

7.1. Introduction

During the past 20 years it became clear that plume persistence after removal, isolation or complete dissolution of DNAPL sources can be caused by back-diffusion from aquitards due to the reversal of the concentration gradient between aquifer and aquitard (Chapman and Parker, 2005; Liu and Ball, 2002; Parker et al., 2008; Seyedabbasi et al., 2012). To estimate the longevity of contamination plumes associated to back-diffusion, several studies used numerical modelling showing that back-diffusion can generate aquifer concentrations far above Maximum drinking water Concentration Limits (MCL, based on US EPA) for decades or even centuries (Chapman and Parker, 2005; Hwang et al., 2008; Seyedabbasi et al., 2012). These studies did not take into account reactive processes in the aquitard in their models. However, the more reducing conditions in aquitards may frequently trigger degradation of chlorinated hydrocarbons, which are otherwise stable under oxic aquifer conditions. Field studies reported in the previous chapter (chp. 6) and recent publications (Damgaard et al., 2013; Takeuchi et al., 2011) confirmed that chlorinated hydrocarbons can indeed be degraded in aquitards potentially influencing the plume persistence due to back-diffusion. Hence, an investigation of the effect of degradation in aquitards on plume persistence is warranted. On the one hand degradation could reduce plume longevity and one the other hand if only partial degradation occurs, more toxic by-products might be released in the aquifer. Furthermore, it remains unclear how reactive processes in aquitards are reflected isotope ratio profiles in aquifer – aquitard systems and as to what extent stable isotope methods provide more insight into the relation between degradation activities in aquitards and plume persistence due to back-diffusion.

To address these gaps, numerical modelling was performed to investigate the impact of degradation in aquitards on the longevity of the contamination source due to back-diffusion. In addition, it was evaluated, whether the degradation products in the low permeability sediments also significantly contaminate the adjacent aquifer as reactants and products can simultaneously diffuse into and out of the aquitard, respectively due to opposite concentration gradients. Moreover, it is investigated whether carbon isotope measurements in the aquifer can be used to track reactive processes in the aquitard, which would facilitate the identification of degradation activities in aquitards as aquifers are normally easier to access than aquitards. Furthermore, it is evaluated whether isotope ratio measurements in the aquifer also allow differentiating between

degradation activities in the aquifer and the aquitard, respectively. For this purpose a previously described 2D numerical model simulating a migrating TCE plume in an aquifer overlying an aquitard (Chapman and Parker, 2005) was adopted and reactive processes were added to the model in the aquitard and in the aquifer.

7.2. Numerical simulation methods

The 2D numerical model of an aquifer-aquitard system developed by Chapman and Parker (2005) was adopted by using the finite element computer code Comsol Multiphysics®. The 2D modelling approach is justified by the assumption that transverse horizontal dispersion in the simulated aquifer is not affecting the concentration evolution in the center of the contaminant plume. The selected model parameters are summarized in table 7-1 and a detailed description of the 2D numerical model can be found in Chapman and Parker (2005). Briefly, the modelling domain was 15 meters high and 300 meters long, whereby the aquifer was 5 m and the aquitard 10 m thick (Tab. 7-1). A highly resolved rectangular mesh was generated, especially refined at the aquifer – aquitard interface, where the rectangular elements were 20 times smaller than in the rest of the modelling domain. The differential equations were solved by using the implicit time dependent solver algorithm, whereby the BDF (backward differentiation formulas) time stepping method was used. In the aquifer a linear groundwater flow velocity of 0.5 m/d was specified, while in the underlying aquitard the velocity was set to zero (Tab. 7-1). At the up and down gradient ends of the modelling domain a continuous in- and outflow were defined, respectively, while at the other boundaries no flow was imposed. A trichloroethene (TCE) DNAPL source of 20 m length and 0.1 m height, with an initial concentration at the aqueous solubility limit (1100 mg/L,) was emplaced at the up gradient end of the modelling domain at the bottom of the aquifer. The migration of the emanating TCE plume from the TCE DNAPL source was simulated by advection and dispersion in the aquifer and by diffusion in the underlying aquitard. The source was emplaced for 42 years. After its removal clean water flushed though the aquifer for 100 years causing back-diffusion from the aquitard towards the aquifer. For simulating degradation in the aquitard and in the aquifer, reactive processes (first order kinetics) were included in the model by considering the degradation of TCE to cis-dichloroethene (cDCE). The choice of a one-step

degradation process has the advantage that the effect of a degrading parent (TCE) and an accumulating product compound (cDCE) can be evaluated in the different degradation scenarios. To simulate carbon isotope fractionation, species containing one heavy (^{13}C) and only light (^{12}C) carbon isotopes, respectively, were defined for TCE and cDCE (^{13}TCE, ^{12}TCE, $^{13}cDCE$, $^{12}cDCE$). A $\delta^{13}C$ value of -29.3‰ was used for the TCE DNAPL source, which corresponds to an average value (n=10) of different TCE manufacturers (Aelion et al., 2010). Beside degradation, it was assumed that diffusion and sorption have also an influence on carbon isotope ratios of TCE and cDCE. Isotope enrichment factors for sorption ($\varepsilon_{Sorption}$ = -0.40‰) and diffusion ($\varepsilon_{Diffusion}$ = -0.33‰) were selected based on experimentally determined values in chapter 3 and 5. To assess the impact of reactive processes in the aquitard on plume persistence due to back-diffusion and to investigate whether carbon isotopes can be used to track different aquitard degradation conditions, three different aquitard degradation scenarios were simulated: A no-degradation scenario, a uniform and a non-uniform degradation scenario. For the uniform and the non-uniform aquitard degradation scenarios, the same enrichment factor (ε_C = -18.2‰) for TCE to cDCE transformation was selected as obtained for core 15-13 by calibration in chapter 6. In the uniform degradation scenario, a high vertically constant degradation rate was imposed (half-life = 30 days), while in the non-uniform degradation scenario, the rate varied vertically according to core 15-13 (chp. 6), i.e. the rate decreased exponentially from fast (half-life = 30 days) to zero degradation with increasing depth within the upper 10 cm of the aquitard. Concentration and carbon isotope profiles were evaluated 280 m downgradient from the source zone. The temporal concentration evolution was assessed in a virtual well with a 1.5 m screened interval located at the same location placed on top of the aquitard to cover the main part of the contaminant plume.

To examine whether carbon isotope ratios can be used to track if degradation takes place in the aquifer or in the aquitard, an aquifer degradation scenario was simulated and compared with the different aquitard degradation scenarios. For the aquifer degradation scenario, the same enrichment factor was used as for the aquitard degradation scenarios (ε_C = -18.2‰) with a slower degradation rate (half-life = 170 days). To compare carbon isotope ratios for the aquifer and aquitard degradation scenarios, the spatial carbon isotope ratio evolution along the plume axis was assessed before and during 100 years after source removal.

Table 7-1. Model parameters for simulating the TCE plume in the aquifer – aquitard system according to Chapman and Parker (2005). Degradation rates of the non-uniform degradation scenario were defined according to core 15-13 in chapter 6.

Parameter	**Unit**	**Value**
Tortuosity factor	-	0.40
K_{OC} TCE	L/Kg	126
K_{OC} cDCE	L/Kg	86
Diffusion coefficient in free solution: $D_{0,TCE}$	m^2/s	1.01E-09
Diffusion coefficient in free solution: $D_{0,cDCE}$	m^2/s	1.13E-09
Aquifer		
Height	m	5
Length	m	300
Hydraulic conductivity: K	m/s	2.0E-04
Porosity: ϕ	-	0.35
Linear groundwater flow velocity:v	m/d	0.5
Organic carbon content: f_{OC}	%	0.038
Bulk density: ρ	g/cm^3	1.70
Transverse dispersivity	m	1.0
Vertical dispersitvity	m	0.002
Aquitard		
Height	m	10
Length	m	300
Hydraulic conductivity: K	m/s	5.0E-10
Porosity: ϕ	-	0.43
Organic carbon content: f_{OC}	%	0.054
Bulk density: ρ	g/cm^3	1.95
Uniform degradation rate	1/s	2.7E-7
Non-uniform degradation rate	1/s	$2.7E\text{-}7 \cdot \mathrm{erfc}(20z)$[a]
TCE Source		
Height	m	0.1
Length	m	20
Concentration	mg/L	1100
Persistence time	y	42

[a] z corresponds to the vertical depth

7.3. Simulation results and discussion

7.3.1. Vertical aquifer – aquitard concentration profiles

For all simulated degradation scenarios, aquifer-aquitard concentration profiles were evaluated 280 m down gradient of the TCE DNAPL source. In the no-degradation scenario, just before TCE DNAPL source removal at 42 years, the highest TCE concentration of 250 mg/L was observed at the aquifer – aquitard interface (Fig. 7-1A). In the aquitard, TCE reached a depth of 4.5 m, whereby the concentration gradually decreased with depth showing a distinct diffusion profile. Five years after source removal, the TCE concentration at the aquifer – aquitard interface decreased to 10 mg/L, while in the aquitard typical back-diffusion profiles were observed showing the highest TCE concentration of 138 mg/L 55 cm below the aquifer – aquitard interface (Fig 7-1A). With increasing time (10 – 100 years after source removal), the TCE aquifer – aquitard interface concentrations further decreased and in the aquitard the peak concentrations of the back-diffusion profiles declined and migrated to greater depth.

In the uniform aquitard degradation scenario, a lower TCE concentration of 128 mg/L was observed at the aquifer - aquitard interface compared to the no-degradation scenario (250 mg/L) after 42 years, just before source removal (Fig. 7-1B). Furthermore, the TCE diffused into the aquitard at a lower concentration and to a shallower depth than in the no-degradation scenario, due to the uniform degradation activities in the aquitard. Five years after source removal TCE was no longer detected neither in the aquifer nor in the aquitard (Fig. 7-1B). Thus, the uniform degradation activities in the aquitard have completely eliminated the TCE from the aquifer – aquitard systems five years after cessation of the mass flux from the contamination source. In contrast to the degraded TCE, the cDCE produced in the aquitard was detected in the aquifer and in the aquitard before and after source removal (Fig. 7-1C). In the aquitard, cDCE showed back diffusion like profiles with gradually decreasing concentrations with depth and towards the aquifer – aquitard interface. During the presence of the TCE DNAPL source, the peak concentration (145 mg/L) of the cDCE profile was observed next to the aquitard – aquifer interface. After source removal, the cDCE concentrations in the aquitard declined and the peak concentration decreased and moved downwards into the aquitard (Fig. 7-1C).

In the non-uniform degradation scenario, in which degradation rates decreased exponentially in the upper 10 cm of the aquitard as observed in core 15-13 (chp. 6), the detected TCE concentration of 160 mg/L at the aquifer – aquitard interface was higher than in the uniform (128 mg/L) but lower than in the no-degradation scenario (280 mg/L) after simulating a constant TCE DNAPL source for 42 years (Fig. 7-1D). In the aquitard, a typical TCE diffusion profile was observed with a penetration depth of 3 m, which was deeper compared to the uniform degradation scenario but shallower than in the no-degradation scenario. In contrast to the uniform degradation scenario, TCE was still detected in the aquifer as well as in the aquitard up to 100 years after the TCE DNAPL source was removed. In the aquitard TCE showed distinct back-diffusion profiles at about three times lower concentrations than in the no-degradation scenario. The produced cDCE in the aquitard also showed back-diffusion like concentration patterns at approximately 1.5 time lower concentrations before and after source removal compared to the uniform degradation scenario (Fig. 7-1E).

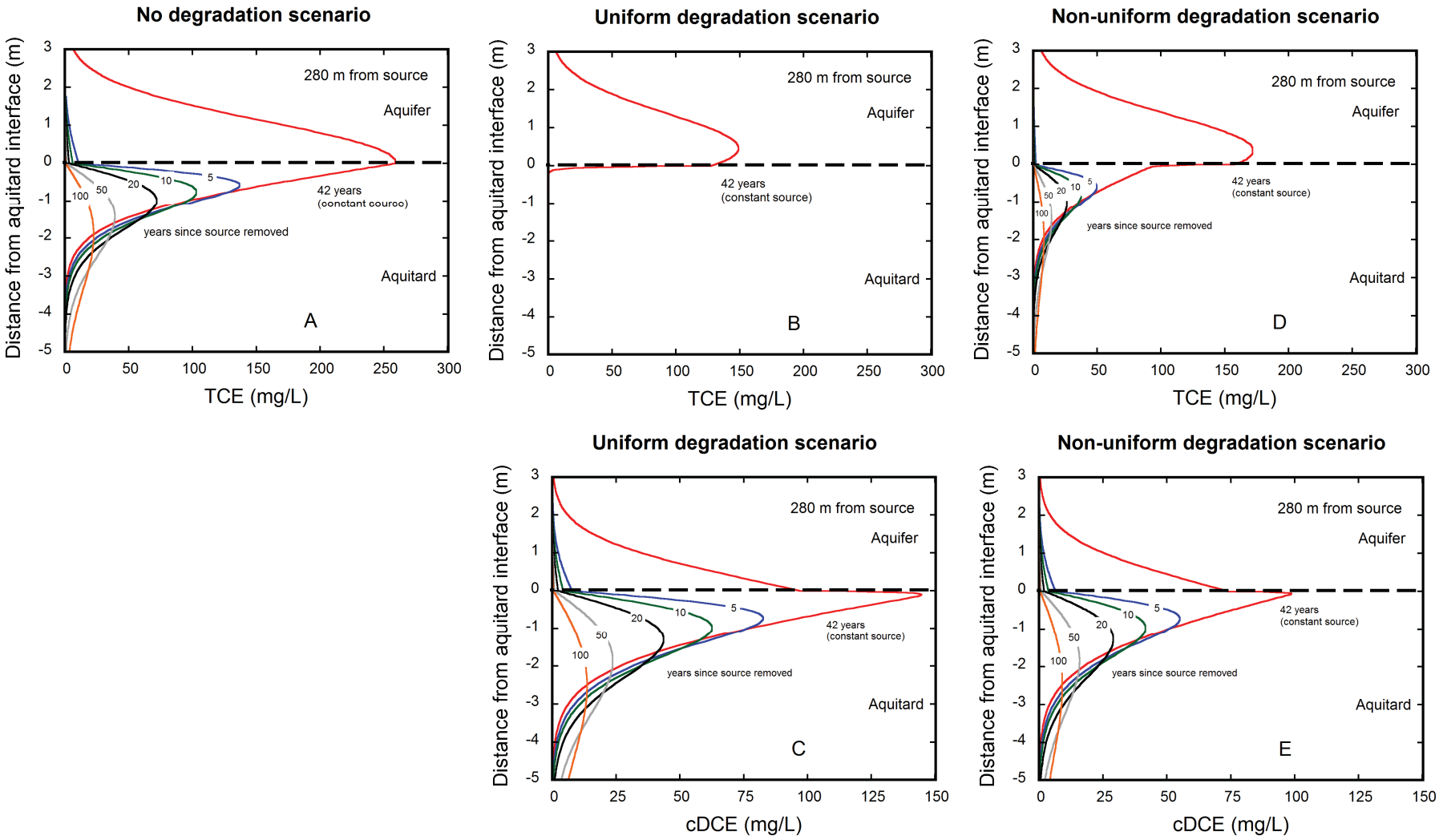

Figure 7-1.Simulated TCE and cDCE concentration profiles 280 m down gradient of the TCE DNAPL source for the no-degradation scenario (Fig. 7-1A), the uniform degradation scenario (Figs. 7-1B and 7-1C) and the non-uniform degradation scenario (Figs. 7-1D and 7-1E). Concentration profiles are shown at the end of the 42 years constant source period and at 5, 10, 20, 50 and 100 years after source removal.

7.3.2. Temporal evolution of aquifer concentrations

To evaluate the effect of the different degradation scenarios in the aquitard on plume persistence, breakthrough curves in a virtual 1.5 m screened well, placed in the lowest aquifer part 280 m down gradient of the TCE DNAPL source, were assessed (Fig. 7-2). For the no-degradation scenario, the TCE concentration in the well remained on a constant level of 300 mg/L during the presence of the TCE DNAPL source, while after source removal the TCE concentration decreased rapidly by more than one order of magnitude (Fig. 7-2A). However, a strong long-term tailing persisted with TCE concentrations around 1 mg/L. Hence, in the no-degradation scenario the TCE concentrations remained far above the MCL (0.005 mg/L, based on US EPA) for more than 100 years after source removal in the simulated well, which is consistent with the findings of Chapman and Parker (2005).

In the uniform degradation scenario, TCE concentrations remained on a lower level (185 mg/L) compared to the no-degradation scenario (300 mg/L) during the presence of the TCE DNAPL source (Fig. 7-2A). The lower concentrations are likely due to a stronger diffusive mass flux into the aquitard during the migration of the TCE plume caused by the steeper aquifer - aquitard concentration gradient generated by the uniform degradation activities in the aquitard. After source removal, the TCE concentration declined in the simulated well immediately below the MCL showing that the uniform degradation in the aquitard prevents the persistence of a long-term tailing for TCE in contrast to the no-degradation scenario (Fig. 7-2A). However, in the uniform degradation scenario not only TCE but also cDCE, which was produced in the aquitard, was detected in the simulated well (Fig. 7-2B). This indicates that significant diffusive mass transfer of the produced cDCE occurred from the aquitard into the aquifer. During the presence of the source the diffusive transport of cDCE was largest causing a cDCE aquifer concentration of 75 mg/L (Fig 7-2B). After the source was removed, the diffusive transport was less strong and the cDCE concentrations dropped but a long-term tailing persisted with cDCE concentrations (1.0 - 0.1 mg/L) above the MCL (0.07 mg/L, based on US EPA) for more than 100 years after source removal (Fig. 7-2B). This shows that although the uniform degradation activities in the aquitard impeded a long term tailing for TCE, aquifer contamination still persists for more than 100 years due to the accumulation of cDCE in the aquitard followed by diffusion into the aquifer.

In the non-uniform degradation scenario, TCE concentrations in the simulated well prevailed on an intermediate level (222 mg/L) compared to the no-degradation (300 mg/L) and

uniform degradation (185 mg/L) scenario during the presence of the TCE DNAPL source (Fig. 7-2A). The aquifer – aquitard concentration gradient and the associated diffusive mass flux into the aquitard is likely stronger than in the no-degradation but weaker than in the uniform degradation scenario during the presence of the source leading to the intermediate concentration level. After the source was removed TCE persisted in the aquifer (Fig 7-2A). Although TCE occurred at a lower concentration than in the no-degradation scenario, the concentrations remained above the MCL for more than 100 years (Fig. 7-2A). The persistence of TCE above MCL in the aquifer in the non-uniform degradation scenario contrasts the uniform degradation scenario, in which no TCE was observed after source removal. This demonstrates that the vertical extent of degradation in the aquitard affects the TCE plume persistence due to back-diffusion. In addition to TCE, also the cDCE produced in the aquitard was observed in the simulated well (Fig. 7-2B). Hence, significant diffusive transport of the produced cDCE from the aquitard towards the aquifer also occurred in the non-uniform degradation scenario. Similar to the uniform degradation scenario the diffusive transport rate of cDCE was fastest during the presence of source resulting in a concentration of 55 mg/L. After the source was removed, the cDCE concentrations decreased rapidly but also remained on a concentration level above the MCL for more than a century after the source was removed (Fig. 7-2B). Hence, the non-uniform degradation scenario generated a two-fold contamination of the aquifer by TCE and cDCE showing both long-term tailings of concentrations above the MCL for more than 100 years after source removal.

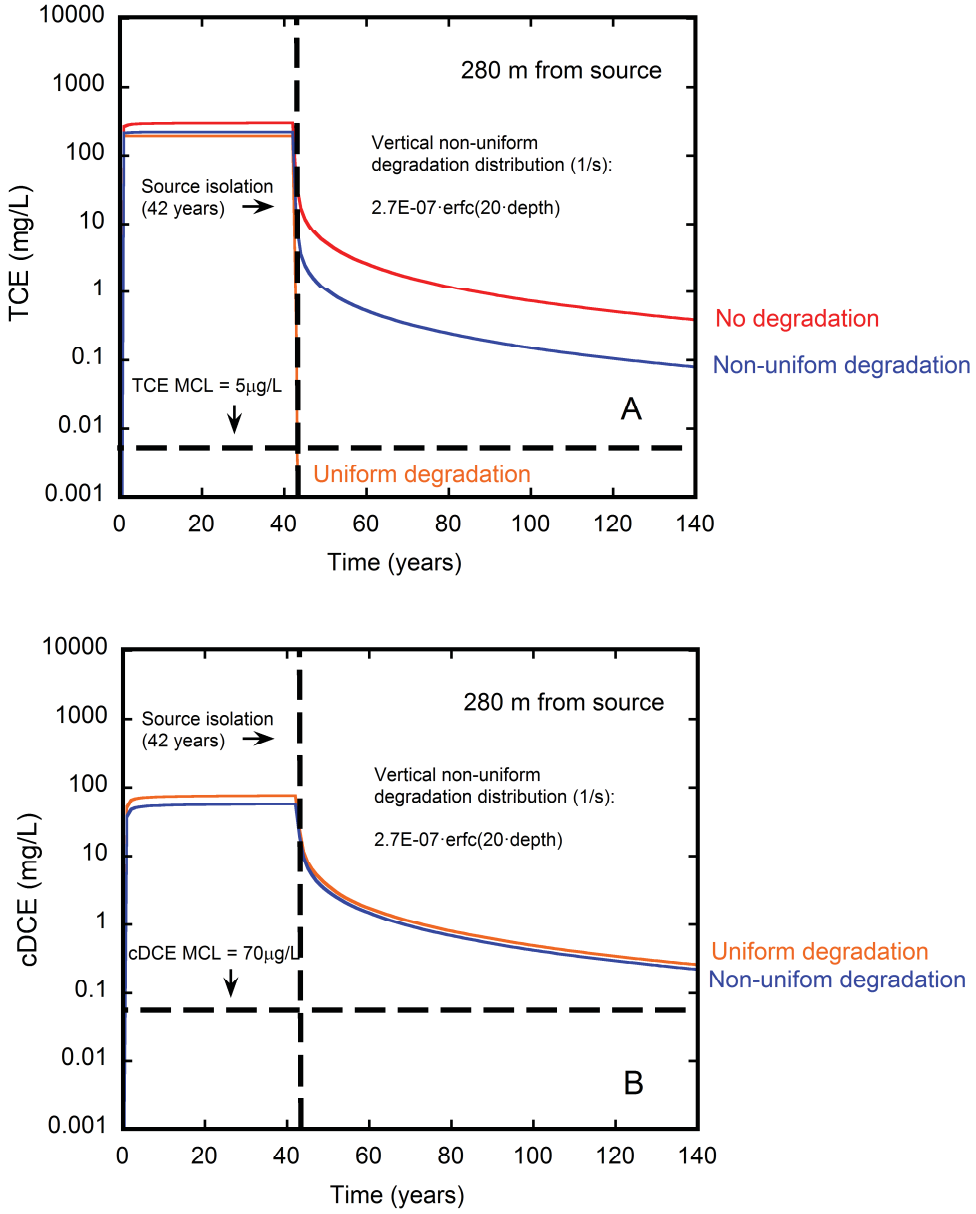

Figure 7-2. Temporal TCE (Fig. 7-2A) and cDCE (Fig. 7-2B) concentration evolution in a virtual 1.5 m screened well, located 280 m downgradient of the TCE DNAPL source on top of the aquitard for the no-degradation, the uniform and the non-uniform degradation scenario. MCLs for TCE (5 μg/L) and cDCE (70 μg/L) are indicated based on the US EPA.

7.3.3. Vertical aquifer – aquitard carbon isotope ratio profiles

Similar as for the concentration profiles, aquifer-aquitard carbon isotope ratio profiles were evaluated 280 m down gradient of the TCE DNAPL source for all simulated degradation scenarios. The profiles were assessed to investigate how the different degradation conditions are reflected in isotope ratio profiles and to investigate if the different degradation scenarios lead to unique isotope ratio patterns compared to diffusion/back-diffusion scenario without degradation. In the no-degradation scenario, TCE carbon isotope ratios were temporally constant close to the aquifer – aquitard interface corresponding to the TCE DNAPL source signature ($\delta^{13}C$ = -29.3‰). With increasing vertical distance from the aquifer – aquitard interface the TCE became slightly depleted in ^{13}C in the aquitard and in the aquifer (Fig. 7-3A). The small shifts can be likely explained by the faster diffusive transport rate for the isotopically light compared to the heavy species into the aquitard and the diffusive contribution to dispersion in the aquifer (Fig. 7-3A). This indicates that for a linear sorption behavior the diffusive isotope effect is not compensated by sorption even though the isotope fractionation factor is slightly larger for sorption compared to diffusion (c.f. section 7.2.).

In the uniform degradation scenario during the present of the TCE DNAPL source, TCE was strongly enriched in ^{13}C next to the aquifer – aquitard interface due to the strong uniform degradation activities in the aquitard (Fig. 7-3B). The produced cDCE reached the initial carbon isotope signature of TCE at 20 cm depth in the aquitard as TCE was completely converted to cDCE (Fig. 7-3C). With increasing depth an inverse carbon isotope trend of cDCE was observed with a slight depletion of ^{13}C due to the diffusive transport process. After source removal, the inverse shift of cDCE carbon isotope ratios with depth in the aquitard was less pronounced as the concentration gradient was flatter than during the presence of the source (Fig. 7-1C). Such a positive correlation between the steepness of the concentration gradient and the magnitude of the shift of isotope ratios has been also observed beneath the chemical waste landfill as described in chapter 3 (Figs. 3-6A and B). In the aquifer the cDCE carbon isotope profiles became heavier after source removal as isotopically heavier cDCE was transported by diffusion from the aquitard towards the aquifer compared to prior source removal. Furthermore, the cDCE carbon isotope profiles look similar as the TCE profiles in the no-degradation scenario after source removal as

cDCE acts as a contamination source and back-diffuses similarly as TCE in the no-degradation scenario due to the rapid and complete conversion of TCE to cDCE in the aquitard (Fig. 7-3A).

In the non-uniform degradation scenario, TCE and cDCE showed similar carbon isotope ratio profiles in the aquifer and in the aquitard (Figs. 7-3D and 7-3E). During the presence of the TCE DNAPL source, a pronounced enrichment of ^{13}C was observed in the upper 20 cm of the aquitard that is however, less strong than in the uniform degradation scenario (TCE: $\Delta\delta^{13}C$ = 8.0‰, cDCE: $\Delta\delta^{13}C$= 1.2‰). With increasing depth an inverse trend with slight depletion of ^{13}C was detected (Figs. 7-3D and 7-3E). After source removal, TCE and cDCE carbon isotope ratios were more enriched in ^{13}C in the upper 20 cm of the aquitard TCE compared to the uniform degradation scenario due to the ongoing degradation of the remaining TCE. The magnitude of the shift was largest adjacent to the aquifer – aquitard interface and decreased with depth due to vertically non-uniformly distributed degradation activities (Fig. 7-3D). At greater depth, TCE and cDCE were depleted in ^{13}C caused by the diffusive transport process as already observed during the presence of the TCE DNAPL source. Furthermore, the diffusion induced isotope shift decreased with increasing time as the concentration gradient in the aquitard became flatter as observed in the uniform degradation scenario and in chapter 3 (Figs. 3-6A and B). In the aquifer, TCE and cDCE was more enriched in ^{13}C after source removal. This can be explained by the further degradation of the remaining TCE to cDCE during the back-diffusive transport after source removal through the bioactive zone in the upper 10 cm of the aquitard towards the aquifer, which caused the enriched TCE and cDCE in ^{13}C in the aquifer compared to prior source removal (Figs. 7-3D and E).

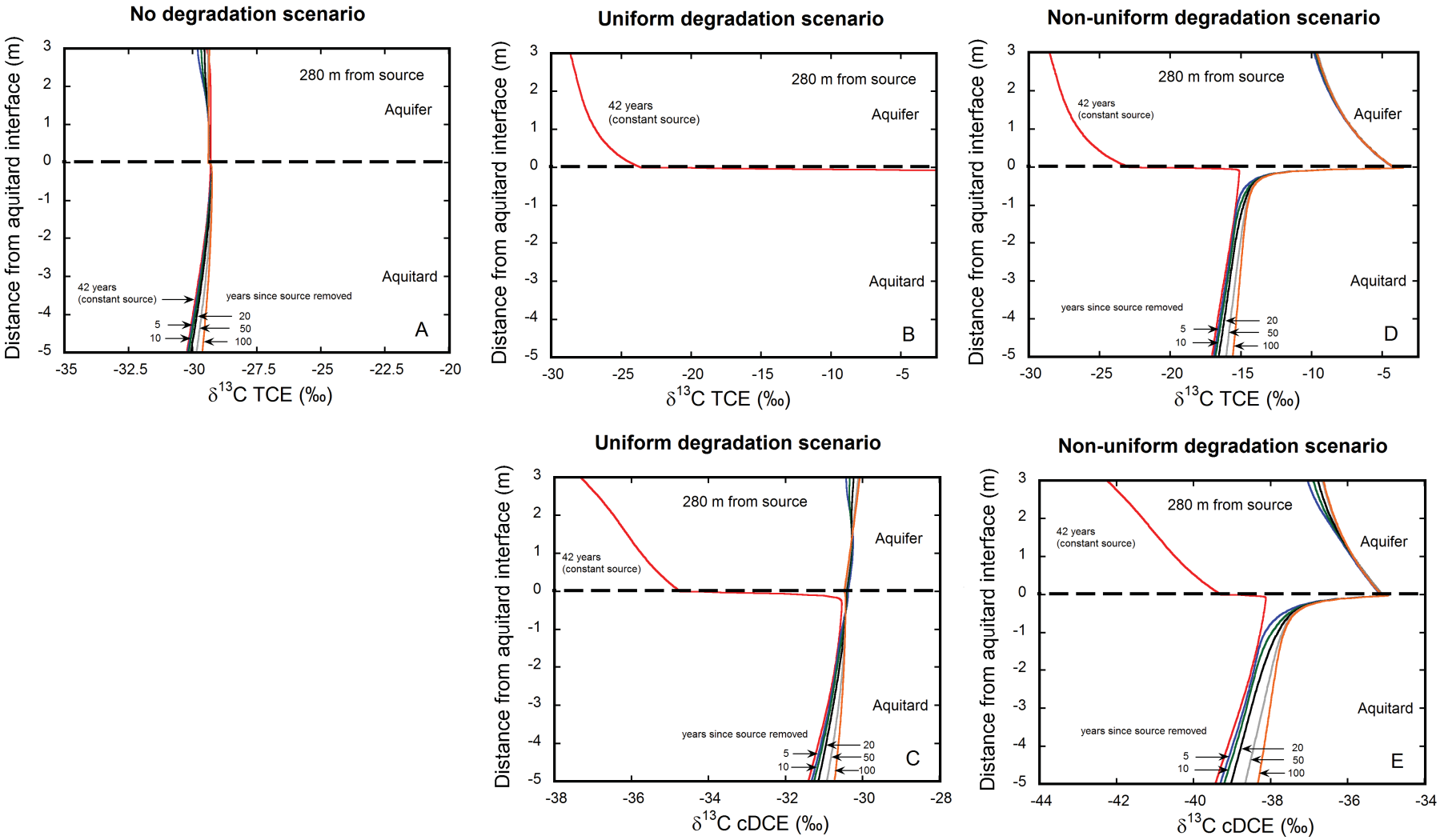

Figure 7-3.Simulated TCE and cDCE carbon isotope ratio profiles 280 m down gradient of the TCE DNAPL source ($\delta^{13}C$ = -29.3‰) for the no-degradation scenario (Fig. 7-3A), the uniform degradation scenario (Figs. 7-3B and 7-3C) and the non-uniform degradation scenario (Figs. 7-3D and 7-3E). Carbon isotope ratio profiles are shown at the end of the 42 years constant source period and at 5, 10, 20, 50 and 100 years after source removal.

7.3.4. Carbon isotope signatures in the aquifer for different aquitard degradation scenarios

To investigate the impact of the different degradation scenarios in the aquitard on carbon isotope ratios in the aquifer, the temporal evolution of the TCE and cDCE carbon isotope signatures in the 1.5 m screen well located 280 m down gradient on top of the aquitard was assessed. For the no-degradation scenario, the TCE carbon isotope ratios in the simulated well remained constant (Fig. 7-4A) indicating that physical isotope effects such as sorption and diffusion are not significantly modifying the TCE carbon isotope signature in the aquifer.

In the uniform degradation scenario, the TCE carbon isotope signature remained also constant but TCE was more enriched in ^{13}C ($\delta^{13}C$ = -25.9‰) than in the no-degradation scenario ($\Delta\delta^{13}C$ = -29.3‰) during the presence of the TCE DNAPL source (Fig. 7-4A). Due to the more rapid degradation of light compared to heavy TCE in the aquitard, concentrations gradients are steeper and thus, the diffusive mass flux into the aquitard is larger for light compared to heavy TCE, leading to the enrichment of ^{13}C in TCE in the aquifer. The cDCE carbon isotope signature was also constant ($\delta^{13}C$ = -35.4‰) during the presence of the source (Fig. 7-4B). In contrast, after source removal, cDCE became immediately enriched in ^{13}C ($\Delta\delta^{13}C$ = 5‰), followed by a constant temporal carbon isotope ratio evolution, which corresponded to the initial TCE isotope signature due to the complete degradation of TCE to cDCE in the aquitard followed by back-diffusion towards the aquifer.

In the non-uniform degradation scenario, TCE and cDCE showed a similar $\delta^{13}C$ trend in the simulated 1.5 m screened well. During the presence of the source the signatures remained constant but they were slightly more depleted in ^{13}C than in the uniform degradation scenario (TCE: $\delta^{13}C$ = -26.3‰; cDCE: $\delta^{13}C$ = -40.0‰) (Fig. 7-4A-B), while after source removal, TCE and cDCE became suddenly enriched in ^{13}C. The immediate enrichment of TCE and cDCE in ^{13}C after source removal can be explained by the further degradation and enrichment in ^{13}C of the remaining TCE in the aquitard during its back-diffusive transport through the bioactive zone in the upper 10 cm of the aquitard towards the aquifer (Fig. 7-4A). Furthermore, after source removal, carbon isotope signatures of TCE and cDCE remained constant again in the aquifer despite transient TCE and cDCE concentration evolutions (Figs. 7-2A and B) likely due to the applied first order kinetic degradation approach, for which the magnitude of isotope fractionation shows no concentration dependency.

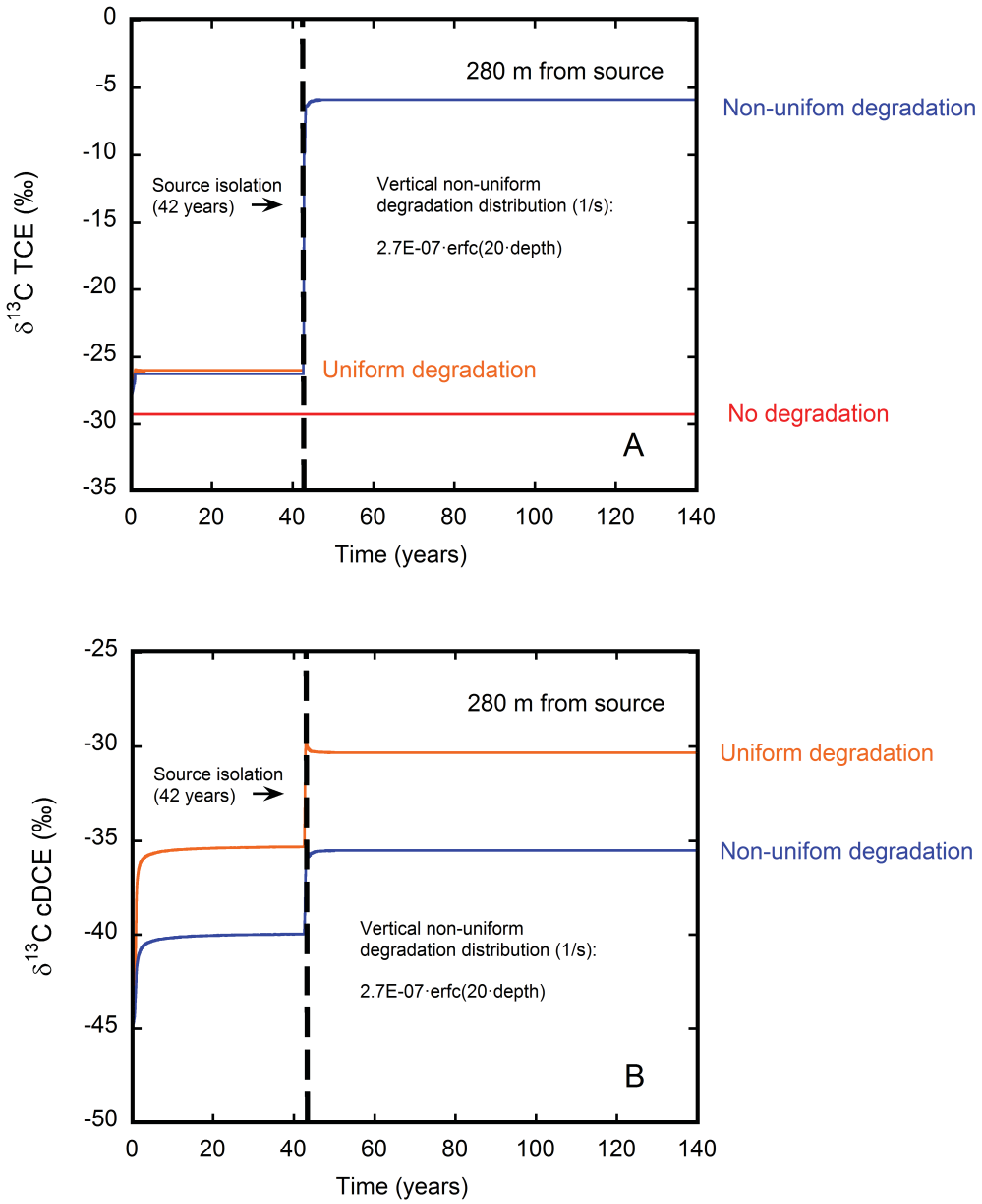

Figure 7-4. Temporal TCE (Fig. 7-4A) and cDCE (Fig. 7-4B) carbon isotope ratio evolution in a virtual 1.5 m screened well, located 280 m downgradient of the TCE DNAPL source on top of the aquitard for the no-degradation, the uniform and the non-uniform aquitard degradation scenario.

7.3.5. Spatial carbon isotope signature evolution for degradation in the aquifer and for uniform and non-uniform degradation in the aquitard

To explore if carbon isotope ratio aquifer measurements can be used to distinguish between reactive processes occurring in the aquifer or in the aquitard, the evolution of carbon isotope ratios along the plume axis was assessed in the aquifer and in the aquitard degradation scenarios (uniform, non-uniform). The spatial evolution of carbon isotope ratios along the plume axis was investigated just before and during 100 years after source removal.

In the aquifer degradation scenario, a continuous enrichment of ^{13}C in TCE and cDCE was observed with increasing distance from the TCE DNAPL source (Figs. 7-5A and 7-5B). The enrichment of heavy cDCE and TCE carbon isotopes along the plume axis was equal before and during 100 years after the source was removed (Figs. 7-5A and 7-5B). This can be explained by the identical carbon isotope signature of TCE, which acts as contamination source before (TCE DNAPL) and after (back-diffusion of TCE from aquitard, mainly from source zone) source removal. A similar continuous enrichment of ^{13}C in TCE and cDCE was observed for the aquitard degradation scenarios (uniform and non-uniform) during the presence of the source. The enrichment of ^{13}C along the plume axis was less strong than in the aquifer degradation scenarios although the degradation rate was faster (Figs. 7-5A and 7-5B). However, in contrast to the aquifer degradation scenario, TCE and cDCE became enriched in ^{13}C five years after source removal in the aquitard degradation scenarios and remained equal for 100 years (Figs. 7-5A and 7-5B). This is due to the back-diffusive transport of TCE and cDCE, which were enriched in ^{13}C caused by the degradation activities in the aquitard. Therefore, degradation in the aquitard and in the aquifer produced distinct spatial carbon isotope ratio trends after source removal. Consequently, the assessment of the spatial carbon isotope ratio evolution along the plume axis before and after source removal is useful to identify whether organic contaminants are affected by degradation in the aquifer or in the aquitard. When degradation occurs in the aquitard the assessment of isotope ratios along the plume axis can also be used for assessing the success of the remediation of DNAPL sources located in the aquifer since the contaminants become enriched in ^{13}C along the plume axis when the DNAPL was removed (Figs. 7-5A and 7-5B).

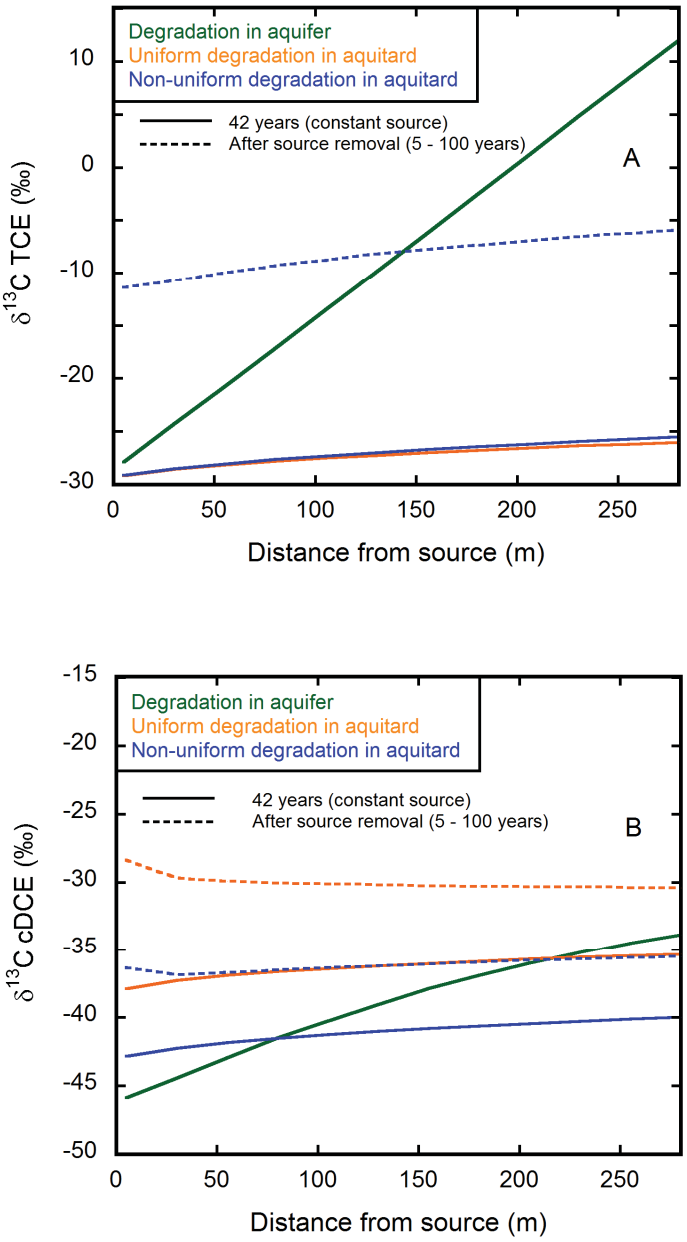

Figure 7-5. TCE (Fig. 7-5A) and cDCE (Fig. 7-5B) carbon isotope ratio evolution as a function of the distance of TCE DNAPL source for the degradation scenario in the aquifer and the uniform and the non-uniform degradation scenario in the aquitard just before and during 100 years after source removal.

7.3. Conclusions

Three different aquitard degradation scenarios (no-degradation, uniform degradation, non-uniform degradation), which included the degradation of TCE to cDCE, were simulated to assess their impact on plume persistence in the adjacent aquifer due to back-diffusion. Furthermore, it was evaluated if carbon isotope ratios measurements in the aquifer can be used to track degradation activities in the aquitard and if they allow distinguishing between reactive processes in the aquifer and in the aquitard.

The aquitard degradation scenarios showed that plume persistence due back-diffusion depends on whether or not degradation takes place in the aquitard and on their vertical distribution. In the no-degradation scenario a strong TCE long-term tailing persists in the aquifer after source removal due back-diffusion with concentration above the MCL for more than 100 years. In contrast in the uniform degradation scenario, TCE disappeared completely after source removal but the produced cDCE was transported by diffusion from the aquitard towards the aquifer causing concentrations above MCL for more than 100 years after source removal. Therefore, as cDCE was not further degraded, the uniform degradation activities were not impeding the occurrence of a long-term persistence of the contamination source due to back-diffusion. In the non-uniform degradation scenario, in which the degradation rate decreased exponentially in the topmost 10 cm of the aquitard as observed in core 15-13 in chapter 6, the parent compound (TCE) as well as the daughter product (cDCE) persist in the aquifer due to back-diffusion form the aquitard. Hence, the partial degradation of TCE in the non-uniform degradation scenario in the aquitard led to a dual contamination and aggravated the plume persistence due to back-diffusion compared to a situation in which no degradation or uniform degradation occurs.

The aquitard degradation scenarios (uniform, non-uniform) were also reflected in characteristic temporal carbon isotope ratio evolutions compared to the no-degradation scenario in the aquifer in the 1.5 m screened well located 280 m down gradient of the TCE DNAPL source. This demonstrated that carbon isotope ratios measurements in the aquifer are able to track whether or not degradation occurs in aquitards, which simplifies the identification of aquitard degradation activities as aquifers are usually easier accessible than aquitards. Furthermore, the comparison between an aquifer degradation scenario and the aquitard degradation scenarios

(uniform/non-uniform) revealed that depending on whether degradation occurs in the aquifer or in the aquitard carbon isotope ratios evolve distinctively along the plume axis after the contaminant source has been removed. This indicates that stable carbon isotope ratios are also beneficial for distinguishing reactive processes in the aquitard and the aquifer. When degradation occurs in the aquitard the evaluation of isotope ratios along the plume axis can also reveal whether or not the remediation of a DNAPL source located in the aquifer was effective as the contaminants become enriched in ^{13}C when the DNAPL was completely removed.

Overall the present chapter assessed only a few aquifer and aquitard degradation scenarios, respectively. Hence, the results of the simulations and the conclusions might alter if some model parameters are set differently. For instance when in the uniform aquitard degradation scenario the degradation rate is slower not all of the TCE might be degraded, which perhaps also leads to a dual contamination of the aquifer due to back-diffusion as observed in the non-uniform degradation scenario. Furthermore, if reactive processes in the aquitard degradation scenario are associated with smaller isotope fractionation factors, the difference between isotope ratios before and after source removal is perhaps not as distinct as in the conducted simulations. Hence, degradation activities in the aquifer and in the aquitard might be not well distinguishable. This demands for a sensitivity analysis for the simulation parameters, which would increase the comprehension of the impact of different degradation activities in aquitard on plume persistence due to back-diffusion and which would improve the understanding for to what extent carbon isotope ratio measurements in aquifers can be used to identify degradation activities in aquifer – aquitard systems.

7.4. References

Aelion, C.M., Höhener, P., Hunkeler, D., Aravena, R., 2010. Environmental Isotopes in Biodegradation and Bioremediation CRC Press, USA, 450 pp.

Chapman, S.W., Parker, B.L., 2005. Plume persistence due to aquitard back diffusion following dense nonaqueous phase liquid source removal or isolation. Water Resources Research, 41(12).

Damgaard, I. et al., 2013. Identification of chlorinated solvents degradation zones in clay till by high resolution chemical, microbial and compound specific isotope analysis. Journal of Contaminant Hydrology, 146: 37-50.

Hwang, Y.K., Endres, A.L., Piggott, S.D., Parker, B.L., 2008. Long-term ground penetrating radar monitoring of a small volume DNAPL release in a natural groundwater flow field. Journal of contaminant hydrology, 97(1): 1-12.

Liu, C.X., Ball, W.P., 2002. Back diffusion of chlorinated solvent contaminants from a natural aquitard to a remediated aquifer under well-controlled field conditions: Predictions and measurements. Ground Water, 40(2): 175-184.

Parker, B.L., Chapman, S.W., Guilbeault, M.A., 2008. Plume persistence caused by back diffusion from thin clay layers in a sand aquifer following TCE source-zone hydraulic isolation. Journal of Contaminant Hydrology, 102(1-2): 86-104.

Seyedabbasi, M.A., Newell, C.J., Adamson, D.T., Sale, T.C., 2012. Relative contribution of DNAPL dissolution and matrix diffusion to the long-term persistence of chlorinated solvent source zones. Journal of Contaminant Hydrology, 134: 69-81.

Takeuchi, M. et al., 2011. Comparative study of microbial dechlorination of chlorinated ethenes in an aquifer and a clayey aquitard. Journal of Contaminant Hydrology, 124(1-4): 14-24.

Chapter 8: Conclusions and outlook

8.1. Conclusions

This PhD thesis addressed the following four research questions: A) Does aqueous phase diffusion and sorption lead to measurable shifts of isotope ratios? B) Are isotope effects due to diffusion and sorption detectable under field conditions? C) Do isotope effects associated with sorption and diffusion impair the identification of reactive processes in aquifer - aquitard systems by using stable isotope methods? and D) Can stable isotope methods provide insight into the impact of reactive processes in aquitards on plume persistence due to back diffusion? The focus of this PhD study lied on chlorinated solvents (denominated as chlorinated hydrocarbons when dissolved in water or air) as they are among the most persistent subsurface contaminants and are degradable under reducing conditions, which are often encountered in aquitards. In the following, the main conclusions of these four questions will be presented.

A) Does aqueous phase diffusion and sorption lead to measurable shifts of isotope ratios?

To investigate the effect of aqueous phase diffusion and sorption on isotope ratios, controlled laboratory experiments were performed. The laboratory diffusion experiment revealed a small but measurable shift of isotope ratios of TCE and 1,2-DCA, whereby light isotopocules diffused faster compared to heavy. The isotope enrichment factors were larger for chlorine ($\varepsilon_{Cl,TCE}$ = -0.27‰, $\varepsilon_{Cl,1,2\text{-}DCA}$ = -0.61‰) compared to carbon isotopes ($\varepsilon_{C,TCE}$ = -0.22‰, $\varepsilon_{C,1,2\text{-}DCA}$ = -0.23‰), which was consistent with the larger absolute mass difference between stable chlorine (two mass units) compared to carbon isotopes (one mass unit). The magnitude of isotope fractionation due to aqueous phase diffusion was generally smaller than in the gas phase. Molecular dynamic simulations, which have been conducted for the first time for organic compounds, demonstrated that lower magnitude of isotope fractionation during diffusion in aqueous phase compared to the gas phase can be explained by the mode coupling theory. In the aqueous phase the diffusing species is increasingly coupled with the mass-independent hydrodynamic modes of motion, while in the gas phase the strongly mass-dependent kinetic modes of motion dominate.

The laboratory sorption experiment revealed an unusual inverse isotope trend showing that carbon and chlorine isotopocules of 1,2-DCA and DCM containing light isotopes were preferentially sorbed compared to isotopocules containing heavy isotopes. This enhances the

mobility of isotopically heavy species, which is opposite to the observed faster diffusive transport rate for isotopically light compared to heavy species. The preferential sorption of isotopically light compared to heavy species can be explained by reduced Van der Waals interactions between heavy isotope and the sorbent material compared to light isotopes. The magnitude of isotope fractionation due to sorption was similar for 1,2-DCA carbon and chlorine ($\varepsilon_{C,1,2\text{-}DCA}$ = -0.40‰, $\varepsilon_{Cl,1,2\text{-}DCA}$ = -0.55‰) as for DCM carbon isotopes ($\varepsilon_{C,DCM}$ = -0.54‰).

B) Are isotope effects due to diffusion and sorption detectable under field conditions?

To assess whether aqueous phase diffusion and sorption induced isotope fractionation is also detectable at the field scale, and to explore how isotope fractionation due to diffusion and sorption interact, two field studies were carried out in non-reactive low permeability sediments. Key benefit was that sorption and diffusion occur coevally in these low permeable units and that the advancement of the concentration front could be located and sampled at a high spatial resolution. Furthermore, for both sites the contamination source was well characterized (volume, composition, spill time) as at the first site (Sarnia site) a controlled release field experiment had been performed and as at the second site the contamination occurred due to a chemical waste landfill, whereby the contamination history was known in detail. The two sites differed especially regarding their organic carbon content, whereby the Sarnia site showed a five times higher organic matter content than the chemical waste landfill site, which led to a different sorption behavior. The field investigations at these two sites revealed for the first time that isotope effects due to diffusion and sorption are indeed detectable at the field scale. Sorption and diffusion induced isotope effects were superimposed and compensate each other to some degree as both processes fractionate isotopes in opposite directions with increasing depth. Isotopically light species are transported faster by diffusion but at the same time, they are preferentially sorbed making them less mobile compared to isotopically heavy species during the migration in low permeability sediments. At the Sarnia site, the strong sorption behavior led to an enrichment of ^{13}C with increasing depth ($\Delta\delta^{13}C$ = 2.0‰ – 2.4‰) as sorption induced isotope fractionation dominated for carbon. In contrast for chlorine the diffusive isotope effect was larger as the mass difference is two for stable chlorine compared to one for carbon isotopes overruling the sorption effect and leading to a depletion of ^{37}Cl with depth ($\Delta\delta^{37}Cl$ = 1.3‰). On the contrary, at the chemical waste landfill site, where sorption behavior was less strong, diffusion dominated for

both carbon and chlorine isotopes leading to a depletion in ^{13}C and ^{37}Cl with depth ($\Delta\delta^{37}Cl$=2.8‰; $\Delta\delta^{13}C$ = 1.4‰). Furthermore, the simulation of isotope fractionation for different diffusion time scales in low permeability sediments revealed that the duration of the diffusion period has influence on the magnitude of isotope fractionation. During short diffusion periods, the shift of isotope ratios is largest, while for longer diffusion period the heavy isotopes catch up and the magnitude of isotope fractionation becomes smaller.

C*) Do isotope effects associated with sorption and diffusion impair the identification of reactive processes in aquifer - aquitard systems?*

The field investigations in non-reactive low permeable units revealed that sorption and diffusion induced isotope fractionation can lead to shifts of isotope ratios of around 2‰ under field conditions. The US EPA guidelines consider such shifts of isotope ratios as a lower limit for the identification of reactive processes. (Hunkeler et al., 2008). Hence, for slow reaction processes of for organic compounds having small degradation induced isotope enrichment factors (e.g. for BTEX compounds (benzene, toluene, ethylbenzene, xylenes)) a shift of isotope ratios of around 2‰ is not distinctively attributable to degradation processes by using stable isotope methods. However, for chlorinated hydrocarbons, which show usually larger isotope enrichment factors associated with degradation than BTEX compounds, an impairment of sorption and diffusion induced isotope fractionation can be likely neglected. This has been confirmed by the second controlled release field experiment at the Borden site, which was initiated nearly 15 years ago by infiltrating a mixture of chlorinated solvents in an aquifer overlying an aquitard. The isotope ratios profiles of the chlorinated hydrocarbons, which had diffused into the aquitard, showed large shifts towards lighter isotopes (up to 24‰) with depth. Hence, the observed shifts of isotope ratios were clearly larger than 2‰ and could be unequivocally attributed to degradation processes in the aquitard. However, the isotope trend was opposite to what was expected for reactive processes for which an enrichment of heavy isotopes with depth would be awaited. The inverse isotope trend could be attributed to a delay of the commencement of the degradation activities in the aquitard followed by non-uniformly distributed degradation activities in the aquitard, which were strongest close to the aquifer – aquitard interface and decreased exponentially with increasing depth within the upper 10 cm of the aquitard. With the help of numerical modelling the start of the degradation activities could be identified (2500 days after

DNAPL) and degradation rates could be estimated. Therefore, the field investigations at the Borden site demonstrated for the first time that stable isotope methods can be used to quantify reactive processes including spatial and temporal variability in aquitards.

D) Can stable isotope methods provide insight into the impact of reactive processes in aquitards on plume persistence in aquifers?

To assess if stable isotope methods can provide insight into the effect of degradation activities in aquitards on plume persistence due to back-diffusion a numerical model of a dissolved TCE plume emanating from a TCE DNAPL source in an aquifer – aquitard system was adopted and reactive processes were included in the aquitard. Several aquitard degradation scenarios were simulated, which revealed for the first time that degradation activities in the aquitard have an impact on plume persistence due to back-diffusion. Furthermore, the simulated degradation scenarios showed that longevity of the contamination source and its daughter products due to back-diffusion depends on the spatial variability of the degradation activities in the aquitard and on whether complete or partial degradation of the organic contaminants occurs. Moreover, the different simulated aquitard degradation scenarios showed that degradation activities in the aquitard have an impact on isotope ratios in the aquifer, whereby an immediate shift towards heavier isotope occurred after DNAPL source removal. This characteristic isotope pattern simplifies the identification of degradation activities in aquitards as aquifers are easier accessible than aquitards. In addition, the comparison between an aquifer and the different aquitard degradation scenarios revealed that depending on whether degradation occurs in the aquifer or in the aquitard, isotope ratios evolve differently along the plume axis in the aquifer. In the aquifer degradation scenario a continuous enrichment of heavy carbon isotopes along the plume axis was observed, which was equal before and after source removal. In contrast for the aquitard degradation scenarios, a sudden enrichment of heavy carbon isotopes was observed along the plume axis after source removal. This showed that stable isotope methods are also helpful for differentiating between degradation activities in the aquifer and the aquitard. When degradation occurs in the aquitard, isotope ratio measurements along the plume axis can also be used for evaluating the success of the remediation of DNAPL sources located in the aquifer, since the contaminants become enriched in heavy isotopes in the aquifer when the DNAPL was completely removed.

8.2. Outlook

Although sorption and diffusion induced isotope fractionation and their influence on the identification of reactive processes in aquifer – aquitard systems have been extensively examined in this PhD study, some further research questions, which have been risen during this PhD, remain to be elucidated:

- It has been demonstrated by Bourg et al. (2010) that the diffusive transport rate for ions and noble gases is not only dependent on the mass but also to the residence time of the solvation shell (nearest water molecules surrounding the solute), which is correlated with the polarity of the solute. To assess if the same relationship between the diffusive transport rate and the residence time of the solvation is also valid for organic compounds, the magnitude of isotope fractionation should be determined for additional organic compounds having different polarities.

- Isotope fractionation of organic compounds due to diffusion should also be determined for hydrogen isotopes. This would open the possibility to evaluate the mass dependency of the diffusive transport rate in the aqueous phase for chlorinated hydrocarbons not only in a dual but also in a multi-element approach (C, Cl, H).

- So far, the magnitude of isotope fractionation due to diffusion and sorption was investigated at a specified temperature. To evaluate to what extent the magnitude of diffusion and sorption induced isotope fractionation depends on temperature, serveral laboratory experiments should be performed at different temperatures.

- It remains unclear, which properties of organic compounds and of the clayey sorbate material govern the magnitude of isotope fractionation due to sorption processes. Hence, additional laboratory sorption experiments should be performed for different organic compound having different properties and by using clayey sorbate material with and without organic matter. This would clarify which properties of organic compounds have an influence on the magnitude of sorption induced isotope fractionation. Furthermore, it

would gain more insight into the relative contribution of sorption processes on clayey minerals and on organic matter to the overall isotope fractionation due to sorption. The laboratory sorption experiments could be also verified by molecular dynamic simulations addressing isotopocially different organic molecules being in contact with clay layers with and without organic matter.

- At the field scale, the understanding of the reactive processes affecting chlorinated hydrocarbons in low permeability sediments should be improved. In particular it is not clear whether chlorinated hydrocarbons are degraded biotically and/or abiotically in clays and whether stable isotope methods can be used to distinguish between different degradation pathways. If chlorinated hydrocarbons are degraded abiotically, further questions arise, which minerals or dissolved species in the pore water of the clay act as electron donors. Moreover, when the degradation occurs biotically it needs to be investigated what kind of bacteria can live in the small pore sizes of clays and can degrade chlorinated hydrocarbons.

- It also needs to be investigated in more detail how plume persistence due to back-diffusion depends on degradation activities in aquitards and how its role can be tracked with stable isotope methods. For that purpose a wider range of aquitard degradation scenarios should be simulated. It would be especially useful to vary the degradation rates in the aquitard to investigate their impact on the longevity of the contamination source and its daughter products due to back-diffusion.

8.3. References

Bourg, I.C., Richter, F.M., Christensen, J.N., Sposito, G., 2010. Isotopic mass dependence of metal cation diffusion coefficient in liquid water. Geochimica et Cosmochimica, 74: 2249 - 2256.

Hunkeler, D., Meckenstock, R.U., Sheerwood Lollar, B., Schmidt, T.C., Wilson, J.T., 2008. A Guide for Assessing Biodegradation and Source Identification of Organic Ground Water Contaminants using Compound Specific Isotope Analysis. Environental Protection Agency (EPA), 600(R-08): 68.

Appendix

Control files for molecular dynamic simulations of TCE carbon isotopocules with Lammps

```
#121C_TCE input file


units metal
dimension 3
atom_style full
pair_style lj/cut/coul/long 10.0 10.0
bond_style harmonic
angle_style harmonic
dihedral_style opls
pair_modify mix arithmetic

read_restart 121C_TCE_03.save
reset_timestep 0

pair_coeff 1 1 6.73853e-3 3.16556
pair_coeff 2 2 0.0 0.0
pair_coeff 3 3 3.2984e-3 3.55
pair_coeff 4 4 3.2984e-3 3.55
pair_coeff 5 5 1.3020e-2 3.40
pair_coeff 6 6 1.3020e-2 3.40
pair_coeff 7 7 0.0 0.0

kspace_style pppm 0.0001

group water type 1 2
group Ow type 1
group C type 3 4

timestep 0.001
run_style verlet
fix 1 water shake 0.0001 20 0000 t 1 2


fix avePT all ave/time 1 250000 250000 c_thermo_temp c_thermo_press[1] c_thermo_press[2] c_thermo_press[3]
thermo_style custom step etotal f_avePT[1] f_avePT[2] f_avePT[3] f_avePT[4] lx ly lz
thermo 250000

dump 1 all dcd 1000 121C_TCE_04.dcd
dump 2 all xyz 10000000000 121C_TCE_04.xyz


fix 2 all nvt temp 298.0 298.0 0.1
run 50000000


write_restart 121C_TCE_04.save
```

```
#181C_TCE input file

units metal
dimension 3
atom_style full
pair_style lj/cut/coul/long 10.0 10.0
bond_style harmonic
angle_style harmonic
dihedral_style opls
pair_modify mix arithmetic

read_restart 181C_TCE_03.save
reset_timestep 0

pair_coeff 1 1 6.73853e-3 3.16556
pair_coeff 2 2 0.0 0.0
pair_coeff 3 3 3.2984e-3 3.55
pair_coeff 4 4 3.2984e-3 3.55
pair_coeff 5 5 1.3020e-2 3.40
pair_coeff 6 6 1.3020e-2 3.40
pair_coeff 7 7 0.0 0.0

kspace_style pppm 0.0001

group water type 1 2
group Ow type 1
group C type 3 4

timestep 0.001
run_style verlet
fix 1 water shake 0.0001 20 0000 t 1 2


fix avePT all ave/time 1 250000 250000 c_thermo_temp c_thermo_press[1] c_thermo_press[2]
c_thermo_press[3]
thermo_style custom step etotal f_avePT[1] f_avePT[2] f_avePT[3] f_avePT[4] lx ly lz
thermo 250000

dump 1 all dcd 1000 181C_TCE_04.dcd
dump 2 all xyz 10000000000 181C_TCE_04.xyz


fix 2 all nvt temp 298.0 298.0 0.1
run 50000000


write_restart 181C_TCE_04.save
```

```
#271C_TCE input file

units metal
dimension 3
atom_style full
pair_style lj/cut/coul/long 10.0 10.0
bond_style harmonic
angle_style harmonic
dihedral_style opls
pair_modify mix arithmetic

read_restart 271C_TCE_03.save
reset_timestep 0

pair_coeff 1 1 6.73853e-3 3.16556
pair_coeff 2 2 0.0 0.0
pair_coeff 3 3 3.2984e-3 3.55
pair_coeff 4 4 3.2984e-3 3.55
pair_coeff 5 5 1.3020e-2 3.40
pair_coeff 6 6 1.3020e-2 3.40
pair_coeff 7 7 0.0 0.0

kspace_style pppm 0.0001

group water type 1 2
group Ow type 1
group C type 3 4

timestep 0.001
run_style verlet
fix 1 water shake 0.0001 20 0000 t 1 2


fix avePT all ave/time 1 250000 250000 c_thermo_temp c_thermo_press[1] c_thermo_press[2] c_thermo_press[3]
thermo_style custom step etotal f_avePT[1] f_avePT[2] f_avePT[3] f_avePT[4] lx ly lz
thermo 250000

dump 1 all dcd 1000 271C_TCE_04.dcd
dump 2 all xyz 10000000000 271C_TCE_04.xyz


fix 2 all nvt temp 298.0 298.0 0.1
run 50000000


write_restart 271C_TCE_04.save
```

```
#331C_TCE input file

units metal
dimension 3
atom_style full
pair_style lj/cut/coul/long 10.0 10.0
bond_style harmonic
angle_style harmonic
dihedral_style opls
pair_modify mix arithmetic

read_restart 331C_TCE_03.save
reset_timestep 0

pair_coeff 1 1 6.73853e-3 3.16556
pair_coeff 2 2 0.0 0.0
pair_coeff 3 3 3.2984e-3 3.55
pair_coeff 4 4 3.2984e-3 3.55
pair_coeff 5 5 1.3020e-2 3.40
pair_coeff 6 6 1.3020e-2 3.40
pair_coeff 7 7 0.0 0.0

kspace_style pppm 0.0001

group water type 1 2
group Ow type 1
group C type 3 4

timestep 0.001
run_style verlet
fix 1 water shake 0.0001 20 0000 t 1 2


fix avePT all ave/time 1 250000 250000 c_thermo_temp c_thermo_press[1] c_thermo_press[2]
c_thermo_press[3]
thermo_style custom step etotal f_avePT[1] f_avePT[2] f_avePT[3] f_avePT[4] lx ly lz
thermo 250000

dump 1 all dcd 1000 331C_TCE_04.dcd
dump 2 all xyz 10000000000 331C_TCE_04.xyz


fix 2 all nvt temp 298.0 298.0 0.1
run 50000000


write_restart 331C_TCE_04.save
```

Control files for molecular dynamic simulations of TCE chlorine isotopocules with Lammps

```
#31Cl_TCE input file

units metal
dimension 3
atom_style full
pair_style lj/cut/coul/long 10.0 10.0
bond_style harmonic
angle_style harmonic
dihedral_style opls
pair_modify mix arithmetic

read_restart 31Cl_TCE_03.save
reset_timestep 0

pair_coeff 1 1 6.73853e-3 3.16556
pair_coeff 2 2 0.0 0.0
pair_coeff 3 3 3.2984e-3 3.55
pair_coeff 4 4 3.2984e-3 3.55
pair_coeff 5 5 1.3020e-2 3.40
pair_coeff 6 6 1.3020e-2 3.40
pair_coeff 7 7 0.0 0.0

kspace_style pppm 0.0001

group water type 1 2
group Ow type 1
group C type 3 4

timestep 0.001
run_style verlet
fix 1 water shake 0.0001 20 0000 t 1 2


fix avePT all ave/time 1 250000 250000 c_thermo_temp c_thermo_press[1] c_thermo_press[2] c_thermo_press[3]
thermo_style custom step etotal f_avePT[1] f_avePT[2] f_avePT[3] f_avePT[4] lx ly lz
thermo 250000

dump 1 all dcd 1000 31Cl_TCE_04.dcd
dump 2 all xyz 10000000000 31Cl_TCE_04.xyz


fix 2 all nvt temp 298.0 298.0 0.1
run 50000000


write_restart 31Cl_TCE_04.save
```

```
#91Cl_TCE input file

units metal
dimension 3
atom_style full
pair_style lj/cut/coul/long 10.0 10.0
bond_style harmonic
angle_style harmonic
dihedral_style opls
pair_modify mix arithmetic

read_restart 91Cl_TCE_03.save
reset_timestep 0

pair_coeff 1 1 6.73853e-3 3.16556
pair_coeff 2 2 0.0 0.0
pair_coeff 3 3 3.2984e-3 3.55
pair_coeff 4 4 3.2984e-3 3.55
pair_coeff 5 5 1.3020e-2 3.40
pair_coeff 6 6 1.3020e-2 3.40
pair_coeff 7 7 0.0 0.0

kspace_style pppm 0.0001

group water type 1 2
group Ow type 1
group C type 3 4

timestep 0.001
run_style verlet
fix 1 water shake 0.0001 20 0000 t 1 2


fix avePT all ave/time 1 250000 250000 c_thermo_temp c_thermo_press[1] c_thermo_press[2]
c_thermo_press[3]
thermo_style custom step etotal f_avePT[1] f_avePT[2] f_avePT[3] f_avePT[4] lx ly lz
thermo 250000

dump 1 all dcd 1000 91Cl_TCE_04.dcd
dump 2 all xyz 10000000000 91Cl_TCE_04.xyz


fix 2 all nvt temp 298.0 298.0 0.1
run 50000000


write_restart 91Cl_TCE_04.save
```

```
#130Cl_TCE input file

units metal
dimension 3
atom_style full
pair_style lj/cut/coul/long 10.0 10.0
bond_style harmonic
angle_style harmonic
dihedral_style opls
pair_modify mix arithmetic

read_restart 130Cl_TCE_03.save
reset_timestep 0

pair_coeff 1 1 6.73853e-3 3.16556
pair_coeff 2 2 0.0 0.0
pair_coeff 3 3 3.2984e-3 3.55
pair_coeff 4 4 3.2984e-3 3.55
pair_coeff 5 5 1.3020e-2 3.40
pair_coeff 6 6 1.3020e-2 3.40
pair_coeff 7 7 0.0 0.0

kspace_style pppm 0.0001

group water type 1 2
group Ow type 1
group C type 3 4

timestep 0.001
run_style verlet
fix 1 water shake 0.0001 20 0000 t 1 2


fix avePT all ave/time 1 250000 250000 c_thermo_temp c_thermo_press[1] c_thermo_press[2]
c_thermo_press[3]
thermo_style custom step etotal f_avePT[1] f_avePT[2] f_avePT[3] f_avePT[4] lx ly lz
thermo 250000

dump 1 all dcd 1000 130Cl_TCE_04.dcd
dump 2 all xyz 10000000000 130Cl_TCE_04.xyz


fix 2 all nvt temp 298.0 298.0 0.1
run 50000000


write_restart 130Cl_TCE_04.save
```

```
#235Cl_TCE input file

units metal
dimension 3
atom_style full
pair_style lj/cut/coul/long 10.0 10.0
bond_style harmonic
angle_style harmonic
dihedral_style opls
pair_modify mix arithmetic

read_restart 235Cl_TCE_03.save
reset_timestep 0

pair_coeff 1 1 6.73853e-3 3.16556
pair_coeff 2 2 0.0 0.0
pair_coeff 3 3 3.2984e-3 3.55
pair_coeff 4 4 3.2984e-3 3.55
pair_coeff 5 5 1.3020e-2 3.40
pair_coeff 6 6 1.3020e-2 3.40
pair_coeff 7 7 0.0 0.0

kspace_style pppm 0.0001

group water type 1 2
group Ow type 1
group C type 3 4

timestep 0.001
run_style verlet
fix 1 water shake 0.0001 20 0000 t 1 2


fix avePT all ave/time 1 250000 250000 c_thermo_temp c_thermo_press[1] c_thermo_press[2]
c_thermo_press[3]
thermo_style custom step etotal f_avePT[1] f_avePT[2] f_avePT[3] f_avePT[4] lx ly lz
thermo 250000

dump 1 all dcd 1000 235Cl_TCE_04.dcd
dump 2 all xyz 10000000000 235Cl_TCE_04.xyz


fix 2 all nvt temp 298.0 298.0 0.1
run 50000000


write_restart 235Cl_TCE_04.save
```

```
#421Cl_TCE input file

units metal
dimension 3
atom_style full
pair_style lj/cut/coul/long 10.0 10.0
bond_style harmonic
angle_style harmonic
dihedral_style opls
pair_modify mix arithmetic

read_restart 421Cl_TCE_03.save
reset_timestep 0

pair_coeff 1 1 6.73853e-3 3.16556
pair_coeff 2 2 0.0 0.0
pair_coeff 3 3 3.2984e-3 3.55
pair_coeff 4 4 3.2984e-3 3.55
pair_coeff 5 5 1.3020e-2 3.40
pair_coeff 6 6 1.3020e-2 3.40
pair_coeff 7 7 0.0 0.0

kspace_style pppm 0.0001

group water type 1 2
group Ow type 1
group C type 3 4

timestep 0.001
run_style verlet
fix 1 water shake 0.0001 20 0000 t 1 2


fix avePT all ave/time 1 250000 250000 c_thermo_temp c_thermo_press[1] c_thermo_press[2]
c_thermo_press[3]
thermo_style custom step etotal f_avePT[1] f_avePT[2] f_avePT[3] f_avePT[4] lx ly lz
thermo 250000

dump 1 all dcd 1000 421Cl_TCE_04.dcd
dump 2 all xyz 10000000000 421Cl_TCE_04.xyz


fix 2 all nvt temp 298.0 298.0 0.1
run 50000000


write_restart 421Cl_TCE_04.save
```

Control files for molecular dynamic simulations of 1,2-DCA carbon isotopocules with Lammps

```
#90C_DCA input file

units metal
dimension 3
atom_style full
pair_style lj/cut/coul/long 10.0 10.0
bond_style harmonic
angle_style harmonic
dihedral_style opls
pair_modify mix arithmetic

read_restart 90C_DCA_03.save
reset_timestep 0

pair_coeff 1 1 6.73853e-3 3.16556
pair_coeff 2 2 0.0 0.0
pair_coeff 3 3 2.6040e-3 3.50
pair_coeff 4 4 2.6040e-3 3.50
pair_coeff 5 5 1.3020e-2 3.40
pair_coeff 6 6 1.3020e-2 3.40
pair_coeff 7 7 1.3020e-3 2.50
pair_coeff 8 8 1.3020e-3 2.50
pair_coeff 9 9 1.3020e-3 2.50
pair_coeff 10 10 1.3020e-3 2.50

kspace_style pppm 0.0001

group water type 1 2
group Ow type 1
group C type 3 4

timestep 0.001
run_style verlet
fix 1 water shake 0.0001 20 0000 t 1 2
fix avePT all ave/time 1 250000 250000 c_thermo_temp c_thermo_press[1] c_thermo_press[2] c_thermo_press[3]
thermo_style custom step etotal f_avePT[1] f_avePT[2] f_avePT[3] f_avePT[4] lx ly lz
thermo 250000

dump 1 all dcd 1000 90C_DCA_04.dcd
dump 2 all xyz 10000000000 90C_DCA_04.xyz

fix 2 all nvt temp 298.0 298.0 0.01
run 50000000


write_restart 90C_DCA_04.save
```

```
#99_DCA input file

units metal
dimension 3
atom_style full
pair_style lj/cut/coul/long 10.0 10.0
bond_style harmonic
angle_style harmonic
dihedral_style opls
pair_modify mix arithmetic

read_restart DCA_03.save
reset_timestep 0

pair_coeff 1 1 6.73853e-3 3.16556
pair_coeff 2 2 0.0 0.0
pair_coeff 3 3 2.6040e-3 3.50
pair_coeff 4 4 2.6040e-3 3.50
pair_coeff 5 5 1.3020e-2 3.40
pair_coeff 6 6 1.3020e-2 3.40
pair_coeff 7 7 1.3020e-3 2.50
pair_coeff 8 8 1.3020e-3 2.50
pair_coeff 9 9 1.3020e-3 2.50
pair_coeff 10 10 1.3020e-3 2.50

kspace_style pppm 0.0001

group water type 1 2
group Ow type 1
group C type 3 4

timestep 0.001
run_style verlet
fix 1 water shake 0.0001 20 0000 t 1 2
fix avePT all ave/time 1 250000 250000 c_thermo_temp c_thermo_press[1] c_thermo_press[2] c_thermo_press[3]
thermo_style custom step etotal f_avePT[1] f_avePT[2] f_avePT[3] f_avePT[4] lx ly lz thermo 250000

dump 1 all dcd 1000 DCA_04.dcd
dump 2 all xyz 10000000000 DCA_04.xyz

fix 2 all nvt temp 298.0 298.0 0.01
run 50000000


write_restart DCA_04.save
```

```
#178_DCA input file

units metal
dimension 3
atom_style full
pair_style lj/cut/coul/long 10.0 10.0
bond_style harmonic
angle_style harmonic
dihedral_style opls
pair_modify mix arithmetic

read_restart 178C_DCA_03.save
reset_timestep 0

pair_coeff 1 1 6.73853e-3 3.16556
pair_coeff 2 2 0.0 0.0
pair_coeff 3 3 2.6040e-3 3.50
pair_coeff 4 4 2.6040e-3 3.50
pair_coeff 5 5 1.3020e-2 3.40
pair_coeff 6 6 1.3020e-2 3.40
pair_coeff 7 7 1.3020e-3 2.50
pair_coeff 8 8 1.3020e-3 2.50
pair_coeff 9 9 1.3020e-3 2.50
pair_coeff 10 10 1.3020e-3 2.50

kspace_style pppm 0.0001
group water type 1 2
group Ow type 1
group C type 3 4

timestep 0.001
run_style verlet
fix 1 water shake 0.0001 20 0000 t 1 2
fix avePT all ave/time 1 250000 250000 c_thermo_temp c_thermo_press[1] c_thermo_press[2]
c_thermo_press[3]
thermo_style custom step etotal f_avePT[1] f_avePT[2] f_avePT[3] f_avePT[4] lx ly lz thermo 250000

dump 1 all dcd 1000 178C_DCA_04.dcd
dump 2 all xyz 10000000000 178C_DCA_04.xyz

fix 2 all nvt temp 298.0 298.0 0.01
run 50000000


write_restart 178C_DCA_04.save
```

```
#223C_DCA input file

units metal
dimension3
atom_style full
pair_style lj/cut/coul/long 10.0 10.0
bond_style harmonic
angle_style harmonic
dihedral_style opls
pair_modify mix arithmetic

read_restart 223C_DCA_03.
save reset_timestep 0

pair_coeff 1 1 6.73853e-3 3.16556
pair_coeff 2 2 0.0 0.0
pair_coeff 3 3 2.6040e-3 3.50
pair_coeff 4 4 2.6040e-3 3.50
pair_coeff 5 5 1.3020e-2 3.40
pair_coeff 6 6 1.3020e-2 3.40
pair_coeff 7 7 1.3020e-3 2.50
pair_coeff 8 8 1.3020e-3 2.50
pair_coeff 9 9 1.3020e-3 2.50
pair_coeff 10 10 1.3020e-3 2.50

kspace_style pppm 0.0001
group water type 1 2
group Ow type 1
group C type 3 4

timestep 0.00
run_style verlet
fix 1 water shake 0.0001 20 0000 t 1 2
fix avePT all ave/time 1 250000 250000 c_thermo_temp c_thermo_press[1] c_thermo_press[2]
c_thermo_press[3]
thermo_style custom step etotal f_avePT[1] f_avePT[2] f_avePT[3] f_avePT[4] lx ly lz thermo 250000

dump 1 all dcd 1000 223C_DCA_04.dcd
dump 2 all xyz 10000000000 223C_DCA_04.xyz

fix 2 all nvt temp 298.0 298.0 0.01
run 50000000


write_restart 223C_DCA_04.save
```

```
#283C_DCA input file

units metal
dimension 3
atom_style full
pair_style lj/cut/coul/long 10.0 10.0 bond_style harmonic
angle_style harmonic
dihedral_style opls
pair_modify mix arithmetic

read_restart 283C_DCA_03
save reset_timestep 0

pair_coeff 1 1 6.73853e-3 3.16556
pair_coeff 2 2 0.0 0.0
pair_coeff 3 3 2.6040e-3 3.50
pair_coeff 4 4 2.6040e-3 3.50
pair_coeff 5 5 1.3020e-2 3.40
pair_coeff 6 6 1.3020e-2 3.40
pair_coeff 7 7 1.3020e-3 2.50
pair_coeff 8 8 1.3020e-3 2.50
pair_coeff 9 9 1.3020e-3 2.50
pair_coeff 10 10 1.3020e-3 2.50

kspace_style pppm 0.0001
group water type 1 2
group Ow type 1
group C type 3 4

timestep 0.001
run_style verlet
fix 1 water shake 0.0001 20 0000 t 1 2
fix avePT all ave/time 1 250000 250000 c_thermo_temp c_thermo_press[1] c_thermo_press[2]
c_thermo_press[3]
thermo_style custom step etotal f_avePT[1] f_avePT[2] f_avePT[3] f_avePT[4] lx ly lz thermo 250000

dump 1 all dcd 1000 283C_DCA_04.dcd
dump 2 all xyz 10000000000 283C_DCA_04.xyz

fix 2 all nvt temp 298.0 298.0 0.01
run 50000000


write_restart 283C_DCA_04.save
```

```
#353C_DCA input file

units metal
dimension 3
atom_style full
pair_style lj/cut/coul/long 10.0 10.0
bond_style harmonic
angle_style harmonic
dihedral_style opls
pair_modify mix arithmetic

read_restart 353C_DCA_03.save
reset_timestep 0

pair_coeff 1 1 6.73853e-3 3.16556
pair_coeff 2 2 0.0 0.0
pair_coeff 3 3 2.6040e-3 3.50
pair_coeff 4 4 2.6040e-3 3.50
pair_coeff 5 5 1.3020e-2 3.40
pair_coeff 6 6 1.3020e-2 3.40
pair_coeff 7 7 1.3020e-3 2.50
pair_coeff 8 8 1.3020e-3 2.50
pair_coeff 9 9 1.3020e-3 2.50
pair_coeff 10 10 1.3020e-3 2.50

kspace_style pppm 0.0001
group water type 1 2
group Ow type 1
group C type 3 4

timestep 0.001
run_style verlet
fix 1 water shake 0.0001 20 0000 t 1 2
fix avePT all ave/time 1 250000 250000 c_thermo_temp c_thermo_press[1] c_thermo_press[2]
c_thermo_press[3]
thermo_style custom step etotal f_avePT[1] f_avePT[2] f_avePT[3] f_avePT[4] lx ly lz thermo 250000

dump 1 all dcd 1000 353C_DCA_04.dcd
dump 2 all xyz 10000000000 353C_DCA_04.xyz

fix 2 all nvt temp 298.0 298.0 0.01
run 50000000


write_restart 353C_DCA_04.save
```

Control files for molecular dynamic simulations of 1,2-DCA chlorine isotopocules with Lammps

```
#35Cl_DCA input file

units metal
dimension 3
atom_style full
pair_style lj/cut/coul/long 10.0 10.0
bond_style harmonic
angle_style harmonic
dihedral_style opls
pair_modify mix arithmetic

read_restart 35Cl_DCA_03
save reset_timestep 0

pair_coeff 1 1 6.73853e-3 3.16556
pair_coeff 2 2 0.0 0.0
pair_coeff 3 3 2.6040e-3 3.50
pair_coeff 4 4 2.6040e-3 3.50
pair_coeff 5 5 1.3020e-2 3.40
pair_coeff 6 6 1.3020e-2 3.40
pair_coeff 7 7 1.3020e-3 2.50
pair_coeff 8 8 1.3020e-3 2.50
pair_coeff 9 9 1.3020e-3 2.50
pair_coeff 10 10 1.3020e-3 2.50

kspace_style pppm 0.0001
group water type 1 2
group Ow type 1
group C type 3 4

timestep 0.00
 run_style verlet
fix 1 water shake 0.0001 20 0000 t 1 2
fix avePT all ave/time 1 250000 250000 c_thermo_temp c_thermo_press[1] c_thermo_press[2] c_thermo_press[3]
thermo_style custom step etotal f_avePT[1] f_avePT[2] f_avePT[3] f_avePT[4] lx ly lz thermo 250000

dump 1 all dcd 1000 35Cl_DCA_04.dcd
dump 2 all xyz 10000000000 35Cl_DCA_04.xyz

fix 2 all nvt temp 298.0 298.0 0.01
run 50000000


write_restart 35Cl_DCA_04.save
```

```
#55Cl_DCA input file

units metal
dimension 3
atom_style full
pair_style lj/cut/coul/long 10.0 10.0
bond_style harmonic
angle_style harmonic
dihedral_style opls
pair_modify mix arithmetic

read_restart 55Cl_DCA_03
save reset_timestep 0

pair_coeff 1 1 6.73853e-3 3.16556
pair_coeff 2 2 0.0 0.0
pair_coeff 3 3 2.6040e-3 3.50
pair_coeff 4 4 2.6040e-3 3.50
pair_coeff 5 5 1.3020e-2 3.40
pair_coeff 6 6 1.3020e-2 3.40
pair_coeff 7 7 1.3020e-3 2.50
pair_coeff 8 8 1.3020e-3 2.50
pair_coeff 9 9 1.3020e-3 2.50
pair_coeff 10 10 1.3020e-3 2.50

kspace_style pppm 0.0001
group water type 1 2
group Ow type 1
group C type 3 4

timestep 0.001
run_style verlet
fix 1 water shake 0.0001 20 0000 t 1 2
fix avePT all ave/time 1 250000 250000 c_thermo_temp c_thermo_press[1] c_thermo_press[2]
c_thermo_press[3]
thermo_style custom step etotal f_avePT[1] f_avePT[2] f_avePT[3] f_avePT[4] lx ly lz thermo 250000

dump 1 all dcd 1000 55Cl_DCA_04.dcd
dump 2 all xyz 10000000000 55Cl_DCA_04.xyz

fix 2 all nvt temp 298.0 298.0 0.01
run 50000000


write_restart 55Cl_DCA_04.save
```

```
#145Cl_DCA input file

units metal
dimension 3
atom_style full
pair_style lj/cut/coul/long 10.0 10.0
bond_style harmonic
angle_style harmonic
dihedral_style opls
pair_modify mix arithmetic

read_restart 145Cl_DCA_03
save reset_timestep 0

pair_coeff 1 1 6.73853e-3 3.16556
pair_coeff 2 2 0.0 0.0
pair_coeff 3 3 2.6040e-3 3.50
pair_coeff 4 4 2.6040e-3 3.50
pair_coeff 5 5 1.3020e-2 3.40
pair_coeff 6 6 1.3020e-2 3.40
pair_coeff 7 7 1.3020e-3 2.50
pair_coeff 8 8 1.3020e-3 2.50
pair_coeff 9 9 1.3020e-3 2.50
pair_coeff 10 10 1.3020e-3 2.50

kspace_style pppm 0.0001
group water type 1 2
group Ow type 1
group C type 3 4

timestep 0.001
run_style verlet
fix 1 water shake 0.0001 20 0000 t 1 2
fix avePT all ave/time 1 250000 250000 c_thermo_temp c_thermo_press[1] c_thermo_press[2]
c_thermo_press[3]
thermo_style custom step etotal f_avePT[1] f_avePT[2] f_avePT[3] f_avePT[4] lx ly lz thermo 250000

dump 1 all dcd 1000 145Cl_DCA_04.dcd
dump 2 all xyz 10000000000 145Cl_DCA_04.xyz

fix 2 all nvt temp 298.0 298.0 0.01
run 50000000


write_restart 145Cl_DCA_04.save
```

```
#235Cl_DCA input file

units metal
dimension 3
atom_style full
pair_style lj/cut/coul/long 10.0 10.0
bond_style harmonic
angle_style harmonic
dihedral_style opls
pair_modify mix arithmetic

read_restart 235Cl_DCA_03
save reset_timestep 0

pair_coeff 1 1 6.73853e-3 3.16556
pair_coeff 2 2 0.0 0.0
pair_coeff 3 3 2.6040e-3 3.50
pair_coeff 4 4 2.6040e-3 3.50
pair_coeff 5 5 1.3020e-2 3.40
pair_coeff 6 6 1.3020e-2 3.40
pair_coeff 7 7 1.3020e-3 2.50
pair_coeff 8 8 1.3020e-3 2.50
pair_coeff 9 9 1.3020e-3 2.50
pair_coeff 10 10 1.3020e-3 2.50

kspace_style pppm 0.0001
group water type 1 2
group Ow type 1
group C type 3 4

timestep 0.001
run_style verlet
fix 1 water shake 0.0001 20 0000 t 1 2
fix avePT all ave/time 1 250000 250000 c_thermo_temp c_thermo_press[1] c_thermo_press[2]
c_thermo_press[3]
thermo_style custom step etotal f_avePT[1] f_avePT[2] f_avePT[3] f_avePT[4] lx ly lz thermo 250000

dump 1 all dcd 1000 235Cl_DCA_04.dcd
dump 2 all xyz 10000000000 235Cl_DCA_04.xyz

fix 2 all nvt temp 298.0 298.0 0.01
run 50000000


write_restart 235Cl_DCA_04.save
```

```
#385Cl_DCA input file

units metal
dimension 3
atom_style full
pair_style lj/cut/coul/long 10.0 10.0
bond_style harmonic
angle_style harmonic
dihedral_style opls
pair_modify mix arithmetic

read_restart 385Cl_DCA_03
save reset_timestep 0

pair_coeff 1 1 6.73853e-3 3.16556
pair_coeff 2 2 0.0 0.0
pair_coeff 3 3 2.6040e-3 3.50
pair_coeff 4 4 2.6040e-3 3.50
pair_coeff 5 5 1.3020e-2 3.40
pair_coeff 6 6 1.3020e-2 3.40
pair_coeff 7 7 1.3020e-3 2.50
pair_coeff 8 8 1.3020e-3 2.50
pair_coeff 9 9 1.3020e-3 2.50
pair_coeff 10 10 1.3020e-3 2.50

kspace_style pppm 0.0001
group water type 1 2
group Ow type 1
group C type 3 4

timestep 0.001 run_style verlet
fix 1 water shake 0.0001 20 0000 t 1 2
fix avePT all ave/time 1 250000 250000 c_thermo_temp c_thermo_press[1] c_thermo_press[2]
c_thermo_press[3]
thermo_style custom step etotal f_avePT[1] f_avePT[2] f_avePT[3] f_avePT[4] lx ly lz thermo 250000

dump 1 all dcd 1000 385Cl_DCA_04.dcd
dump 2 all xyz 10000000000 385Cl_DCA_04.xyz

fix 2 all nvt temp 298.0 298.0 0.01
run 50000000


write_restart 385Cl_DCA_04.save
```

Curriculum Vitae

Philipp Wanner

PhD candidate
Centre for Hydrogeology and Geothermics (CHYN)
Rue Emil-Argand 11
2000 Neuchâtel
Switzerland
Phone: +41 32 718 26 22; email: philipp.wanner@unine.ch

Education

Academic education:

2012 – Present:	University of Neuchâtel, Switzerland. Centre for Hydrogeology and Geothermics (CHYN), PhD candidate.
2010 – 2012:	University of Bern, Switzerland, Institute of Geological Sciences, MSc in Environmental and Resource Geochemistry.
2007 – 2010:	University of Bern, Switzerland, Institute of Geological Sciences, BSc in General Geology

Further education:

2016:	Certificate of advanced studies in Management of polluted sites (specialization module).
2010:	Certificate of advanced studies in Management of polluted sites (foundation module).

Publications

Wanner, P., Parker B.L., Chapman S.W., Aravena, R., Hunkeler, D., 2016.
Investigations of sorption effects on isotope ratios during diffusion of chlorinated hydrocarbons in low permeability sediments (in preparation)

Wanner, P., Parker B.L., Chapman S.W., Aravena, R., Hunkeler, D., 2016.
Quantification of degradation of chlorinated hydrocarbons in low permeability sediments using compound-specific isotope analysis.
Environmental Science and Technology, DOI: 10.1021/acs.est.5b06330

Wanner, P., Hunkeler, D., 2015.
Carbon and chlorine isotopologue fractionation of chlorinated hydrocarbons during diffusion in water and low permeability sediments.
Geochimica et Cosmochimica Acta, 157: 198-212.

Wanner, P., Al-Sulaimani, M.Y.N., Waber, N., Wanner, C., 2015.
Assessing the environmental hazard of using seawater for ore processing at the Lasail mine site in the Sultanate of Oman.
Mine Water and the Environment, 34(1): 59-74.

Theses

Master thesis (2012): Evaluation of salinity and heavy metal contamination in groundwater of Wadi Suq, Oman.

Bachelor thesis (2010): Paleoclimatic evidences in the basal tertiary sediments of the central Jura Mountains. (Paläoklimatische Indizien in den basalen Tertiärsedimenten des zentralen Juras).

Presentations

June 2014:	University Consortium for Field-Focused Groundwater Contamination Research Annual Progress Meeting, University of Guelph, Canada.
September 2014:	"In-Situ" Remediation Conference, London, United Kingdom.
October 2014:	University Consortium for Field-Focused Groundwater Contamination Focus Meeting, Denver, USA.
September 2015:	Annual Conference of International Association of Hydrologeologists (IAH), Rome, Italy.
November 2015:	Swiss Geoscience Meeting, Basel, Switzerland.
March 2016:	Meeting of the German Association for Hydrogeology, Karlsruhe, Germany.

Teaching experience

Spring 2015:	Practical course in general geology for first year bachelor students.

Practical work experience

2009 – 2012:	Technical assistant (part time position): Grain density measurements at the Institute of Geological Sciences at the University of Bern, Switzerland.
July – August 2008:	Technical assistant (part time position): Preparation of pellets for XRF-diffractometry at the Institute of Geological Sciences at the University of Bern, Switzerland.
June - July 2006:	Internship in a private consulting company (Kellerhals und Haefeli AG) in Bern, Switzerland.

Sports activities

2003 – 2013:	Semi-professional floorball player in highest Swiss national division.
2007 – 2011:	Member of the Swiss National floorball team and participation in two World Championships: In 2008 in Prag, Czech Republic (3rd place) and in 2010 in Helsinki, Finland (4th place).